THESIS

STATISTICS FOR STRUCTURE FORMATION IN THE UNIVERSE

Takahiko Matsubara

A dissertation submitted to
Department of Physics
Faculty of Science
Hiroshima University

January, 1995

UTAP-200/95

Contents

1

Introduction

The study of the structure of our Universe is one of the most active and exciting research fields in cosmology. In these several years, new and sensational facts in observational cosmology have been unveiled and our understanding of the large-scale structure of the Universe is improving rapidly. There are various structures in the Universe. The purpose of cosmological models is to explain the origin of the structure and the processes to form the present structure. Among others, the widely accepted view for the time being is that the small fluctuations of energy density in the early Universe are amplified mainly by the gravitational interaction and become the origin of structures in the present Universe. This view is called as *gravitational instability theory*. This theory is favorable for number of reasons. The small fluctuations of 2.75K cosmic microwave background radiation (CMBR) recently detected by COBE satellite (Smoot et al. 1992) further support that the primordial Universe is almost homogeneous but has the small fluctuations of order 10^{-5}.

Many people have been studying how the primordial fluctuations can be generated, but until now, we have not the fully convincing theories for this subject yet. One of the possible theories is that the quantum fluctuations of some kind in the early Universe become classical in the later Universe as many inflationary models assume. Because the Universe is expanding, if we go back in time, the state of very high density and high temperature is achieved where the presently known physical laws break down. There is not any convincing model that can generate reasonable primordial fluctuations using only processes which are well established in elementary particle physics. So the properties of primordial fluctuations do not seem to be predicted just using known laws of elementary physics. Thus the primordial fluctuations are most likely caused by unknown physics including quantum gravity etc.

Using gravitational instability theory, the structures in the present Universe can be related to the primordial fluctuations. This fact arises the hope that the sufficient observation of the large-scale structure of the present Universe as well as the accurate detection of the fluctuations of CMBR can probe the unknown physics. To pursue this possibility, the processes to form the observable astrophysical objects should be clarified.

One of the popular probe of the large-scale structure of the Universe is the distribution of galaxies. Recently, the redshift data of galaxies are widely collected systematically and have been exhibiting rich structures in the Universe. In the next several years, the redshift surveys will make rapid progress both in quantity and in quality. Redshift surveys have been unveiling that the Universe has structures even on scales $\sim$ 100Mpc and is far from homogeneous. In the gravitational instability theory, such large-scale structure should be formed by gravitational interaction. For the formation of galaxies itself, however, the dissipative processes other than the gravitational interaction concern much. Galaxies are not guaranteed to trace the density field of the Universe and this fact makes the problem complicated. The formation of galaxies is one of the most difficult issues which has been widely debated so far. We can only say that the galaxies are the biased tracers of a density field in the Universe and what kind of bias is subjected should be clarified in future investigations.

The statistics of galaxy distribution are fundamental tools in the analysis of the large-scale structure. To quantify the present universe, the statistical properties of the galaxy distribution should be identified. Because of the observational limitation, which statistic is efficient for analyzing is not obvious. Many statistical measures to quantify the large-scale structure are proposed so far. In this *Thesis*, author's recent published work concerning the connection of statistics and dynamics of the universe based on gravitational instability theory is summarized. Materials from more recent work mostly concerning biasing and statistics are also included.

More in detail, this *Thesis* is organized as follows.

In chapter 2, the ingredients for the theory of large-scale structure are reviewed briefly. After reviewing the evolution of background metric in section 2.1, the linear and higher order perturbation theories for collisionless non-relativistic fluid in expanding background are summarized in section 2.2. The correlation functions are the traditional tools to quantifying the clustering pattern of galaxies. Some basic concepts of the correlation statistics are explained in section 2.3. We have never

had the definite theory for primordial fluctuations. Some candidates and its present status are briefly described in section 2.4.

In chapter 3, the dynamical evolution of several statistical quantities are studied. First the observational and theoretical overview on cosmological correlation functions is described in section 3.1.

Two-, three- and four-point correlation functions of galaxies in several cosmological models are examined in detail by using cosmological N-body simulation data in section 3.2. Particular attention is paid to see whether or not they obey the hierarchical clustering ansatz which states that N-point correlation functions of cosmological gravitating systems are written down as $N-1$ products of two-point correlation functions. In this analysis, different geometrical configurations of three and four points are treated separately, which enable us to quantify for the first time configuration-dependent behavior of the correlation functions up to the fourth order. It is found that the hierarchical clustering ansatz holds only very approximately, and that there is clear evidence against the ansatz especially in strongly nonlinear regimes of fluctuations. The effect of peculiar velocity field makes the correlation functions in redshift space obey the hierarchical clustering ansatz better than in real space. Thus a straightforward analysis of redshift surveys would lead to a misleading result in this sense.

In section 3.3, statistics of isodensity contours are considered. The gravitational evolution of the genus and other statistics of isodensity contours of the density field is derived analytically in a weakly nonlinear regime using second-order perturbation theory. The effect of final smoothing in perturbation theory on the statistics of isodensity contours is also evaluated. The resulting analytic expression for the genus is compared with N-body numerical simulations and exhibits a good agreement.

In section 3.4, the distortion of the apparent distribution of galaxies in redshift space contaminated by the peculiar velocity effect is studied. Specifically the expressions for N-point correlation functions are obtained in redshift space with given functional form for velocity distribution $f(v)$, and are evaluated for two- and three-point correlation functions quantitatively. The effect of velocity correlations is also discussed. When the two-point correlation function in real space has a power-law form, $\xi^{(r)}(r) \propto r^{-\gamma}$, the redshift-space counterpart *on small scales* also has a power-law form but with an increased power-law index: $\xi^{(s)}(s) \propto s^{1-\gamma}$. When the three-point correlation function has the hierarchical form and the two-point correlation function has the power-law form in real space, the hierarchical form of the

three-point correlation function is almost preserved in redshift space. The above analytic results are compared with the direct analysis based on N-body simulation data for cold dark matter models. Implications on the hierarchical clustering ansatz are discussed in detail.

In section 3.6, the peculiar velocity effect on the statistics of isodensity contours is examined by linear theory. The statistics considered in this section are the three- and two-dimensional genus of isodensity contours, the area of isodensity contours, the length of isodensity contours in the 2-dimensional slice and the level crossing statistics on the line. It is found that all these statistics in redshift space as functions of density threshold of contours have the same shape as in real space. The redshift space distortion affects only amplitudes of these statistics. The three-dimensional genus and the area hardly suffer from the redshift space distortion for $0 \leq \Omega b^{-5/3} \leq 1$, where b is a linear bias parameter. The other statistics are defined in one- or two-dimensional slices of the sample volume and depend on the direction of these slices relative to the line of sight. These dependences on direction of these statistics provide ways to determine the density parameter of the universe.

In chapter 4, Technique concerning statistical analyses of the large-scale structure of the universe in the presence of biasing in the structure formation is developed. The diagrammatic method are formulated to calculate the correlation functions of the nonlocally biased field from a generally non-Gaussian density field. This method is based on generalized Wiener-Hermite expansion of the density field. The present formalism has not only general applicability, but also practical significance, too. To show the effectiveness of this method, we revisit the problems on biasing that have been considered previously, i.e., various approximations for peak statistics and hierarchical structure of correlation functions of locally biased field. Further analyses which have not been possible so far on these problems can be performed by our formalism. The gravitational evolution of primordial fluctuations or other structure-forming processes can be described by nonlocal biasing, so can be treated by our new formalism in principle.

The brief summary of previous work on this subject is presented in section 4.1. In section 4.2, the generalized Wiener-Hermite functionals which play essential roles in the analysis are introduced. Average value of any functional of a field is expanded by Wiener-Hermite functionals. In section 4.3, the diagrammatic method to calculate the mean density and N-point correlation functions of biased field is presented. More compact expressions or methods of calculation are given when the biasing is local

or semi-local, that are defined below. The Fourier-space version of our methods is also explained. The methods are applied to several theoretical problems in section 4.4. The first application is not relevant to bias, but the relation to Edgeworth expansion is discussed. The Edgeworth expansion was recently used in analyses of astrophysical density fields. The second application is on peak theory. We show that our methods improve the technique which is available so far for peak statistics. The next application is on hierarchical relations of correlation functions in the presence of local biasing which is investigated recently by Fry & Gaztañaga (1993; and references therein). We show our method complements their results. The last application is on the gravitational nonlinear evolution as a nonlocal biasing. We apply our methods to the calculation of three-point correlation function induced by gravity.

Finally, we present the summary in chapter 5. Appendices are devoted to the details of derivation, calculation and proof.

2

Ingredients of the Analyses

2.1 BACKGROUND COSMOLOGY

The fundamental assumption in standard cosmology, called *cosmological principle*, is the global homogeneity and isotropy of our Universe. As described in the previous chapter, the inhomogeneity is seen on scales of even about 100 Mpc, but on scales much larger than 100 Mpc, observations of the isotropy of the CMBR and the X-ray background and the number counts of radio sources, support the cosmological principle. When the spatial hypersurface is homogeneous and isotropic, one can find (e.g., Weinberg 1972) coordinates with the following Friedmann-Lemaître-Robertson-Walker (FLRW) metric:

$$ds^2 = dt^2 - a^2(t)\left[\frac{dx^2}{1-kx^2} + x^2 d\theta^2 + x^2 \sin^2\theta d\phi^2\right]. \tag{2.1.1}$$

In this coordinate, t is called the proper time and $\boldsymbol{x} = (x, \theta, \phi)$ are called comoving coordinates. In the space with this metric, $k = 0$, $k > 0$ and $k < 0$ corresponds to the spatially flat Universe, the closed Universe with positive curvature and open Universe with negative curvature, respectively. The behavior of the expansion factor $a(t)$ is determined by the Einstein equation.

The stress-energy tensor $T_{\mu\nu}$ should be diagonal so as to have the solution of the Einstein equation for the metric of equation (2.1.1), and, because of the spatial homogeneity, the spatial components should be identical. Thus, $T_{\mu\nu}$ has the same form as for the perfect fluid with energy density $\rho(t)$ and pressure $p(t)$:

$$T^{\mu}{}_{\nu} = \mathrm{diag}(\rho, -p, -p, -p). \tag{2.1.2}$$

The Einstein equation reduces to the following two equations:

$$H^2 \equiv \left(\frac{\dot{a}}{a}\right)^2 = \frac{8\pi G}{3}\rho + \frac{\Lambda}{3} - \frac{k}{a^2}, \tag{2.1.3}$$

$$\frac{d}{da}(\rho a^3) = -3a^2 p, \tag{2.1.4}$$

where G is a gravitational constant, Λ is a cosmological constant and dot denotes the time derivative, d/dt. In the FLRW Universe, the two objects which are at an interval of $r = ax$ in a physical unit and both of which do not move with respect to the background metric ($\dot{x} = 0$) move apart each other at a velocity $v = \dot{a}x = Hr$ in a physical unit. This expansion rate H is called Hubble parameter. The present value of the Hubble parameter H_0 is not accurately determined but is estimated roughly as

$$H_0 = 100h\text{km s}^{-1}\text{ Mpc}^{-1}, \quad 0.4 \lesssim h \lesssim 1. \tag{2.1.5}$$

The recent observations favor the higher value $h \sim 0.8$ (e.g., Pierce et al. 1994; Freedman et al. 1994), but the uncertainty remains in any case.

Owing to equation (2.1.3),

$$k = a^2 H^2(\Omega + \lambda - 1), \tag{2.1.6}$$

where

$$\Omega = \frac{8\pi G}{3H^2}\rho, \tag{2.1.7}$$

$$\lambda = \frac{\Lambda}{3H^2}. \tag{2.1.8}$$

are the density parameter and the dimensionless cosmological constant*. Therefore, $\Omega + \lambda = 0, > 0, < 0$ correspond to spatially flat Universe, closed Universe with positive curvature, and open Universe with negative curvature, respectively. The present value of the density parameter Ω_0 is also not accurately determined but only the rough estimation as $0.2 \lesssim \Omega_0 \lesssim 1$ are available. As for the cosmological constant, we could not say more than that the present value of the dimensionless cosmological constant λ_0 is of order unity or less. It is hopeless to determine observationally the geometry of the Universe from the value $\Omega_0 + \lambda_0$ and we proceed leaving Ω_0, λ_0, H_0 as parameters. The present value of the expansion factor a_0 can be fixed arbitrarily choosing an unit of length of the present Universe. The conventional one is chosen so that the constant k takes the value $\pm 1, 0$ (c.f., equation [2.1.6] at the present). Other choice is $a_0 = 1$. The latter choice is also popular, but note that k is not restricted to $\pm 1, 0$ generally in this choice. In this Thesis, a_0 is not fixed but is left explicitly in equations below.

*Note that dimensionless cosmological constant λ is no longer a constant but varies with time.

The equation (2.1.4), together with the equation of state for the content of the Universe, determine the behavior of ρ as a function of a. When the Universe is matter-dominated ($p = 0$), then $\rho \propto a^{-3}$, when radiation-dominated ($p = \rho/3$), then $\rho \propto a^{-4}$.

In cases of vanishing cosmological constant, $\Lambda = 0$, from equation (2.1.6),

$$\Omega^{-1} - 1 = \frac{\rho_0 a_0^2}{\rho a^2}\left(\Omega_0^{-1} - 1\right). \tag{2.1.9}$$

In the radiation-dominated Universe, $\rho \propto a^{-4}$, or non-relativistic matter-dominated Universe, $\rho \propto a^{-3}$, this relation shows $\Omega = 1$ is an unstable fixed point: as a grows, a small deviation from $\Omega = 1$ becomes large. The case $\Omega = 1$ is special because only in this case the density parameter does not depend on time. This special Universe with $\Omega = 1$, $\Lambda = 0$ is called Einstein-de Sitter Universe.

In this Thesis, the Universe dominated by collisionless, non-relativistic matter is focused on. In such a situation, the Friedmann equation (2.1.3) reduces to

$$\left(\frac{dR}{d\tau}\right)^2 = \frac{\Omega_0}{R} + \lambda_0 R^2 + (1 - \Omega_0 - \lambda_0), \tag{2.1.10}$$

where the dimensionless quantities,

$$R \equiv \frac{a}{a_0}, \quad \tau \equiv H_0 t, \tag{2.1.11}$$

are introduced. This equation (2.1.10) is the same as a energy equation for a particle moving on a one-dimensional line under the potential $-\Omega_0/R - \lambda_0 R^2$, having energy of $(1 - \Omega_0 - \lambda_0)$. The solution of this equation is generally represented by elliptical integrals. In some special cases, equation (2.1.10) is integrated elementarily. The results are summarized below.

a) Einstein-de Sitter Universe, $\Omega_0 = 1$, $\lambda_0 = 0$:

$$\frac{a(t)}{a_0} = \left(\frac{3}{2}H_0 t\right)^{2/3}. \tag{2.1.12}$$

b) Open Universe without cosmological term, $\Omega_0 < 1$, $\lambda_0 = 0$: in parametric representation,

$$\frac{a(t)}{a_0} = \frac{\Omega_0}{2(\Omega_0 - 1)}(1 - \cos\theta), \tag{2.1.13}$$

$$H_0 t = \frac{\Omega_0}{2(\Omega_0 - 1)^{3/2}}(\theta - \sin\theta). \tag{2.1.14}$$

c) Closed Universe without cosmological term, $\Omega_0 > 1$, $\lambda_0 = 0$: in parametric representation,

$$\frac{a(t)}{a_0} = \frac{\Omega_0}{2(1-\Omega_0)}(\cosh\theta - 1), \tag{2.1.15}$$

$$H_0 t = \frac{\Omega_0}{2(1-\Omega_0)^{3/2}}(\sinh\theta - \theta). \tag{2.1.16}$$

d) Flat Universe with cosmological term, $\Omega_0 + \lambda_0 = 1$:

$$\frac{a(t)}{a_0} = \left(\frac{\Omega_0}{1-\Omega_0}\right)^{1/3} \sinh^{2/3}\left(\frac{3}{2}\sqrt{1-\Omega_0}H_0 t\right) \quad (\Omega_0 < 1, \lambda_0 > 0), \tag{2.1.17}$$

$$\frac{a(t)}{a_0} = \left(\frac{\Omega_0}{\Omega_0-1}\right)^{1/3} \sin^{2/3}\left(\frac{3}{2}\sqrt{\Omega_0-1}H_0 t\right) \quad (\Omega_0 > 1, \lambda_0 < 0). \tag{2.1.18}$$

2.2 PERTURBATION THEORY FOR DENSITY FLUCTUATION

The density fluctuation evolves by self-gravity in the background geometry described in the previous section after non-relativistic matter dominates in the Universe. We assume that the dominant content in the Universe is approximated by self-gravitating Newtonian fluid with negligible pressure. The evolution equations of density fluctuation are continuity equation, Euler equation of motion and Poisson equation of gravitational field (e.g., Peebles 1980):

$$\dot{\delta} + \nabla\cdot\boldsymbol{v} + \nabla\cdot(\delta\boldsymbol{v}) = 0, \tag{2.2.1}$$

$$\dot{\boldsymbol{v}} + 2H\boldsymbol{v} + (\boldsymbol{v}\cdot\nabla)\boldsymbol{v} + \nabla\Phi = \boldsymbol{0}, \tag{2.2.2}$$

$$\nabla^2\Phi = \frac{3}{2}H^2\Omega\delta, \tag{2.2.3}$$

where $\boldsymbol{x}$, $\boldsymbol{v}(\boldsymbol{x},t)$, $\Phi(\boldsymbol{x},t)$ are position, peculiar velocity, peculiar potential in comoving coordinate, respectively, which correspond to $a\boldsymbol{x}$, $a\boldsymbol{v}(\boldsymbol{x},t)$, $a^2\Phi(\boldsymbol{x},t)$ in physical units, respectively. Dot denotes time derivative and $\nabla \equiv \partial/\partial\boldsymbol{x}$ denotes and spatial derivative with respect to comoving coordinates. Density contrast δ is defined by

$$\delta(\boldsymbol{x},t) = \frac{\rho(\boldsymbol{x},t) - \overline{\rho}(t)}{\overline{\rho}(t)}, \tag{2.2.4}$$

where $\overline{\rho}(t)$ is a mean density per physical volume, which is denoted simply by $\rho(t)$ in the previous section. Instead, $\rho(\boldsymbol{x},t)$ means local density per physical volume. Using equations (2.2.1) and (2.2.2), one finds

$$\ddot{\delta} + 2H\dot{\delta} - \frac{3}{2}H^2\Omega\delta = \frac{3}{2}H^2\Omega\delta^2 + \nabla\delta\cdot\nabla\Phi + \partial_i\partial_j\left[(1+\delta)v_i v_j\right], \tag{2.2.5}$$

which turn out to be useful below. The inversion of the Poisson equation (2.2.3) is standard,

$$\Phi(\boldsymbol{x},t) = \frac{3}{2}H^2\Omega\triangle^{-1}\delta(\boldsymbol{x},t) = -\frac{3}{8\pi}H^2\Omega\int d^3x'\frac{\delta(\boldsymbol{x}',t)}{|\boldsymbol{x}'-\boldsymbol{x}|}. \tag{2.2.6}$$

These nonlinear field equations could not be solved generally and exact solutions are known only for extremely limited cases as in spherically symmetric perturbation (Peebles 1980). So we need approximations to integrate these equations. One way is to integrate the system numerically as N-body simulations. While numerical simulations provide almost only way to investigate the nonlinear process reasonably, analytic approximations to the problem are useful in some cases. When $|\delta|$, $|\boldsymbol{v}| \ll 1$, the equations are solved approximately. In linear perturbation theory, the nonlinear terms other than first order in the equations are neglected. In higher order perturbation theory, the weak nonlinearity is taken into account by solving the equations using perturbative expansion as described below.

2.2.1 Linear theory

Equation (2.2.5) is linearized as

$$\ddot{\delta} + 2H\dot{\delta} - \frac{3}{2}H^2\Omega\delta = 0. \tag{2.2.7}$$

This equation does not couple deferent points, so the fluctuation evolves independently on each points. The solution of second order differential equation (2.2.7) is a linear combination of growing mode $D(t)$ and decaying mode $D'(t)$. The growing mode dominates at later epoch, so the solution of the linear perturbation theory is approximated by

$$\delta^{(1)}(\boldsymbol{x},t) = D(t)\epsilon(\boldsymbol{x}). \tag{2.2.8}$$

The growing mode of equation (2.2.7) is generally given by (Peebles 1980)

$$D(t) \propto a\Omega\int_0^1 \frac{dx}{(\Omega/x + \lambda x^2 + 1 - \Omega - \lambda)^{3/2}}, \tag{2.2.9}$$

where Ω and λ are time-dependent parameters. The lower limit in the integration is set to be zero because we are interested in the Universe which has the beginning and are now in a expanding phase. In some special cases considered at the end of the last section, the above equation expressed differently.

a) Einstein-de Sitter Universe, $\Omega_0 = 1$, $\lambda_0 = 0$:

$$D \propto a \propto t^{2/3}. \tag{2.2.10}$$

b,c) Universe without cosmological term, $\lambda_0 = 0$:

$$D \propto aF\left(1, 2, \frac{7}{2}; 1 - \Omega^{-1}\right) \tag{2.2.11}$$

$$\propto \begin{cases} 1 + 3/x + 3\sqrt{(1+x)/x^3}\ln(\sqrt{1+x} - \sqrt{x}), & (\Omega_0 < 1) \\ -1 + 3/x - 3\sqrt{(1-x)/x^3}\tan^{-1}\sqrt{x/(1-x)}, & (\Omega_0 > 1) \end{cases} \tag{2.2.12}$$

where $x = |\Omega^{-1}(t) - 1| = |\Omega_0^{-1} - 1|a/a_0$.

d) Flat Universe with cosmological term, $\Omega_0 + \lambda_0 = 1$:

$$D \propto aF\left(\frac{1}{3}, 1, \frac{11}{6}; 1 - \Omega^{-1}\right). \tag{2.2.13}$$

In the above list, $F(\alpha, \beta, \gamma; z)$ is the Gauss' hypergeometric function.

As for the velocity field, linearized equation (2.2.2) can be integrated using equation (2.2.7), resulting in

$$\boldsymbol{v}^{(1)} = -\nabla\triangle^{-1}\dot{\delta}^{(1)} + \frac{\boldsymbol{F}(\boldsymbol{x})}{a^2}, \qquad \nabla \cdot \boldsymbol{F} = 0. \tag{2.2.14}$$

The growing mode of this equation is

$$\boldsymbol{v}^{(1)}(\boldsymbol{x}, t) = -fHD\nabla\triangle^{-1}\epsilon(\boldsymbol{x}), \tag{2.2.15}$$

where

$$f(t) \equiv \frac{d\ln D}{d\ln a}. \tag{2.2.16}$$

From equation (2.2.9), $f(t)$ is explicitly given by

$$f(\Omega, \lambda) = -1 - \frac{\Omega}{2} + \lambda + \left[\int_0^1 \frac{dx}{(\Omega/x + \lambda x^2 + 1 - \Omega - \lambda)^{3/2}}\right]^{-1} \tag{2.2.17}$$

$$\approx \begin{cases} \Omega^{0.6} + \lambda/30, & (0.05 \le \Omega \le 1.5,\ 0 \le \lambda \le 1.5) \\ \Omega^{0.6} + \lambda(1 + \Omega/2)/70. & (0.03 \le \Omega \le 2,\ -5 \le \lambda \le 5) \end{cases} \tag{2.2.18}$$

The fits in equation (2.2.18) are due to Martel (1991) and Lahav et al. (1991), respectively. This function depends on cosmological constant very weakly. In the cases for vanishing cosmological constant and for flat Universe,

$$f(\Omega, 0) = \Omega\frac{F(2, 3/2, 7/2; 1 - \Omega)}{F(1, 3/2, 7/2; 1 - \Omega)} \approx \Omega^{0.6}, \tag{2.2.19}$$

$$f(\Omega, 1 - \Omega) = \Omega\frac{F(4/3, 5/6, 11/6; 1 - \Omega)}{F(1/3, 5/6, 11/6; 1 - \Omega)}$$

$$\approx \Omega^{0.6} + \frac{1}{70}\left[1 - \frac{1}{2}\Omega(1 + \Omega)\right], \tag{2.2.20}$$

The fit in equation (2.2.19) is due to Peebles (1980) and the fit in equation (2.2.20) is an analogy of the fit in equation (2.2.18).

The growing mode of linear velocity field is irrotational

$$\nabla \times \boldsymbol{v}^{(1)} = \mathbf{0}, \tag{2.2.21}$$

so the vorticity in the present Universe could not be generated by linear theory.

2.2.2 Higher order perturbation theory

The weakly nonlinear effect can be evaluated by solving the system of differential equations (2.2.1)–(2.2.3) perturbatively adding the higher order terms to the linear solution. First, we consider the following perturbative expansion:

$$\delta = \sum_{n=1}^{\infty} \delta^{(n)}, \quad \boldsymbol{v} = \sum_{n=1}^{\infty} \boldsymbol{v}^{(n)}, \tag{2.2.22}$$

where $\delta^{(n)}$, $\boldsymbol{v}^{(n)}$ are of order $(\delta^{(1)})^n$. Then the differential equations can be solved order by order for each terms in equation (2.2.22). That is, the following equations should be solved for $n = 2, 3, 4, \ldots$, one by one.

$$\dot{\delta}^{(n)} + \nabla \cdot \boldsymbol{v}^{(n)} + \sum_{k=1}^{n-1} \nabla \cdot (\delta^{(k)} \boldsymbol{v}^{(n-k)}) = 0, \tag{2.2.23}$$

$$\dot{\boldsymbol{v}}^{(n)} + 2H\boldsymbol{v}^{(n)} + \sum_{k=1}^{n-1} (\boldsymbol{v}^{(k)} \cdot \nabla)\boldsymbol{v}^{(n-k)} + \nabla\Phi^{(n)} = \mathbf{0}, \tag{2.2.24}$$

$$\begin{aligned} \ddot{\delta}^{(n)} + 2H\dot{\delta}^{(n)} - \frac{3}{2}H^2\Omega\delta^{(n)} &= \frac{3}{2}H^2\Omega \sum_{k=1}^{n-1} \delta^{(k)}\delta^{(n-k)} + \sum_{k=1}^{n-1} \nabla\delta^{(k)} \cdot \nabla\Phi^{(n-k)} \\ &+ \sum_{k=1}^{n-1} \partial_i\partial_j \left[v_i^{(k)} v_j^{(n-k)} \right] + \sum_{k=1}^{n-1} \sum_{l=1}^{k-1} \partial_i\partial_j \left[\delta^{(l)} v_i^{(k-l)} v_j^{(n-k)} \right], \end{aligned} \tag{2.2.25}$$

where

$$\Phi^{(n)} = \frac{3}{2}H^2\Omega\triangle^{-1}\delta^{(n)}. \tag{2.2.26}$$

Two of equations (2.2.23) – (2.2.25) are independent. Although there are independent solutions for $\delta^{(n)}$ and $\boldsymbol{v}^{(n)}$, only the leading growing modes are left in the following. In the perturbative solution by this procedure, the velocity field is still irrotational in the leading growing mode:

$$\nabla \times \boldsymbol{v}^{(n)} = \mathbf{0}, \tag{2.2.27}$$

so the vorticity in the present Universe could not be generated by weakly nonlinear effect. It would be generated by strongly nonlinear effect. This is proved by

induction as follows. The case $n = 1$ is linear theory result (2.2.21). For $n \geq 2$, the rotation of equation (2.2.24) reduces to

$$\frac{\partial}{\partial t}\left[a^2 \mathrm{rot}\boldsymbol{v}^{(n)}\right] = a^2 \sum_{k=1}^{n-1}\left[(\mathrm{rot}\boldsymbol{v}^{(k)}\cdot\nabla)\boldsymbol{v}^{(n-k)} - (\boldsymbol{v}^{(n-k)}\cdot\nabla)\mathrm{rot}\boldsymbol{v}^{(k)} - \mathrm{rot}\boldsymbol{v}^{(k)}(\nabla\cdot\boldsymbol{v}^{(n-k)})\right]. \tag{2.2.28}$$

To derive this equation, note that $\partial_i v_j - \partial_j v_i = \epsilon_{lij}(\mathrm{rot}\boldsymbol{v})_l$. The right hand side in equation (2.2.28) does not contribute to the leading time-dependence by the assumption of induction, so $\mathrm{rot}\boldsymbol{v}^{(n)}$ also does not contribute to the leading growing mode. Thus equation (2.2.27) is proved for leading growing mode.

The irrotational velocity field can be represented by $\boldsymbol{v}^{(n)} = \nabla\triangle^{-1}\theta^{(n)}$, where $\theta^{(n)} = \nabla\cdot\boldsymbol{v}^{(n)}$ is a velocity divergence. At this stage, it is convenient to work in the Fourier space:

$$\delta^{(n)}(\boldsymbol{x},t) = \int \frac{d^3k}{(2\pi)^3} e^{i\boldsymbol{k}\cdot\boldsymbol{x}}\tilde{\delta}^{(n)}(\boldsymbol{k},t), \tag{2.2.29}$$

$$\theta^{(n)}(\boldsymbol{x},t) = \int \frac{d^3k}{(2\pi)^3} e^{i\boldsymbol{k}\cdot\boldsymbol{x}}\tilde{\theta}^{(n)}(\boldsymbol{k},t). \tag{2.2.30}$$

The Fourier-space representation of equations (2.2.23) – (2.2.25) are as follows:

$$\dot{\tilde{\delta}}^{(n)}(\boldsymbol{k}) + \tilde{\theta}^{(n)}(\boldsymbol{k}) + \sum_{k=1}^{n-1}\int \frac{d^3p}{(2\pi)^3}\frac{d^3p'}{(2\pi)^3}(2\pi)^3\delta_{\mathrm{D}}^3(\boldsymbol{p}+\boldsymbol{p}'-\boldsymbol{k})\frac{\boldsymbol{k}\cdot\boldsymbol{p}'}{p'^2}\tilde{\delta}^{(k)}(\boldsymbol{p})\tilde{\theta}^{(n-k)}(\boldsymbol{p}') = 0, \tag{2.2.31}$$

$$\dot{\tilde{\theta}}^{(n)}(\boldsymbol{k}) + 2H\tilde{\theta}^{(n)}(\boldsymbol{k}) + \frac{3}{2}H^2\Omega\tilde{\delta}^{(n)}(\boldsymbol{k}) + \sum_{k=1}^{n-1}\int \frac{d^3p}{(2\pi)^3}\frac{d^3p'}{(2\pi)^3}(2\pi)^3\delta_{\mathrm{D}}^3(\boldsymbol{p}+\boldsymbol{p}'-\boldsymbol{k}) \times \frac{(\boldsymbol{k}\cdot\boldsymbol{p}')(\boldsymbol{p}\cdot\boldsymbol{p}')}{p^2p'^2}\tilde{\theta}^{(k)}(\boldsymbol{p})\tilde{\theta}^{(n-k)}(\boldsymbol{p}') = 0, \tag{2.2.32}$$

$$\ddot{\tilde{\delta}}^{(n)}(\boldsymbol{k}) + 2H\dot{\tilde{\delta}}^{(n)}(\boldsymbol{k}) - \frac{3}{2}H^2\Omega\tilde{\delta}^{(n)}(\boldsymbol{k}) = \sum_{k=1}^{n-1}\int \frac{d^3p}{(2\pi)^3}\frac{d^3p'}{(2\pi)^3}(2\pi)^3\delta_{\mathrm{D}}^3(\boldsymbol{p}+\boldsymbol{p}'-\boldsymbol{k})\left[\frac{3}{2}H^2\Omega\left(1+\frac{\boldsymbol{p}\cdot\boldsymbol{p}'}{p'^2}\right)\tilde{\theta}^{(k)}(\boldsymbol{p})\tilde{\theta}^{(n-k)}(\boldsymbol{p}')\right] + \sum_{k=1}^{n-1}\sum_{l=1}^{k-1}\int \frac{d^3p}{(2\pi)^3}\frac{d^3p'}{(2\pi)^3}\frac{d^3p''}{(2\pi)^3}(2\pi)^3\delta_{\mathrm{D}}^3(\boldsymbol{p}+\boldsymbol{p}'+\boldsymbol{p}''-\boldsymbol{k}) \times \frac{\boldsymbol{k}\cdot\boldsymbol{p}'}{p'^2}\frac{\boldsymbol{k}\cdot\boldsymbol{p}''}{p''^2}\tilde{\delta}^{(l)}(\boldsymbol{p})\tilde{\theta}^{(k-l)}(\boldsymbol{p}')\tilde{\theta}^{(n-k)}(\boldsymbol{p}'') \tag{2.2.33}$$

The solution of the second order perturbation theory is, using (2.2.33) and

(2.2.31),

$$\widetilde{\delta}^{(2)}(\boldsymbol{k},t) = D^2 \int \frac{d^3p_1}{(2\pi)^3}\frac{d^3p_2}{(2\pi)^3}(2\pi)^3\delta_{\rm D}^3(\boldsymbol{p}_1+\boldsymbol{p}_2-\boldsymbol{k})P_2(\boldsymbol{p}_1,\boldsymbol{p}_2,t)\widetilde{\epsilon}(\boldsymbol{p}_1)\widetilde{\epsilon}(\boldsymbol{p}_2), \tag{2.2.34}$$

$$\widetilde{\theta}^{(2)}(\boldsymbol{k},t) = D^2 \int \frac{d^3p_1}{(2\pi)^3}\frac{d^3p_2}{(2\pi)^3}(2\pi)^3\delta_{\rm D}^3(\boldsymbol{p}_1+\boldsymbol{p}_2-\boldsymbol{k})Q_2(\boldsymbol{p}_1,\boldsymbol{p}_2,t)\widetilde{\epsilon}(\boldsymbol{p}_1)\widetilde{\epsilon}(\boldsymbol{p}_2), \tag{2.2.35}$$

where

$$P_2(\boldsymbol{p}_1,\boldsymbol{p}_2,t) = \frac{1}{2}(1+K) + \frac{\boldsymbol{p}_1\cdot\boldsymbol{p}_2}{2p_1p_2}\left(\frac{p_1}{p_2}+\frac{p_2}{p_1}\right) + \frac{1}{2}(1-K)\left(\frac{\boldsymbol{p}_1\cdot\boldsymbol{p}_2}{p_1p_2}\right)^2 \tag{2.2.36}$$

$$Q_2(\boldsymbol{p}_1,\boldsymbol{p}_2,t) = -Hf\left[C + \frac{\boldsymbol{p}_1\cdot\boldsymbol{p}_2}{2p_1p_2}\left(\frac{p_1}{p_2}+\frac{p_2}{p_1}\right) + (1-C)\left(\frac{\boldsymbol{p}_1\cdot\boldsymbol{p}_2}{p_1p_2}\right)^2\right]. \tag{2.2.37}$$

In the above expressions, $K(t) \equiv F/D^2$ and $C(t) \equiv \dot{F}/(2D\dot{D})$ are defined using the growing solution $F(t)$ of the following ordinary differential equation:

$$\ddot{F} + 2H\dot{F} - \frac{3}{2}H^2\Omega F = \frac{3}{2}H^2\Omega D^2. \tag{2.2.38}$$

The growing mode of this equation can be expressed by a closed form (Matsubara 1995b) as

$$K(\Omega,\lambda) = \frac{\Omega}{4} - \frac{\lambda}{2} - \frac{1}{U_{3/2}}\left[1 - \frac{3}{2}\frac{U_{5/2}}{U_{3/2}}\right], \tag{2.2.39}$$

$$C(\Omega,\lambda) = \frac{1}{8f}\left\{-3\Omega + \frac{1}{(U_{3/2})^2}\left[2 + 4U_{3/2} - 3(2+\Omega-2\lambda)U_{5/2}\right]\right\}, \tag{2.2.40}$$

where

$$U_\alpha(\Omega,\lambda) = \int_0^1 dx[\Omega/x + \lambda x^2 + 1 - \Omega - \lambda]^{-\alpha}. \tag{2.2.41}$$

In Einstein-de Sitter, Friedmann and flat models,

$$U_\alpha(1,0) = \frac{1}{1+\alpha}, \tag{2.2.42}$$

$$U_\alpha(\Omega,0) = \frac{1}{1+\alpha}F(1,\alpha,\alpha+2;1-\Omega), \tag{2.2.43}$$

$$U_\alpha(\Omega,1-\Omega) = \frac{1}{1+\alpha}F\left(1,\alpha,\frac{\alpha+4}{3};1-\Omega\right), \tag{2.2.44}$$

where F is the hypergeometric function. Moreover, in Friedmann models, $U_{3/2}$ and $U_{5/2}$ are actually elementary functions (Bouchet et al. 1992).

For practical purposes, equations (2.2.39) and (2.2.40) are accurately approximated by

$$K \approx \frac{3}{7}\Omega^{-1/30} - \frac{\lambda}{80}\left(1 - \frac{3}{2}\lambda \log_{10}\Omega\right), \tag{2.2.45}$$

$$C \approx \frac{3}{7}\Omega^{-11/200} - \frac{\lambda}{70}\left(1 - \frac{7}{3}\lambda \log_{10}\Omega\right), \tag{2.2.46}$$

within maximum error 0.6% for both for $-1 \leq \log_{10}\Omega \leq 0$ and $0 \leq \lambda \leq 1$. Quite obviously from this fitting, dependence on parameters Ω and λ is weak (Bernardeau 1994; Bernardeau et al. 1994; Matsubara 1995b). In fact K and C for the above ranges of Ω and λ are different from the Einstein-de Sitter values within 8% and 14%, respectively. In the Einstein-de Sitter Universe, or $t \to 0$, the solution of equation (2.2.38) is $F = 3D^2/7$, thus,

$$P_2(\boldsymbol{p}_1, \boldsymbol{p}_2) = \left[\frac{5}{7} + \frac{\boldsymbol{p}_1 \cdot \boldsymbol{p}_2}{2p_1p_2}\left(\frac{p_1}{p_2} + \frac{p_2}{p_1}\right) + \frac{2}{7}\left(\frac{\boldsymbol{p}_1 \cdot \boldsymbol{p}_2}{p_1p_2}\right)^2\right], \tag{2.2.47}$$

$$Q_2(\boldsymbol{p}_1, \boldsymbol{p}_2) = -Hf\left[\frac{3}{7} + \frac{\boldsymbol{p}_1 \cdot \boldsymbol{p}_2}{2p_1p_2}\left(\frac{p_1}{p_2} + \frac{p_2}{p_1}\right) + \frac{4}{7}\left(\frac{\boldsymbol{p}_1 \cdot \boldsymbol{p}_2}{p_1p_2}\right)^2\right]. \tag{2.2.48}$$

This expression is exact for Einstein-de Sitter Universe, and is an approximation for the general Universe.

The perturbation of order higher than three is similarly obtained but is complicated. In the Einstein-de Sitter Universe, one can see

$$\delta^{(n)} \propto t^{2n/3}, \tag{2.2.49}$$

$$\boldsymbol{v}^{(n)} \propto t^{2n/3-1}, \tag{2.2.50}$$

by induction and the dependence on space and time decouples in each terms in perturbative expansion, so the calculation is relatively simplified. The result of higher order solution is expressed by recursion relations (Goroff et al. 1986). The solution takes the form,

$$\tilde{\delta}^{(n)}(\boldsymbol{k}, t) = t^{2n/3}\int \frac{d^3p_1}{(2\pi)^3}\cdots\frac{d^3p_n}{(2\pi)^3}(2\pi)^3\delta_{\rm D}^3(\boldsymbol{p}_1 + \cdots + \boldsymbol{p}_n - \boldsymbol{k}) \times R_n(\boldsymbol{p}_1, \ldots, \boldsymbol{p}_n, t)\tilde{\epsilon}(\boldsymbol{p}_1)\cdots\tilde{\epsilon}(\boldsymbol{p}_n), \tag{2.2.51}$$

$$\tilde{\theta}^{(n)}(\boldsymbol{k}, t) = -t^{2n/3-1}\int \frac{d^3p_1}{(2\pi)^3}\cdots\frac{d^3p_n}{(2\pi)^3}(2\pi)^3\delta_{\rm D}^3(\boldsymbol{p}_1 + \cdots + \boldsymbol{p}_n - \boldsymbol{k}) \times S_n(\boldsymbol{p}_1, \ldots, \boldsymbol{p}_n, t)\tilde{\epsilon}(\boldsymbol{p}_1)\cdots\tilde{\epsilon}(\boldsymbol{p}_n), \tag{2.2.52}$$

and R_n, S_n is determined by the following recursion relations

$$R'_n(\boldsymbol{k}_1,\ldots,\boldsymbol{k}_n) = \frac{9}{2(2n^2+n-3)} \times \sum_{m=1}^{n-1}\left[\left(\frac{2n+3}{3}\right)\frac{\boldsymbol{k}\cdot(\boldsymbol{k}_1+\cdots+\boldsymbol{k}_m)}{|\boldsymbol{k}_1+\cdots+\boldsymbol{k}_m|^2}R'_{n-m}(\boldsymbol{k}_{m+1},\ldots,\boldsymbol{k}_n)S'_m(\boldsymbol{k}_1,\ldots,\boldsymbol{k}_m) + \frac{1}{2}k^2\frac{(\boldsymbol{k}_1+\cdots+\boldsymbol{k}_m)\cdot(\boldsymbol{k}_{m+1}+\cdots+\boldsymbol{k}_n)}{|\boldsymbol{k}_1+\cdots+\boldsymbol{k}_m|^2|\boldsymbol{k}_{m+1}+\cdots+\boldsymbol{k}_n|^2} \times S'_m(\boldsymbol{k}_1,\ldots,\boldsymbol{k}_m)S'_{n-m}(\boldsymbol{k}_{m+1},\ldots,\boldsymbol{k}_n)\right], \quad (2.2.53)$$

$$S'_n(\boldsymbol{k}_1,\ldots,\boldsymbol{k}_n) = \frac{2n}{3}R'_n(\boldsymbol{k}_1,\ldots,\boldsymbol{k}_n) - \sum_{m=1}^{n-1}\frac{\boldsymbol{k}\cdot(\boldsymbol{k}_1+\cdots+\boldsymbol{k}_m)}{|\boldsymbol{k}_1+\cdots+\boldsymbol{k}_m|^2}R'_{n-m}(\boldsymbol{k}_{m+1},\ldots,\boldsymbol{k}_n)S'_m(\boldsymbol{k}_1,\ldots,\boldsymbol{k}_m), \quad (2.2.54)$$

and initial values $R'_1 = 1$, $S'_1 = 2/3$ and the symmetrization procedure,

$$R_n(\boldsymbol{k}_1,\ldots,\boldsymbol{k}_n) = \sum_{\text{all perm.:}p}\frac{1}{n!}R'_n(\boldsymbol{k}_{p(1)},\ldots,\boldsymbol{k}_{p(n)}), \quad (2.2.55)$$

$$S_n(\boldsymbol{k}_1,\ldots,\boldsymbol{k}_n) = \sum_{\text{all perm.:}p}\frac{1}{n!}S'_n(\boldsymbol{k}_{p(1)},\ldots,\boldsymbol{k}_{p(n)}). \quad (2.2.56)$$

In equations (2.2.53), (2.2.54), $\boldsymbol{k} = \boldsymbol{k}_1 + \cdots + \boldsymbol{k}_n$ and sums in equations (2.2.55), (2.2.56) are taken for all n-permutations.

2.2.3 Lagrangian perturbation theory

So far, the dynamical variables are defined in Eulerian space. There is another perturbative treatment that is defined in Lagrangian space (see, e.g., Buchert 1994; Bouchet et al. 1995), which is called Lagrangian perturbation theory. This theory considers motion of mass elements labeled by unperturbed Lagrangian coordinates $\boldsymbol{q}$. The comoving Eulerian position of mass element $\boldsymbol{q}$ at time t is denoted by $\boldsymbol{x}(\boldsymbol{q},t)$. The displacement field $\boldsymbol{\Psi}(\boldsymbol{q},t)$ defined by

$$\boldsymbol{x}(\boldsymbol{q},t) = \boldsymbol{q} + \boldsymbol{\Psi}(\boldsymbol{q},t), \quad (2.2.57)$$

is a dynamical variable in this formulation. Density contrast and a velocity field are derived from a displacement field as

$$\delta[\boldsymbol{x}(\boldsymbol{q},t),t] = J^{-1} - 1, \quad (2.2.58)$$

$$\boldsymbol{v}[\boldsymbol{x}(\boldsymbol{q},t),t] = \dot{\boldsymbol{x}}(\boldsymbol{q},t) = \dot{\boldsymbol{\Psi}}(\boldsymbol{q},t), \quad (2.2.59)$$

where $J \equiv \det[\partial x_i/\partial q_j] = \det[\delta_{ij} + \partial\Psi_i/\partial q_j]$ is the Jacobian from Lagrangian space to Eulerian space. A dot denotes time derivative fixing Lagrangian coordinate $\boldsymbol{q}$, so should not be confused with the Eulerian time derivative in equations (2.2.1)-(2.2.3). These Eulerian equations (2.2.1)-(2.2.3) are transformed to the Lagrangian equations governing displacement field as

$$J\nabla_x \cdot [\ddot{\boldsymbol{\Psi}} + 2H\dot{\boldsymbol{\Psi}}] + \frac{3}{2}H^2\Omega(1-J) = 0, \tag{2.2.60}$$

$$\nabla_x \times [\ddot{\boldsymbol{\Psi}} + 2H\dot{\boldsymbol{\Psi}}] = \mathbf{0}. \tag{2.2.61}$$

Again, a dot denotes Lagrangian time derivative and ∇_x is the spacial derivative with respect to Eulerian coordinates $\boldsymbol{x}$, so $(\nabla_x)_i = J^{-1}\tilde{J}_{ij}(\nabla_q)_j$, where $\tilde{J}_{ij}$ are cofactors of the Jacobian J.

In usual treatment of Lagrangian perturbation theory, one assumes an additional condition, i.e., vorticity-free condition:

$$\nabla_x \times \boldsymbol{v} = \nabla_x \times \dot{\boldsymbol{\Psi}} = \mathbf{0}. \tag{2.2.62}$$

This is not unreasonable requirement because vorticity is expected to be diluted by expansion before 'turn-around' in some sense (Peebles 1980). The condition (2.2.62) is a sufficient condition for dynamical equation (2.2.61) (Buchert 1992), so the solutions with vorticity-free condition are in a subclass of the general solutions [rotational perturbation is argued by Buchert (1992) and Buchert & Ehlers (1993)]. This subclass is achieved if one limit the initial condition to irrotational field because irrotational velocity field at one time remains irrotational at later times from Kelvin's circulation theorem. Therefore, equations (2.2.60) and (2.2.62) are solved perturbatively for displacement field $\boldsymbol{\Psi} = \boldsymbol{\Psi}^{(1)} + \boldsymbol{\Psi}^{(2)} + \cdots$, keeping only terms of leading time-dependence. For irrotational initial displacement field, the result, up to second-order [see Buchert & Ehlers (1993) and Bouchet et al. (1995) for detail], is

$$\boldsymbol{\Psi}^{(1)} = -D(t)\nabla\triangle^{-1}\epsilon(\boldsymbol{x}), \tag{2.2.63}$$

$$\boldsymbol{\Psi}^{(2)} = -\frac{1}{2}K(t)\nabla\triangle^{-1}\sum_{i\neq j}\left(\Psi^{(1)}_{i,i}\Psi^{(1)}_{j,j} - \Psi^{(1)}_{i,j}\Psi^{(1)}_{i,j}\right). \tag{2.2.64}$$

The first-order solution is equivalent to the Zel'dovich approximation (Zel'dovich (1970; 1973). The factors D and K are the same quantities in Eulerian perturbation theory.

2.3 CORRELATION STATISTICS

One of the very important issues in cosmology is to investigate the statistical properties of the density field in the Universe. The conventional tools to represent the statistical properties are correlation functions of the field. The set of correlation functions of all orders have the complete information of the statistics of the field.

2.3.1 The two-point correlation function and the power spectrum

The two-point correlation statistics is relatively popular in cosmology. Two-point correlation function of smoothed field $\delta(\boldsymbol{x})$ with zero-mean is defined by

$$\xi(\boldsymbol{x}_1, \boldsymbol{x}_2) = \langle \delta(\boldsymbol{x}_1)\delta(\boldsymbol{x}_2) \rangle. \tag{2.3.1}$$

When the field is statistically homogeneous, this quantity is a function of $\boldsymbol{x}_1 - \boldsymbol{x}_2$ and when the field is statistically isotropic, this quantity is a function of $|\boldsymbol{x}_1 - \boldsymbol{x}_2|$. Thus, the above quantity is denoted also as $\xi(\boldsymbol{x}_1 - \boldsymbol{x}_2)$ or $\xi(|\boldsymbol{x}_1 - \boldsymbol{x}_2|)$ for statistically homogeneous and isotropic field. The average $\langle \cdots \rangle$ means mathematically the one for 'ensemble of Universes'. Of course we can never observe another realizations of statistically equivalent Universes not of ours, so, observationally, only the spatial average can be done. These two averaging are equivalent if ergodic theorem holds, but this theorem have not been proven for general situation. It is known that when the field is an Gaussian random field, the ergodic theorem holds if and only if its power spectrum is continuous (Adler 1981). We assume that the ergodic theorem holds in our Universe in comparing the theories and observations.

The two-point correlation in Fourier space defines the power spectrum $P(k)$ through

$$\langle \widetilde{\delta}(\boldsymbol{k}_1)\widetilde{\delta}(\boldsymbol{k}_2) \rangle = (2\pi)^3 \delta_{\rm D}^3(\boldsymbol{k}_1 + \boldsymbol{k}_2) P(k_1), \tag{2.3.2}$$

where delta-function must appear for the homogeneity of the space (this can be seen by that ξ is a function of $\boldsymbol{x}_1 - \boldsymbol{x}_2$). The power spectrum depends only on the magnitude of $\boldsymbol{k}_1$ for the isotropy of the space (this can be seen by that ξ is a function of $|\boldsymbol{x}_1 - \boldsymbol{x}_2|$). Approximating the Universe by a cube of volume V imposed periodic boundary condition,

$$P(k) = V^{-1} \langle |\widetilde{\delta}(\boldsymbol{k})|^2 \rangle, \tag{2.3.3}$$

where the reality condition,

$$\widetilde{\delta}^*(\boldsymbol{k}) = \widetilde{\delta}(-\boldsymbol{k}), \tag{2.3.4}$$

is used. The two-point correlation function $\xi(|\boldsymbol{x}|)$ as a function of $\boldsymbol{x}$ and the power spectrum $P(|\boldsymbol{k}|)$ as a function of $\boldsymbol{k}$ is related by three-dimensional Fourier transforms (Wiener-Khintchine relation):

$$P(k) = \int d^3x e^{-i\boldsymbol{k}\cdot\boldsymbol{x}}\xi(x) = 4\pi\int_0^\infty x^2 dx \frac{\sin kx}{kx}\xi(x) \tag{2.3.5}$$

$$\xi(x) = \int \frac{d^3k}{(2\pi)^3} e^{i\boldsymbol{k}\cdot\boldsymbol{x}}P(k) = \frac{1}{2\pi^2}\int_0^\infty k^2 dx \frac{\sin kx}{kx}P(k) \tag{2.3.6}$$

Instead of equation (2.3.3), sometimes the power spectrum is defined by $P(k) = \langle|\widetilde{\delta}(\boldsymbol{k})|^2\rangle$. The latter definition is unnatural because it depends on the volume of the Universe for $P(k)$ of our notation is independent of the volume; see equation (2.3.5). The same argument is seen in Bertschinger (1992).

2.3.2 Higher order correlation functions

Not only the two-point correlation function, or equivalently the power spectrum, determines all the statistical property, of course. All the statistical property is expressed as a probability distribution functional $\mathcal{P}[\delta]$. The expectation value of an arbitrary functional of the field δ is, using distribution functional,

$$\langle F[\delta]\rangle = \int [d\delta]\mathcal{P}[\delta]F[\delta]. \tag{2.3.7}$$

To investigate the distribution functional directly by observation is awkward and almost impossible. We need other statistics which is equivalent to the distribution functional.

The infinite dimensional Fourier transform of the distribution functional is a moment generating functional $Z[J]$:

$$Z[J] = \left\langle \exp\left[-i\int d^3x J(\boldsymbol{x})\delta(\boldsymbol{x})\right]\right\rangle \tag{2.3.8}$$

$$= \sum_{N=0}^{\infty}\frac{(-i)^N}{N!}\int d^3x_1\cdots d^3x_N J(\boldsymbol{x}_1)\cdots J(\boldsymbol{x}_N)\langle\delta(\boldsymbol{x}_1)\cdots\delta(\boldsymbol{x}_N)\rangle. \tag{2.3.9}$$

As seen from (2.3.9), the set of all the moment

$$\mu^{(N)}(\boldsymbol{x}_1,\ldots,\boldsymbol{x}_N) = \langle\delta(\boldsymbol{x}_1)\cdots\delta(\boldsymbol{x}_N)\rangle, \tag{2.3.10}$$

determines $Z[J]$. The inverse transform of equation (2.3.8),

$$\mathcal{P}[\delta] = \int\left[\frac{dJ}{2\pi}\right] Z[J]\exp\left[i\int d^3x J(\boldsymbol{x})\delta(\boldsymbol{x})\right] \tag{2.3.11}$$

determines the distribution functional from the moment generating functional. Thus, the set of all the moment determines the statistical property of the field δ completely and all the statistical quantities are expressed by moments (2.3.10).

It is popular to use the connected N-point correlation function

$$\xi^{(N)}(\boldsymbol{x}_1, \ldots, \boldsymbol{x}_N) = \langle \delta(\boldsymbol{x}_1) \cdots \delta(\boldsymbol{x}_N) \rangle_{\rm c}, \tag{2.3.12}$$

rather than mere moments. This quantity is defined by eliminating the lower order contribution to the N-moment and represents the true N-point correlation. Explicitly, it is defined by following relations iteratively:

$$\mu^{(2)}_{12} = \xi^{(2)}_{12}, \tag{2.3.13}$$

$$\mu^{(3)}_{123} = \xi^{(3)}_{123,} \tag{2.3.14}$$

$$\mu^{(4)}_{1234} = \xi^{(2)}_{12}\xi^{(2)}_{34} + \xi^{(2)}_{13}\xi^{(2)}_{24} + \xi^{(2)}_{14}\xi^{(2)}_{23} + \xi^{(4)}_{1234}, \tag{2.3.15}$$

$$\begin{aligned}\mu^{(5)}_{12345} = {} & \xi^{(2)}_{12}\xi^{(3)}_{345} + \xi^{(2)}_{13}\xi^{(3)}_{245} + \xi^{(2)}_{14}\xi^{(3)}_{235} + \xi^{(2)}_{15}\xi^{(3)}_{234} + \xi^{(2)}_{23}\xi^{(3)}_{145} \\ & + \xi^{(2)}_{24}\xi^{(3)}_{135} + \xi^{(2)}_{25}\xi^{(3)}_{134} + \xi^{(2)}_{34}\xi^{(3)}_{125} + \xi^{(2)}_{35}\xi^{(3)}_{124} + \xi^{(2)}_{45}\xi^{(3)}_{123} + \xi^{(5)}_{12345},\end{aligned} \tag{2.3.16}$$

$$\vdots \qquad\qquad \vdots$$

where the notation $\mu^{(2)}_{12} = \mu^{(2)}(\boldsymbol{x}_1, \boldsymbol{x}_2)$ etc. are used. The N-th moment is determined by connected correlation functions of order less than or equal to N, so the set of all the connected function has complete information of statistics of the field δ. There are beautiful relation, called *cumulant expansion theorem* (e.g., Ma 1985), that is widely used in statistical theory and quantum field theory. This theorem states that 'the logarithm of a generating functional of moments, $\ln Z[J]$, is a generating functional of connected correlation functions', i.e.,

$$\ln Z[J] = \sum_{N=0}^{\infty} \frac{(-i)^N}{N!} \int d^3x_1 \cdots d^3x_N J(\boldsymbol{x}_1) \cdots J(\boldsymbol{x}_N) \langle \delta(\boldsymbol{x}_1) \cdots \delta(\boldsymbol{x}_N) \rangle_{\rm c}. \tag{2.3.17}$$

Since this theorem is very important, the proof is presented in Appendix A. This theorem simplify the statistical calculation concerning connected correlation function, and plays an essential role in later part (chapter 4) in this thesis.

2.3.3 Gaussian random fields

Fields with distribution in which connected correlation functions of order more than or equal to three vanish are called *Gaussian random fields*. The moments of a

Gaussian random field $\delta(\boldsymbol{x})$ are given by

$$\langle\delta(\boldsymbol{x}_1)\delta(\boldsymbol{x}_2)\rangle = \xi(\boldsymbol{x}_1,\boldsymbol{x}_2), \tag{2.3.18}$$

$$\langle\delta(\boldsymbol{x}_1)\cdots\delta(\boldsymbol{x}_{2n+1})\rangle = 0, \tag{2.3.19}$$

$$\langle\delta(\boldsymbol{x}_1)\cdots\delta(\boldsymbol{x}_{2n})\rangle = \frac{1}{2^n n!}\sum_{p\in\text{perm.}}\langle\delta(\boldsymbol{x}_{p(1)})\delta(\boldsymbol{x}_{p(2)})\rangle\cdots\langle\delta(\boldsymbol{x}_{p(2n-1)})\delta(\boldsymbol{x}_{p(2n)})\rangle. \tag{2.3.20}$$

The distribution functional of Gaussian random fields are, from the cumulant expansion theorem (2.3.17) and equation (2.3.11),

$$\mathcal{P}[\delta] = \frac{1}{\sqrt{\det(2\pi\xi)}}\exp\left[-\frac{1}{2}\int d^3x_1 d^3x_2\,\delta(\boldsymbol{x}_1)\xi^{-1}(\boldsymbol{x}_1,\boldsymbol{x}_2)\delta(\boldsymbol{x}_2)\right], \tag{2.3.21}$$

where $[\det(2\pi\xi)]^{1/2}$ is a normalization factor,

$$\sqrt{\det(2\pi\xi)} = \int[d\delta]\exp\left[-\frac{1}{2}\int d^3x_1 d^3x_2\,\delta(\boldsymbol{x}_1)\xi^{-1}(\boldsymbol{x}_1,\boldsymbol{x}_2)\delta(\boldsymbol{x}_2)\right], \tag{2.3.22}$$

and ξ^{-1} is the inverse (or Green's function) of the two-point correlation function which satisfies

$$\int d^3y\,\xi(|\boldsymbol{x}-\boldsymbol{y}|)\,\xi^{-1}(|\boldsymbol{y}-\boldsymbol{z}|) = \delta_{\rm D}^3(\boldsymbol{x}-\boldsymbol{z}), \tag{2.3.23}$$

or, equivalently, it is defined in Fourier space as

$$\xi^{-1}(|\boldsymbol{x}|) = \int\frac{d^3k}{(2\pi)^3}\frac{e^{i\boldsymbol{k}\cdot\boldsymbol{x}}}{P(k)}. \tag{2.3.24}$$

The distribution functional in Fourier space is, from (2.3.21),

$$\mathcal{P}[\widetilde{\delta}] \propto \exp\left(-\frac{1}{2}\int\frac{d^3k}{(2\pi)^3}\frac{|\widetilde{\delta}(\boldsymbol{k})|^2}{P(k)}\right), \tag{2.3.25}$$

where the reality condition (2.3.4) is taken into account. This expression implies that each Fourier modes are distributed independently. To see the precise form of this property, it is convenient to move in the discrete space. The real space and the Fourier space is approximated by the discretized lattice in which the real space is the finite box of volume $V = L^3$ imposed by periodic boundary condition. The lattice spacing in real space is $\Delta x = (V/N)^{1/3}$, where N is the number of total lattice sites. The lattice spacing in Fourier space is given by $\Delta k = 2\pi/L$. The integral is represented in this discretized space as

$$\int d^3x \longrightarrow \sum_{\boldsymbol{x}}(\Delta x)^3 = \frac{V}{N}\sum_{\boldsymbol{x}}, \tag{2.3.26}$$

$$\int\frac{d^3k}{(2\pi)^3} \longrightarrow \sum_{\boldsymbol{k}}\left(\frac{\Delta k}{2\pi}\right)^3 = \frac{1}{V}\sum_{\boldsymbol{k}}. \tag{2.3.27}$$

In fact, the treatments of the functional integrations above can be defined only in those discretized space and the continuum limit $L \to \infty$, $N \to \infty$, $V/N \to \infty$ is assumed. Thus, the decoupling of modes in equation (2.3.25) is described precisely in this discretized space and the distribution function of each mode $\widetilde{\delta}(\boldsymbol{k})$ is

$$P(\widetilde{\delta}(\boldsymbol{k})) \propto \exp\left(-\frac{|\widetilde{\delta}(\boldsymbol{k})|^2}{VP(k)}\right). \tag{2.3.28}$$

From the reality condition (2.3.4), all the Fourier modes are not independent but, e.g., only the upper half of $\boldsymbol{k}$-space, $k_z \geq 0$, (uhs) is sufficient. Such double contributions in exponential of equation (2.3.25) compensate the factor 1/2. Corresponding two kinds of representation,

$$\widetilde{\delta}(\boldsymbol{k}) = \mathrm{Re}\widetilde{\delta}(\boldsymbol{k}) + i\,\mathrm{Im}\widetilde{\delta}(\boldsymbol{k}) \tag{2.3.29}$$

$$= |\widetilde{\delta}(\boldsymbol{k})|e^{i\theta(\boldsymbol{k})}, \tag{2.3.30}$$

the distribution (2.3.28) reduces to, including normalization factor,

$$P(\mathrm{Re}\widetilde{\delta}(\boldsymbol{k}), \mathrm{Im}\widetilde{\delta}(\boldsymbol{k}))d\mathrm{Re}\widetilde{\delta}(\boldsymbol{k})d\mathrm{Im}\widetilde{\delta}(\boldsymbol{k})$$
$$= \frac{1}{\pi VP(k)} \exp\left(-\frac{(\mathrm{Re}\widetilde{\delta}(\boldsymbol{k}))^2 + (\mathrm{Im}\widetilde{\delta}(\boldsymbol{k}))^2}{VP(k)}\right) d\mathrm{Re}\widetilde{\delta}(\boldsymbol{k})d\mathrm{Im}\widetilde{\delta}(\boldsymbol{k}), \tag{2.3.31}$$

$$P(|\widetilde{\delta}(\boldsymbol{k})|, \theta(\boldsymbol{k}))d|\widetilde{\delta}(\boldsymbol{k})|d\theta(\boldsymbol{k})$$
$$= \frac{2|\widetilde{\delta}(\boldsymbol{k})|}{VP(k)} \exp\left(-\frac{|\widetilde{\delta}(\boldsymbol{k})|^2}{VP(k)}\right) d|\widetilde{\delta}(\boldsymbol{k})|\frac{d\theta(\boldsymbol{k})}{2\pi} \tag{2.3.32}$$

One of the characteristic feature of Gaussian random fields is that the phase $\theta(\boldsymbol{k})$ of each mode $\widetilde{\delta}(\boldsymbol{k})$ distribute randomly as seen from equation (2.3.32). The unrecommended notation $P(k) = \langle|\widetilde{\delta}(\boldsymbol{k})|^2\rangle$ can simplify the above distribution, but it is natural that the volume V appeared explicitly in the discretized space. If we adopt this unrecommended notation, we have to deal with the volume of the space explicitly in the representations in the continuum limit.

The Gaussian random fields are expected to appear in various situations because of the central limit theorem, and it is the key distribution of the fields. In addition, standard inflationary models predict that the primordial distribution should be a Gaussian random field (Guth & Pi 1982; Starobinskii 1982; Hawking 1982; Bardeen, Steinhardt & Turner 1983). From these things, and for simplicity, the primordial fluctuation of our Universe is often assumed to be a Gaussian random field.

2.4 THE PRIMORDIAL SPECTRUM

In this section, some models are described briefly concerning what type of fluctuation is expected when the gravitational force became the prominent source of evolution of the structure.

2.4.1 Harrison-Zel'dovich spectrum

Although there are no guarantee that the primordial fluctuation is a Gaussian random field, let us assume that standpoint here. Then, the degree of freedom of the primordial fluctuation reduce to the functional form of the primordial power spectrum, $P_{\rm i}(k)$. We do not know the definite feature of the origin of the primordial fluctuation, it is common to assume the simple power-law spectrum

$$P_{\rm i}(k) = Ak^n, \tag{2.4.1}$$

which has not characteristic scales. This assumption greatly reduces the degree of freedom of primordial fluctuation to two parameters, amplitude A and power-law index n.

The index n should not be too small or too large. For smaller values of n, relatively large fluctuation on small scales produces excessive black holes in the Universe. For larger values of n, relatively large fluctuation on large scales breaks the global homogeneity and isotropy and produces excessive CMBR anisotropy. If $n = 1$, these constraints are balanced with the present Universe (Harrison 1970; Zel'dovich 1972). Such primordial spectrum, $P(k) \propto k$ is called as Harrison-Zel'dovich spectrum or scale-invariant spectrum and considered to be important. The Harrison-Zel'dovich spectrum has a property that the amplitude of fluctuation of the scale which enters the horizon has the same amplitude for every scales. The simpler inflationary models predict the Harrison-Zel'dovich spectrum. Harrison-Zel'dovich spectrum itself does not fix the overall amplitude A, it is determined by the fluctuation of the present Universe or the CMBR anisotropy.

The primordially scale-free spectrum of the form (2.4.1) is deformed for the radiation-dominated epoch. The fluctuation on scales which enter the horizon in the radiation-dominated epoch could not be amplified because of the pressure of radiation (the Jeans length is about the horizon size for radiation-dominated epoch) while the fluctuation on super-horizon scales is amplified. The deformation of scale-free spectrum by this effect has the characteristic scale that is the horizon scale

$2\pi/k_{\rm H,eq}$ ($k_{\rm H,eq} \simeq 0.64\Omega_0 h^2{\rm Mpc}$) at the time matter start to dominated the Universe (equal time). The power spectrum on $k \leq k_{\rm H,eq}$ is amplified independently on wavenumber and keeps its shape, $P(k) \propto k^n$, but on $k \geq k_{\rm H,eq}$, the fluctuation can be amplified only before entering the horizon. Smaller scales enter the horizon earlier, so the amplitude on smaller scales is suppressed compared with that on larger scales. The asymptotic form of the power spectrum by this deformation effect is $P(k) \propto k^{n-4}$ on $k \ll k_{\rm H,eq}$. In addition, according to the main component of matter in the Universe, another process to damp the amplitude of fluctuation on some smaller scales can work.

Thus, by the decoupling time, at which the interaction between baryons and radiation effectively breaks, the power spectrum of density fluctuation suffers from deformations. After the decoupling time, the density fluctuation evolves by self-gravitation alone. As long as the fluctuation is in linear regime $|\delta| \ll 1$, the spectrum does not deformed and only the amplitude is increased according to equation (2.2.8).

2.4.2 Dark matter and the initial spectrum

There exists a lot of invisible matter which we could not observe directly. Actually, it is known that the most of the mass in our Universe is in the form of such 'dark matter'. What is the dark matter is one of the fundamental issues in astrophysics and cosmology which has not been solved yet.

The natural idea is to identify the dark matter with the usual baryons which is well known to us. This model is called as a baryonic dark matter (BDM) model. This model, however, has many problems. The very strict constraint to this model is from a theory of primordial nucleosynthesis and observations of the abundance of light elements in the Universe which predict (Olive et al. 1990; Walker et al. 1991; Smith, Kawano & Malaney 1993)

$$0.010 \leq \Omega_{\rm B} h^2 \leq 0.015, \tag{2.4.2}$$

where $\Omega_{\rm B}$ is the contribution of the baryons to the density parameter at present. This constraint is strict because the observations suggest $0.2 \lesssim \Omega_0 \lesssim 1$. Moreover, in the BDM model, fluctuation on scales smaller than the size of typical clusters of galaxies are erased by a mechanism called Silk damping: at about the decoupling time, the mean length of photon diffusion become gradually longer. In this process, photons drag baryons and the baryonic fluctuation is erased. To obtain the fluctuation on

scales about galaxies in BDM model, the fluctuation on large scales collapse first, and then it should be segregated to galaxies (pancake model). It is doubtful that such top-down scenario, in which the structures on smaller scales are generated from structures on larger scales, can work well. Furthermore, the baryonic fluctuation at decoupling time on scales of large-scale structure (super-cluster scale) of present day or on smaller scales than that is constrained from CMBR isotropy to be $\lesssim 2 \times 10^{-4}$ (e.g., Uson & Wilkinson 1984; Readhead et al. 1989; Smoot et al. 1992). The amplification of the fluctuation after decoupling is roughly proportional to scale factor, so in the BDM model, the fluctuation can be amplified at most by 1000 times from decoupling time to present day. This can not explain the observed fluctuation on such scales at present. The mass fluctuation at decoupling time should be larger than the fluctuation of baryons, so non-baryonic dark matter is needed.

As the non-baryonic dark matter, the hot dark matter (HDM) model and the cold dark matter (CDM) model are considered frequently. In the HDM model, the dark matter particles decouple from thermal contact with each other when the particles are relativistic. The light neutrinos of mass $m_\nu = 10$–100 eV are candidates of HDM particles. In this model, the neutrino is relativistic until equal time and the fluctuation on scales smaller than $2\pi/k_{\rm H,eq}$ is smoothed out by the motion of neutrino (free streaming damping). By an accurate estimation (Bond & Szalay 1983), the resulting deformation of power spectrum is fitted by

$$P(k) = Ak^n 10^{-2(k/k_\nu)^{1.5}}, \tag{2.4.3}$$

where $k_\nu = 0.49\Omega_0 h^2 {\rm Mpc}^{-1}$ is a neutrino damping scale. In HDM model, the sharp cut-off of fluctuation on about $25h^{-1}$Mpc appeared if $\Omega_0 h \sim 0.5$. Thus the structures should form by extreme top-down scenario and the it is difficult to explain the origin of the fluctuation on galaxy-scales.

On the other hand, in the CDM model, either the dark matter particles decouple from thermal contact with each other when the particles are non-relativistic or the particles have never been in thermal contact. In either cases, when the dark matter particles concerned with the formation of large-scale structure, the particles was non-relativistic and did not interact with radiation. The extra damping of small scales as in BDM or HDM models never occurred and only the suppression of the evolution on sub-horizon scales in radiation-dominated era is the source of deformation of power spectrum. According to an accurate estimation (Bardeen et al. 1986), the power

spectrum of CDM model at decoupling time is fitted by

$$P(k) = Ak^n \left(\frac{\ln(1+2.34q)}{2.34q} \right)^2 \left[1 + 3.89q + (16.1q)^2 + (5.46q)^3 + (6.71q)^4 \right]^{-1/2}, \tag{2.4.4}$$

where $q = k/(\Omega_0 h^2 \mathrm{Mpc}^{-1})$. The fluctuation on small scales remain relatively in CDM model, so the structure formation proceeds by bottom-up scenario: structures on small scales form first, and they gather to form larger structures.

3

Dynamics and Statistics in the Universe

3.1 CORRELATION HIERARCHY IN THE UNIVERSE

Quantifying the large-scale structure of the Universe rigorously is of fundamental importance. For this purpose, N-point correlation functions, $\xi^{(N)}$, are supposed to be the most natural and powerful measures applicable to existing galaxy catalogues.

Two-point correlation function of galaxies $\xi(r) \equiv \xi_2$ is the first of this hierarchy, and has been extensively explored both observationally and theoretically since the pioneering work by Totsuji & Kihara (1969). A mostly accepted expression for the observed ξ for galaxies in real space (corrected for the peculiar velocity contamination; see Davis & Peebles 1983) is

$$\begin{array}{c} \xi(r) = (r/r_0)^{-\gamma} \qquad (0.1h^{-1}\mathrm{Mpc} < r < 10h^{-1}\mathrm{Mpc}) \\ r_0 = (5.4 \pm 0.3)h^{-1}\mathrm{Mpc} \quad \text{and} \quad \gamma = 1.77 \pm 0.04. \end{array} \tag{3.1.1}$$

The next hierarchy, the three-point correlation function of galaxies $\zeta_{123} \equiv \zeta(\boldsymbol{r}_1, \boldsymbol{r}_2, \boldsymbol{r}_3)$, is not determined so precisely as $\xi(r)$. Nevertheless previous analysis consistently suggested that the observed ζ satisfies the following empirical relation:

$$\zeta_{123} = Q[\xi_{12}\xi_{23} + \xi_{23}\xi_{31} + \xi_{31}\xi_{12}], \tag{3.1.2}$$

where Q is almost independent of the specific configuration of the galaxy triplet $(\boldsymbol{r}_1, \boldsymbol{r}_2, \boldsymbol{r}_3)$ and is given approximately as

$$Q = 0.8 \sim 1.3 \tag{3.1.3}$$

in the range $0.1h^{-1}$Mpc to $10h^{-1}$Mpc (Peebles & Groth 1975; Groth & Peebles 1977). The four-point correlation function of galaxies $\eta_{1234} \equiv \eta(\boldsymbol{r}_1, \boldsymbol{r}_2, \boldsymbol{r}_3, \boldsymbol{r}_4)$, is also not determined so precisely. The observed η satisfies the following empirical relation:

$$\eta_{1234} = R_a[\xi_{12}\xi_{23}\xi_{34} + \xi_{23}\xi_{34}\xi_{41} + \xi_{24}\xi_{41}\xi_{12} + \xi_{13}\xi_{32}\xi_{24} + \xi_{32}\xi_{24}\xi_{41} + \xi_{24}\xi_{41}\xi_{13}$$

$$+\xi_{12}\xi_{24}\xi_{43}+\xi_{24}\xi_{43}\xi_{31}+\xi_{31}\xi_{12}\xi_{24}+\xi_{13}\xi_{34}\xi_{42}+\xi_{34}\xi_{42}\xi_{21}+\xi_{42}\xi_{21}\xi_{13}]$$
$$+R_b[\xi_{12}\xi_{13}\xi_{14}+\xi_{21}\xi_{23}\xi_{24}+\xi_{31}\xi_{32}\xi_{34}+\xi_{41}\xi_{42}\xi_{43}] \quad (3.1.4)$$

where R_a and R_b are given by

$$R_a = 2.5 \pm 0.6, \quad R_b = 4.3 \pm 1.2, \quad (3.1.5)$$

in the range $0.5h^{-1}$Mpc to $4h^{-1}$Mpc (Fry & Peebles 1978). At this stage, the above results are equally compatible with the interesting cases including $R_a = R_b$, $R_a = R_b/3$. Tóth et al. (1989) and Gott et al. (1991) found that equation (3.1.2) also holds for clusters of galaxies, although the statistical significance is not so high. If Q, R_a, and R_b are constants and $\xi(r)$ follows a single power-law (equation [3.1.1]), then ζ and η scale as

$$\zeta(\lambda \boldsymbol{r}_1, \lambda \boldsymbol{r}_2, \lambda \boldsymbol{r}_3) = \lambda^{-2\gamma}\zeta(\boldsymbol{r}_1, \boldsymbol{r}_2, \boldsymbol{r}_3), \quad (3.1.6)$$
$$\zeta(\lambda \boldsymbol{r}_1, \lambda \boldsymbol{r}_2, \lambda \boldsymbol{r}_3, \lambda \boldsymbol{r}_4) = \lambda^{-3\gamma}\zeta(\boldsymbol{r}_1, \boldsymbol{r}_2, \boldsymbol{r}_3, \boldsymbol{r}_4). \quad (3.1.7)$$

It is tempting to generalize the above relation for reduced (connected) N-point correlation functions as follows:

$$\xi^{(N)}(\lambda \boldsymbol{r}_1, \ldots, \lambda \boldsymbol{r}_N) = \lambda^{-(N-1)\gamma}\xi^{(N)}(\boldsymbol{r}_1, \ldots, \boldsymbol{r}_N). \quad (3.1.8)$$

In fact, the above scaling relation (3.1.8) provides a self-similar solution to the BBGKY equations in a strongly nonlinear limit ($\xi \gg 1$) in an Einstein-de Sitter universe. The above relation (3.1.8) suggests the hierarchical ansatz for the N-point correlation function which claims the N-point correlation function is a linear combination of the $(N-1)$-product of two-point correlation functions:

$$\xi^{(N)}(\boldsymbol{r}_1, \ldots, \boldsymbol{r}_N) = \sum_{\text{trees}(a)} Q_{N,a} \sum_{\text{labelings}} \prod_{\text{edges}(AB)}^{N-1} \xi_2(r_{AB}). \quad (3.1.9)$$

In the above notations, the edge (AB) is one of the edges in some tree graph (a) which is a set of connected $N-1$ edges linking N-points $\boldsymbol{r}_1, \ldots, \boldsymbol{r}_N$. All the distinct tree graphs are labelled by (a) and "labelings" indicate the symmetric sum with respect to the N-points (see Fry 1984b for details).

This relation is known to be satisfied approximately in observations (Sharp 1981; Sharp, Bonometto & Lucchin 1984; Meiksin, Szapudi & Szalay 1992; Szapudi, Szalay & Boschán 1992). but has not been proven to be exact in spite of a number

of theoretical studies on the relation (3.1.9) (Davis & Peebles 1977; Fry 1984a,b; Goroff, Grinstein, Rey & Wise 1986; Hamilton 1988; Balian & Schaeffer 1989a,b; Bernardeau 1992). Fry (1984b) explicitly computed the functional forms of ζ and η in perturbation theory. Basically he found that the ansatz (3.1.9) does not hold strictly in the sense that the amplitude Q, R_a and R_b in equations (3.1.2) and (3.1.4) depend on the geometric configuration of the triplet $(\boldsymbol{r}_1, \boldsymbol{r}_2, \boldsymbol{r}_3)$ and of the quartet $(\boldsymbol{r}_1, \boldsymbol{r}_2, \boldsymbol{r}_3, \boldsymbol{r}_4)$, although the dependence is fairly weak and Q, R_a and R_b are always of order unity. The validity of the ansatz for ζ in a strongly nonlinear regime has been directly examined by Suto (1993) using N-body simulation data of a low-density unbiased cold dark matter model in which $\Omega_0 = 0.2$, $\lambda_0 = 0.8$, $h = 1.0$. The result indicates that the ansatz (3.1.2) holds in an average sense, and a simple arithmetic averaging gives $Q = 1.2 \pm 0.8$. In addition, the scatter around the mean value reflects some dependence of Q on the triplet configuration.

There exist several studies to examine the hierarchical ansatz *after* averaging over the N-point configuration including counts-in-cell analyses (Park 1991; Coles & Frenk 1991; Lahav et al. 1993). This approach corresponds to dealing with the volume averaged N-point correlation function:

$$\overline{\xi^{(N)}} \equiv \frac{1}{V^N} \int_V d^3 r_1 \cdots d^3 r_N \xi^{(N)}(\boldsymbol{r}_1, \ldots, \boldsymbol{r}_N) \tag{3.1.10}$$

rather than $\xi^{(N)}$ itself. Therefore it is difficult to detect the configuration dependence of Q, R_a and R_b, if any, depending on how to average over different configuration. Lahav et al. (1993), for instance, found a scale-dependence of skewness and kurtosis from numerical simulations, but Colombi, Bouchet & Schaeffer (1993) suspected that the dependence is ascribed to the finite volume effect. In order to see whether or not the scale-dependence is real, it is most straightforward to carry out the analysis dealing with ξ_N itself. As will be shown below, the scale-dependence of skewness found by Lahav et al. (1993) is in perfect agreement with the clear configuration dependence of ζ and η (*before* averaging over different triplet configurations). Therefore it is unlikely that the result is a mere artifact of the finite volume effect.

3.2 THREE- AND FOUR-POINT CORRELATION FUNCTIONS: ANALYSIS OF COSMOLOGICAL N-BODY SIMULATIONS

In order to examine the validity of the ansatz (3.1.9) for $N = 3, 4$, we considered simulations with various initial fluctuation spectra, and in fact show that Q, R_a and R_b exhibit weak but clear dependences on the triplet or quartet configurations, the fluctuation spectra, and the degree of nonlinearity in the particle distribution (Matsubara & Suto 1994; Suto & Matsubara 1994). Also of great value is the effect of the peculiar velocity on the estimate of ζ. We will compute ζ in redshift space in order to elucidate its consequence in the low-density cold dark matter (LCDM) model as an example of the most successful scenarios so far (Efstathiou, Sutherland, & Maddox 1990; Suginohara & Suto 1991; Ueda, Itoh, & Suto 1993).

3.2.1 Simulation models

In order to see whether or not the ansatz (3.1.9) holds in general, we analyze six data sets from large N-body simulations; four of them adopt initially scale-free fluctuation spectra:

$$P(k) \propto k^n \qquad (n = -2, -1, 0, \text{and}\, 1), \tag{3.2.1}$$

and assume the Einstein-de Sitter universe. The next one corresponds to an LCDM($\Omega_0 = 0.2, \lambda_0 = 0.8, h = 1.0$) model with a simulation box size L being $100h^{-1}$Mpc. To see if any finite volume size artificially affects the behavior, we use also a larger LCDM model ($\Omega_0 = 0.2$, $\lambda_0 = 0.8$, $h = 0.75$, and $L = 300h^{-1}$Mpc). All models were assigned initially random Gaussian particle distribution at expansion factor $a = 1.0$, and then are evolved with a hierarchical tree code implementing the fully periodic boundary condition in a cubic volume of L^3. The LCDM model with $L = 300h^{-1}$Mpc employs $N_{\rm D} = 128^3$ particles and the gravitational softening length $\epsilon_g = L/2560$ (comoving), while the other five models have $N_{\rm D} = 64^3$ and $\epsilon_g = L/1280$. Further details of the simulation models are described in Suginohara et al. (1991) and Suginohara & Suto (1991).

3.2.2 Method to compute correlation functions

We estimate two-, three- and four-point correlation functions for cosmological N-body simulation data by directly counting particles. The new method presented

below save the computational time greatly and enable us to directly estimate three- and four-point correlation function accurately. The two-, three-, and four-point correlation functions are defined through the joint probability of finding objects in volume elements δV as follows:

$$\delta P_{12} = \bar{n}^2 \delta V_1 \delta V_2 \ [1 + \xi_{12}], \tag{3.2.2}$$

$$\delta P_{123} = \bar{n}^3 \delta V_1 \delta V_2 \delta V_3 \ [1 + \xi_{12} + \xi_{23} + \xi_{31} + \zeta_{123}], \tag{3.2.3}$$

$$\begin{aligned}\delta P_{1234} = \bar{n}^4 \delta V_1 \delta V_2 \delta V_3 \delta V_4 \ [1 &+ \xi_{12} + \xi_{13} + \xi_{14} + \xi_{23} + \xi_{24} + \xi_{34} \\ &+ \zeta_{123} + \zeta_{124} + \zeta_{134} + \zeta_{234} + \xi_{12}\xi_{34} + \xi_{13}\xi_{24} + \xi_{14}\xi_{23} + \eta_{1234}],\end{aligned} \tag{3.2.4}$$

where $\bar{n}$ is the number density of the objects, and $\xi_{12} \equiv \xi(\boldsymbol{r}_1, \boldsymbol{r}_2)$, $\zeta_{123} \equiv \zeta(\boldsymbol{r}_1, \boldsymbol{r}_2, \boldsymbol{r}_3)$, and $\eta_{1234} \equiv \eta(\boldsymbol{r}_1, \boldsymbol{r}_2, \boldsymbol{r}_3, \boldsymbol{r}_4)$ denote two-, three-, and four-point correlation functions, respectively with $\boldsymbol{r}_i$ being the coordinate of the i-th object. Strictly speaking, this definition of correlation functions for point process differs from the definition of correlation functions for continuous field in chapter 2. The main difference is the existence of the shot noise in point process which dominates on very small scales comparable to the mean separation of particles of the point process. For the details of this difference and the correction for shot noise, see Bertschinger (1992). On scales where the particle distribution is well described by continuous density field, the two definitions for correlation functions can be identified.

Global homogeneity and isotropy of the distribution reduces the degree of freedom for those functions to one, three, and six, respectively, corresponding the pair-separation of the i-th and the j-th objects, $r_{ij} \equiv |\boldsymbol{r}_i - \boldsymbol{r}_j|$. To be more specific, $\xi_{12} = \xi(r_{12})$, $\zeta_{123} = \zeta(r_{12}, r_{23}, r_{13})$, and $\eta_{1234} = \eta(r_{12}, r_{23}, r_{13}, r_{34}, r_{14}, r_{24})$. Obviously, ξ_{12}, ζ_{123} and η_{1234} are symmetric with respect to the indices.

If $\mathrm{DD}(r)$ denotes the number of particle pairs from simulation data in separation $r \sim r + dr$ and $\mathrm{DR}(r)$ is its counterpart for simulation particles (N_D in total) and randomly distributed particles (N_R in total), ξ is obtained by

$$\xi(r) = \frac{N_\mathrm{R}}{N_\mathrm{D}} \frac{\mathrm{DD}(r)}{\mathrm{DR}(r)} - 1. \tag{3.2.5}$$

Our estimate of the (reduced) three-point correlation function ζ_{123} is based on equation (3.2.3), which defines ζ in terms of the probability of finding three objects, and proceeds as follows; first, we compute separations of pairs of particles using logarithmically equal bins. In practice, we use the total of N_bin bins between r_min and r_max. Therefore the pair-separation in the n-th bin lies between $r_\mathrm{min}\alpha^{n-1}$ and

$r_{\rm min}\alpha^n$ where $\alpha \equiv (r_{\rm max}/r_{\rm min})^{1/N_{\rm bin}}$. Second we randomly choose $N_{\rm p}(r_1)$ pairs each for all the $N_{\rm bin}$ separation bins. This fixes one side r_1 of the triplets, and then we accumulate the number of triplets, DDD(r_1, r_2, r_3), looping over the rest of all particles. We decided to use the same constant value for $N_{\rm p}$ irrespective of r_1 in order to guarantee the same statistical significance for the pair separation r_1, although this resulted in requiring a large computational cost in small separations where the number of such particle pairs is very small. The latter becomes serious especially in the early epochs when the clustering is not so strong. That forced us to adopt $N_{\rm p} = 1000$ in the analysis of the less evolved models while we could use $N_{\rm p} = 2500$ for the fully nonlinear models with the same (or less) CPU time. As for the rest of the parameters, we adopted $r_{\rm min} = 0.0008L$, $r_{\rm max} = 0.25L$, $N_{\rm bin} = 20$, throughout the present analysis. Third, we compute the corresponding number of triplets, DDR(r_1, r_2, r_3), in the case of a Poisson distribution by using $N_{\rm R}(= 10^6)$ randomly distributed particles. This was performed just once for the smallest r_1 bin, and the counts for the rest of r_1 bins were obtained simply by multiplying the appropriate proportional coefficient because our simulations assume a fully periodic boundary condition. Finally given the two-point correlation function ξ, ζ is estimated from those countings as follows:

$$\zeta(r_1, r_2, r_3) = \frac{N_{\rm R}}{N_{\rm D} N_{\rm p}(r_1)} \frac{{\rm DDD}(r_1, r_2, r_3)}{{\rm DDR}(r_1, r_2, r_3)} \{1+\xi(r_1)\} - \xi(r_1) - \xi(r_2) - \xi(r_3) - 1. \quad (3.2.6)$$

Since ζ is symmetric with respect to r_1, r_2 and r_3, we simply use the above expression only if $r_1 \leq r_2$ and $r_1 \leq r_3$, and then symmetrize the result with respect to r_2 and r_3.

Now we obtain $\zeta(r_1, r_2, r_3)$ evaluated at the logarithmically discretized bins. If $r_i (i = 1, 2, 3)$ belongs to the n_i-th bin, respectively, we will refer this triplet as (n_1, n_2, n_3). Since $\zeta(r_1, r_2, r_3)$ is symmetric with respect to r_i, the triplets satisfying

$$\begin{array}{c} 1 \leq n_1 \leq n_2 \leq n_3 \leq N_{\rm bin} \\ r_1 + r_2 \geq r_3 \quad \text{(triangular inequality)} \end{array} \quad (3.2.7)$$

are relevant for the further analysis below. These constraints reduce the number of triplet configurations available in our analysis to 298. According to our choice of separation binning, a triplet (i, j, k) is similar in shape to one $(i + l, j + l, k + l)$ except that the latter is a factor of α^l larger in linear dimension. For instance, a triplet (n_1, n_2, n_3) is similar to a triplet $(1, n_2 - n_1 + 1, n_3 - n_1 + 1)$. Thus we will use a notation of $[1, n_2 - n_1 + 1, n_3 - n_1 + 1]$ to indicate all such triplets similar in

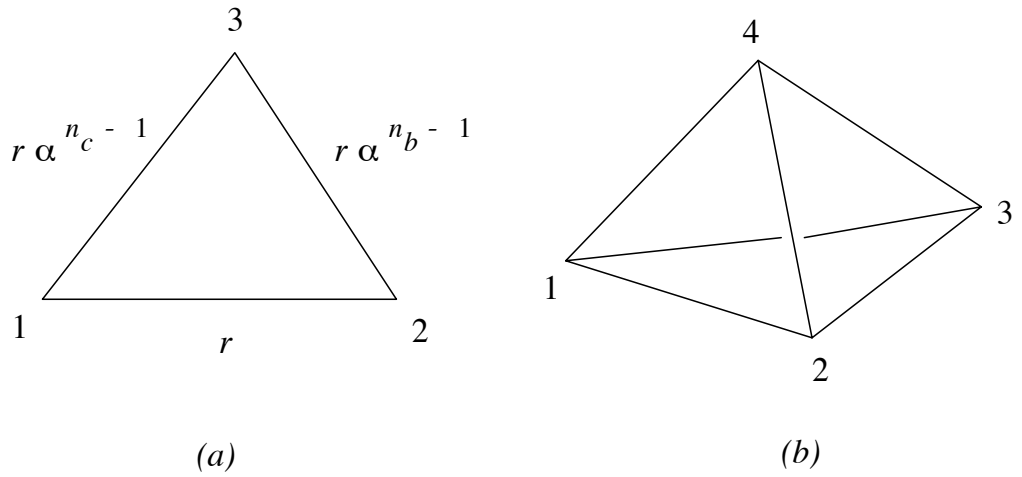

Figure 3.1: Geometrical configuration for our three- and four-point correlation analysis. (a) A triplet corresponding to a shape $[1, n_b, n_c]$, and (b) a tetrahedron.

shape. For example, the shape $[1,2,3]$ refers to triples $(1,2,3)$, $(2,3,4)$, $(3,4,5)$, ..., $(N_{\rm bin}-2, N_{\rm bin}-1, N_{\rm bin})$ (we will classify 298 kinds of triplets into 25 "irreducible" shapes accordingly).

We evaluated the error in the estimate of ζ according to equation (3.2.6) by taking account of the statistical errors in ξ, DDD(r_1, r_2, r_3), and DDR(r_1, r_2, r_3). The former is computed simultaneously in estimating ξ from simulations data. To the latter two countings, we simply assigned a Poisson error:

$$\Delta(\mathrm{DDD}) = \sqrt{\mathrm{DDD}}, \qquad \Delta(\mathrm{DDR}) = \sqrt{\mathrm{DDR}}. \tag{3.2.8}$$

Our estimate of the (reduced) four-point correlation function η_{1234} is based on equation (3.2.4), which defines η in terms of the probability of finding four objects, and proceeds as follows; first, we compute separations of pairs of particles using bins ($N_{\rm bin}$ in total) with logarithmically equal interval between $r_{\rm min}$ and $r_{\rm max}$. Then, we randomly choose $N_{\rm p}(r_{12})$ pairs each for all the $N_{\rm bin}$ separation bins. This fixes one side, r_{12}, of tetrahedra (Figure 3.1(b)). We decided to use the same constant value for $N_{\rm p}$ (4000 for real-space analysis and 1400 for redshift-space analysis) irrespective of r_{12} in order to guarantee the same statistical significance for the pair separation r_{12}.

Second, we select the *third* particles so that the resulting triplets (r_{12}, r_{23}, r_{13}) belong to a specified shape. We use $[1, n_b, n_c]$ to indicate a shape of triangles with $r_{12} \equiv r$, $r_{23} \equiv r\alpha^{n_b-1}$, and $r_{13} \equiv r\alpha^{n_c-1}$ (Figure 3.1(a)). In the present binning, the

number of all the irreducible shapes of triplets is 25. We selected the total number of $N_t(123) \equiv N_t(r_{12}, r_{23}, r_{13})$ triplets of particles from the simulation data *for* a given shape $[1, n_b, n_c]$. When the third particle satisfying the above shape condition with the preselected pair of particles is found, we used the next pair as the baseline of the triplet search, r_{12}. Thus $N_t(123)$ for a specific shape is in most cases equal to the number of preselected pairs $N_{\rm p}(r_{12})$. When all the separation bins for r_{12}, r_{23}, and r_{13} are much smaller than the mean particle separation in the simulation data, it happens that no particle can form the specified shape with the given pairs of particles, and only in such cases $N_t(123)$ becomes smaller than $N_{\rm p}(r_{12})$. For instance, $N_t(123)$ is 1518 and 27 for the base triplet $(r_{\rm min}, r_{\rm min}, r_{\rm min})$ in real space and in redshift space, respectively.

Third, the number of four-points $\mathrm{DDDD}(123;4) \equiv \mathrm{DDDD}(r_{12}, r_{23}, r_{13}, r_{34}, r_{14}, r_{24})$ is accumulated according to the location of the *fourth* particles (r_{14}, r_{24}, r_{34}) with respect to the *base* triplets. We looped over the rest of all simulation particles to find the fourth particles which form a proper tetrahedron with the $N_t(123)$ base triplets of a specified shape $[1, n_b, n_c]$. The corresponding number $\mathrm{DDDR}(123;4) \equiv \mathrm{DDDR}(r_{12}, r_{23}, r_{13}, r_{34}, r_{14}, r_{24})$ was computed by using randomly distributed $N_{\rm R}(= 10^7)$ particles as the fourth particle candidates. The latter procedure was performed just once for a given shape $[1, n_b, n_c]$ of triplets. Then the resulting counts were scaled with respect to the overall size of the triplets r by multiplying the appropriate proportional coefficient since our simulations were carried out in a fully periodic computational cube. Then finally we estimate the four-point correlation functions as

$$\begin{aligned}\eta_{1234} = \frac{N_{\rm R}}{N_{\rm D} N_t(123)} \frac{\mathrm{DDDD}(123;4)}{\mathrm{DDDR}(123;4)} (1 + \xi_{12} + \xi_{23} + \xi_{13} + \zeta_{123}) \\ -1 - \xi_{12} - \xi_{23} - \xi_{13} - \xi_{34} - \xi_{14} - \xi_{24} - \zeta_{123} - \zeta_{234} - \zeta_{134} - \zeta_{124} \\ -\xi_{12}\xi_{34} - \xi_{23}\xi_{14} - \xi_{13}\xi_{24}. \end{aligned} \tag{3.2.9}$$

As in the case of ξ_{12} and ζ_{123}, all the above procedure used the $N_{\rm bin}$ bins with logarithmically equal interval between $r_{\rm min}$ and $r_{\rm max}$. If r_{ij} $(ij = 12, 23, 13, 34, 14, 24)$ belongs to the n_{ij}-th bin of separation, we will refer the tetrahedron as $(n_{12}, n_{23}, n_{13}, n_{34}, n_{14}, n_{24})$. The resulting four-point correlation functions should satisfy the following symmetry:

$$\begin{aligned}&\eta(r_{12}, r_{23}, r_{13}, r_{34}, r_{14}, r_{24}) = \eta(r_{12}, r_{13}, r_{23}, r_{34}, r_{24}, r_{14}) = \eta(r_{23}, r_{12}, r_{13}, r_{14}, r_{34}, r_{24}) \\ = \;&\eta(r_{12}, r_{14}, r_{24}, r_{34}, r_{23}, r_{13}) = \eta(r_{34}, r_{23}, r_{24}, r_{12}, r_{14}, r_{13}) = \eta(r_{34}, r_{14}, r_{13}, r_{12}, r_{23}, r_{24}) \quad , \end{aligned} \tag{3.2.10}$$

as well as the triangular inequalities for four surface triangles of the tetrahedron, and the positiveness of the volume of the tetrahedron (see , e.g., Appendix B of Friedberg & Lee 1984). In addition, according to our choice of logarithmic separation binning, a configuration of $(n_{12}, n_{23}, n_{13}, n_{34}, n_{14}, n_{24})$ is similar in shape to that of $(n_{12}+j, n_{23}+j, n_{13}+j, n_{34}+j, n_{14}+j, n_{24}+j)$ except that the latter is a factor of α^j larger in linear dimension. All the configurations can be classified to the similar shape denoted by $[1, n_{23}-n_{12}+1, \ldots, n_{24}-n_{12}+1]$. For example, the shape $[1,2,3,3,1,1]$ refers to four-points of $(1,2,3,3,1,1)$, $(2,3,4,4,2,2)$,$(3,4,5,5,3,3)$, ..., $(N_{\rm bin}-2, N_{\rm bin}-1, N_{\rm bin}, N_{\rm bin}, N_{\rm bin}-2, N_{\rm bin}-2)$.

The error of η_{1234} quoted in the rest of this section takes into account of the statistical errors in ξ, ζ, DDDD(123;4), and DDDR(123;4). The former two are computed simultaneously in estimating ξ and ζ from simulations data. As for the latter two, we simply assigned Poissonian errors:

$$\Delta(\mathrm{DDDD}) = \sqrt{\mathrm{DDDD}}, \qquad \Delta(\mathrm{DDDR}) = \sqrt{\mathrm{DDDR}}. \tag{3.2.11}$$

The above error estimate does not reflect properly the (complicated) statistical nature of DDDD and DDDR, although it would not be an unreasonable guess. Since sample-to-sample variations might make somewhat larger contribution to the overall errors after all, we will not attempt to refine the error estimate here; the reader should understand the significance of the errors which we will quote below with the above caution.

3.2.3 The result of two-, three- and four-point correlation functions in N-body simulations

The two-point correlation functions ξ for the scale-free models with $n = -2$, -1, 0, and 1 are plotted in Figures 3.2(a) to 3.2(d), respectively. Also in Figures 3.2(e) and 3.2(f) is plotted ξ for LCDM models with $L = 100h^{-1}$Mpc and $300h^{-1}$Mpc, respectively. Note the slope and amplitude of ξ of LCDM models are in beautiful agreement with equation (3.1.1). Although ξ of the scale-free models does not match equation (3.1.1) well, their analysis is useful in examining the dependence of Q on the underlying fluctuation spectra.

For the analysis of the three-point correlation function, it is useful to work with the normalized three-point correlation function

$$Q(r_1, r_2, r_3) = \frac{\zeta(r_1, r_2, r_3)}{\xi(r_1)\xi(r_2) + \xi(r_2)\xi(r_3) + \xi(r_3)\xi(r_1)} \tag{3.2.12}$$

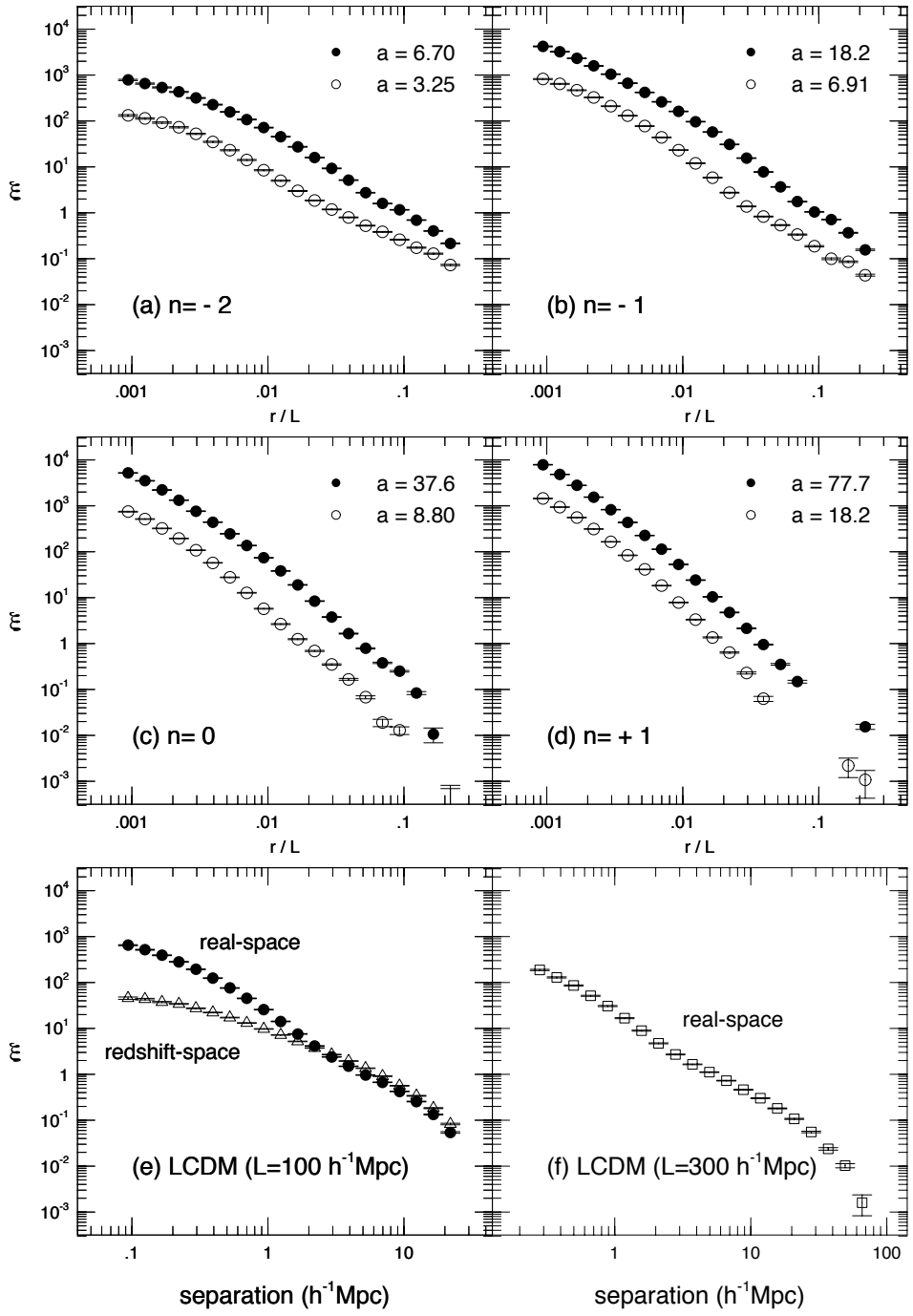

Figure 3.2: Two-point correlation functions of several cosmological models described in text: (a) $n = -2$ at $a = 3.25$ ($\circ$) and $a = 6.70$ ($\bullet$); (b) $n = -1$ at $a = 6.91$ ($\circ$) and $a = 18.2$ ($\bullet$); (c) $n = 0$ at $a = 8.80$ ($\circ$) and $a = 37.6$ ($\bullet$); (d) $n = 1$ at $a = 18.2$ ($\circ$) and $a = 77.7$ ($\bullet$); (e) LCDM with $L = 100h^{-1}$Mpc and $h = 1.0$ in real space ($\bullet$) and in redshift space ($\triangle$); and (f) LCDM model with $L = 300h^{-1}$Mpc and $h = 0.75$ in real space ($\square$).

rather than ζ itself which varies up to nine orders of magnitude in the dynamic range of our simulations. The hierarchical ansatz (3.1.2) states that $Q(r_1, r_2, r_3)$ be independent of the shapes of triangles and is equal to a constant value, Q.

In Figures 3.3 to 3.7 is plotted the behavior of Q for different models. We calculated Q for all possible 25 shapes, but their characteristic behavior is illustrated clearly in the eight typical shapes selected there. Let us call the first four shapes [1,1,1], [1,1,2], [1,1,3], and [1,2,2] 'non-singular' triplets, in the sense that the size of the three sides is similar. In the same spirit, we call the next two shapes [1,4,4] and [1,4,5] 'quasi-singular', and the remaining two [1,10,10] and [1,15,15] 'singular'.

Those figures clearly show how Q depends on specific configuration $[n_1, n_2, n_3]$ and also the fluctuation spectral index n (mainly on small scales): as n increases, the normalized three-point function decreases and becomes flat. This tendency is in agreement with the previous analyses although they are fairly crude compared with our present approach: Efstathiou et al. (1988) and Kauffmann & While (1992) computed '$Q(r_1)$' by averaging over the two other sides r_2 and r_3, and found a similar scale-dependence to ours in the case of scale-free and LCDM models, respectively. Fry et al. (1992) examined the equilateral configurations of various scales, which correspond to our [1,1,1] shape, in Fourier space using their two-dimensional simulation data. They concluded that the departure from the hierarchical ansatz (3.1.2) become more significant for smaller n. Although their findings are qualitatively consistent with ours, we showed for the first time the explicit dependence of Q on both sizes and shapes of the triplets in each model. It is interesting to note that Q in 'singular' shapes are almost constant even in the $n = -2$ case where scale-dependence for other shapes is strongest.

The function Q in the LCDM models behaves similar to the power-law models with $n = -2 \sim -1$ as expected from the fact that the initial spectrum of the LCDM models is fairly similar to that of the latter on scales considered here. The reason why the values of Q in two LCDM models are somewhat different would be explained by the following differences: shape of the initial fluctuation spectrum (which depends on the adopted value for h), spatial resolution (which is determined by simulation box size L, employed number of particles $N_{\rm D}$, and the softening length ϵ_g), and/or the sample-to-sample variation (Itoh, Suginohara & Suto 1992) due to the realization of the initial condition. The basic conclusion, however, is clear and secure: there exists a weak but unambiguous scale-dependence in Q which cannot be ascribed to a possible artificial finite volume effect.

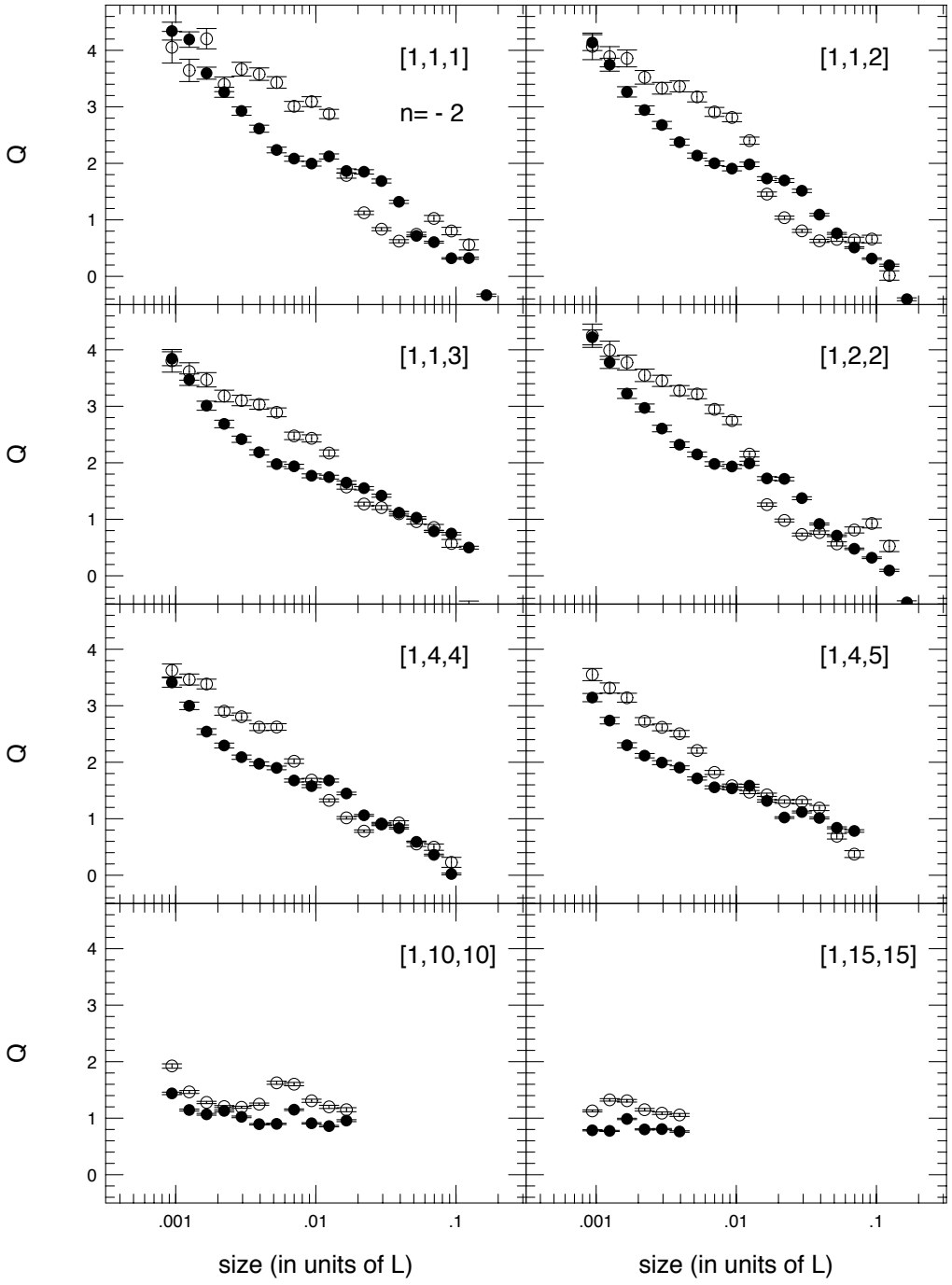

Figure 3.3: Normalized three-point correlation functions for $n = -2$ model plotted against the size of the shortest side of the triplets. The filled and open circles denote the estimates at different epochs corresponding to Figure 3.2. See text for the meaning of the shape $[n_1, n_2, n_3]$.

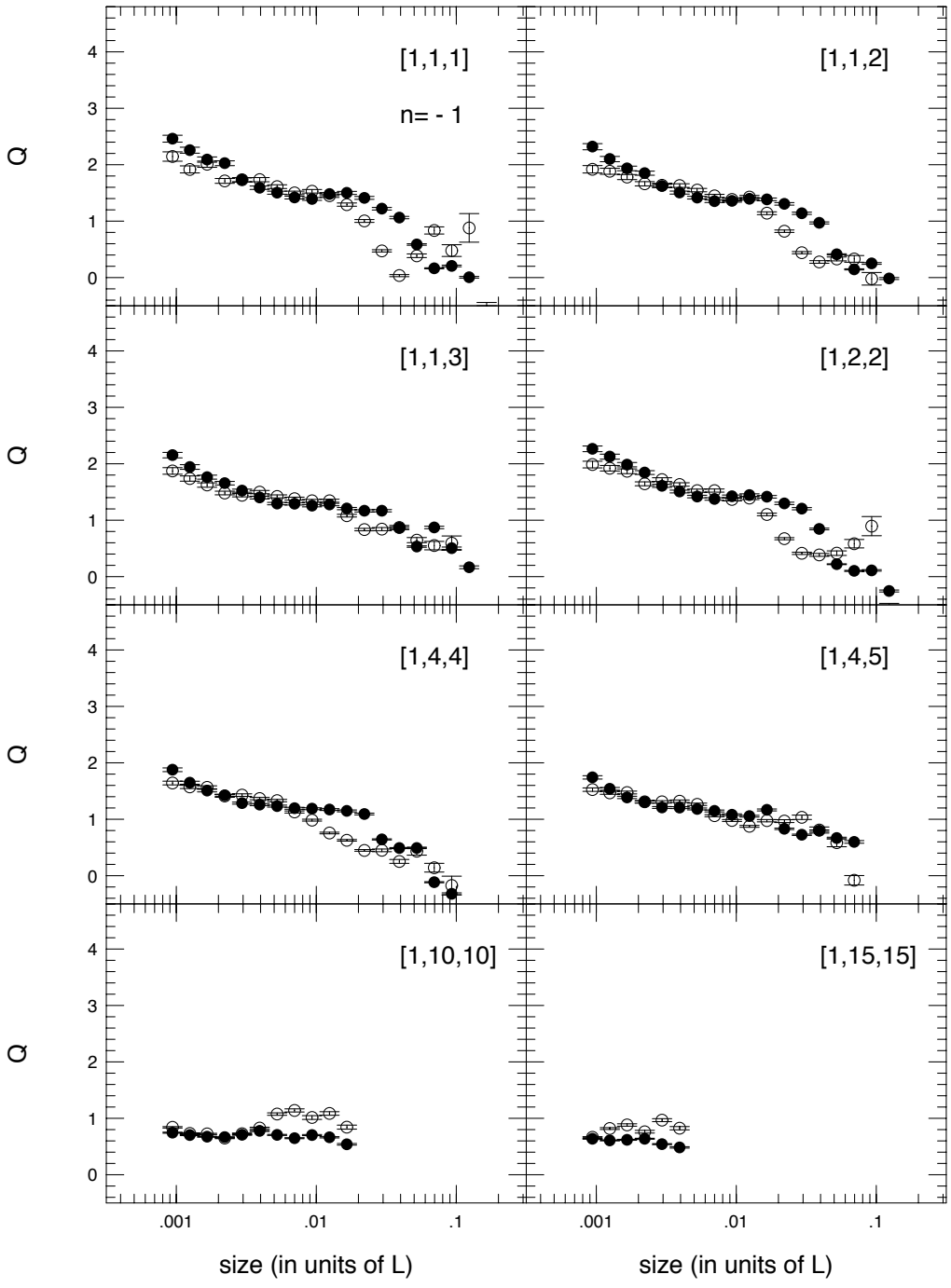

Figure 3.4: Same as Figure 3.3 for $n = -1$ model.

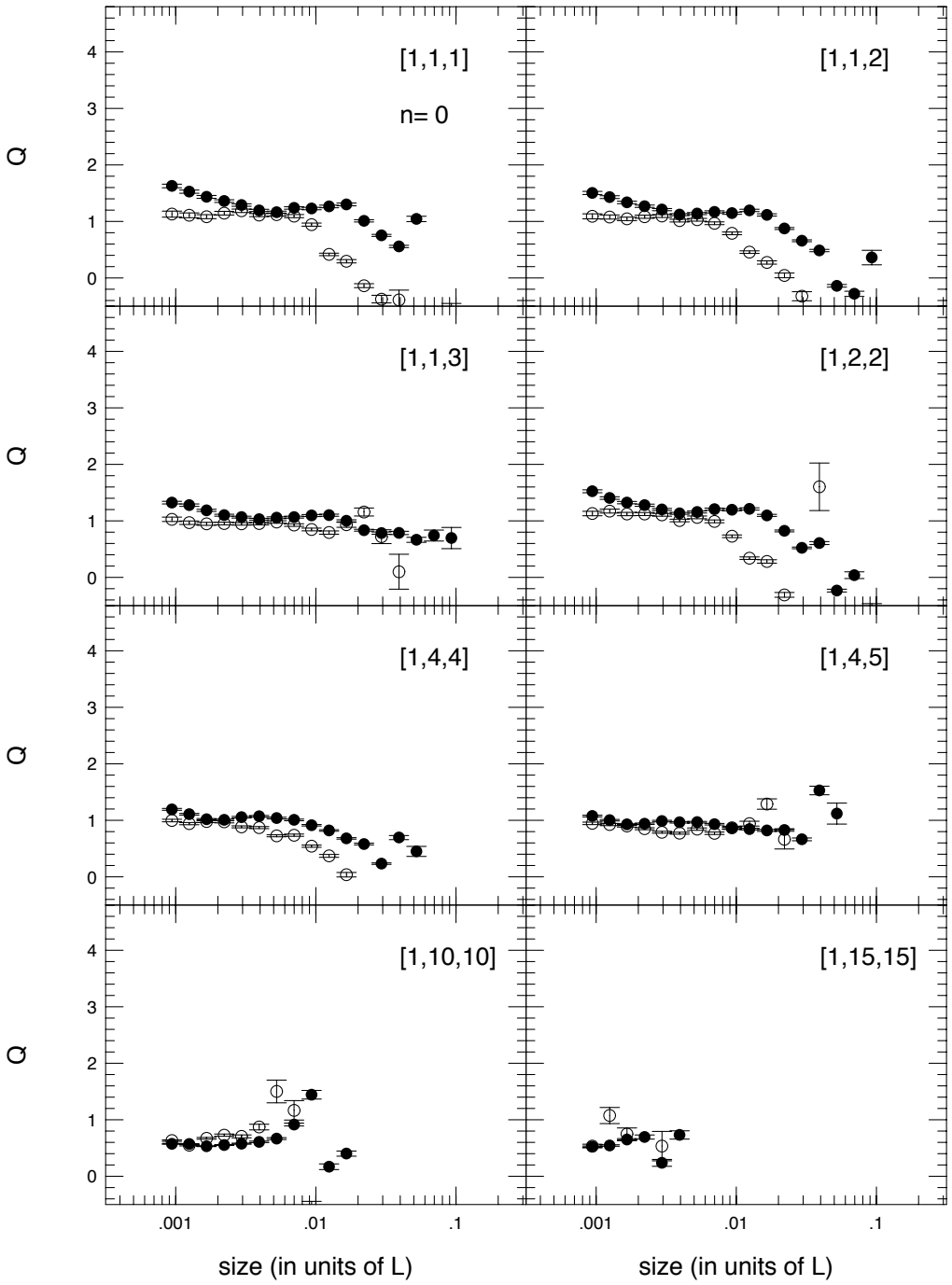

Figure 3.5: Same as Figure 3.3 for $n = 0$ model.

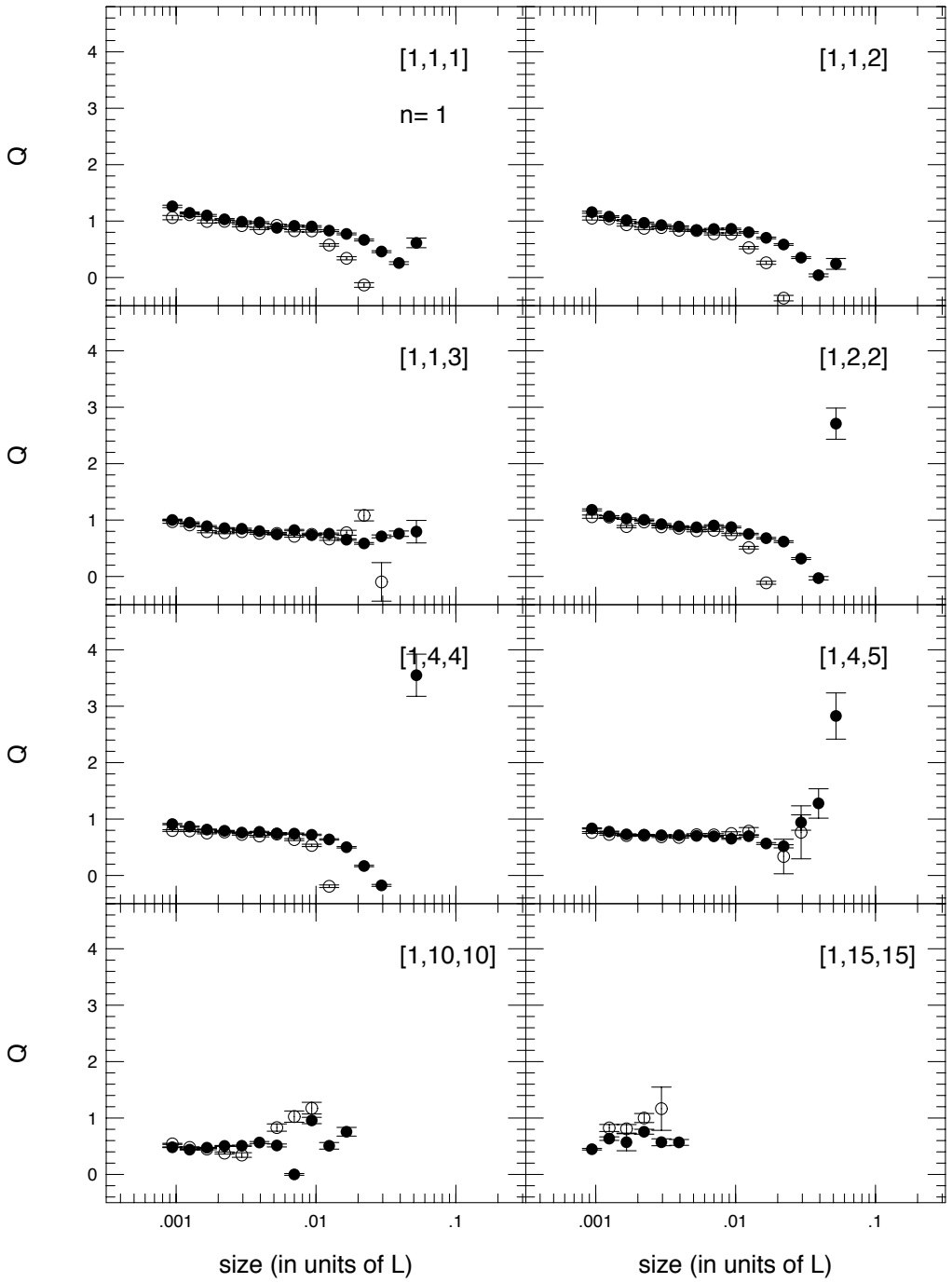

Figure 3.6: Same as Figure 3.3 for $n = 1$ model.

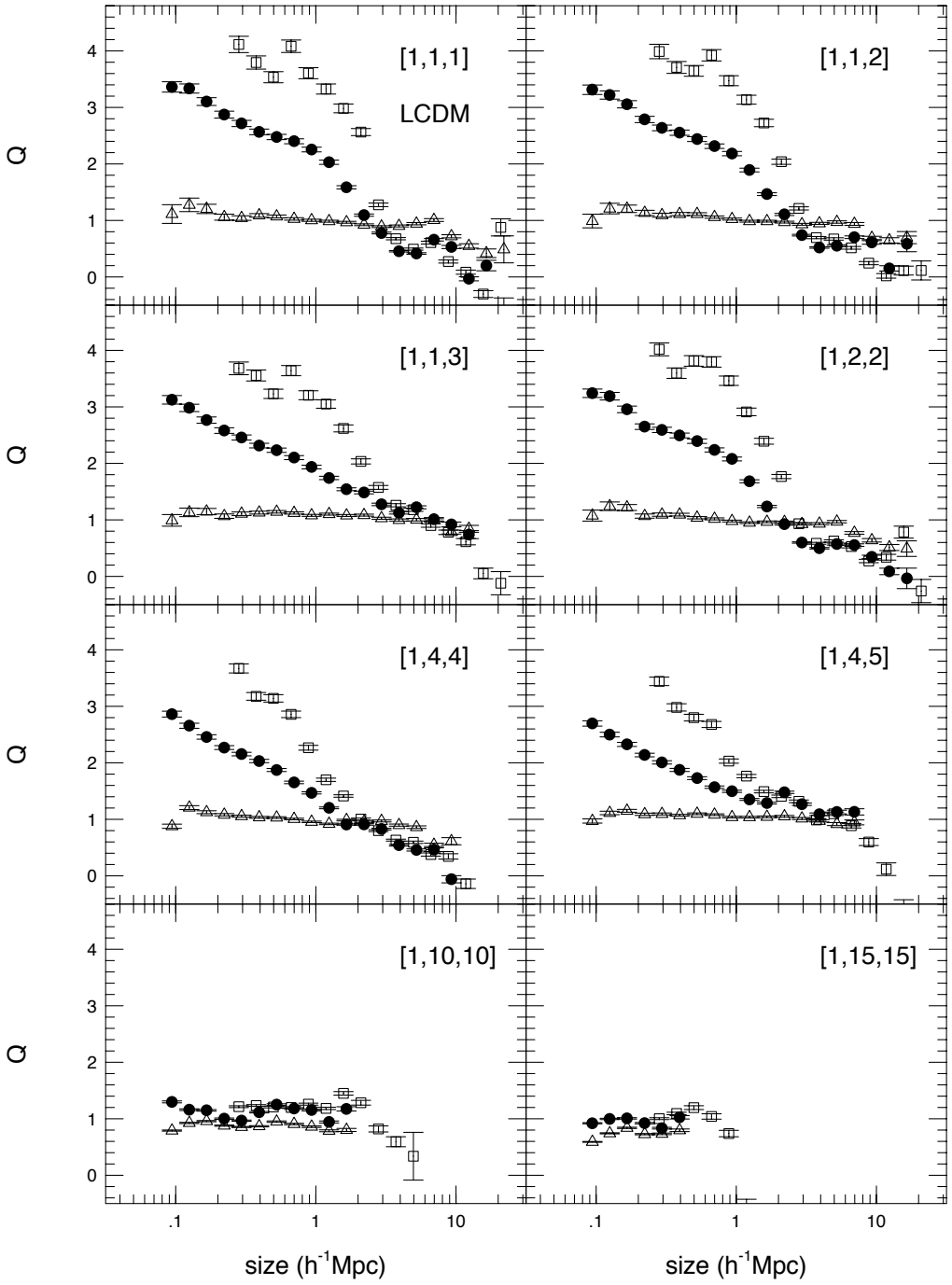

Figure 3.7: Same as Figure 3.3 for LCDM models. Open squares and filled circles indicate the normalized three-point correlation functions in real space for $L = 300h^{-1}$Mpc and $L = 100h^{-1}$Mpc models, respectively, while open triangles correspond to those in redshift space for $L = 100h^{-1}$Mpc model.

Although we have shown that the hierarchical ansatz clearly breaks down especially on small scales in models with large-scale fluctuations ($n = -1 \sim -2$), the deviation is fairly small. Therefore simple-minded analysis of observational and/or simulation data would likely lead to a misleading conclusion that the ansatz holds very accurately. If one averages 'Q' without making shape-wise analysis, the result is very dependent on the way of weighting over the various configurations of the triplets. If we select triplets randomly from the particle distribution, almost all triplets contain a large separation and the scale-dependence of the normalized three-point correlation function we have found can hardly be detected.

For the analysis of the four-point correlation function, it is useful to work with the normalized four-point correlation function

$$R(r_{12}, r_{23}, r_{13}, r_{34}, r_{14}, r_{24}) = \frac{\eta_{1234}}{\xi_{12}\xi_{23}\xi_{34} + \text{sym.}(12) + \xi_{12}\xi_{13}\xi_{14} + \text{sym.}(4)} \qquad (3.2.13)$$

rather than η itself which varies up to nine orders of magnitude in the dynamic range of our simulations. The hierarchical ansatz (3.1.4) with $R_a = R_b$ states that R be independent of the shapes of triangles and is equal to a constant value.

Figure 3.8 shows R as a function of the size of the shortest side $r_a \equiv r_{12}$ ($s_a \equiv s_{12}$) in real (redshift) space of a tetrahedron in units of the computational boxsize L for typical shapes $[1, n_b, n_c, n_d, n_e, n_f]$. Results for the low-density CDM model in real space, in redshift space, and for the $n = 0$ model in real space are plotted in filled circles, open triangles, and open squares, respectively. This figure clearly exhibits basic features of scale-dependent behavior of η_{1234}; the scale dependence is strong when the six lengths of the tetrahedron are nearly the same (e.g., $[1, 1, 1, 1, 1, 1]$). When the shape becomes 'singular', the dependence becomes weak (e.g., $[1, 10, 10, 4, 10, 10]$).

Since our results suggest that the normalized four-point correlation functions R are not constant but dependent on the separations of the four points, it does not make much sense to compute their average values unless specifying the weighting method. In this respect, we should note that our entire data for four-points are biased; we preselected a fixed number of the base triplets from particle data to increase the statistical significance. Although simple arithmetic averaging is not relevant at all, our LCDM model is potentially consistent with the values of R_a and R_b (eq.[3.1.5]) observationally estimated by Fry & Peebles (1978), while $n = 0$ model would lead to much smaller values ($0.5 \sim 1$) (Figure 6(a)). In addition, it should be emphasized here that Fry & Peebles (1978) noted a possible departure from the simply hierarchical form for four-point functions (their Figures 4 to 7 and section

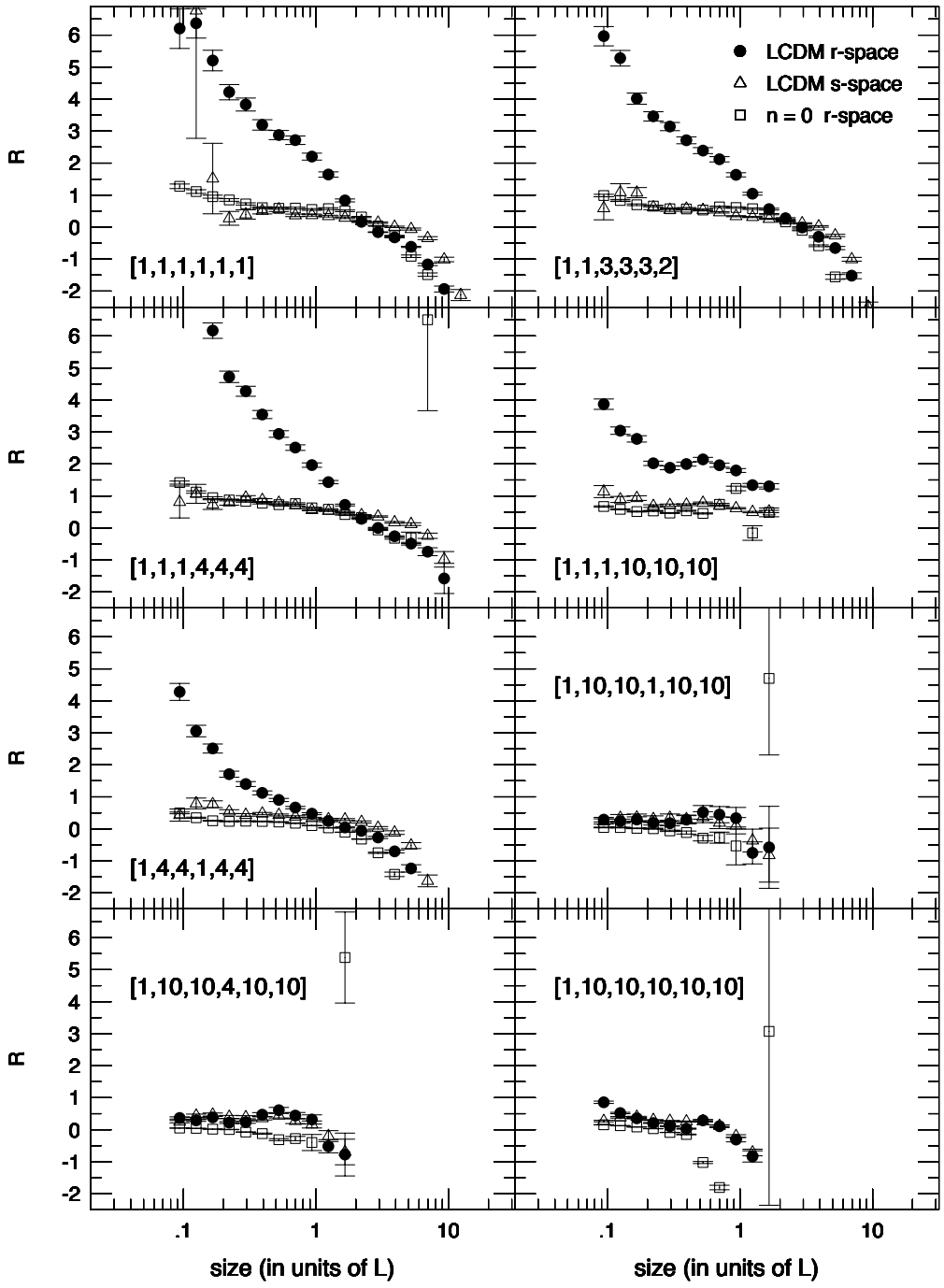

Figure 3.8: Scale-dependence of R as a function of the size of the shortest side $r_a \equiv r_{12}$ ($s_a \equiv s_{12}$) in real (redshift) space of a tetrahedron in units of the computational boxsize L for typical shapes $[1, n_b, n_c, n_d, n_e, n_f]$. Results for the low-density CDM model in real space, in redshift space, and for the $n = 0$ model in real space are plotted in filled circles, open triangles, and open squares, respectively.

IIIc). Unfortunately any further detailed comparison between our and their results is not feasible because of the completely different sample and techniques in deriving the correlation functions. Naturally this should be left for the future project when much deeper and wider galaxy survey data are available.

3.2.4 Redshift-space contamination

The two-, three- and four-point correlation functions in real space investigated above are not directly observable from three-dimensional redshift catalogues of galaxies and/or clusters. In fact they inevitably suffer from the contamination due to the peculiar velocity field. This effect was studied analytically by Kaiser (1987) in a linear regime and then by Suto & Suginohara(1991) in a nonlinear regime using N-body simulations. The two-point correlation function in redshift space $\xi_s(s)$ is quite different from that in real space $\xi_r(r)$; in a nonlinear regime random peculiar velocities tend to wipe out the actual correlation $\xi_r(r)$, while in a linear regime $\xi_s(s)$ is enhanced relative to $\xi_r(r)$ owing to the coherence of the velocity and density fluctuation fields. Therefore to explore the effect of the redshift-space contamination on the three- and four-point correlation function is of great interest.

For this purpose, we placed a fiducial observer at a certain point in the LCDM model with $L = 100h^{-1}$Mpc. Then we constructed a particle distribution in redshift space convolving with the radial components of the peculiar velocities of all particles. Then we repeated the same procedure described in the previous section to compute the three- and four-point correlation function ζ_s, η_s in redshift space. The results Q_s, R_s are plotted in Figures 3.7, 3.8 as open triangles which should be compared with their real space counterparts (filled circles).

The contamination effect is most impressive for ζ_s which seems to be consistent with hierarchical ansatz in contrast to ζ_r. Therefore direct analysis of the redshift survey data would conclude that the hierarchical relations hold very accurately for ζ_{123} even though that is not the case in real distribution of galaxies. For η_{1234}, such effects are not so dramatic and the departure from the hierarchical relations is significant both in real and in redshift spaces. An semi-analytic description of two- and three-point correlation functions in redshift space is presented in section 3.4 below.

3.3 STATISTICS OF ISODENSITY CONTOURS IN WEAKLY NONLINEAR FIELD

3.3.1 Statistics of isodensity contours

There are many statistical tools to investigate the three-dimensional pattern of the galaxy distribution including two-point correlation function, power spectrum, cluster correlations, higher-order correlations, probability distribution function, etc. Among others, there is a class of statistics using a smoothed density field which cut the noisy property of galaxy distribution.

For example, Gott, Melott & Dickinson (1986) proposed to use the Euler characteristic of surfaces of constant density as a quantitative measure for the topology of large-scale structure. The genus G, which is defined by $-1/2$ times the Euler characteristics of two-dimensional surfaces, divided by the total volume, can be a quantitative measure of the topology. More intuitively, the genus corresponds to "the number of holes" of the surfaces minus "the number of isolated regions" surrounded by the surfaces per unit volume. The genus is a function of smoothing scales and the density threshold. The genus as a function of density threshold for a fixed smoothing scale is called the genus curve and is analyzed both in numerical simulations and in redshift surveys of galaxies by many people (Gott, Weinberg & Melott 1987; Weinberg, Gott & Melott 1987; Melott, Weinberg & Gott 1988; Gott et al. 1989; Park & Gott 1991; Park, Gott & da Costa 1992; Weinberg & Cole 1992; Moore et al. 1992; Vogeley, Park, Geller, Huchra & Gott 1994; Rhoads, Gott & Postman 1994). Analytic expressions of the genus for some cases are known so far, including Gaussian random field (Doroshkevich 1970; Adler 1981; Bardeen et al. 1986; Hamilton, Gott & Weinberg 1986), Rayleigh-Lévy random-walk fractal (Hamilton 1988), union of overlapping balls (Okun 1990) and weakly non-Gaussian random fields (Matsubara 1994b).

There are other statistics of isodensity contours, which include the 2D genus in two-dimensional slices of density field G_2 (Melott et al. 1989; Gott et al. 1992; Park et al. 1992), the area of isodensity contours N_3, the length of isodensity contours in two-dimensional slices of density field N_2 and the level crossing statistics N_1 (Ryden 1988; Ryden et al. 1989).

The analytical expression of these statistics are known for Gaussian random density field (Melott et al. 1989; Ryden 1988; Ryden et al. 1989; Adler 1981; Doroshkevich 1970; Bardeen et al. 1986; Hamilton, Gott & Weinberg 1986; Bond & Efstathiou

1987). They are

$$G(\nu) = \frac{1}{4\pi^2}\left(\frac{\langle k^2\rangle}{3}\right)^{3/2}(1-\nu^2)e^{-\nu^2/2}, \tag{3.3.1}$$

$$G_2(\nu) = \frac{1}{(2\pi)^{3/2}}\left(\frac{\langle k^2\rangle}{3}\right)\nu e^{-\nu^2/2}, \tag{3.3.2}$$

$$2N_1(\nu) = \frac{4}{\pi}N_2(\nu) = N_3(\nu) = \frac{2}{\pi}\left(\frac{\langle k^2\rangle}{3}\right)^{1/2}e^{-\nu^2/2}, \tag{3.3.3}$$

where ν is the difference between density threshold and mean density in units of standard deviation of density and

$$\langle k^2\rangle = \frac{\int k^2 P(k) d^3k}{\int P(k) d^3k}, \tag{3.3.4}$$

with $P(k)$ being the power spectrum of the density fluctuation.

Previous analyses mainly compared the observed genus etc. with the random Gaussian prediction (3.3.1)–(3.3.3). With sufficiently large smoothing scales, this comparison could tell us if initial density fluctuation is random Gaussian or not. With the finite smoothing scale of cosmological interest, the effect of nonlinear gravitational evolution would be substantial. This nonlinear effect has been explored only by using N-body numerical simulations so far. In the following, general formulae of the isodensity contours for the field with weak non-Gaussianity is presented. These formulae is incorporated in the second order perturbation theory. The smoothing effect on perturbation theory is also considered (Matsubara 1994b; Matsubara 1995a).

3.3.2 Isodensity Statistics for Quasi-Gaussian Random Field

First, we introduce the seven quantities for a non-Gaussian random field $\delta(x,y,z)$ with zero mean as $(A_\mu) = \sigma^{-1}(\delta, \partial\delta/\partial x, \partial\delta/\partial y, \partial\delta/\partial z, \partial^2\delta/\partial x^2, \partial^2\delta/\partial y^2, \partial^2\delta/\partial x\partial y)$ where $\sigma \equiv \sqrt{\langle\delta^2\rangle}$ is *rms* of the field and the field is defined in Cartesian coordinates x, y, z. The statistics of isodensity contours G, G_2, N_1, N_2, N_3 of constant surfaces $\delta = \nu\sigma$ is given by (Ryden 1988; Ryden et al. 1989; Adler 1981; Doroshkevich 1970; Bardeen et al. 1986; Bond & Efstathiou 1987)

$$G(\nu) = -\frac{1}{2}\left\langle\delta_D(A_1-\nu)\delta_D(A_2)\delta_D(A_3)|A_4|(A_5A_6-A_7^2)\right\rangle, \tag{3.3.5}$$

$$G_2(\nu) = -\frac{1}{2}\left\langle\delta(A_1-\nu)\delta_D(A_2)|A_3|A_5\right\rangle, \tag{3.3.6}$$

$$2N_1(\nu) = \frac{4}{\pi}N_2(\nu) = N_3(\nu) = 2\left\langle\delta(A_1-\nu)\,|A_2|\right\rangle, \tag{3.3.7}$$

where δ_D is a Dirac's delta-function. This expression is valid for general homogeneous and isotropic non-Gaussian random fields.

Let us proceed to evaluating the expectation value (equations [3.3.5]–[3.3.7]) for weakly non-Gaussian field. As usual, we define a partition function $Z(J_\mu)$ as a Fourier transform of a distribution function $P(A_\mu)$ of quantities A_μ: with the partition function for a distribution function $P(A_\mu)$,

$$Z(J_\mu) = \int_{-\infty}^{\infty} d^7A\, P(A_\mu) \exp\left(i \sum_\nu J_\nu A_\nu\right), \tag{3.3.8}$$

the cumulant expansion theorem (see section 2.3 and Appendix A) states that $\ln Z(J_\mu)$ is a generating function of connected correlation function $\psi^{(N)}_{\mu_1 \cdots \mu_N} = \langle A_{\mu_1} \cdots A_{\mu_N} \rangle_{\rm c}$. Then one obtains the inverse Fourier transform of equation (3.3.8) in the following useful form:

$$P(A_\mu) = \exp\left(\sum_{N=3}^{\infty} \frac{(-)^N}{N!} \sum_{\mu_1,\ldots,\mu_N} \psi^{(N)}_{\mu_1 \cdots \mu_N} \frac{\partial^N}{\partial A_{\mu_1} \cdots \partial A_{\mu_N}}\right) P_{\rm G}(A_\mu), \tag{3.3.9}$$

where

$$P_{\rm G}(A_\mu) = \frac{1}{\sqrt{(2\pi)^7 \det\left(\psi^{(2)}_{\mu\nu}\right)}} \exp\left(-\frac{1}{2} \sum_{\mu,\nu} A_\mu \left(\psi^{(2)-1}\right)_{\mu\nu} A_\nu\right), \tag{3.3.10}$$

is a multivariate Gaussian distribution function characterized by a correlation matrix $\psi^{(2)}_{\mu\nu}$. The inverse of this correlation matrix is denoted as $\psi^{(2)-1}$. In a weakly non-Gaussian case, the exponential function in equation (3.3.9) is expanded in Taylor series and equations (3.3.5)–(3.3.7) is expanded by higher-order correlations. In the following, we assume that $\psi^{(N)} \sim \mathcal{O}(\sigma^{N-2})$. This relation is a very definition of "weak non-Gaussianity" in this letter and is a result of perturbation theory (Fry 1984b; Goroff et al. 1986; Bernardeau 1992). Thus to the first order in σ, the expectation value of some function $F(A_\mu)$ is

$$\langle F \rangle = \langle F \rangle_{\rm G} + \frac{1}{6} \sum_{\mu,\nu,\lambda} \psi^{(3)}_{\mu\nu\lambda} \left\langle \frac{\partial^3 F}{\partial A_\mu \partial A_\nu \partial A_\lambda} \right\rangle_{\rm G} + \mathcal{O}(\sigma^2), \tag{3.3.11}$$

where $\langle \cdots \rangle_{\rm G}$ denotes averaging by multivariate Gaussian distribution (eq.[3.3.10]). This expansion can be regarded as based on a multi-dimensional version of the Edgeworth expansion. The usual one-dimensional Edgeworth expansion was recently applied to gravitational instability theory (Juszkiewicz et al. 1994; Bernardeau & Kofman 1994). All the terms in *r.h.s.* of equation (3.3.11) can be evaluated by

straightforward but tedious Gaussian integrals. Spatial homogeneity and isotropy simplify the final result as

$$G(\nu) = -\frac{1}{(2\pi)^2}\left(\frac{\langle k^2\rangle}{3}\right)^{3/2} e^{-\nu^2/2} \times\left[H_2(\nu)+\sigma\left(\frac{S}{6}H_5(\nu)+\frac{3T}{2}H_3(\nu)+3UH_1(\nu)\right)+\mathcal{O}(\sigma^2)\right], \quad (3.3.12)$$

$$G_2(\nu) = \frac{1}{(2\pi)^{3/2}}\frac{\langle k^2\rangle}{3}e^{-\nu^2/2} \times\left[H_1(\nu)+\sigma\left(\frac{S}{6}H_4(\nu)+TH_2(\nu)+U\right)+\mathcal{O}(\sigma^2)\right], \quad (3.3.13)$$

$$2N_1(\nu) = \frac{4}{\pi}N_2(\nu) = N_3(\nu) = \frac{2}{\pi}\left(\frac{\langle k^2\rangle}{3}\right)^{1/2} e^{-\nu^2/2}\left[1+\sigma\left(\frac{S}{6}H_3(\nu)+\frac{T}{2}H_1(\nu)\right)+\mathcal{O}(\sigma^2)\right], \quad (3.3.14)$$

where $H_n(\nu) = (-)^n e^{\nu^2/2}(d/d\nu)^n e^{-\nu^2/2}$ are Hermite polynomials, and we have defined three quantities,

$$\begin{aligned} S &= \frac{1}{\sigma^4}\langle\delta^3\rangle, \\ T &= -\frac{1}{2\langle k^2\rangle\sigma^4}\langle\delta^2\nabla^2\delta\rangle, \\ U &= -\frac{3}{4\langle k^2\rangle^2\sigma^4}\langle\nabla\delta\cdot\nabla\delta\nabla^2\delta\rangle. \end{aligned} \quad (3.3.15)$$

The quantity S is usually called "skewness". The first term in square brackets of equations (3.3.12)–(3.3.14) corresponds to Gaussian contribution and the other terms correspond to non-Gaussian contribution.

As an illustrative application of this result, we consider the case that correlation functions are given by hierarchical model. In hierarchical model, connected correlation function of N-th order is modeled as a sum of $N-1$ products of ξ, thus our previous assumption $\psi^{(N)} \sim \mathcal{O}(\sigma^{N-2})$ is satisfied. Specifically, third order correlation function $\zeta(\boldsymbol{x},\boldsymbol{y},\boldsymbol{z}) = \langle\delta(\boldsymbol{x})\delta(\boldsymbol{y})\delta(\boldsymbol{z})\rangle$ is related to $\xi(|\boldsymbol{x}-\boldsymbol{y}|) = \langle\delta(\boldsymbol{x})\delta(\boldsymbol{y})\rangle$ by

$$\zeta(\boldsymbol{x},\boldsymbol{y},\boldsymbol{z}) = Q[\xi(|\boldsymbol{x}-\boldsymbol{y}|)\xi(|\boldsymbol{y}-\boldsymbol{z}|)+\xi(|\boldsymbol{y}-\boldsymbol{z}|)\xi(|\boldsymbol{z}-\boldsymbol{x}|)+\xi(|\boldsymbol{z}-\boldsymbol{x}|)\xi(|\boldsymbol{x}-\boldsymbol{y}|)], \quad (3.3.16)$$

where Q is a constant (undetermined in this model). If this equation (3.3.16) is exact for some large smoothing scale such that $\xi(0) = \sigma^2 \ll 1$, the quantities S,

T and U reduces to $3Q$, $2Q$ and Q, respectively, and the statistics of isodensity contours with correction terms of non-Gaussianity are

$$G^{(\mathrm{hi.})}(\nu) = \frac{1}{4\pi^2}\left(\frac{\langle k^2\rangle}{3}\right)^{3/2} e^{-\nu^2/2}\left[1-\nu^2-\frac{Q}{2}\nu(\nu^2-1)(\nu^2-3)\sigma\right]+\mathcal{O}(\sigma^2), \tag{3.3.17}$$

$$G_2^{(\mathrm{hi.})}(\nu) = \frac{1}{(2\pi)^{3/2}}\frac{\langle k^2\rangle}{3}e^{-\nu^2/2}\left[\nu+\frac{Q}{2}(\nu^2-1)^2\sigma\right]+\mathcal{O}(\sigma^2), \tag{3.3.18}$$

$$\begin{aligned} 2N_1(\nu) &= \frac{4}{\pi}N_2(\nu) = N_3(\nu) \\ &= \frac{2}{\pi}\left(\frac{\langle k^2\rangle}{3}\right)^{1/2} e^{-\nu^2/2}\left[1+\frac{Q}{2}\nu(\nu^2-1)\sigma\right]+\mathcal{O}(\sigma^2). \end{aligned} \tag{3.3.19}$$

Figures 3.9(a) – 3.11(a) plot the results for $Q\sigma = 0, 0.2, 0.4, 0.6$.

3.3.3 Gravitational evolution of statistics of isodensity contour in second order perturbation theory

Gravitational nonlinear evolution give rise to S, T, U even from the initial Gaussian random density fluctuation which has vanishing S, T, U. We use second order perturbation theory of the non-relativistic collisionless self-gravitating system in the fluid limit (e.g., Peebles 1980, §18) to compute S, T, U to lowest order in σ in Einstein-de Sitter universe. Considering growing mode only, third order correlation function in Fourier space is given by (Fry 1984; Goroff et al. 1986)

$$\begin{aligned} \left\langle\tilde{\delta}(\boldsymbol{k}_1)\tilde{\delta}(\boldsymbol{k}_2)\tilde{\delta}(\boldsymbol{k}_3)\right\rangle &= (2\pi)^3\delta_D^3(\boldsymbol{k}_1+\boldsymbol{k}_2+\boldsymbol{k}_3) \\ &\times\left\{\left[\frac{10}{7}+\left(\frac{k_1}{k_2}+\frac{k_2}{k_1}\right)\frac{\boldsymbol{k}_1\cdot\boldsymbol{k}_2}{k_1k_2}+\frac{4}{7}\left(\frac{\boldsymbol{k}_1\cdot\boldsymbol{k}_2}{k_1k_2}\right)^2\right]P(k_1)P(k_2)+\mathrm{cyc.}\right\}, \end{aligned} \tag{3.3.20}$$

where $P(k)$ is a power spectrum of linear theory. Evaluating S, T, U (eq.[3.3.15]) in Fourier space with equation (3.3.20) results in,

$$S = \frac{34}{7}, \quad T = \frac{82}{21}, \quad U = \frac{54}{35} \tag{3.3.21}$$

This value of the skewness S was already given by Peebles (1980). Note that S, T, U are independent on the shape of the initial power spectrum. The resulting genus curve etc. are plotted in Figures 3.9(b)–3.11(b) for $\sigma = 0, 0.2, 0.4, 0.6$.

In fact, the observable curve is obtained by smoothing of density fluctuation while the above result is not for a smoothed field. Next we evaluate the smoothing effect in the case that the smoothed density fluctuation with sufficiently large

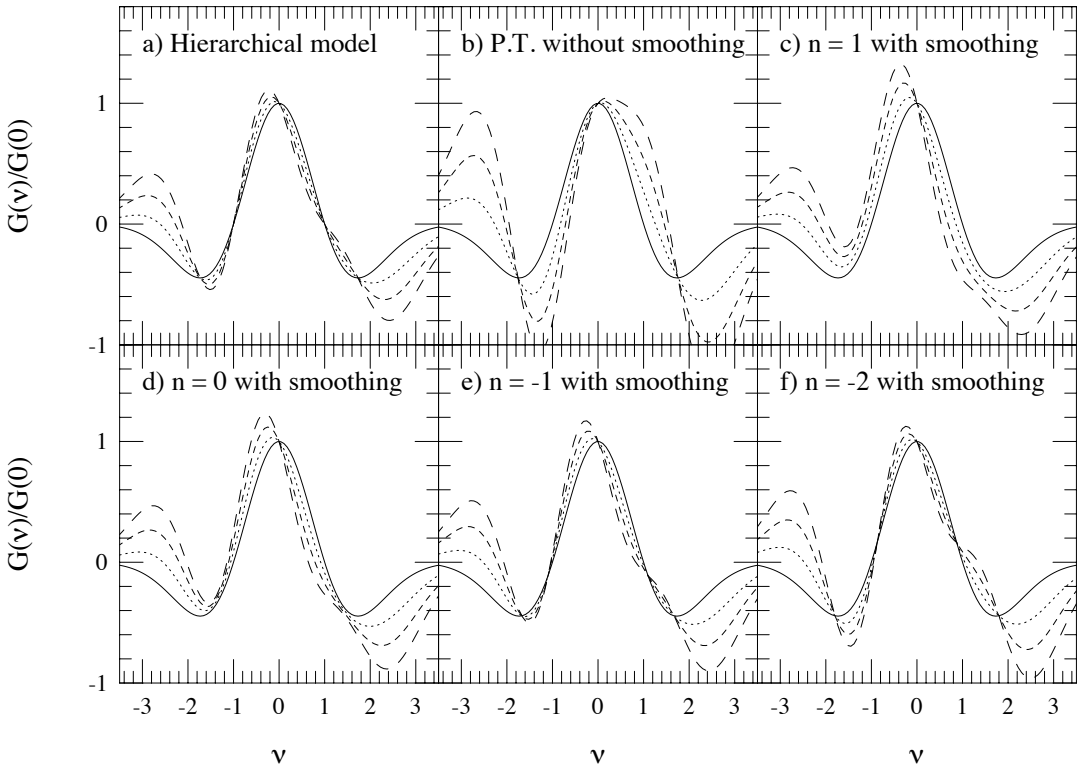

Figure 3.9: Asymmetries of the normalized genus curves $G(\nu)/G(0)$ induced by non-Gaussianity to first order of *rms* σ of fluctuation. The sources of non-Gaussianity are (a) hierarchical model, (b) unsmoothed perturbation theory with Gaussian initial fluctuations, Gaussian-smoothed perturbation theory with Gaussian initial fluctuations of power-law spectra, (c) $P(k) \propto k$, (d) $P(k) = \text{const.}$, (e) $P(k) \propto k^{-1}$, (f) $P(k) \propto k^{-2}$. Solid lines, dotted lines, dashed lines, long-dashed lines show $\sigma =$ (in (a), $Q\sigma =$) $0, 0.2, 0.4, 0.6$ cases, respectively.

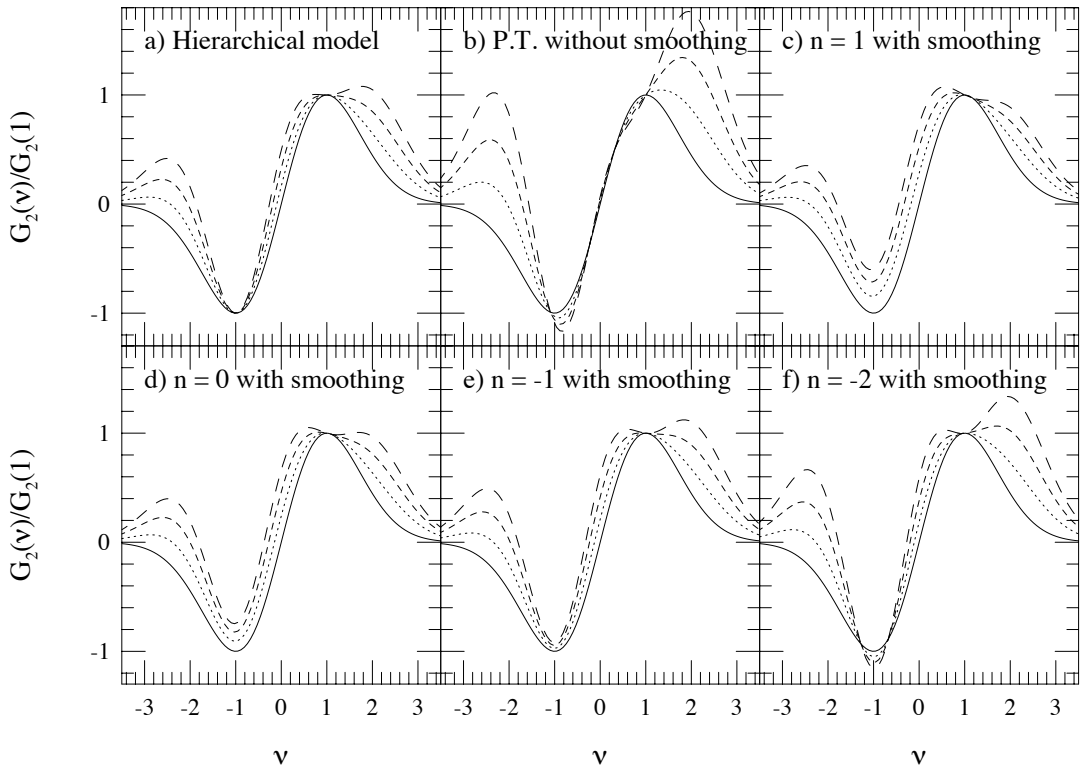

Figure 3.10: Asymmetries of the normalized 2D genus curves $G_2(\nu)/G_2(1)$ as in the previous figure.

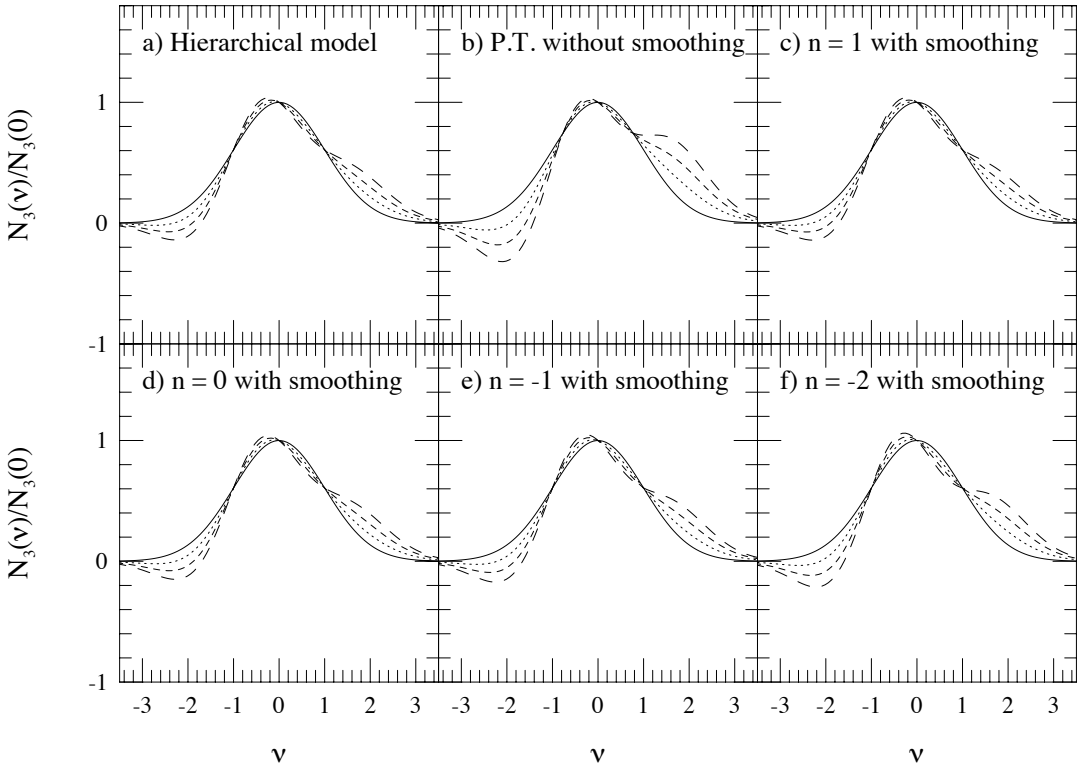

Figure 3.11: Asymmetries of the area of isodensity contour $N_3(\nu)/N_3(0)$ as in the previous figure.

smoothing scale is well described by second order perturbation theory. Recently, Juszkiewicz, Bouchet & Colombi (1993) gave the smoothing effect on the skewness S for Gaussian and top-hat filter. In the following, we use the Gaussian filter $\delta_R(\boldsymbol{x}) = (2\pi R^2)^{-3/2} \int d^3y \delta(\boldsymbol{y}) \exp(-|\boldsymbol{x}-\boldsymbol{y}|^2/2R^2)$ which is usually adopted in smoothing noisy observational data. The quantities S, T, U for Gaussian smoothed field δ_R are obtained similarly as in the unsmoothed case, and the result is

$$
\begin{aligned}
S &= \frac{1}{4\pi^4}\left[(2+K)L_{220} + 3L_{131} + (1-K)L_{222}\right], \\
T &= \frac{1}{60\pi^4}[5(5+2K)L_{240} + 3(9+K)L_{331} + 15L_{151} \\
&\qquad +10(2-K)L_{242} + 3(1-K)L_{333}], \qquad (3.3.22) \\
U &= \frac{1}{140\pi^4}\left[7(3+2K)L_{440} + 21L_{351} - 5(3+4K)L_{442} - 21L_{353} - 6(1-K)L_{444}\right].
\end{aligned}
$$

Here we introduce the following integrals:

$$
\begin{aligned}
L_{\alpha\beta n}(R) &\equiv \frac{\langle k^2 \rangle^{2-(\alpha+\beta)/2}}{\sigma_R^4} \\
&\times \int_0^\infty dx \int_0^\infty dy \int_{-1}^1 d\mu e^{-R^2(x^2+y^2+\mu xy)} x^\alpha y^\beta P_n(\mu) P(x) P(y) \qquad (3.3.23) \\
&= (-)^n \sqrt{2\pi} \frac{\langle k^2 \rangle^{2-(\alpha+\beta)/2}}{\sigma_R^4 R} \\
&\times \int_0^\infty dx \int_0^\infty dy e^{-R^2(x^2+y^2)} x^{\alpha-1/2} y^{\beta-1/2} I_{n+1/2}(xyR^2) P(x) P(y), \qquad (3.3.24)
\end{aligned}
$$

where σ_R is the rms amplitude of the Gaussian smoothed density fluctuation with R, P_n is the Legendre polynomial, and I_ν is a modified Bessel function. The above results hold for arbitrary cosmological models with Ω and λ. The latter effect manifests only through $K = K(\Omega, \lambda)$ defined by equation (2.2.39) which very weakly depends on Ω and λ. When $R \to 0$, the dependence of equation (3.3.22) on the initial power spectrum is canceled and equation (3.3.19) is rederived. The statistics of isodensity contours for smoothed field is dependent on the specific shape of initial power spectrum on the contrary to the unsmoothed one. For the power-law fluctuation spectra $P(k) \propto k^n$, S, T and U can be written down explicitly in terms of the hypergeometric function as

$$
\begin{aligned}
S &= 3F\left(\frac{n+3}{2}, \frac{n+3}{2}, \frac{3}{2}; \frac{1}{4}\right) - (n+2-2K)F\left(\frac{n+3}{2}, \frac{n+3}{2}, \frac{5}{2}; \frac{1}{4}\right), \\
T &= 3F\left(\frac{n+3}{2}, \frac{n+5}{2}, \frac{3}{2}; \frac{1}{4}\right) - (n+3-K)F\left(\frac{n+3}{2}, \frac{n+5}{2}, \frac{5}{2}; \frac{1}{4}\right) \\
&\qquad + \frac{(n-2)(1-K)}{15} F\left(\frac{n+3}{2}, \frac{n+5}{2}, \frac{7}{2}; \frac{1}{4}\right), \qquad (3.3.25)
\end{aligned}
$$

	unsmoothed	$n=1$	$n=0$	$n=-1$	$n=-2$	$n=-3$	CDM	HDM
S	4.857	3.029	3.144	3.468	4.022	4.857	3.443	4.018
T	3.905	2.020	2.096	2.312	2.681	3.238	2.335	2.970
U	1.543	1.431	1.292	1.227	1.222	1.272	1.223	1.306

Table 3.1: The numerical values of S, T, U for unsmoothed perturbation theory and smoothed perturbation theory for power-law spectra, $n = 1$ to -3, CDM and HDM models.

$$U = F\left(\frac{n+5}{2}, \frac{n+5}{2}, \frac{5}{2}; \frac{1}{4}\right) - \frac{n+4-4K}{5} F\left(\frac{n+5}{2}, \frac{n+5}{2}, \frac{7}{2}; \frac{1}{4}\right).$$

The expressions for S in equations (3.3.22) and (3.3.25) are derived by Lokas et al. (1995) which are equivalent to the other form independently derived by Matsubara (1994b). Similarly we transform the expressions for T and U presented in Matsubara (1994b; eqs. [16] and [18]) using the function $L_{\alpha\beta n}(R)$, which are given in equations (3.3.22) and (3.3.25). Numerical values of S, T, U for power-law initial spectra, CDM and HDM models are summarized in Table 3.1. In CDM and HDM models, we set $\Omega_0 = 1$, $h = 0.5$ and smoothing length = 10 Mpc. The values of skewness S in this table was first obtained by Juszkiewicz et al. (1994). The corresponding genus curves etc. for $n = 1, 0, -1, -2$ are shown in Figures 3.9(c–f)–3.11(c–f) for $\sigma = 0, 0.2, 0.4, 0.6$.

The prominent feature of the results, equations (3.3.12)–(3.3.14) is that weakly non-Gaussian correction introduces asymmetry to the symmetric or anti-symmetric curves. The pattern of the asymmetry is dependent on initial power spectra through smoothing effect of S, T, U. Thus, in principle, accurate observations on the statistics presented here can restrict the properties of initial fluctuation, such as Gaussianity, the shape of the spectrum, by the amplitude and the pattern of asymmetry of the curve. The projects as Sloan Digital Sky Survey (SDSS) will enable us to have a large amount of redshift data in near future and the analysis indicated here will be important.

3.3.4 Comparisons with numerical simulations

We found that the analytic expression of the genus curve agrees well with the numerical N-body simulations for power-law initial fluctuations $P(k) \propto k^n$ and CDM models (Matsubara & Suto 1995). In Figure 3.12 is plotted the normalized genus $G(\nu)/G(0)$ as an example of the comparison. The initial fluctuation is the Pois-

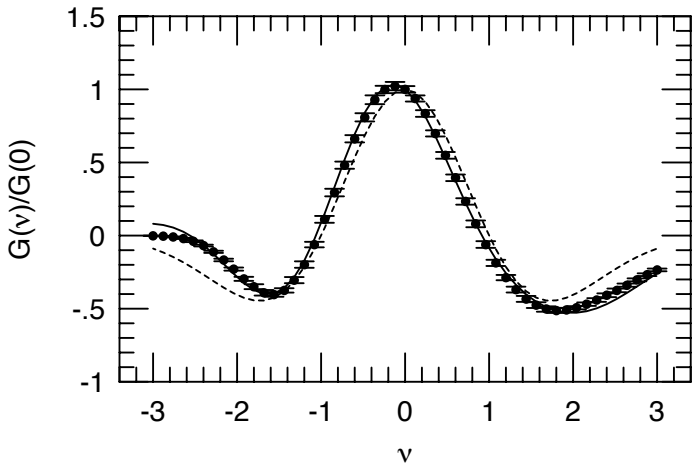

Figure 3.12: Comparison of the analytic genus curve (a solid line) with that from an N-body simulation (symbols) for the Poisson model at $\sigma = 0.2$. A dashed line indicate the Gaussian prediction.

son model $P(k) = \text{const}$. The *rms* of the fluctuation at the stage of comparison is $\sigma = 0.2$.

3.4 STRONGLY NONLINEAR CLUSTERING IN REDSHIFT SPACE

3.4.1 Statistics in redshift space

Conventional cosmological observations provide direct information on large-scale structure in redshift space which, however, is not necessarily the same as that in real space due to the presence of peculiar velocities of galaxies. If galaxies move purely with the uniform Hubble expansion, redshift surveys would tell us the real distribution of galaxies. In reality, however, the peculiar velocities of galaxies distort the distribution in mapping from real space to redshift space. The distortion is along the line of sight and the clustering pattern of galaxies in redshift space becomes anisotropic.

There are two characteristic features in the redshift space distortion. On small scales, the random peculiar motions in virializing clusters stretch the shape of clusters along the line of sight: the 'finger of God' effect. As a result, the strength of the clustering is weaker in redshift space than in real space (e.g., Lilje & Efstathiou 1989; Suto & Suginohara 1991; Peacock 1993; Matsubara 1994a). On large scales, the coherent velocity field falling in the region with the excess mass make the pertur-

bation enhanced along the line of sight, in contrast to the small-scale case (Sargent & Turner 1977; Kaiser 1987; Lilje & Efstathiou 1989; McGill 1990; Hamilton 1992). Peacock (1992) phenomenologically represented this small-scale effect by assuming Gaussian smearing of the density contrast in Fourier space. These effects on two-, three- and four-point correlation functions were studied numerically in Suto & Suginohara (1991), Matsubara & Suto (1994) and Suto & Matsubara (1994) using N-body simulations (section 3.2).

One possible way to check the scaling relation (3.1.8) and/or hierarchical model (3.1.9) in real space is to study redshift surveys of galaxies at the cost of the contamination by the peculiar velocities. De Lapparent, Geller & Huchra (1988), for example, estimated the two-point correlation in redshift space:

$$\xi(s) = \left(\frac{s}{s_0}\right)^{-\gamma} \qquad (3h^{-1}\mathrm{Mpc} < s < 14h^{-1}\mathrm{Mpc}) \tag{3.4.1}$$

$$s_0 = (7.5^{+1.9}_{-1.5})h^{-1}\mathrm{Mpc} \quad \text{and} \quad \gamma = 1.6 \pm 0.3. \tag{3.4.2}$$

There are many papers which claim indirectly the validity of the relation (3.1.8) and/or (3.1.9) using redshift surveys (e.g., Alimi, Blanchard & Schaeffer 1990; Maurogordato, Schaeffer & da Costa 1992; Gaztañaga 1992; but see Vogeley Geller & Huchra 1991). Redshift surveys are sometimes studied without any inversion to real-space distribution nor correction for the peculiar velocity contamination. Thus it is important to clarify the effect of the contamination on the models for the N-point correlation functions (3.1.8) $\sim$ (3.1.9) as we will attempt in the following section (Matsubara 1994a).

3.4.2 A model for correlation functions on small scales in redshift space

To specify the model below, we need a distribution function of peculiar velocities. For that purpose, we will use, in this subsection, the particle-averaged distribution function $f(\boldsymbol{v})$. Therefore we do not take account of, for instance, the difference of velocities in high density or low density region. In fact, it is found observationally that the dependence of distribution function of velocities on its location is weak: the observed two-point velocity correlation $\langle v_{12}^2 \rangle^{1/2}$ varies as $\sim r_{12}^{0.1}$ (Davis & Peebles 1983) where v_{12} is a relative velocity of a pair of galaxies with separation r_{12}. The cosmic virial theorem (Peebles 1980 §75) also indicates this behavior provided that three-point correlation function has the hierarchical form (3.1.2) at least approximately. Because the dependence on the separation is weak, we can reasonably assume that

all the galaxies have the same velocity distribution independently of their locations. The effect of velocity correlations will be discussed in the next subsection.

We are interested in the line-of-sight component of the peculiar velocity, v, and denote the probability distribution function for v as $f_\sigma(v)$ where σ is the root-mean-square value of the velocity dispersion $\sqrt{\langle v^2 \rangle}$ where the averaging $\langle v^2 \rangle$ is particle-weighted. Independence of $f_\sigma(v)$ on location reflects the above assumption. It should be noted that the coherent motion of galaxies according to linear theory (Kaiser 1987) is not included in our model. The coherent motion would enhance the correlations on large scales $\gtrsim (5 \sim 10)h^{-1}$Mpc, so our model should be applied on small scales $\lesssim$ a few h^{-1}Mpc, which corresponds to a typical size for clusters of galaxies.

The relation between number densities in real space $\rho^{(r)}(\boldsymbol{r})$ and in redshift space $\rho^{(s)}(\boldsymbol{s})$ is given by

$$\rho^{(s)}(\boldsymbol{s}) = \int_{-\infty}^{\infty} dv f_\sigma(v) \rho^{(r)}(\boldsymbol{s} + H_0^{-1} v \hat{\boldsymbol{s}}), \tag{3.4.3}$$

where an observer is at the origin of the coordinate and $\hat{\boldsymbol{s}} \equiv \boldsymbol{s}/|\boldsymbol{s}|$. To see the relation (3.4.3), it is useful to consider the infinitesimal cylinder at $\boldsymbol{s}$ with each base ΔS and a length $\Delta l^{(s)}$ with its bases normal to the line of sight. Then the probability that a galaxy is in that cylinder in redshift space is

$$\rho^{(s)}(\boldsymbol{s}) \Delta S \Delta l^{(s)} = \int_{-\infty}^{\infty} dl \Delta S \rho^{(r)}(\boldsymbol{s} + l\hat{\boldsymbol{s}}) f_\sigma(H_0 l) H_0 \Delta l^{(s)}. \tag{3.4.4}$$

This proves the relation (3.4.3). In terms of density contrast, $\delta \equiv (\rho - \bar{\rho})/\bar{\rho}$, where $\bar{\rho}$ denotes the mean density, relation (3.4.3) is given by

$$\delta^{(s)}(\boldsymbol{s}) = \int_{-\infty}^{\infty} dv f_\sigma(v) \delta^{(r)}(\boldsymbol{s} + H_0^{-1} v \hat{\boldsymbol{s}}), \tag{3.4.5}$$

where we used the normalization condition, $\int dv f(v) = 1$, and the fact that the mean densities take the same value both in real and in redshift space.

If two galaxies in redshift space at $\boldsymbol{s}_1$ and $\boldsymbol{s}_2$ are far enough from the observer compared to the separation of the galaxies $s_{12} \equiv |\boldsymbol{s}_1 - \boldsymbol{s}_2|$, i.e., $s_{12} \ll |\boldsymbol{s}_1|, |\boldsymbol{s}_2|$, we can approximate $\widehat{\boldsymbol{s}_1} = \widehat{\boldsymbol{s}_2} \equiv \hat{\boldsymbol{n}}$, where $\hat{\boldsymbol{n}}$ represents the direction of the line-of-sight to the pair of galaxies. Then we can calculate the two-point correlation function in redshift space using equation (3.4.5):

$$\begin{aligned} \xi_\sigma^{(s)}(s_{12}; \theta_{12}) &\equiv \left\langle \delta^{(s)}(\boldsymbol{s}_1) \delta^{(s)}(\boldsymbol{s}_2) \right\rangle \\ &= \int_{-\infty}^{\infty} dv_1 dv_2 f_\sigma(v_1) f_\sigma(v_2) \xi^{(r)} \left[r_{12}(v_1 - v_2; s_{12}, \theta_{12}) \right], \end{aligned} \tag{3.4.6}$$

where

$$r_{12}(v_1 - v_2; s_{12}, \theta_{12}) = H_0^{-1}\sqrt{(v_1 - v_2)^2 - 2H_0(v_1 - v_2)s_{12}\cos\theta_{12} + H_0^2 s_{12}^2}, \quad (3.4.7)$$

and θ_{12} is the angle between line-of-sight and the direction of a vector $\boldsymbol{s}_{21} \equiv \boldsymbol{s}_2 - \boldsymbol{s}_1$, i.e., $\cos\theta_{12} = \hat{\boldsymbol{n}} \cdot \boldsymbol{s}_{21}/|\boldsymbol{s}_{21}|$. Using equation (3.4.5), the three-point correlation function in redshift space can be derived similarly:

$$\begin{aligned}\zeta_\sigma^{(s)}(s_{12}, s_{23}, s_{31}; \theta_{12}, \theta_{23}, \theta_{31}) &= \left\langle \delta^{(s)}(\boldsymbol{s}_1)\delta^{(s)}(\boldsymbol{s}_2)\delta^{(s)}(\boldsymbol{s}_3)\right\rangle \\ &= \int_{-\infty}^{\infty} dv_1 dv_2 dv_3 f_\sigma(v_1) f_\sigma(v_2) f_\sigma(v_3) \zeta^{(r)}\left[r_{12}, r_{23}, r_{31}\right], \quad (3.4.8)\end{aligned}$$

where r_{ij}, θ_{ij} $(ij = 12, 23, 31)$ are defined in equation (3.4.7) with permutations of its indices. More generally, the reduced (connected) N-point correlation function $\xi_N^{(s)}$ in redshift space is related to its real space counterpart $\xi_N^{(r)}$ as

$$\xi_{N,\sigma}^{(s)}(\{s_{ij}\}; \{\theta_{ij}\}) = \left\langle \prod_{i=1}^{N} \delta^{(s)}(\boldsymbol{s}_i)\right\rangle_{\rm c} = \int_{-\infty}^{\infty} \left(\prod_{i=1}^{N} dv_i f_\sigma(v_i)\right) \xi_N^{(r)}\left[\{r_{ij}\}\right], \quad (3.4.9)$$

where

$$r_{ij}(v_i - v_j; s_{ij}, \theta_{ij}) = H_0^{-1}\sqrt{(v_i - v_j)^2 - 2H_0(v_i - v_j)s_{ij}\cos\theta_{ij} + H_0^2 s_{ij}^2}, \quad (3.4.10)$$

and θ_{ij} is the angle between the line of sight and the direction of $\boldsymbol{s}_j - \boldsymbol{s}_i$, and $\langle\cdots\rangle_{\rm c}$ indicates the cumulants (or connected part). The arguments $\{s_{ij}\}$ and $\{\theta_{ij}\}$ of $\xi_N^{(s)}$ are not completely independent for $N \geq 3$; the condition that all the triangles in redshift space should be closed imposes the following constraints:

$$s_{ij}\cos\theta_{ij} + s_{jk}\cos\theta_{jk} + s_{ki}\cos\theta_{ki} = 0, \quad (3.4.11)$$

where i, j, k are all different positive integers and are less than or equal to N.

We will apply this model to examine the correlations in redshift space and the hierarchical ansatz. As for the velocity distribution $f_\sigma(v)$, we mainly adopt the exponential distribution:

$$f_\sigma(v) = \frac{1}{\sqrt{2}\sigma} e^{-\sqrt{2}|v|/\sigma}, \quad (3.4.12)$$

which is observationally favorable compared to Gaussian distribution:

$$f_\sigma(v) = \frac{1}{\sqrt{2\pi}\sigma} e^{-v^2/(2\sigma^2)}. \quad (3.4.13)$$

In fact, the available observations of galaxies (Davis & Peebles 1983) and numerical simulations (Ueda, Itoh & Suto 1993) suggest the form (3.4.12) rather than equation (3.4.13). We will also use the Gaussian form (3.4.13) later for the purpose of comparison.

Note that if the characteristic scale of distribution f_σ is only its *rms* σ, the dimensional argument shows that f scales as $f_{\nu\sigma}(v) = \nu^{-1} f_\sigma(\nu^{-1}v)$, as explicitly seen in equations (3.4.12) and (3.4.13). In addition to that, if the scaling property (3.1.8) is correct, the following scaling relation is derived:

$$\xi^{(s)}_{N,\nu\sigma}(\{s_{ij}\}) = \nu^{-(N-1)\gamma}\xi^{(s)}_{N,\sigma}\left(\{\nu^{-1}s_{ij}\}\right), \tag{3.4.14}$$

where $\xi^{(s)}_{N,\sigma}(\{s_{ij}\})$ are direction averaged N-point correlation functions in redshift space $\xi^{(s)}_{N,\sigma}(\{s_{ij}\}) \equiv \langle\xi^{(s)}_{N,\sigma}(\{s_{ij}\};\{\theta_{ij}\})\rangle_{\rm direction}$ and their explicit forms are given below for $N = 2$ and 3.

3.4.3 Velocity correlations

In the previous section, we obtained a simple formula (3.4.9) by ignoring the velocity correlations. Because the velocity correlations are weak as noted in the previous subsection, our formula (3.4.9) is considered to be a first approximation. We discuss here how the velocity correlations affect this formula and propose a modified formula (3.4.27) below.

For that purpose, let us first consider the conditional probability that line-of-sight velocities of N-galaxies are between v_i and $v_i + \delta v_i$, $(i = 1, \ldots, N)$ when these N-galaxies are at $\boldsymbol{r}_1, \ldots, \boldsymbol{r}_N$. We denote the probability as

$$R_N(v_1, \ldots, v_N|\boldsymbol{r}_1, \ldots, \boldsymbol{r}_n)\prod_{i=1}^{N}\delta v_i. \tag{3.4.15}$$

In the previous subsection, R_N was approximated simply by $\prod_{i=1}^N f_\sigma(v_i)$. More generally, however, the distribution of line-of-sight component of peculiar velocity v_i for i-th galaxy is the function of $\boldsymbol{r}_1, \ldots, \boldsymbol{r}_N$ and possibly of $v_1, \ldots, v_{i-1}, v_{i+1}, \ldots, v_N$. To take this dependence fully into consideration is complicated and is beyond the scope of this paper. Our approximation here is to assume that this dependence is only through the dispersion of line-of-sight velocities $\sigma(\boldsymbol{r}_1, \ldots, \boldsymbol{r}_N)$ for each galaxy, and then the probability (3.4.15) is given by

$$R_N(v_1, \ldots, v_N|\boldsymbol{r}_1, \ldots, \boldsymbol{r}_n) = \prod_{i=1}^{N} f(v_i; \sigma(\boldsymbol{r}_1, \ldots, \boldsymbol{r}_N)), \tag{3.4.16}$$

where

$$f(v,\sigma) \equiv f_\sigma(v). \tag{3.4.17}$$

Next we denote the probability density that the galaxies are at $\boldsymbol{r}_1,\ldots,\boldsymbol{r}_N$ as $P_N(\boldsymbol{r}_1,\ldots,\boldsymbol{r}_N)$. This quantity is related to real-space N-point correlation function $\xi_N^{(r)}$ as

$$P_N(\boldsymbol{r}_1,\ldots,\boldsymbol{r}_N) = \bar{\rho}^N \left[\xi_N^{(r)}(\boldsymbol{r}_1,\ldots,\boldsymbol{r}_N) + \text{disconnected parts}\right], \tag{3.4.18}$$

where "disconnected parts" represents the terms expressed by lower order correlation functions (see, e.g., Peebles 1980; Bertschinger 1992). The joint probability density S_N that the galaxies are at $\boldsymbol{r}_1,\ldots,\boldsymbol{r}_N$ and line-of-sight velocities are $v_1,\ldots,v_N$ is expressed as

$$\begin{aligned} S_N(\boldsymbol{r}_1,\ldots,\boldsymbol{r}_N; v_1,\ldots,v_N) &= P_N R_N \\ &= P_N(\boldsymbol{r}_1,\ldots,\boldsymbol{r}_N) \prod_{i=1}^{N} f(v_i;\sigma(\boldsymbol{r}_1,\ldots,\boldsymbol{r}_N)). \end{aligned} \tag{3.4.19}$$

Using these quantities, the probability density that the galaxies are at $\boldsymbol{s}_1,\ldots,\boldsymbol{s}_N$ in redshift space is given by

$$\begin{aligned} & P_N^{(s)}(\boldsymbol{s}_1,\ldots,\boldsymbol{s}_N) \\ &= \int_{-\infty}^{\infty} \prod_{i=1}^{N} dv_i S_N\left[\boldsymbol{r}(\boldsymbol{s}_1,v_1),\ldots,\boldsymbol{r}(\boldsymbol{s}_N,v_N); v_1,\ldots,v_N\right] \\ &= \int_{-\infty}^{\infty} \left(\prod_{i=1}^{N} dv_i f\left[v_i;\sigma\left(\boldsymbol{r}(\boldsymbol{s}_1,v_1),\ldots,\boldsymbol{r}(\boldsymbol{s}_N,v_N)\right)\right]\right) P_N\left[\boldsymbol{r}(\boldsymbol{s}_1,v_1),\ldots,\boldsymbol{r}(\boldsymbol{s}_N,v_N)\right], \end{aligned} \tag{3.4.20}$$

where

$$\boldsymbol{r}(\boldsymbol{s},v) \equiv \boldsymbol{s} + H_0^{-1} v \hat{\boldsymbol{s}}. \tag{3.4.21}$$

The mean velocity $\sigma\left(\boldsymbol{r}(\boldsymbol{s}_1,v_1),\ldots,\boldsymbol{r}(\boldsymbol{s}_N,v_N)\right)$ is not expected to vary strongly as noted in section 3.4.2 and we denote a rough estimate of this quantity by $\bar{\sigma}$. The major contribution to the integral of equation (3.4.20) is from $v_i \lesssim \bar{\sigma}$ because of the factor f. In this region,

$$|\boldsymbol{r}(\boldsymbol{s}_i,v_i) - \boldsymbol{r}(\boldsymbol{s}_j,v_j)| \lesssim H_0^{-1}\bar{\sigma} \tag{3.4.22}$$

is satisfied on small scales such that $|\boldsymbol{s}_i - \boldsymbol{s}_j| \ll H_0^{-1}\bar{\sigma}$. The mean velocity σ is a function of left hand side of inequality (3.4.22) because of statistical homogeneity and

isotropy of the universe. At this point we make a second approximation: on small scales with inequality (3.4.22) for $i, j = 1, \ldots, N$, σ is considered to be a constant σ_N dependent only on N. Thus equation (3.4.20) is approximated as follows:

$$P_N^{(s)}(\boldsymbol{s}_1, \ldots, \boldsymbol{s}_N) = \int_{-\infty}^{\infty} \left(\prod_{i=1}^{N} dv_i f_{\sigma_N}(v_i) \right) P_N\left(\boldsymbol{r}(\boldsymbol{s}_1, v_1), \ldots, \boldsymbol{r}(\boldsymbol{s}_N, v_N)\right). \quad (3.4.23)$$

Roughly speaking, σ_N is the mean line-of-sight velocity of one of N-galaxies under condition that these N-galaxies have the mutual separations less than $H_0^{-1}\bar{\sigma}$. Thus we naturally expect that σ_N is a increasing function of N because the expected gravitational potential decreases as N increases.

We are mainly interested in the N-point correlation function ξ_N rather than the probability density P_N and we can express the above equation in terms of ξ_N using relation (3.4.18). In $N = 2$ case, two-point correlation function in redshift space in approximations in this subsection, $\xi_{\rm new}^{(s)}$, is

$$\xi_{\rm new}^{(s)}(\boldsymbol{s}_1, \boldsymbol{s}_2) = \xi_{\sigma_2}^{(s)}(s_{12}; \theta_{12}), \quad (3.4.24)$$

where $\xi_{\sigma_2}^{(s)}$ denotes the two-point function in the previous subsection defined by equation (3.4.6). In $N = 3$ case, the corresponding relation is

$$\begin{aligned} \zeta_{\rm new}^{(s)}(\boldsymbol{s}_1, \boldsymbol{s}_2, \boldsymbol{s}_3) &= \zeta_{\sigma_3}^{(s)}(s_{12}, s_{23}, s_{31}; \theta_{12}, \theta_{23}, \theta_{31}) \\ &+ \left(\xi_{\sigma_3}^{(s)}(s_{12}; \theta_{12}) - \xi_{\sigma_2}^{(s)}(s_{12}; \theta_{12})\right) + \left(\xi_{\sigma_3}^{(s)}(s_{23}; \theta_{23}) - \xi_{\sigma_2}^{(s)}(s_{23}; \theta_{23})\right) \\ &+ \left(\xi_{\sigma_3}^{(s)}(s_{31}; \theta_{31}) - \xi_{\sigma_2}^{(s)}(s_{31}; \theta_{31})\right) \end{aligned} \quad (3.4.25)$$

On small scales, $\xi^{(s)} \ll \zeta^{(s)}$ is generally satisfied in observations and in numerical simulations. Then the last three terms in the right hand side are much smaller than the first term if σ_2 and σ_3 are not much different with each other. This approximation leads the following:

$$\zeta_{\rm new}^{(s)}(\boldsymbol{s}_1, \boldsymbol{s}_2, \boldsymbol{s}_3) \simeq \zeta_{\sigma_3}^{(s)}(s_{12}, s_{23}, s_{31}; \theta_{12}, \theta_{23}, \theta_{31}). \quad (3.4.26)$$

The same argument can be extended to higher order correlations:

$$\xi_{N,\rm new}^{(s)}(\boldsymbol{s}_1, \ldots, \boldsymbol{s}_N) \simeq \xi_{N,\sigma_N}^{(s)}(\{s_{ij}\}; \{\theta_{ij}\}). \quad (3.4.27)$$

In summary, the main effect of velocity correlations on our previous formula is to make the parameter σ in equation (3.4.9) dependent on N. In spite of many approximations in this subsection, we see that equation (3.4.27) is in good agreement with numerical simulations. Before that, we examine the analytical structure of equation (3.4.9) or equation (3.4.27) using models for correlation functions in real space and velocity distribution functions in $N = 2, 3$ cases in detail.

3.4.4 Two-point correlation function in redshift space

In this section, the relation (3.4.6) is examined assuming the power-law model $\xi^{(r)}(r) = (r_0/r)^\gamma$ for the two-point correlation function in real space. After transforming variables to $u = v_1 + v_2, u' = v_1 - v_2$, and symmetrizing the integrand with respect to transformations $u \leftrightarrow u'$, $u \leftrightarrow -u$, $u' \leftrightarrow -u'$, equation (3.4.6) reduces to

$$\begin{aligned}\xi_\sigma^{(s)}(s;\theta) &= r_0^\gamma \int_0^\infty du \int_0^u du' f_\sigma\left(\frac{u+u'}{2}\right) f_\sigma\left(\frac{u-u'}{2}\right) \\ &\quad \times \Big[r_{12}(u,s,\theta)^{-\gamma} + r_{12}(-u,s,\theta)^{-\gamma} \\ &\quad + r_{12}(u',s,\theta)^{-\gamma} + r_{12}(-u',s,\theta)^{-\gamma}\Big], \end{aligned} \tag{3.4.28}$$

where we used the isotropy $f_\sigma(-v) = f_\sigma(v)$. Correlations in redshift space are anisotropic in the sense that the clustering is elongated along the line of sight on small scales due to random peculiar motions (finger of God effect). This is why correlation functions in redshift space $\xi_N^{(s)}$ should have the arguments for directions $\{\theta_{ij}\}$ in addition to the arguments for scales $\{s_{ij}\}$ in equation (3.4.9). It is usual, however, to consider the direction-averaged correlation function in redshift space (e.g., de Lapparent et al. 1988). In the case of two-point correlation function, the direction (θ, ϕ) of the line linking two points are randomly oriented in three-dimensional space, so we should average it by integrating over $SO(3)$ invariant measure, $\sin\theta d\theta d\phi/(4\pi)$. Then the direction-averaged two-point correlation function reduces to

$$\xi_\sigma^{(s)}(s) = \frac{1}{2}\int_0^\pi \sin\theta \; d\theta \; \xi^{(s)}(s;\theta). \tag{3.4.29}$$

This averaging for equation (3.4.28) can be carried out explicitly, resulting in

$$\begin{aligned}\xi^{(s)}(s) &= \frac{(H_0 r_0)^\gamma}{(2-\gamma)H_0 s}\int_0^\infty du \int_0^u du' f_\sigma\left(\frac{u+u'}{2}\right) f_\sigma\left(\frac{u-u'}{2}\right) \\ &\times \left[\frac{|u+H_0 s|^{2-\gamma} - |u-H_0 s|^{2-\gamma}}{u} + \frac{|u'+H_0 s|^{2-\gamma} - |u'-H_0 s|^{2-\gamma}}{u'}\right]. \end{aligned} \tag{3.4.30}$$

Now we adopt velocity distributions (3.4.12) and (3.4.13) to compute the above integral. First we consider the exponential case (3.4.12). Performing partial integration gives

$$\xi^{(s)}(s) = \frac{1}{2\sqrt{2}(2-\gamma)}\frac{H_0 r_0^\gamma}{\sigma} s^{1-\gamma} F\left(\frac{H_0 s}{\sigma}\right), \tag{3.4.31}$$

where

$$F(x) \equiv \int_0^\infty dt \left(1+\sqrt{2}xt\right) e^{-\sqrt{2}xt} \frac{|t+1|^{2-\gamma} - |t-1|^{2-\gamma}}{t}. \tag{3.4.32}$$

It is useful to derive the asymptotic expansion of $F(x)$. When $x \to \infty$, it can be evaluated by Laplace's method as

$$F(x) \overset{x\to\infty}{\approx} \sum_{k=0}^{\infty} \frac{k+1}{2k+1} 2^{3/2-k} \left(\prod_{j=0}^{2k} (2-\gamma-j) \right) \frac{1}{x^{2k+1}}. \tag{3.4.33}$$

On the other hand, when $x \to 0$, it approaches a constant:

$$F_0(\gamma) \equiv \int_0^\infty dt \frac{|t+1|^{2-\gamma} - |t-1|^{2-\gamma}}{t}. \tag{3.4.34}$$

For $\gamma = 1.8$, the above constant is given numerically as

$$F_0(1.8) = 1.02077\cdots. \tag{3.4.35}$$

The corresponding asymptotic limits of $\xi^{(s)}(s)$ are

$$\xi^{(s)}(s) \overset{H_0 s/\sigma\to\infty}{\to} \left(\frac{s}{r_0}\right)^{-\gamma} \left\{ 1 + \frac{\gamma(\gamma-1)}{3} \left(\frac{\sigma}{H_0 s}\right)^2 + O\left(\left(\frac{\sigma}{H_0 s}\right)^4 \right) \right\}, \tag{3.4.36}$$

$$\xi^{(s)}(s) \overset{H_0 s/\sigma\to 0}{\to} \frac{F_0(\gamma)}{2\sqrt{2}(2-\gamma)} \frac{H_0 r_0^\gamma}{\sigma} s^{1-\gamma}. \tag{3.4.37}$$

The limit (3.4.36) simply gives the small deviation of the redshift-space correlation from the real-space correlation caused by the random peculiar velocities on scales above σ/H_0. We can see, even if we ignore the coherent motion of galaxies, that the two-point function in redshift space on scales $\sim \sigma/H_0$ is somewhat greater than the one in real space. This is qualitatively understood by the decrease of the correlation on small scales and the particle conservation:

$$\int_0^\infty r^2 \xi^{(r)}(r) dr = \int_0^\infty s^2 \xi^{(s)}(s) ds. \tag{3.4.38}$$

As noted in section 3.4.1, the coherent motion increases $\xi^{(s)}(s)$ on large scales. Random peculiar velocities also provide another mechanism that increases $\xi^{(s)}$ with respect to $\xi^{(r)}$ on scales $\gtrsim \sigma/H_0$ though the latter effect is much smaller than the former as we will show in the next section using N-body simulation. The other limit (3.4.37) implies that the power-law index of the two-point correlation function in redshift space is $1-\gamma$ on small scales ($\ll \sigma/H_0$). In the intermediate region, the power-law index takes an intermediate value, $-\gamma \sim 1-\gamma$, and this is exactly what is observed (de Lapparent et al. 1988).

Corresponding to the scaling relation (3.4.14), the behavior of $\xi^{(s)}$ with respect to the velocity dispersion σ in two limits (3.4.36) and (3.4.37) is

$$\xi^{(s)}_{\nu\sigma}(s) = \begin{cases} \nu^{-1} \xi^{(s)}_\sigma(s) & (s \ll \nu\sigma/H_0) \\ \xi^{(s)}_\sigma(s) & (s \gg \nu\sigma/H_0) \end{cases}. \tag{3.4.39}$$

The correlation on small scales is in inverse proportion to the velocity dispersion σ, but the correlation on large scales is independent of the value of σ.

We next compare the results obtained above to the case of Gaussian velocity distribution (equation [3.4.13]). Let us distinguish the case of Gaussian (3.4.13) from the exponential case (3.4.12) by adding the suffix G. Substituting equation (3.4.13) in equation (3.4.30), we obtain

$$\xi_G^{(s)}(s) = \frac{1}{2\sqrt{\pi}(2-\gamma)} \frac{H_0 r_0^\gamma}{\sigma} s^{1-\gamma} F_G\left(\frac{H_0 s}{\sigma}\right), \tag{3.4.40}$$

where

$$F_G(x) \equiv \int_0^\infty dt e^{-x^2t^2/4} \frac{|t+1|^{2-\gamma} - |t-1|^{2-\gamma}}{t}. \tag{3.4.41}$$

The asymptotic expansion of $F_G(x)$ for $x \to \infty$ is

$$F_G(x) \overset{x\to\infty}{\approx} \sum_{k=0}^{\infty} \frac{2\sqrt{\pi}}{(2k+1)k!} \left(\prod_{j=0}^{2k}(2-\gamma-j)\right) \frac{1}{x^{2k+1}}, \tag{3.4.42}$$

and $F_G(0) = F_0(\gamma)$. Corresponding to limits (3.4.36) and (3.4.37), we have the following for the Gaussian case:

$$\xi_G^{(s)}(s) \overset{H_0 s/\sigma\to\infty}{\to} \left(\frac{s}{r_0}\right)^{-\gamma} \left(1 + \frac{\gamma(\gamma-1)}{3}\frac{\sigma^2}{H_0^2 s^2} + O\left(\frac{1}{s^4}\right)\right), \tag{3.4.43}$$

$$\xi_G^{(s)}(s) \overset{H_0 s/\sigma\to 0}{\to} \frac{F_0(\gamma)}{2\sqrt{\pi}(2-\gamma)} \frac{H_0 r_0^\gamma}{\sigma} s^{1-\gamma} \tag{3.4.44}$$

The scaling (3.4.39) also holds in this case.

On large scales, the lowest two terms are the same in both exponential and Gaussian cases, so they behave very similarly for the same σ. Correlations on small scales also behave in a similar way except that the magnitude in Gaussian case is somewhat less than in exponential case with the factor $\sqrt{2/\pi} \sim 0.8$ for the same σ. Functions (3.4.31) and (3.4.40) are plotted in Figure 3.13 for $\gamma = 1.8$. In the upper panel of Figure 3.14 is plotted the function (3.4.31) for various values for σ.

3.4.5 Three-point correlation function in redshift space

Unlike in the case of ξ, it is difficult to derive even the limiting behavior analytically in the case of three-point correlation function, and we have to resort to numerical integrations. First, we need the explicit direction-average of the triangles corresponding to (3.4.29). The result of the direction-averaged three-point correlation

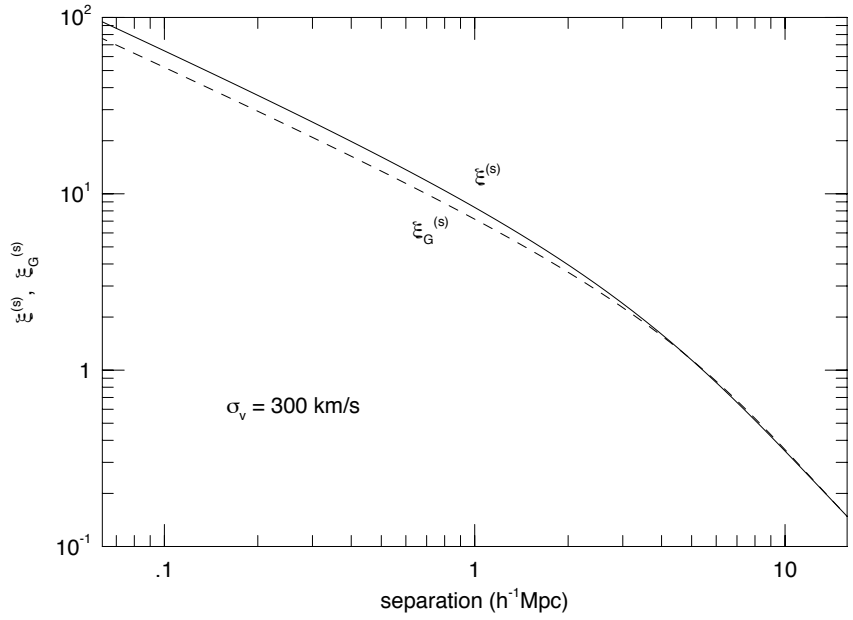

Figure 3.13: Two-point correlation functions in redshift space for the power-law model in real space. Solid line shows the function in exponential case. Dashed line shows the function in Gaussian case. In both cases, the velocity dispersion σ is set to be 300km/s and the power-law index $\gamma = 1.8$.

function in redshift space (see Appendix A of Matsubara 1994a) is

$$\zeta^{(s)}(s_{12}, s_{23}, s_{31}) = \int_{-\infty}^{\infty} dv_1 dv_2 dv_3 f_\sigma(v_1) f_\sigma(v_2) f_\sigma(v_3) \frac{1}{2\pi} \int_0^\pi d\theta_{12} \sin\theta_{12} \int_0^\pi d\phi \zeta^{(r)}(r_{12}, r_{23}, r_{31}), \tag{3.4.45}$$

where

$$\begin{aligned}
r_{12} &= H_0^{-1}\sqrt{(v_1 - v_2)^2 - 2H_0(v_1 - v_2)s_{12}\cos\theta_{12} + H_0^2 s_{12}^2} \\
r_{23} &= H_0^{-1}\sqrt{(v_2 - v_3)^2 - 2H_0(v_2 - v_3)s_{23}\cos\theta_{23}(\theta_{12}, \phi) + H_0^2 s_{23}^2} \\
r_{31} &= H_0^{-1}\sqrt{(v_3 - v_1)^2 - 2H_0(v_3 - v_1)s_{31}\cos\theta_{31}(\theta_{12}, \phi) + H_0^2 s_{31}^2} \\
\cos\theta_{23}(\theta_{12}, \phi) &= -\sin\varphi\sin\theta_{12}\cos\phi - \cos\varphi\cos\theta_{12}, \\
\cos\theta_{31}(\theta_{12}, \phi) &= -\left(s_{12}\cos\theta_{12} + s_{23}\cos\theta_{23}(\theta_{12}, \phi)\right)/s_{31} \\
\varphi &= \arccos\left(\frac{s_{12}^2 + s_{23}^2 - s_{31}^2}{2s_{12}s_{23}}\right) \quad (0 \le \varphi \le \pi).
\end{aligned}$$

The upper panel of Figure 3.14 shows the result of numerical integration of equation (3.4.45) with various σ in the case of $s_{12} = s_{23} = s_{31}$ (equilateral configurations*),

*We display the result concerning three-point correlation function only for equilateral configu-

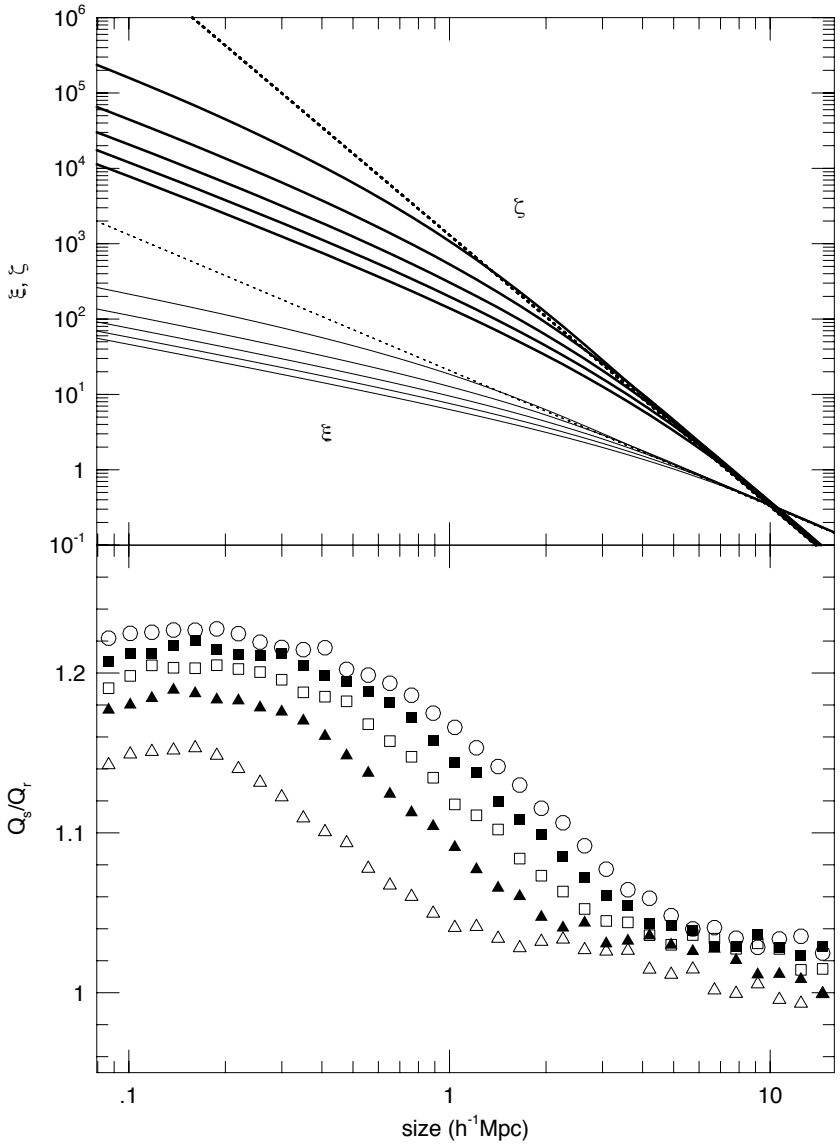

Figure 3.14: *upper panel*: The two- (lower lines) and three- (upper lines) point correlation functions in redshift space. The assumed two- and three-point correlation functions in real space are power-law and hierarchical forms, respectively, which are shown by dotted lines. For the three-point correlation functions, horizontal axis shows the size of equilateral configurations. These functions are displayed for five different velocity dispersions $\sigma = 100, 200, 300, 400, 500$km/s (from top to bottom). In each case, the power-law index γ is set to be 1.8 . *lower panel*: The value Q_s from two- and three-point correlation functions in redshift space in the upper panel of this figure. Open triangles for $\sigma = 100$km/s, filled triangles for $\sigma = 200$km/s, open squares for $\sigma = 300$km/s, filled squares for $\sigma = 400$km/s, open circles for $\sigma = 500$km/s.

where we assumed that the hierarchical ansatz (3.1.2) with $Q = 1$ and power-law property (3.1.1) are exact, i.e.,

$$\zeta^{(r)}(r_{12}, r_{23}, r_{31}) = r_0^{2\gamma}\left[(r_{12}r_{23})^{-\gamma} + (r_{23}r_{31})^{-\gamma} + (r_{31}r_{12})^{-\gamma}\right]. \tag{3.4.46}$$

with $\gamma = 1.8$ and adopted the exponential distribution for $f_\sigma(v)$ (equation [3.4.12]).

3.4.6 Hierarchical relations in real and redshift spaces

We have obtained the relation between the correlation function in real space and direction averaged correlation function in redshift space especially for two- and three-point in our model (3.4.9) or (3.4.27). We next consider whether or not the (lowest) hierarchical relation (3.1.2) is preserved under the transformation from real to redshift space. When the hierarchical relation (3.1.2) holds in real space, the left and right hand sides of (3.1.2) in redshift space can be estimated as in the previous section. We define the scale-dependent Q by equation (3.2.12). We will denote these quantities in real space by Q_r and in redshift space by Q_s. The value Q_s/Q_r for equilateral configuration ($s_{12} = s_{23} = s_{31}$) in redshift space is plotted in the lower panel of Figure 3.14 where we assume the power-law two-point function (3.1.1) and the hierarchical three-point function (3.1.2), so $Q_r = $ const. In Figure 3.14, the model (3.4.9) where σ is common for $N = 2, 3$ is used to see the qualitative scaling of Q_s. From Figure 3.14, hierarchical relation is weakly broken on small scales, $\lesssim \sigma/H_0$, with Q_s 20% larger than Q_r.

Let us note some technical points in evaluating the five-dimensional integral (3.4.45), using the Monte-Carlo method. The integrand here has singularities at either $r_{12} = 0$, $r_{23} = 0$, or $r_{31} = 0$ which need careful treatment in the Monte-Carlo integration. In order to remove the singularities, we have introduced a cut-off r_c to the hierarchical three-point correlation function in real space:

$$\zeta^{(r)}_{\rm hierarchial} \equiv Q_r r_0^{2\gamma}\left[(r_1r_2)^{-\gamma} + (r_2r_3)^{-\gamma} + (r_3r_1)^{-\gamma}\right]. \tag{3.4.47}$$

More explicitly, we consider the three-point correlation function in real space of the form,

$$\zeta(r_{12}, r_{23}, r_{31}) = \begin{cases} \zeta^{(r)}_{\rm hierarchical}(r_c, r_c, r_c) & (r_{31} < r_c) \\ \zeta^{(r)}_{\rm hierarchical}(r_c, r_c, r_{31}) & (r_{23} < r_c < r_{31}) \\ \zeta^{(r)}_{\rm hierarchical}(r_c, r_{23}, r_{31}) & (r_{12} < r_c < r_{23}) \\ \zeta^{(r)}_{\rm hierarchical}(r_{12}, r_{23}, r_{31}) & (r_c < r_{12}) \end{cases}. \tag{3.4.48}$$

ration, where the three sides of the triangle have the same size. We will denote the size simply by r and s in real and redshift space, respectively.

when $r_{12} < r_{23} < r_{31}$. We have set $r_c = 0.02h^{-1}$Mpc in Figure 3.14. This value is determined so that the Monte-Carlo integration converges sufficiently. We have to admit this value r_c is not negligible compared to our dynamical range $\gtrsim 0.1h^{-1}$Mpc, but some experiment of varying r_c showed that the value r_c in Figure 3.14 does not affect the region for $r \gtrsim 0.2h^{-1}$Mpc; if we increase r_c, the values Q_s/Q_r decrease a little on scales $\lesssim 0.2h^{-1}$Mpc but does not change on scales $\gtrsim 0.2h^{-1}$Mpc. Thus the lower part of Figure 3.14 for $r \gtrsim 0.2h^{-1}$Mpc is not affected by the artificial cut-off $r_c = 0.02h^{-1}$Mpc.

3.4.7 Comparison with N-body simulations

In this section, we apply our model to N-body simulation data described in section 3.2 and consider whether or not the hierarchical relation in redshift space implies that the similar relation exists in real space. In section 3.2 we find that the low-density cold dark matter (LCDM) model is a counter example of this statement. Our subsequent analysis show that standard cold dark matter (SCDM) model is also consistent with hierarchical relation in redshift space but not in real space. In this section, we use the data of the N-body simulation for both SCDM and LCDM models for the distribution in real space. We will try to reproduce the direct simulation result in the framework of our semi-analytical model presented here.

So far we have assumed the power-law model for two-point correlation function and the hierarchical model for three-point correlation function. Here we use correlations $\xi^{(r)}, \zeta^{(r)}$ of simulation data. They are substituted in equations (3.4.6) and (3.4.8). In Figure 3.15 is plotted the result for the two-point correlation function. The filled circles indicate the two-point function in real space of simulation data. The lines show the direction averaged two-point correlation function in redshift space (eqs.[3.4.6] and [3.4.29]) where the correlation in real space $\xi^{(r)}$ directly evaluated from simulations is substituted in equation (3.4.6). We adjusted the value σ_2 by least square method in linear scale to match the correlation in redshift space in simulation data which is plotted in open triangles. Solid line shows the case for exponential model (3.4.12) and dashed line for Gaussian model (3.4.13). The best fitted values σ_2 are also indicated in the figure. The agreement between our model and the data is surprisingly good on small scales $\lesssim 2h^{-1}$Mpc. The systematic deviation on large scales should be ascribed to the density-velocity coherence in linear theory (Kaiser 1987) which is not included in our model.

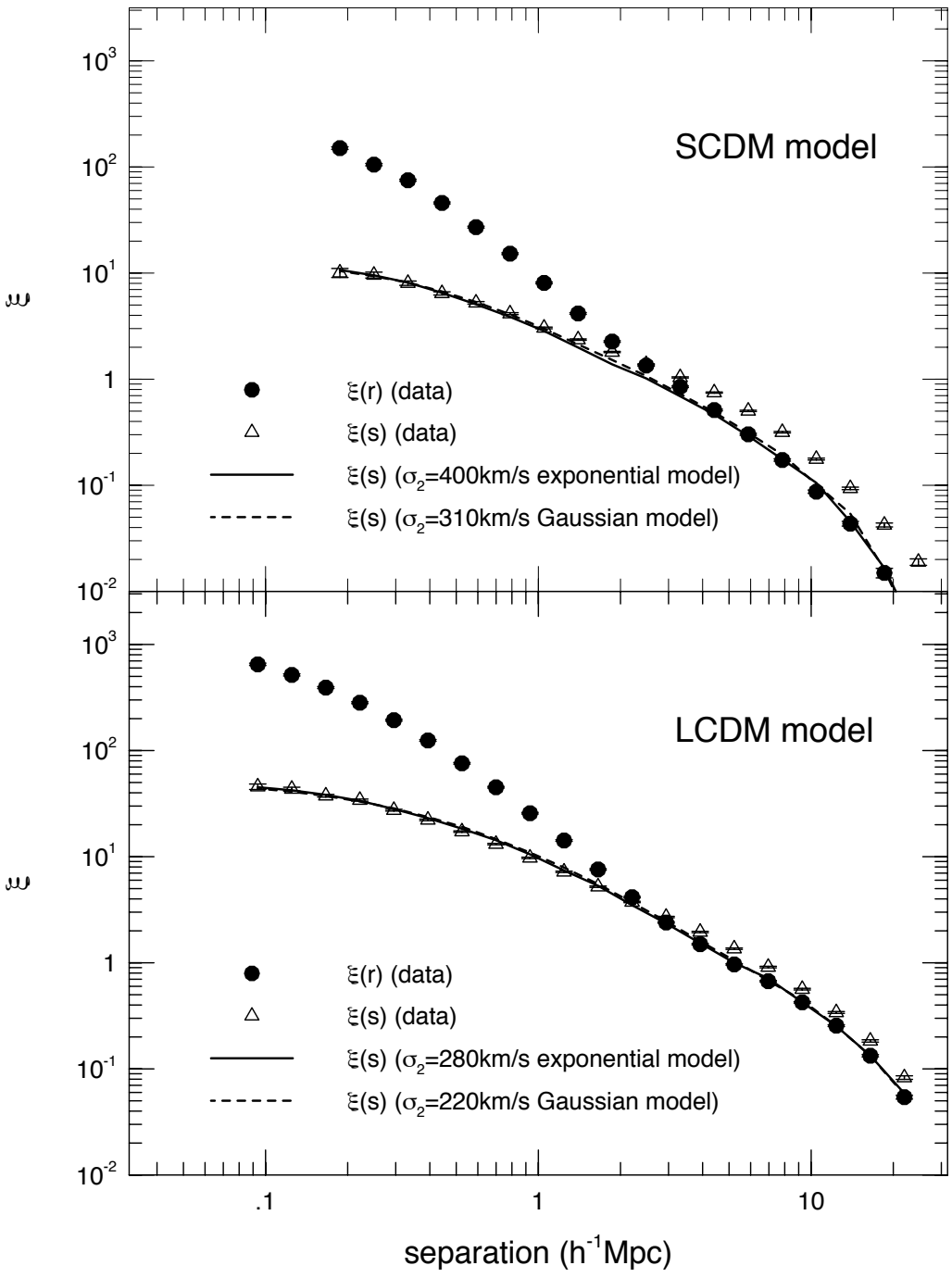

Figure 3.15: The two-point correlation functions in real space (filled circles) and in redshift space (open triangles) for SCDM (upper panel) and LCDM (lower panel) models. The prediction of our exponential model (solid lines) and Gaussian model (dashed lines) are shown. The best fitted values σ_2 are also indicated.

The similar plots and the best fit of σ_3 are shown in the upper panels of Figures 3.16, 3.17 for $\zeta^{(r)}$ and $\zeta^{(s)}$ of the equilateral configuration. As above, the three-point function in real space $\zeta^{(r)}$ is directly evaluated from simulation data. Comparing the best fit of σ_3 with that of σ_2, we can see $\sigma_3 \sim 1.7\sigma_2$ nearly independently of the models considered (SCDM or LCDM, and Gaussian or exponential). Thus, the velocity-correlation-modified model (3.4.27) agrees well with the data while the model (3.4.9) with common σ does not agree well with the data. The agreement is quite good in spite of many approximations in section 3.4.3. The expected property $\sigma_2 < \sigma_3$ discussed in section 3.4.3 is satisfied.

The results for Q_r and Q_s are plotted in the lower panels of Figure 3.16, 3.17. For the denominator in definition (3.2.12) for our model (solid and dashed lines), we employed the value from data (open triangles in Figure 3.15).

Thus, using velocity-correlation-modified model (3.4.27), we can successfully reproduce the direct simulation result in which the redshift-space correlation functions exhibit the hierarchical structure while the real-space correlation functions do not.

3.5 Discussion

We have ignored the Hubble flow for the bound systems and we have considered only peculiar velocities in comoving coordinate. In the case of a pair of galaxies in a gravitationally bound system with physical separation $r_{\rm phys}$, for example, we get the relative peculiar velocity — the Hubble flow — $H_0 r_{\rm phys}$ in addition to the true peculiar velocities in physical coordinate v_1, v_2. Such Hubble flow would not dominate our model because the typical peculiar velocity $v_{\rm pec} \sim v_1 \sim v_2$ are greater than $H_0 r_{\rm phys}$; in our universe, a typical size of gravitationally bound systems, i.e., clusters of galaxies, is $\sim 1h^{-1}$Mpc. So the Hubble flow $H_0 r_{\rm phys}$ for the bound systems in our Universe hardly exceeds ~ 100km/s. Though our analysis on scales $\lesssim 1h^{-1}$Mpc can be affected by the Hubble flow, the effect is expected to be small. The accurate estimation to this effect would be difficult because the corresponding scale in our universe has not yet virialized and is likely in the process of virialization. We will not address further details of this subject because it requires a proper understanding of fully nonlinear dynamical behavior.

At this stage we have to admit that the present analysis does not completely answer the problem why $Q_s \sim 1$ at least in the SCDM and LCDM model. Quantitative account of this is probably too complicated due to the intrinsically nonlinear nature

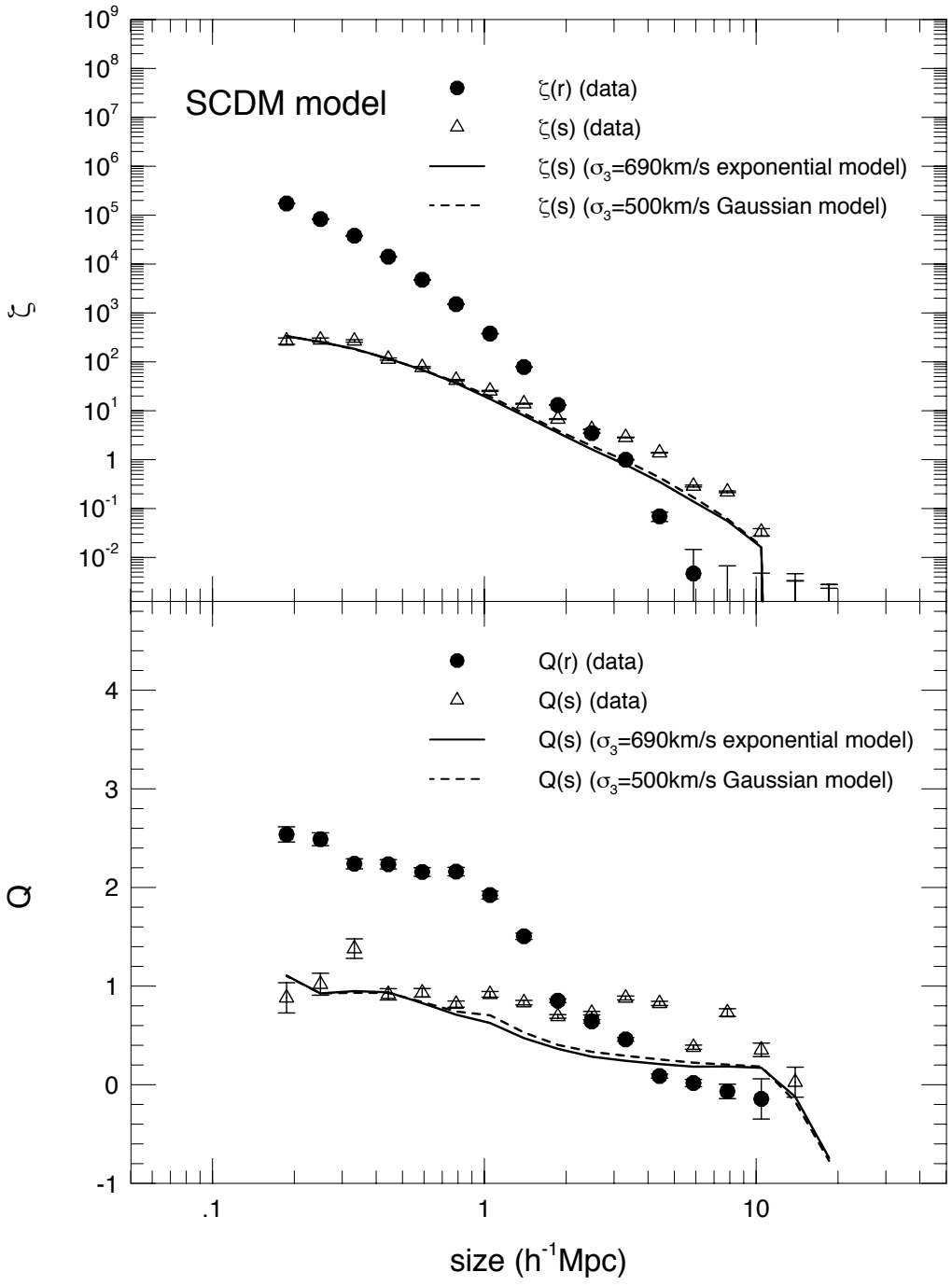

Figure 3.16: *upper panel*: The three-point correlation functions for equilateral configurations in real space (filled circles) and in redshift space (open triangles) for SCDM model. The prediction of our exponential model (solid lines) and Gaussian model (dashed lines) are shown. The best fitted values σ_3 are also indicated. *lower panel*: The value Q_r and Q_s corresponding to the upper panel of this figure. The meaning of symbols are the same as the upper panel.

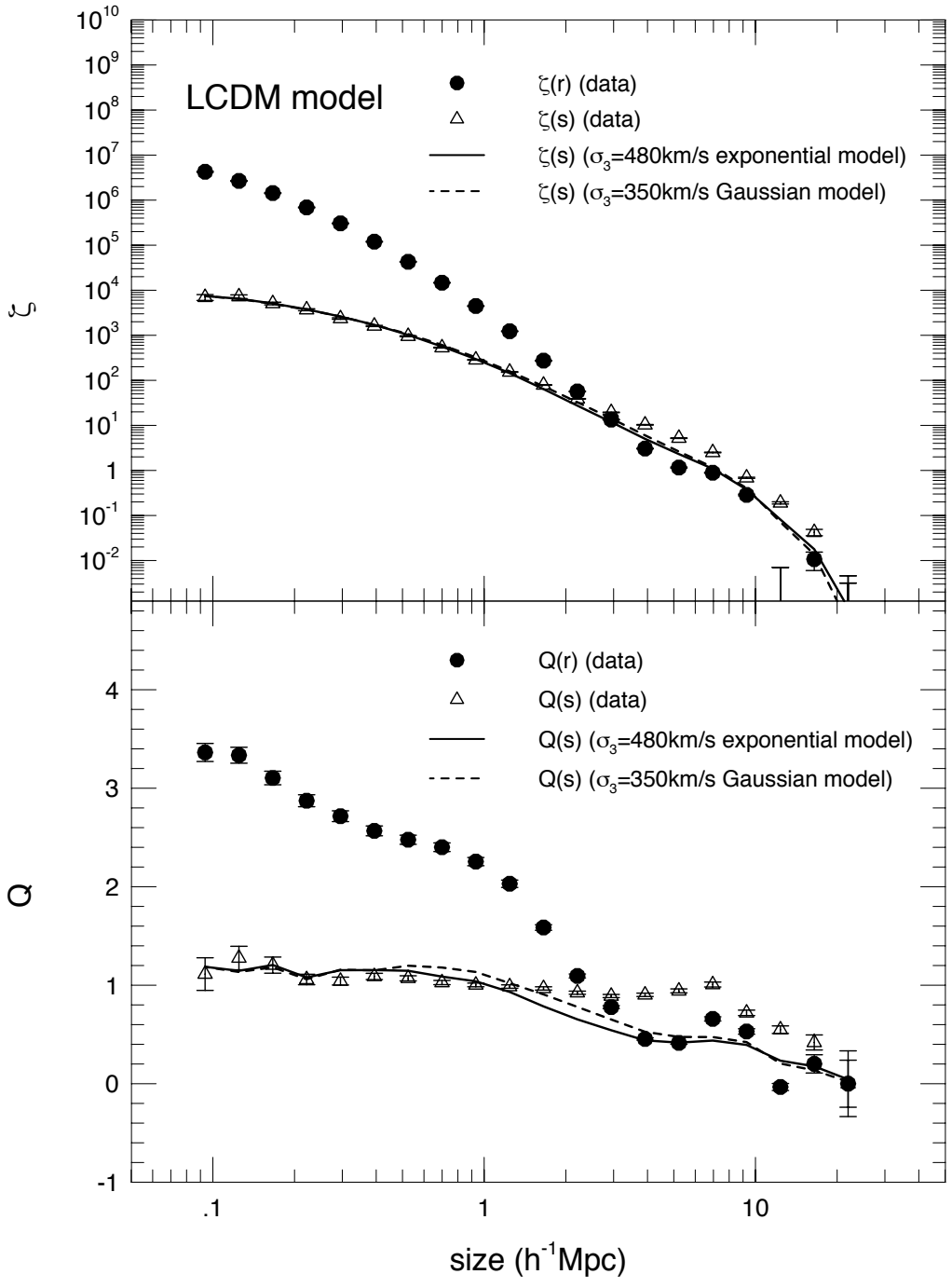

Figure 3.17: Same as the previous Figure for LCDM model.

of the problem. We can, however, qualitatively argue the reason for the tendency; the value Q_r and Q_s depends sensitively on both two- and three-point correlation functions. The three-point correlation functions in real and redshift space, $\zeta^{(r)}$, $\zeta^{(s)}$, behave as $(\xi^{(r)})^2$, $(\xi^{(s)})^2$, respectively, but the deviations in factors from such behavior of order unity result in scale-dependent Q_r and/or Q_s of order unity. In redshift space, however, two- and three-point correlation functions are smoothed through equation (3.4.9). The typical smoothing scale is given by dispersion of peculiar velocities, $\sigma \sim 500$km/s, so it is $\sim 5h^{-1}$Mpc. Thus the deviations in correlation functions in redshift space are smoothed out on scales below $\sim 1h^{-1}$Mpc. As a result, the value Q_s is also smoothed on such a scales and tend to be a constant. Glancing over the lower panels of Figure 3.16, 3.17 we would think that Q_s should be ~ 2. Nevertheless, the property $\sigma_2 < \sigma_3$ decreases the value of Q_s and results in $Q_s \sim 1$. Note that this is a qualitative picture and we have not understood the machinery of why $Q_s \simeq 1$ quantitatively. Is this a universal phenomenon in non-equilibrium gravitational systems or just an accident? It would be interesting to pursue this problem.

3.6 STATISTICS OF ISODENSITY CONTOURS IN REDSHIFT SPACE

The redshift contamination for the statistics of isodensity contours is also of great interest. Practically, the statistical tests of cosmology using the isodensity contours are performed in redshift space in which the density field is statistically anisotropic. So far the analytic expressions for statistics of isodensity contours G, G_2, N_3, N_2, N_1 have been derived only for isotropic fields (section 3.3).

The growth of the density fluctuation of the universe on large scales is described by linear theory in the gravitational instability picture of the structure formation (e.g., Peebles 1980). Thus, if the initial fluctuation is a Gaussian random field as is often assumed, the statistics of isodensity contours of the density field with large smoothing length should obey the random Gaussian prediction. Because the known analytic expression for Gaussian random fields is for the isotropic field, this Gaussianity test of the initial fluctuation should be performed in real space which is not feasible in reality. It is not obvious whether or not the redshift space distortion strongly affects statistics of isodensity contours. As for the genus, Melott, Weinberg & Gott (1988) found by analysis of N-body simulations that genus is hardly affected by redshift space distortion when the smoothing length is larger than the correlation

length $\sim 5h^{-1}$Mpc.

In this section, the redshift space distortions of statistics of isodensity contours G, G_2, N_3, N_2, N_1 are studied analytically by linear theory of gravitational instability assuming that the initial fluctuation is a Gaussian random field (Matsubara 1994c). These statistics will be accurately determined with the future redshift surveys. Our approach provides the Gaussianity test which can be directly performed in redshift space. Moreover, the redshift space distortion generally depends on the density parameter of the universe and our formula could in principle discriminate this parameter.

3.6.1 Field correlations in the distant-observer approximation

Kaiser (1987) showed that the distortion of power spectrum in redshift space $P^{(s)}(\boldsymbol{k})$ from that in real space $P^{(r)}(k)$ is given by the simple formula as

$$P^{(s)}(\boldsymbol{k}) = \left[1 + f\mu^2\right]^2 P^{(r)}(k), \tag{3.6.1}$$

where μ is the cosine of the angle between the line of sight and the direction of $\boldsymbol{k}$ and $f(\Omega) = H^{-1}\dot{D}/D \approx \Omega^{0.6}$, D is the linear growth rate and H is the Hubble parameter. The omega-dependence of $f(\Omega)$ is approximately the same in the presence of cosmological constant Λ (section 2.2.1), and we use this approximation, $f \approx \Omega^{3/5}$, extensively in this section. This simplicity of equation (3.6.1) relies on the approximation that the sample volume is distant from the observer. Inhomogeneity of the redshift samples closer to the observer is not negligible as well as the anisotropy and prevent to give the simple expression as in equation (3.6.1). When the sample volume is distant from the observer, the direction of line of sight is approximately fixed in the sample volume. We call this approximation fixing the line of sight as 'distant-observer approximation'. Adopting this approximation, the Cartesian coordinates in which the line of sight is fixed is convenient for our purpose. The Cartesian coordinates make the calculation of statistics of isodensity contours easy. Our distant-observer approximation exactly reproduces Kaiser's result (equation [3.6.1]) which is derived by first introducing the spherical coordinates and then approximating that the sample is distant from the observer. Our approach depends on the Cartesian coordinates from the beginning and it would be useful to see directly the equivalence of the Kaiser's approximation and our distant-observer approximation. The derivation of Kaiser's result in Cartesian coordinates is simpler as we will see in the following.

In the Cartesian coordinates of our distant-observer approximation, we define the direction of the line of sight by an unit vector $\hat{\boldsymbol{z}}$. Using the line-of-sight component of a peculiar velocity field $U(\boldsymbol{r}) = \boldsymbol{v}(\boldsymbol{r}) \cdot \hat{\boldsymbol{z}}$, the mapping of the coordinates from the real space to the redshift space is given by

$$\boldsymbol{s}(\boldsymbol{r}) = \boldsymbol{r} + \frac{\hat{\boldsymbol{z}}}{H}[U(\boldsymbol{r}) - U(\boldsymbol{0})]. \tag{3.6.2}$$

The observer is placed on the origin of the coordinates, $\boldsymbol{0}$. On large scales we are interested in, we can relate the number density of galaxies in redshift space $\rho_g^{(s)}$ and that in real space $\rho_g^{(r)}$ by evaluating the Jacobian of the mapping (3.6.2) resulting in

$$\rho_g^{(s)}(\boldsymbol{s}(\boldsymbol{r})) = \left(1 + \frac{1}{H}\hat{\boldsymbol{z}} \cdot \nabla U(\boldsymbol{r})\right)^{-1} \rho_g^{(r)}(\boldsymbol{r}). \tag{3.6.3}$$

Leaving only linear order in density contrast $\delta = \rho/\bar{\rho} - 1$ and peculiar velocity field, this relation reduces to

$$\delta_g^{(s)}(\boldsymbol{r}) = \delta_g^{(r)}(\boldsymbol{r}) - \frac{1}{H}\hat{\boldsymbol{z}} \cdot \nabla U(\boldsymbol{r}). \tag{3.6.4}$$

The peculiar velocity field in linear theory (Peebles 1980) is, in growing mode,

$$\boldsymbol{v}(\boldsymbol{r}) = -Hf\nabla\triangle^{-1}\delta_m^{(r)}(\boldsymbol{r}), \tag{3.6.5}$$

where $\triangle^{-1}$ is the inverse Laplacian and $\delta_m^{(r)}$ is the mass density contrast in real space. In the following, δ_g and δ_m are assumed to be proportional to each other. This assumption is called linear biasing: $\delta_g = b\delta_m$, where b is the bias parameter which is a constant. The relation between the density contrast in redshift space and in real space is, up to linear order,

$$\delta_g^{(s)}(\boldsymbol{r}) = \left[1 + f\, b^{-1}(\hat{\boldsymbol{z}} \cdot \nabla)^2\triangle^{-1}\right] \delta_g^{(r)}(\boldsymbol{r}), \tag{3.6.6}$$

or, in Fourier space,

$$\tilde{\delta}_g^{(s)}(\boldsymbol{k}) = \left[1 + f\, b^{-1}\left(\frac{\hat{\boldsymbol{z}} \cdot \boldsymbol{k}}{k}\right)^2\right] \tilde{\delta}_g^{(r)}(\boldsymbol{k}), \tag{3.6.7}$$

which is Kaiser's result.

In the following, we use the parameters σ_j and C_j defined by

$$\sigma_j^2(R) = \int \frac{k^2 dk}{2\pi^2} k^{2j} P^{(r)}(k) W^2(kR), \tag{3.6.8}$$

$$C_j(\Omega) = \frac{1}{2}\int_{-1}^{1} d\mu \mu^{2j} \left(1 + f\, b^{-1}\mu^2\right)^2, \tag{3.6.9}$$

where $W(x)$ is the Fourier transform of the window function to smooth the noisy field of galaxy distribution. The two popular windows are the Gaussian window $W_{\rm G}(x) = \exp(-x^2/2)$ and the top-hat window $W_{\rm TH}(x) = 3(\sin x - x\cos x)/x^3$. We assume that the window function is an isotropic function. The *rms* $\sigma^{(s)}$ of density contrast in redshift space is given by

$$\left(\sigma^{(s)}\right)^2 = C_0\sigma_0^2. \tag{3.6.10}$$

We define the following normalized quantities,

$$\alpha = \frac{\delta_R^{(s)}}{\sigma^{(s)}}, \quad \beta_i = \frac{\partial_i\delta_R^{(s)}}{\sigma^{(s)}}, \quad \omega_{ij} = \frac{\partial_i\partial_j\delta_R^{(s)}}{\sigma^{(s)}}, \tag{3.6.11}$$

where $\delta_R^{(s)}$ is the smoothed density contrast in redshift space. These quantities obey the multivariate Gaussian distribution in linear theory if the primordial fluctuation is a random Gaussian field. The multivariate Gaussian distribution is completely determined by the correlations of all pairs of variables. For our purpose below, the statistics of quantities α, β_i, ω_{IJ} $(i = 1,2,3;\ I,J = 1,2)$ is sufficient. Choosing the coordinates in which the line of sight is the third axis, all the correlations among the above quantities at some point are as follows:

$$\begin{aligned}
&\langle\alpha\alpha\rangle = 1,\\
&\langle\alpha\beta_i\rangle = 0,\\
&\langle\alpha\omega_{IJ}\rangle = \frac{1}{2}\left(\frac{C_1}{C_0} - 1\right)\frac{\sigma_1^2}{\sigma_0^2}\delta_{IJ},\\
&\langle\beta_I\beta_J\rangle = \frac{1}{2}\left(1 - \frac{C_1}{C_0}\right)\frac{\sigma_1^2}{\sigma_0^2}\delta_{IJ},\\
&\langle\beta_I\beta_3\rangle = 0,\\
&\langle\beta_3\beta_3\rangle = \frac{C_1}{C_0}\frac{\sigma_1^2}{\sigma_0^2},\\
&\langle\beta_i\omega_{IJ}\rangle = 0,\\
&\langle\omega_{IJ}\omega_{KL}\rangle = \frac{1}{8}\left(1 - \frac{2C_1}{C_0} + \frac{C_2}{C_0}\right)\frac{\sigma_2^2}{\sigma_0^2}\left(\delta_{IJ}\delta_{KL} + \delta_{IK}\delta_{JL} + \delta_{IL}\delta_{JK}\right).
\end{aligned}$$

It is more convenient to consider

$$\tilde{\omega}_{IJ} = \omega_{IJ} - \alpha\left\langle\alpha\omega_{IJ}\right\rangle, \tag{3.6.12}$$

instead of ω_{IJ}. The new set of variables α, β_i, $\tilde{\omega}_{IJ}$ distribute as multivariate Gaussian and the non-vanishing correlations of these variables are only

$$\langle\alpha\alpha\rangle = 1,$$

$$\langle\beta_1\beta_1\rangle = \langle\beta_2\beta_2\rangle = \frac{1}{2}\left(1-\frac{C_1}{C_0}\right)\frac{\sigma_1^2}{\sigma_0^2},$$
$$\langle\beta_3\beta_3\rangle = \frac{C_1}{C_0}\frac{\sigma_1^2}{\sigma_0^2},$$
$$\langle\tilde{\omega}_{11}\tilde{\omega}_{11}\rangle = \langle\tilde{\omega}_{22}\tilde{\omega}_{22}\rangle = \frac{1}{8}\left[3\left(1-\frac{2C_1}{C_0}+\frac{C_2}{C_0}\right)-2\left(1-\frac{C_1}{C_0}\right)^2\gamma^2\right]\frac{\sigma_2^2}{\sigma_0^2},$$
$$\langle\tilde{\omega}_{11}\tilde{\omega}_{22}\rangle = \frac{1}{8}\left[\left(1-\frac{2C_1}{C_0}+\frac{C_2}{C_0}\right)-2\left(1-\frac{C_1}{C_0}\right)^2\gamma^2\right]\frac{\sigma_2^2}{\sigma_0^2},$$
$$\langle\tilde{\omega}_{12}\tilde{\omega}_{12}\rangle = \frac{1}{8}\left(1-\frac{2C_1}{C_0}+\frac{C_2}{C_0}\right)\frac{\sigma_2^2}{\sigma_0^2},$$

where $\gamma = \sigma_1^2/(\sigma_0\sigma_2)$.

3.6.2 Statistics of isodensity contours

Let us derive the formula of statistics of isodensity contours in redshift space. In the following, the primordial fluctuation is assumed to be a random Gaussian field.

Genus statistics

The genus is minus one-half times the Euler number. The Euler number density of isodensity contours is evaluated by

$$\text{number of maxima} + \text{number of minima} - \text{number of saddle points} \tag{3.6.13}$$

of the contour surfaces with regard to some fixed direction. The expectation value of Euler number of the isodensity contours per unit volume is (Doroshkevich 1970; Adler 1981; Bardeen et al. 1986)

$$n_\chi^{(s)}(\nu) = \left\langle\delta(\alpha-\nu)\delta(\beta_1)\delta(\beta_2)|\beta_3|(\omega_{11}\omega_{22}-\omega_{12}^2)\right\rangle, \tag{3.6.14}$$

where the isodensity contours are defined to be the surface $\delta_R^{(s)} = \nu\sigma^{(s)}$. This expression is valid even for general anisotropic fields. Using new variables $\tilde{\omega}_{IJ}$ in equation (3.6.14), the following result for the expression of genus $G^{(s)}$ in redshift space is derived:

$$G^{(s)}(\nu) = -\frac{1}{2}n_\chi^{(s)}(\nu) = \frac{3\sqrt{3}}{2}\sqrt{\frac{C_1}{C_0}}\left(1-\frac{C_1}{C_0}\right)G^{(r)}(\nu), \tag{3.6.15}$$

where, from equation (3.6.9),

$$\frac{C_1}{C_0} = \frac{1}{3}\,\frac{1+\frac{6}{5}f\,b^{-1}+\frac{3}{7}(f\,b^{-1})^2}{1+\frac{2}{3}f\,b^{-1}+\frac{1}{5}(f\,b^{-1})^2}, \tag{3.6.16}$$

and $G^{(r)}$ is genus in real space (Doroshkevich 1970; Adler 1980; Bardeen et al. 1986; Hamilton et al. 1986) given by

$$G^{(r)}(\nu) = \frac{1}{(2\pi)^2}\left(\frac{\sigma_1}{\sqrt{3}\sigma_0}\right)^3 (1-\nu^2)e^{-\nu^2/2}. \tag{3.6.17}$$

The redshift space distortion does not alter the shape of genus as a function of density threshold and only the amplitude is affected. The Ω dependence of the change in amplitude is plotted in Figure 3.18 (upper panel). The effects of redshift space distortion is small for $\Omega b^{-5/3}$ less than unity. This fact is in agreement with the N-body analysis of Melott, Weinberg & Gott (1988).

2D Genus statistics

The next statistics we consider is 2-dimensional genus. This statistics is defined in the 2-dimensional flat plane S in 3-dimensional space. The density field calculated in 3-dimensional volume defines the high density points in the plane which constitute the excursion set on the plane. The 2D genus is defined by the number of contours surrounding high density region minus the number of contours surrounding low density regions (Adler 1980; Coles 1988; Melott et al 1989; Gott et al. 1990). The redshift space is anisotropic by the presence of the special direction, line of sight, so the 2D statistics depends on the angle θ_S between the plane S and the line of sight. The alternative, equivalent definition of 2D genus is useful in the following. For some arbitrarily fixed direction in the 2D surface, the maximum and minimum points are defined on the contours. These points are classified into upcrossing and downcrossing points with respect to the fixed direction. The 2D genus is defined to be

$$\begin{aligned}\frac{1}{2}(&\text{number of upcrossing minima} - \text{number of upcrossing maxima}\\ &- \text{number of downcrossing minima} + \text{number of downcrossing maxima}),\end{aligned} \tag{3.6.18}$$

of the contour lines with regard to some fixed direction in the plane S. The latter definition can be used to obtain the following expression for 2D genus per unit area of the plane:

$$G_2^{(s)}(\nu,\theta_S) = -\frac{1}{2}\left\langle \delta(\alpha-\nu)\delta(\beta_1)|\beta_2\sin\theta_S + \beta_3\cos\theta_S|\omega_{11}\right\rangle . \tag{3.6.19}$$

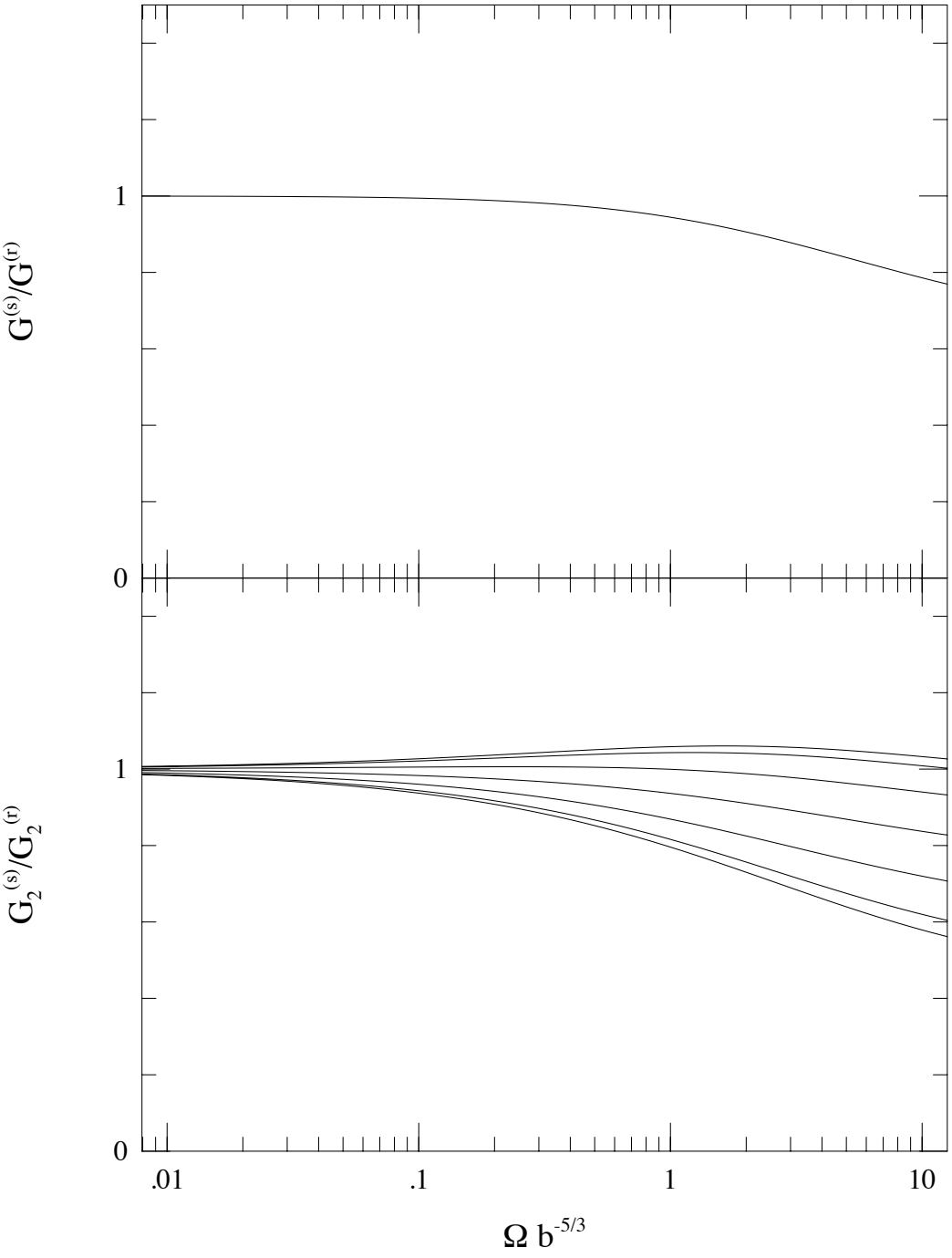

Figure 3.18: *Upper panel*: amplitude of genus in redshift space relative to that in real space. *Lower panel*: relative amplitude of 2D genus. The angles between the slice and the line of sight are $\theta_S = 0°$, $15°$, $30°$, $45°$, $60°$, $75°$, $90°$ (from upper line to lower line).

The corresponding expression in case of the isotropic 2-dimensional field is appeared in Bond & Efstathiou (1987). From this expression, we obtain

$$G_2^{(s)}(\nu,\theta_S) = \frac{3}{2}\sqrt{\left(1-\frac{C_1}{C_0}\right)\left[1-\frac{C_1}{C_0}+\left(\frac{3C_1}{C_0}-1\right)\cos^2\theta_S\right]}G_2^{(r)}(\nu). \tag{3.6.20}$$

To derive this result, we use $\tilde{\omega}_{11}$ rather than ω_{11}, then regard the variables α, β_1, $\beta_2\sin\theta_S+\beta_3\cos\theta_S$ and $\tilde{\omega}_{11}$ as independent variables. The 2D genus in real space $G_2^{(r)}$ has the following form:

$$G_2^{(r)}(\nu) = \frac{1}{(2\pi)^{3/2}}\left(\frac{\sigma_1}{\sqrt{3}\sigma_0}\right)^2 \nu e^{-\nu^2/2}. \tag{3.6.21}$$

The redshift space distortion again affects only amplitude of 2D genus. The dependence on Ω and θ_S of the change in amplitude is plotted in Figure 3.18 (lower panel). The dependence on the direction of the plane θ_S for large Ω can be used to determine the cosmological parameter by this statistics.

Area of isodensity contours

The area of isodensity contours per unit volume (Ryden 1988; Ryden et al. 1989) is given by

$$N_3^{(s)}(\nu) = \left\langle \delta(\alpha-\nu)\sqrt{\beta_1^2+\beta_2^2+\beta_3^2}\right\rangle. \tag{3.6.22}$$

This expression is valid even for general anisotropic fields. Introducing spherical coordinates for β_i, the above expression is calculated to be

$$N_3^{(s)}(\nu) = \frac{\sqrt{3}}{2}\left[\sqrt{\frac{C_1}{C_0}} - \frac{1-\frac{C_1}{C_0}}{2\sqrt{2\left(\frac{3C_1}{C_0}-1\right)}}\ln\left|\frac{\sqrt{\frac{C_1}{C_0}}-\sqrt{\frac{1}{2}\left(\frac{3C_1}{C_0}-1\right)}}{\sqrt{\frac{C_1}{C_0}}+\sqrt{\frac{1}{2}\left(\frac{3C_1}{C_0}-1\right)}}\right|\right] N_3^{(r)}(\nu), \tag{3.6.23}$$

where $N_3^{(r)}$ is the area in real space given by

$$N_3^{(r)}(\nu) = \frac{2}{\sqrt{3}\pi}\frac{\sigma_1}{\sigma_0}e^{-\nu^2/2}. \tag{3.6.24}$$

Again, only the amplitude is affected. The Ω dependence of the amplitude is very weak as plotted in Figure 3.19 (upper panel).

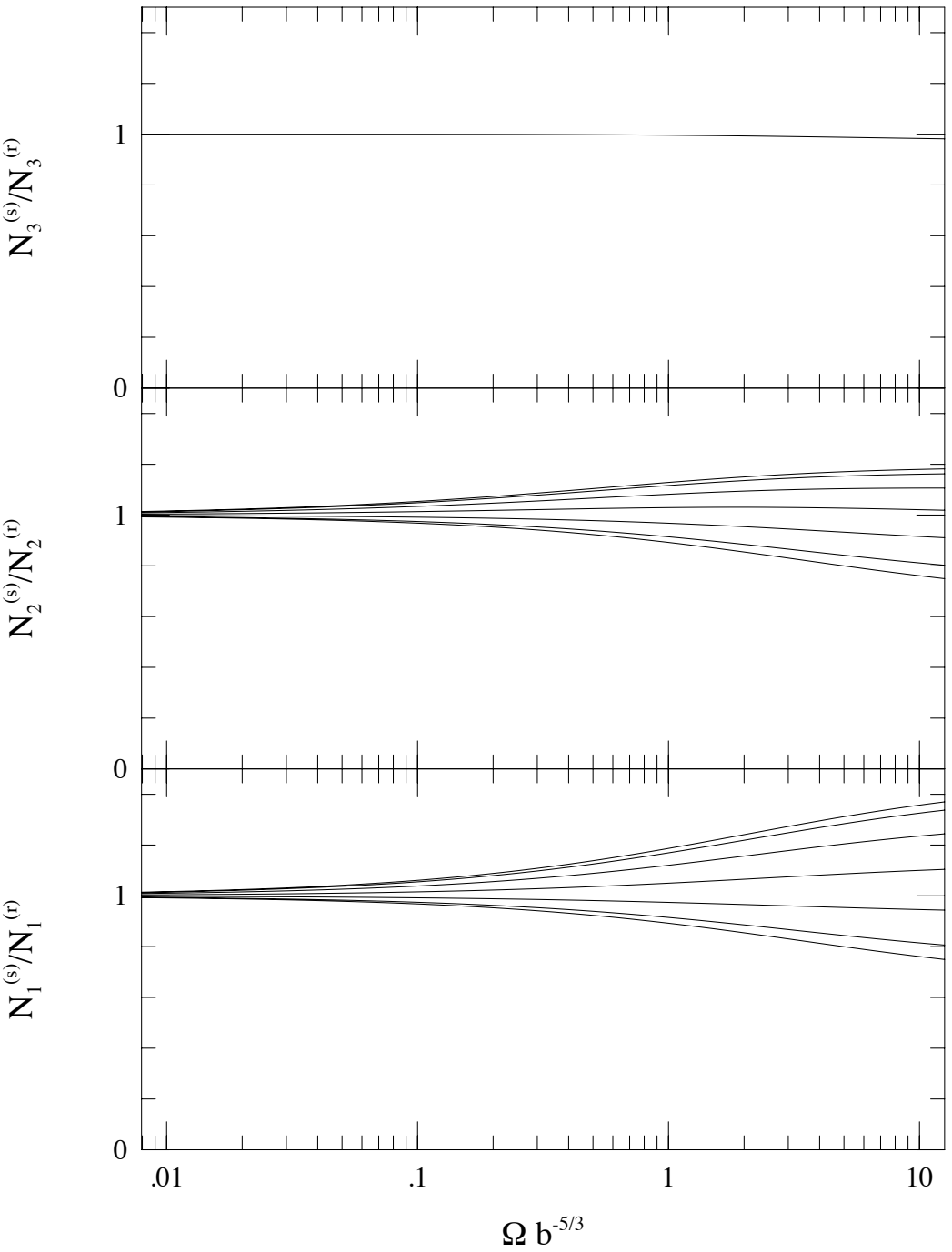

Figure 3.19: *Upper panel*: amplitude of area statistics in redshift space relative to that in real space. *Middle panel*: relative amplitude of length statistics. The angles between the slice and the line of sight are $\theta_S = 0°$, 15°, 30°, 45°, 60°, 75°, 90° (from upper line to lower line). *Lower panel*: relative amplitude of level crossing statistics. The angles between the crossing line and the line of sight are $\theta_L = 0°$, 15°, 30°, 45°, 60°, 75°, 90° (from upper line to lower line).

Length of isodensity contours in planes

As in the case of 2D genus statistics, 2-dimensional flat plane S is considered in the statistics of length of isodensity contours. The length of intersections of isodensity contours and the plane S was introduced by Ryden (1988). For isotropic density fields, this statistics is proportional to the area statistics considered in the previous section. As shown below, for anisotropic fields in redshift space, the proportional factor depends on the direction of the surface S relative to the line of sight. The angle θ_S between the plane S and the line of sight is relevant as in the case of 2D genus statistics. The expectation value of length of isodensity contours in the plane S per unit area of the plane is given by

$$N_2^{(s)}(\nu,\theta_S) = \left\langle \delta(\alpha-\nu)\sqrt{\beta_1^2 + (\beta_2\sin\theta_S + \beta_3\cos\theta_S)^2} \right\rangle. \tag{3.6.25}$$

To evaluate the above equation, note that α, β_1 and $\beta_2\sin\theta_S + \beta_3\cos\theta_S$ are non-correlated, independent variables. Introducing the polar coordinates for the latter two variables, the following expression is obtained:

$$\begin{aligned} N_2^{(s)}(\nu,\theta_S) = \frac{\sqrt{6}}{\pi}&\sqrt{1-\frac{C_1}{C_0}+\left(\frac{3C_1}{C_0}-1\right)\cos^2\theta_S} \\ &\times E\left(\frac{\left(\frac{3C_1}{C_0}-1\right)\cos^2\theta_S}{1-\frac{C_1}{C_0}+\left(\frac{3C_1}{C_0}-1\right)\cos^2\theta_S}\right) N_2^{(r)}(\nu), \end{aligned} \tag{3.6.26}$$

where $E(k)$ is the complete elliptical integral of the second kind:

$$E(k) = \int_0^{\pi/2}\sqrt{1-k^2\sin^2\phi}\,d\phi, \tag{3.6.27}$$

and $N_2^{(r)}$ is the expectation in real space:

$$N_2^{(r)}(\nu) = \frac{\pi}{4}N_3^{(r)}. \tag{3.6.28}$$

The redshift space distortion affects only amplitude as other statistics considered in this section. The dependence on Ω and θ_S of the amplitude is plotted in Figure 3.19 (middle panel).

Contour crossings

Contour crossing statistics is the mean number of intersection of a straight line L and the isodensity contours. This statistics of large-scale structure is introduced

by Ryden (1988) and extensively studied by Ryden et al. (1989) using numerical simulations and redshift observations. For isotropic density fields, this statistics is also proportional to the area statistics. In redshift space, the density field is anisotropic and this statistics depends on the angle θ_L between the direction of the line L and the line of sight. The mean number of crossings per unit length of the line L is given by

$$N_1^{(s)}(\nu, \theta_L) = \langle \delta(\alpha - \nu) \, |\beta_1 \sin\theta_L + \beta_3 \cos\theta_L| \rangle \, . \tag{3.6.29}$$

This expression is evaluated by noting that α and $\beta_1 \sin\theta_L + \beta_3 \cos\theta_L$ are non-correlated, independent variables, resulting in

$$N_1^{(s)}(\nu, \theta_L) = \sqrt{\frac{3}{2}\left[1 - \frac{C_1}{C_0} + \left(\frac{3C_1}{C_0} - 1\right)\cos^2\theta_L\right]} N_1^{(r)}(\nu), \tag{3.6.30}$$

where $N_1^{(r)}$ is the expectation in real space:

$$N_1^{(r)}(\nu) = \frac{1}{2} N_3^{(r)}(\nu). \tag{3.6.31}$$

Again, the redshift space distortion affects only amplitude. The dependence on Ω and θ_L of the amplitude is plotted in Figure 3.19 (lower panel).

3.6.3 On the value of Ω

The strength of the effects of redshift space distortion is different according to which statistics is focused on. The characteristic point in linear theory is that all the statistics in redshift space considered above has the same shapes as in real space as functions of density threshold. The redshift space distortion affects only on the amplitude.

As for genus $G(\nu)$ and area $N_3(\nu)$, the redshift distortion of amplitude is small for $0 \leq \Omega b^{-5/3} \leq 1$ (Figure 3.18, 3.19). This property justifies the comparison of the observational redshift data and the theoretical Gaussian prediction in real space [equation (3.6.17) and equation (3.6.24)] at least in linear regime. In the Gaussianity test of primordial fluctuation using genus and area statistics, the effect of redshift space distortion can be ignored approximately. The similar statistical measure of galaxy clustering, the skewness $\langle \delta_R^3 \rangle / \langle \delta_R^2 \rangle^2$ induced by weakly nonlinear evolution from the Gaussian primordial fluctuation is recently reported not to be affected much also by redshift space distortion (Juszkiewicz, Bouchet, & Colombi 1993; Hivon et al. 1994).

The direction dependent statistics, 2D genus G_2, length statistics N_2 and crossing statistics N_1 are shown to exhibit the dependence on Ω and the direction to define statistics. In Figure 3.20 plotted the direction dependence of these three statistics. The direction dependence of amplitude of these statistics is relatively large: for $\Omega b^{-5/3} = 1$, the amplitude varies more than 20 % while for $\Omega b^{-5/3} = 0$, the amplitude does not varies and is equal to the one in real space. The direction-dependence depends on $\Omega b^{-5/3}$ and the statistics G_2, N_2 and N_1 are three independent indicators to determine the cosmological parameters. The redshift space distortion of power spectrum (equation [3.6.1]) or two-point correlation function of Kaiser's result recently used for determining the parameter $\Omega b^{-5/3}$ (Hamilton 1992; 1993; Fry & Gaztañaga 1994; Cole, Fisher & Weinberg 1994). Gramann, Cen & Gott (1994) introduced the ratio of density gradients $\langle(\partial\delta^{(s)}/\partial r_{||})^2\rangle/\langle(\partial\delta^{(s)}/\partial r_{\perp})^2\rangle$, where $r_{\perp}$, $r_{||}$ are spatial component of line of sight and its perpendicular component, as a discriminator of $\Omega b^{-5/3}$. This ratio is equal to $3C_1/C_0$ in linear theory. Our results can be used as complementary ways of these observations.

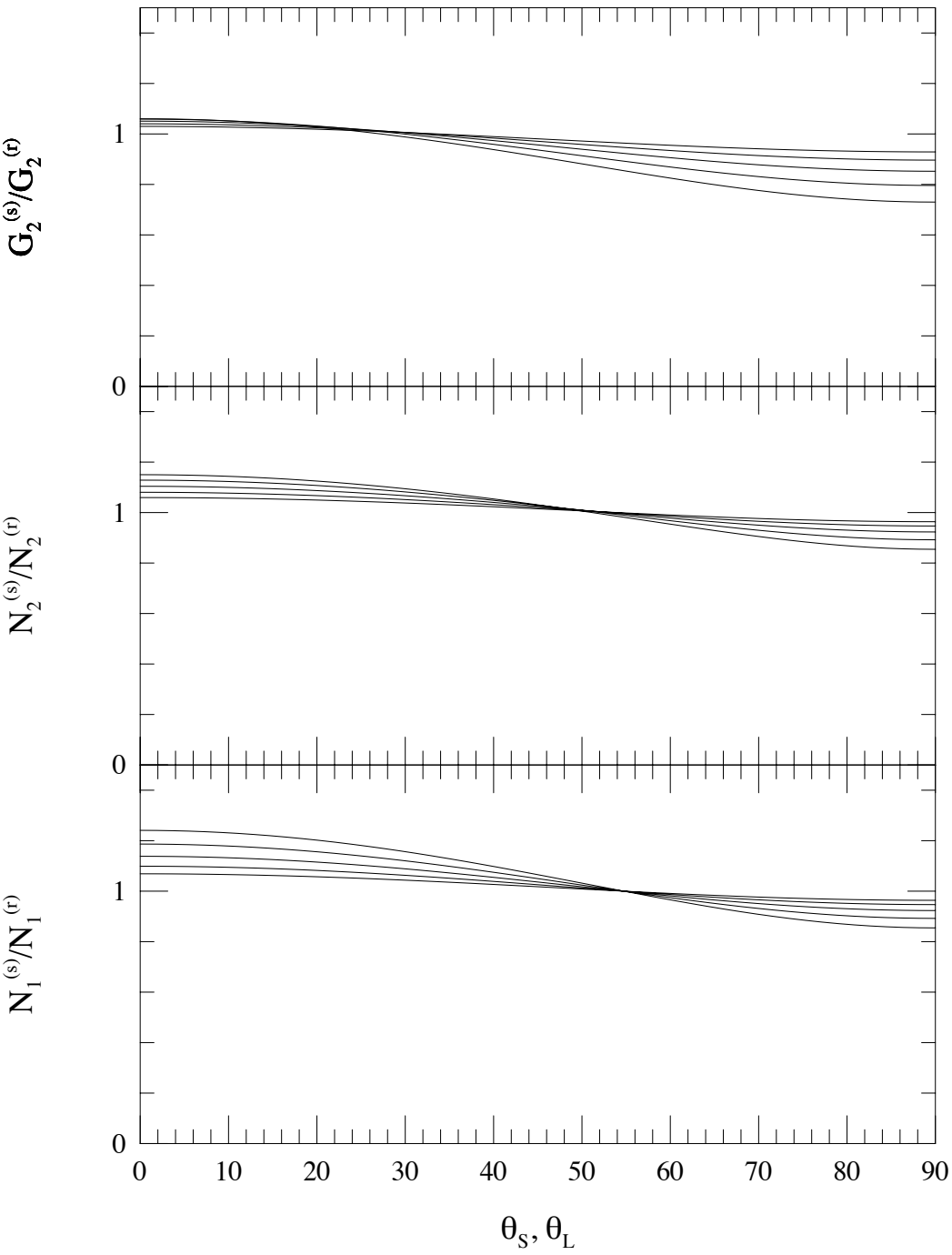

Figure 3.20: Relative amplitude of direction-dependent statistics as functions of the angle between the line-of-sight and the plane or the line on which the statistics are evaluated. Five cases $\Omega b^{-5/3} = 0.125, 0.25, 0.5, 1.0, 2.0$ (from upper line to lower line at $\theta = 90°$) are plotted in each panel. *Upper panel*: 2D genus. *Middle panel*: length statistics *Lower panel*: level crossing statistics.

4

Biasing and Statistics in the Universe

4.1 THE BIASING IN THE UNIVERSE

To compare observations of distribution of cosmic objects with theories of primordial fluctuation, there exist a difficult problem that the present mass density is not the same with the number density of cosmic objects.

Various models on generating the primordial fluctuation of the universe predict different statistical properties of the universe. For instance, simpler inflationary models naturally predict the Gaussian initial fluctuation with scale-invariant primordial power spectrum (Guth & Pi 1982; Starobinskii 1982; Hawking 1982; Bardeen, Steinhardt & Turner 1983). On the other hand, topological defects (see, e.g., Kolb & Turner 1990; Vilenkin 1985) such as global monopoles, cosmic strings, domain walls or textures produce various non-Gaussian fluctuation as well as various non-simpler inflationary models (Allen, Grinstein & Wise 1987; Kofman & Linde 1985; Ortolan, Lucchin & Matarrese 1989; Salopek & Bond 1990; Salopek, Bond & Efstathiou 1989; Hodges et al. 1990; Salopek 1992), the explosion model (Ikeuchi 1981; Ostriker & Cowie 1981), and so on. Density fluctuation generated by various models determines the statistical properties of mass distribution of the present universe which are subjected by the subsequent gravitational evolution.

The mass distribution, however, can not be observed directly. We can directly observe the luminous cosmic objects, such as galaxies, clusters of galaxies, QSOs, X-ray clusters, etc. Generally, the number density of luminous cosmic objects of some kind is not proportional to the mass-density field and is biased tracers of mass. The relation between the number density field $\rho_L(\boldsymbol{r})$ of the luminous objects and the density field $\rho_b(\boldsymbol{x})$ of underlying mass has the essential effects on determining the mass distribution of the present universe. These two fields can be considered as nonlocal functionals of a primordial fluctuation field. If we can express the relation of

those two fields, the relation generally should be a functional as $\rho_L(\boldsymbol{r}) = F_{\boldsymbol{r}}[\rho_b(\boldsymbol{x})]$. We assume this type of relation *exists* in this chapter and explore the statistical consequences of this relation of biasing. This functional depends on the physical process to form the luminous objects and the primordial fluctuation of the universe.

As an example, in usual biased galaxy formation scenarios (Kaiser 1984; Davis et al. 1985; Bardeen et al. 1986; Coles 1989; Lumsden, Heavens & Peacock 1989), the galaxies form at high density peaks of primordial fluctuation. Adopting this hypothesis, the CDM model can explain the observations of two-point correlation function (e.g., Davis & Peebles 1983) on small scales. However, recent observations as Automatic Plate Measuring Facility (APM) survey (Maddox et al. 1990), Queen Mary and West field College Durham, Oxford and Toronto (QDOT) redshift survey (Efstathiou et al. 1990; Saunders, Rowan-Robinson & Lawrence 1992; Moore et al. 1992) suggest that the clustering of galaxies on large-scales $\gtrsim 10h^{-1}$Mpc is stronger than that of standard CDM model. It is pointed out that this discrepancy can be reconciled by introducing nonlocally biasing mechanisms as quasor-modulated galaxy formation (Babul & White 1991) or cooperative galaxy formation (Bower et al. 1993) rather than the simple biasing by peaks.

Though the biasing by peaks is a simple model to investigate, more complicated biasing is certainly present in reality. The real bias is determined by gravitational and hydrodynamical mechanisms (Cen & Ostriker 1992, 1993), but the right form of nonlocal bias is not known yet.

The local bias, represented by a function $\rho_L(\boldsymbol{r}) = f(\rho_b(\boldsymbol{r}))$ instead of a functional, is widely explored so far. Kaiser (1984) showed that the enhancement of two-point correlation function of clusters relative to that of galaxies (see, e.g., Bahcall & Soneira 1983; Klypin & Kopylov 1983; Hauser & Peebles 1973; Postman, Huchra & Geller 1992; Mann, Heavens & Peacock 1993; Croft & Efstathiou 1994; Watanabe, Matsubara & Suto 1994) can be explained by local biasing between galaxy distribution and cluster distribution. He adopted a model that the biased objects are homogeneously formed in the region where the value of underlying field $\delta_b(\boldsymbol{r})$ is larger than the threshold ν in units of *rms* σ of underlying field, and then calculated the two-point correlation function of the biased objects in high ν, and large-separation limit for random Gaussian underlying field. In this model, the biasing is local and represented by a step function as $\rho_B(\boldsymbol{r}) = \theta(\delta_b(\boldsymbol{r}) - \nu\sigma)$. The generalization of this result to N-point correlation functions or to the expressions with loosened restriction on ν and/or separation (Politzer & Wise 1984; Jensen &

Szalay 1986) was performed. Further generalizations to the case in which the underlying field has non-Gaussianity (Fry 1986; Grinstein & Wise 1986; Matarrese, Lucchin & Bonometto 1986), and/or the case of general form of local biasing function which is not necessarily the step function (Szalay 1988; Borgani & Bonometto 1989, 1990). In these generalizations, however, the biasing is restricted to be local.

The biasing by peaks does not fall under the category of local bias. The average peak number density for Gaussian random field was analytically calculated (Doroshkevich 1970; Adler 1981; Bardeen et al. 1986). Some approximations for correlation functions of peaks are known (Bardeen et al. 1986; Otto, Politzer & Wise 1986; Cline et al. 1987). Average peak number density for generally non-Gaussian random fields for high-threshold limit is also known (Catelan, Lucchin & Matarrese 1988). In the following, we provide the unified point of view for these calculation of the statistics of generally biased field, and theoretical applications of our formalism.

4.2 NON-GAUSSIAN RANDOM FLUCTUATIONS

4.2.1 Correlation statistics

We introduce first a homogeneous random field $\alpha(\boldsymbol{x})$ with zero mean in three-dimensional space. For astrophysical applications, this random field corresponds to, e.g., the smoothed density fluctuation,

$$\delta_R(\boldsymbol{x}) = \int d^3y W_R(|\boldsymbol{x}-\boldsymbol{y}|)\delta(\boldsymbol{y}), \tag{4.2.1}$$

or normalized density fluctuation, $\delta_R(\boldsymbol{x})/\langle\delta_R^2\rangle^{1/2}$, etc., depending on specific applications. In the applications below, α is always regarded as normalized density fluctuation. In the above notations, $\delta \equiv \rho/\bar{\rho} - 1$ is the density contrast and W_R is the window function which cut the high frequency component higher than $1/R$. Two popular forms are the Gaussian window:

$$W_R^{(\mathrm{G})}(x) = \frac{1}{(2\pi R^2)^{3/2}} \exp\left(-\frac{x^2}{2R^2}\right), \tag{4.2.2}$$

and the top-hat window:

$$W_R^{(\mathrm{TH})}(x) = \frac{3}{4\pi R^3}\theta(R-x). \tag{4.2.3}$$

We review some correlation statistics for a general field α below (see also section 2.3).

The probability distribution for a field α is specified by a functional $\mathcal{P}[\alpha]$. Averaging $\langle \cdots \rangle$ is represented by a functional integration as

$$\langle \cdots \rangle = \int [d\alpha] \cdots \mathcal{P}[\alpha]. \tag{4.2.4}$$

The mean value of N-product of the field is called N-th moment:

$$\mu^{(N)}(\boldsymbol{x}_1, \ldots, \boldsymbol{x}_N) \equiv \langle \alpha(\boldsymbol{x}_1) \cdots \alpha(\boldsymbol{x}_N) \rangle. \tag{4.2.5}$$

These moments are generated by the following generating functional:

$$Z[J] \equiv \int [d\alpha] \mathcal{P}[\alpha] \exp\left[i \int d^3x J(\boldsymbol{x}) \alpha(\boldsymbol{x}) \right], \tag{4.2.6}$$

through the functional differentiation:

$$\mu^{(N)}(\boldsymbol{x}_1, \ldots, \boldsymbol{x}_N) = \left. \frac{(-i)^N \delta^N Z}{\delta J(\boldsymbol{x}_1) \cdots \delta J(\boldsymbol{x}_N)} \right|_{J=0}. \tag{4.2.7}$$

We usually use reduced moments rather than mere moments. The N-th reduced moment is defined by

$$\psi^{(N)}(\boldsymbol{x}_1, \ldots, \boldsymbol{x}_N) \equiv \langle \alpha(\boldsymbol{x}_1) \ldots \alpha(\boldsymbol{x}_N) \rangle_{\rm c}, \tag{4.2.8}$$

where $\langle \cdots \rangle_{\rm c}$ denotes "connected part" of the moment (Bertschinger 1992) removing the disconnected parts from the moment. The reduced moments are called semi-invariants or cumulants in probability theory and related to the connected Green's function in quantum field theory. When α is identified with the density contrast δ as in section 2.3, the N-point correlation function ξ_N in the continuum limit in cosmology (e.g., Peebles 1980) is identical to the N-th reduced moment, neglecting shot noise effect. When the statistics of a field α is Gaussian, the reduced moments larger than or equal to third order are all vanish.

According to the celebrated "cumulant expansion theorem" (section 2.3, Appendix B), reduced moments are generated by logarithm of moment-generating functional $Z[J]$:

$$\psi^{(N)}(\boldsymbol{x}_1, \ldots, \boldsymbol{x}_N) = \left. \frac{(-i)^N \delta^N \ln Z}{\delta J(\boldsymbol{x}_1) \cdots \delta J(\boldsymbol{x}_N)} \right|_{J=0} \tag{4.2.9}$$

where $\psi^{(0)}$ is set to zero formally. Thus,

$$Z[J] = \exp\left[\sum_{N=2}^{\infty} \frac{i^N}{N!} \int d^3x_1 \cdots d^3x_N \psi^{(N)}(\boldsymbol{x}_1, \ldots, \boldsymbol{x}_N) J(\boldsymbol{x}_1) \cdots J(\boldsymbol{x}_N) \right] \tag{4.2.10}$$

provide a very useful way to tackle non-Gaussian random fields because it relates the probability distribution functional $\mathcal{P}[\alpha]$ and the reduced moments through the equation (4.2.6).

4.2.2 Generalized Wiener-Hermite functionals

We define generalized Wiener-Hermite functionals which play essential roles in our analyses below. For a given random field $\alpha(\boldsymbol{x})$, the generalized Wiener-Hermite functionals are defined by

$$\mathcal{H}^{(m)}(\boldsymbol{x}_1,\ldots,\boldsymbol{x}_m) = \exp\left[\frac{1}{2}\int d^3x d^3y \alpha(\boldsymbol{x})\psi^{-1}(\boldsymbol{x},\boldsymbol{y})\alpha(\boldsymbol{y})\right] \times \frac{(-1)^m\delta^m}{\delta\alpha(\boldsymbol{x}_1)\cdots\delta\alpha(\boldsymbol{x}_m)} \exp\left[-\frac{1}{2}\int d^3x d^3y \alpha(\boldsymbol{x})\psi^{-1}(\boldsymbol{x},\boldsymbol{y})\alpha(\boldsymbol{y})\right], \quad (4.2.11)$$

where ψ^{-1} denotes an infinite dimensional inverse matrix of ψ defined formally by

$$\int d^3y \psi^{-1}(\boldsymbol{x},\boldsymbol{y})\psi(\boldsymbol{y},\boldsymbol{z}) = \delta^3(\boldsymbol{x}-\boldsymbol{z}), \quad (4.2.12)$$

and ψ is an arbitrary function of two points in space in general situations. In the following, we designate ψ in the above definition of generalized Wiener-Hermite functionals as 2nd reduced moment $\psi^{(2)}$ defined by equation (4.2.8) with $N = 2$. The *generalized* Wiener-Hermite functionals are reduced to the Wiener-Hermite functionals in the special case $\psi(\boldsymbol{x},\boldsymbol{y}) = \delta^3(\boldsymbol{x}-\boldsymbol{y})$. The following functionals defined by infinite dimensional linear combinations of equation (4.2.11) as

$$\mathcal{H}_{(m)}(\boldsymbol{x}_1,\ldots,\boldsymbol{x}_m) = \int d^3y_1\cdots d^3y_m \psi(\boldsymbol{x}_1,\boldsymbol{y}_1)\cdots\psi(\boldsymbol{x}_m,\boldsymbol{y}_m)\mathcal{H}^{(m)}(\boldsymbol{y}_1,\ldots,\boldsymbol{y}_m), \quad (4.2.13)$$

are convenient for our purposes below. Note that we distinguish two classes of functionals (4.2.11) and (4.2.13) by the place of (m). The latter functionals are also called generalized Wiener-Hermite functionals. The generalized Wiener-Hermite functionals defined above are the natural generalization of the generalized Wiener-Hermite polynomials (e.g., Appel & de Fériet 1926) which have finite degrees of freedom rather than three dimensional continuum degree of freedom. The first several forms of $\mathcal{H}_{(m)}$ are

$$\mathcal{H}_{(0)} \equiv 1, \quad (4.2.14)$$

$$\mathcal{H}_{(1)}(\boldsymbol{x}) = \alpha(\boldsymbol{x}), \quad (4.2.15)$$

$$\mathcal{H}_{(2)}(\boldsymbol{x}_1,\boldsymbol{x}_2) = \alpha(\boldsymbol{x}_1)\alpha(\boldsymbol{x}_2) - \psi(\boldsymbol{x}_1,\boldsymbol{x}_2), \quad (4.2.16)$$

$$\mathcal{H}_{(3)}(\boldsymbol{x}_1,\boldsymbol{x}_2,\boldsymbol{x}_3) = \alpha(\boldsymbol{x}_1)\alpha(\boldsymbol{x}_2)\alpha(\boldsymbol{x}_3) - [\psi(\boldsymbol{x}_1,\boldsymbol{x}_2)\alpha(\boldsymbol{x}_3) + \psi(\boldsymbol{x}_1,\boldsymbol{x}_3)\alpha(\boldsymbol{x}_2) + \psi(\boldsymbol{x}_2,\boldsymbol{x}_3)\alpha(\boldsymbol{x}_1)], \quad (4.2.17)$$

$$\mathcal{H}_{(4)}(\boldsymbol{x}_1,\boldsymbol{x}_2,\boldsymbol{x}_3,\boldsymbol{x}_4) = \alpha(\boldsymbol{x}_1)\alpha(\boldsymbol{x}_2)\alpha(\boldsymbol{x}_3)\alpha(\boldsymbol{x}_4)$$

$$
\begin{aligned}
&- [\psi(\boldsymbol{x}_1,\boldsymbol{x}_2)\alpha(\boldsymbol{x}_3)\alpha(\boldsymbol{x}_4) + \psi(\boldsymbol{x}_1,\boldsymbol{x}_3)\alpha(\boldsymbol{x}_2)\alpha(\boldsymbol{x}_4) + \psi(\boldsymbol{x}_1,\boldsymbol{x}_4)\alpha(\boldsymbol{x}_2)\alpha(\boldsymbol{x}_3) \\
&+ \psi(\boldsymbol{x}_2,\boldsymbol{x}_3)\alpha(\boldsymbol{x}_1)\alpha(\boldsymbol{x}_4) + \psi(\boldsymbol{x}_2,\boldsymbol{x}_4)\alpha(\boldsymbol{x}_1)\alpha(\boldsymbol{x}_3) + \psi(\boldsymbol{x}_3,\boldsymbol{x}_4)\alpha(\boldsymbol{x}_1)\alpha(\boldsymbol{x}_2)] \\
&+ [\psi(\boldsymbol{x}_1,\boldsymbol{x}_2)\psi(\boldsymbol{x}_3,\boldsymbol{x}_4) + \psi(\boldsymbol{x}_1,\boldsymbol{x}_3)\psi(\boldsymbol{x}_2,\boldsymbol{x}_4) + \psi(\boldsymbol{x}_1,\boldsymbol{x}_4)\psi(\boldsymbol{x}_2,\boldsymbol{x}_3)]\,.
\end{aligned}
\tag{4.2.18}
$$

The generalized Wiener-Hermite functionals $\mathcal{H}^{(m)}, \mathcal{H}_{(m)}$ are symmetric about its argument $\boldsymbol{x}_1,\ldots,\boldsymbol{x}_m$ and are regarded as functionals of a field $\alpha(\boldsymbol{x})$. Under linear transformation of a field α:

$$
\alpha'(\boldsymbol{x}) = \int d^3y M(\boldsymbol{x},\boldsymbol{y})\alpha(\boldsymbol{y}), \tag{4.2.19}
$$

the generalized Wiener-Hermite functionals transform as follows:

$$
\begin{aligned}
&\mathcal{H}'^{(m)}(\boldsymbol{x}_1,\ldots,\boldsymbol{x}_m) \\
&\quad = \int d^3y_1\cdots d^3y_m M^{-1}(\boldsymbol{x}_1,\boldsymbol{y}_1)\cdots M^{-1}(\boldsymbol{x}_m,\boldsymbol{y}_m)\mathcal{H}^{(m)}(\boldsymbol{y}_1,\ldots,\boldsymbol{y}_m), \qquad (4.2.20) \\
&\mathcal{H}'_{(m)}(\boldsymbol{x}_1,\ldots,\boldsymbol{x}_m) \\
&\quad = \int d^3y_1\cdots d^3y_m M(\boldsymbol{x}_1,\boldsymbol{y}_1)\cdots M(\boldsymbol{x}_m,\boldsymbol{y}_m)\mathcal{H}_{(m)}(\boldsymbol{y}_1,\ldots,\boldsymbol{y}_m), \qquad (4.2.21)
\end{aligned}
$$

where M^{-1} is an infinite dimensional inverse matrix of M:

$$
\int d^3y M^{-1}(\boldsymbol{x},\boldsymbol{y})M(\boldsymbol{y},\boldsymbol{z}) = \delta^3(\boldsymbol{x}-\boldsymbol{z}). \tag{4.2.22}
$$

Thus, we can regard $\mathcal{H}^{(m)}$ as infinite dimensional covariant tensors and $\mathcal{H}_{(m)}$ as infinite dimensional contravariant tensors. In physical applications, the linear transformation (4.2.19) is considered as smoothing of a field α if M is a low-pass filter or is considered as the Fourier transform if $M(\boldsymbol{x},\boldsymbol{y}) = \exp(-i\boldsymbol{x}\cdot\boldsymbol{y})$. The following recursion relation,

$$
\left[\alpha(\boldsymbol{x}_m) - \int d^3y\psi(\boldsymbol{x}_{m+1},\boldsymbol{y})\frac{\delta}{\delta\alpha(\boldsymbol{y})}\right]\mathcal{H}_{(m)}(\boldsymbol{x}_1,\ldots,\boldsymbol{x}_m) = \mathcal{H}_{(m+1)}(\boldsymbol{x}_1,\ldots,\boldsymbol{x}_{m+1}), \tag{4.2.23}
$$

are helpful properties of the functionals.

4.2.3 Expectation values

The averaging (4.2.4) for a non-Gaussian random field is reduced to the averaging for a Gaussian random field using the generalized Wiener-Hermite functionals as we

shall see below. First of all, with a given distribution $\mathcal{P}[\alpha]$, we associate a Gaussian distribution $\mathcal{P}_{\rm G}[\alpha]$ constructed by the 2nd reduced moment ψ of the original distribution $\mathcal{P}[\alpha]$:

$$P_{\rm G}[\alpha] = N_{\rm G} \exp\left[-\frac{1}{2}\int d^3x d^3y \alpha(\boldsymbol{x})\psi^{-1}(\boldsymbol{x},\boldsymbol{y})\alpha(\boldsymbol{y})\right], \tag{4.2.24}$$

where $N_{\rm G}$ is a formal normalization constant:

$$N_{\rm G} = \left\{\int [d\alpha] \exp\left[-\frac{1}{2}\int d^3x d^3y \alpha(\boldsymbol{x})\psi^{-1}(\boldsymbol{x},\boldsymbol{y})\alpha(\boldsymbol{y})\right]\right\}^{-1}. \tag{4.2.25}$$

The averaging by this Gaussian distribution $\mathcal{P}_{\rm G}[\alpha]$ is denoted as $\langle\cdots\rangle_{\rm G}$ distinguished from the averaging by the original non-Gaussian field: $\langle\cdots\rangle$.

The relation between the non-Gaussian distribution $\mathcal{P}[\alpha]$ and the Gaussian distribution $\mathcal{P}[\alpha]$ is

$$\mathcal{P}[\alpha] = \exp\left[\sum_{N=3}^{\infty}\frac{(-1)^N}{N!}\int d^3x_1\cdots d^3x_N \psi^{(N)}(\boldsymbol{x}_1,\ldots,\boldsymbol{x}_N)\frac{\delta}{\delta\alpha(\boldsymbol{x}_1)}\cdots\frac{\delta}{\delta\alpha(\boldsymbol{x}_N)}\right] P_{\rm G}[\alpha]. \tag{4.2.26}$$

This relation is proven as follows: the generating functional $Z[J]$ is (infinite dimensional) Fourier transform of distribution functional $\mathcal{P}[\alpha]$. Thus the inverse Fourier transform gives the expression of $\mathcal{P}[\alpha]$ in terms of reduced moments because of equation (4.2.10). Substituting $i\delta/\delta\alpha(\boldsymbol{x})$ for $J(\boldsymbol{x})$, and performing Gaussian integration, we finally arrive at the relation (4.2.26). Expanding the exponential of equation (4.2.26) and using the definition of the generalized Wiener-Hermite functionals, we can express non-Gaussian averaging of arbitrary functional $F[\alpha]$ by Gaussian averaging as follows:

$$\begin{aligned}\langle F[\alpha]\rangle &= \langle F[\alpha]\rangle_{\rm G} \\ &+ \sum_{m=1}^{\infty}\frac{1}{m!}\sum_{n_1=3}^{\infty}\cdots\sum_{n_m=3}^{\infty}\frac{1}{n_1!\cdots n_m!}\int\prod_{l=1}^{m}\prod_{k=1}^{n_l} d^3x_l^{(k)}\cdot\prod_{l=1}^{m}\psi^{(n_l)}(\boldsymbol{x}_l^{(1)},\ldots\boldsymbol{x}_l^{(n_l)}) \\ &\times\left\langle\mathcal{H}^{(n_1+\cdots+n_m)}(\boldsymbol{x}_1^{(1)},\ldots,\boldsymbol{x}_1^{(n_1)},\ldots,\boldsymbol{x}_m^{(1)},\ldots,\boldsymbol{x}_m^{(n_m)})F[\alpha]\right\rangle_{\rm G}.\end{aligned} \tag{4.2.27}$$

This equation is an expansion of a non-Gaussian averaging by higher order reduced moments. The nontrivial part in the equation (4.2.27) is the factor of the form, $\langle\mathcal{H}F\rangle_{\rm G}$. In Appendix B, the methods to calculate the Gaussian averaging of the product of generalized Wiener-Hermite functionals, $\langle\prod\mathcal{H}\rangle_{\rm G}$ are developed. Therefore, if a functional $F[\alpha]$ is expressed by the sum of the product of generalized Wiener-Hermite functionals, the right-hand-side of equation (4.2.27) can be calculated as performed in the next section.

4.3 DIAGRAMMATIC CALCULUS OF N-POINT CORRELATION FUNCTIONS

4.3.1 Generalized Wiener-Hermite expansion and diagrammatic methods

We are interested in the correlations of a density field $\rho_{\rm B}(\boldsymbol{r},[\alpha])$ which appears by some biasing mechanism from a field $\alpha(\boldsymbol{x})$. We formally do not restrict the form of biasing in this subsection and consider a given, generally nonlocal, biasing functional $\rho_{\rm B}(\boldsymbol{r},[\alpha])$ which is both a function of a point $\boldsymbol{r}$ and a functional of a field $\alpha(\boldsymbol{x})$. It is natural to expand this functional by the generalized Wiener-Hermite functionals as follows:

$$\rho_{\rm B}(\boldsymbol{r},[\alpha]) = \sum_{m=0}^{\infty}\frac{1}{m!}\int d^3x^{(1)}\cdots d^3x^{(m)}K^{(m)}(\boldsymbol{r}-\boldsymbol{x}^{(1)},\cdots,\boldsymbol{r}-\boldsymbol{x}^{(m)})\mathcal{H}_{(m)}(\boldsymbol{x}^{(1)},\ldots,\boldsymbol{x}^{(m)}), \tag{4.3.1}$$

where the kernel $K^{(m)}$ is given by

$$K^{(m)}(\boldsymbol{r}-\boldsymbol{x}^{(1)},\ldots,\boldsymbol{r}-\boldsymbol{x}^{(m)}) = \left\langle\mathcal{H}^{(m)}(\boldsymbol{x}^{(1)},\ldots,\boldsymbol{x}^{(m)})\rho_{\rm B}(\boldsymbol{r},[\alpha])\right\rangle_{\rm G} \tag{4.3.2}$$

$$= \left\langle\frac{\delta^m\rho_{\rm B}(\boldsymbol{r},[\alpha])}{\delta\alpha(\boldsymbol{x}^{(1)})\cdots\delta\alpha(\boldsymbol{x}^{(m)})}\right\rangle_{\rm G}. \tag{4.3.3}$$

The equation (4.3.2) is derived from the orthogonality of the generalized Wiener-Hermite functionals (B.20) in appendix B. We assume that the expansion (4.3.1) exists for the nonlocal biasing of our interest. Using equation (4.2.27), the N-th moment of a biased density field $\rho_{\rm B}$ is given by somewhat complicated expression:

$$P_N(\boldsymbol{r}_1,\ldots,\boldsymbol{r}_N)\equiv\langle\rho_{\rm B}(\boldsymbol{r}_1,[\alpha])\cdots\rho_{\rm B}(\boldsymbol{r}_N,[\alpha])\rangle \tag{4.3.4}$$

$$\begin{aligned}
&= \sum_{m_1=0}^{\infty}\cdots\sum_{m_N=0}^{\infty}\int\prod_{i=1}^{N}\prod_{a=1}^{m_i}d^3x_i^{(a)}\cdot\prod_{i=1}^{N}\frac{1}{m_i!}K^{(m_i)}(\boldsymbol{r}_i-\boldsymbol{x}_i^{(1)},\ldots,\boldsymbol{r}_i-\boldsymbol{x}_i^{(m_i)})\\
&\times\left[\left\langle\prod_{i=1}^{N}\mathcal{H}_{m_i}(\boldsymbol{x}_i^{(1)},\ldots,\boldsymbol{x}_i^{(m_i)})\right\rangle_{\rm G}+\sum_{m=1}^{\infty}\frac{1}{m!}\sum_{n_1=3}^{\infty}\cdots\sum_{n_m=3}^{\infty}\frac{1}{n_1!\cdots n_m!}\right.\\
&\times\int\prod_{l=1}^{m}\prod_{k=1}^{n_l}d^3y_l^{(k)}\cdot\prod_{l=1}^{m}\psi^{(n_l)}(\boldsymbol{y}_l^{(1)},\ldots,\boldsymbol{y}_l^{(n_l)})\\
&\left.\times\left\langle\mathcal{H}^{(n_1+\cdots+n_m)}(\boldsymbol{y}_1^{(1)},\ldots,\boldsymbol{y}_1^{(n_1)},\ldots,\boldsymbol{y}_m^{(1)},\ldots,\boldsymbol{y}_m^{(n_m)})\prod_{i=1}^{N}\mathcal{H}_{(m_i)}(\boldsymbol{x}_i^{(1)},\ldots,\boldsymbol{x}_i^{(m_i)})\right\rangle_{\rm G}\right].
\end{aligned} \tag{4.3.5}$$

This expression can be calculated making use of the methods described in Appendix B. The diagrammatic method in calculating Gaussian expectation value of the

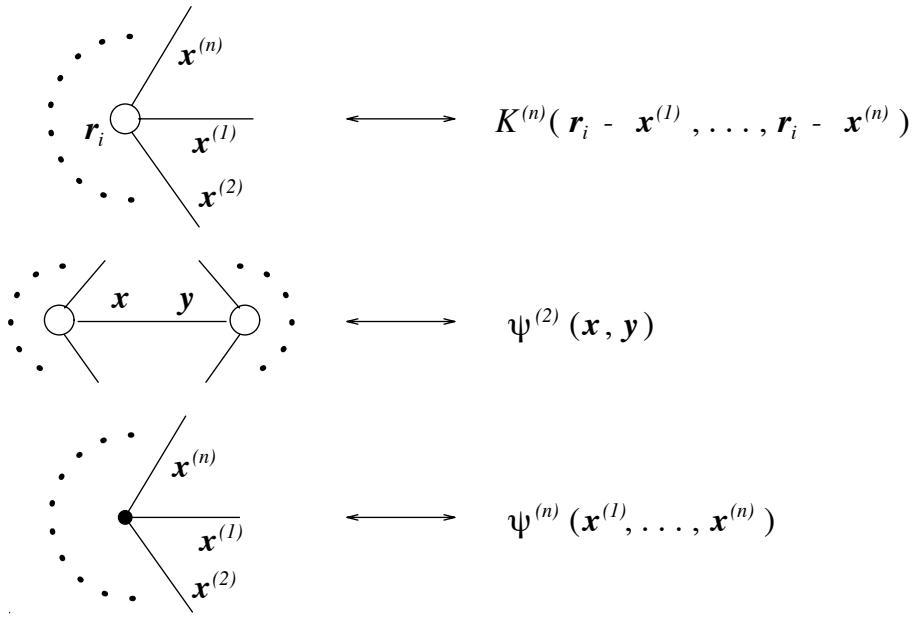

Figure 4.1: Diagrammatic rules for the nonlocal bias. The open circles and filled circles corresponds to external points and vertices, respectively.

product of generalized Wiener-Hermite functionals is translated to the diagrammatic method in calculating moments (4.3.5) of $\rho_{\rm B}$. The result is summarized as the following procedures:

A-i) Draw N open circles corresponding to $\boldsymbol{r}_1, \ldots, \boldsymbol{r}_N$ which we call external points.

A-ii) Consider one of possible graphs with lines between external points or between external points and vertices. Vertices are the parts where three or more ends of lines are gathered. Do not connect two vertices directly with lines. Do not draw any line whose two ends are placed at the same external point or the same vertex.

A-iii) Associate labels like $\boldsymbol{x}, \boldsymbol{y}$, etc. with ends of lines placed at external points (not at vertices).

A-iv) Apply the correspondence of Figure 4.1 for the external points, lines between external points and vertices. Make the product of these factors of the graph.

A-v) Integrate with respect to all the labels and multiply the following statistical factor:

$$\frac{1}{\prod\limits_{\substack{\text{identical}\\ \text{lines}}} n_{\rm L}! \prod\limits_{\substack{\text{identical}\\ \text{vertices}}} n_{\rm V}!}, \tag{4.3.6}$$

where $n_{\rm L}$ and $n_{\rm L}$ are, respectively, the number of lines and vertices whose ends are identical. This statistical factor is for the case we do not distinguish vertices in the graph.

A-vi) Sum up values obtained from all the possible graphs.

The readers are invited to calculate several examples both by equation (4.3.5) and by the above diagrammatic rules. The Appendix C is devoted to the explanation of the statistical factor (4.3.6).

This diagrammatic rules enable us to easily calculate lower order terms about $\psi^{(m)}$ or $K^{(m)}$. Although we are not guaranteed the sufficient convergence of this diagrammatic expansion in the general situation, there are many cases in astrophysics where this expansion is useful as we shall see in section 4.4.

The reduced N-point correlation function of the biased density field $\rho_{\rm B}$:

$$\xi_{\rm B}^{(N)}(\boldsymbol{r}_1,\ldots,\boldsymbol{r}_N) = \frac{1}{\bar{\rho}_{\rm B}^N}\left\langle \rho_{\rm B}(\boldsymbol{r}_1,[\alpha])\cdots\rho_{\rm B}(\boldsymbol{r}_N,[\alpha])\right\rangle_{\rm c}, \tag{4.3.7}$$

is more easily evaluated in this diagrammatic expansion because the contribution to the reduced moment in equation (4.3.7) comes from connected graphs in our approach. This especially simplify the calculation of higher order correlation functions of the biased field. Thus, the above rules are applicable to the calculation of reduced N-point correlation functions substituting the following rule for A-vi).

A-vi) Sum up values obtained from all the connected graphs and multiply $(P_1)^{-N}$.

4.3.2 Local and semi-nonlocal biases

Here we consider special cases of the above general consideration, i.e., the case biasing is local or semi-nonlocal.

The local bias is defined so that the biasing functional $\rho_{\rm B}(\boldsymbol{r},[\alpha])$ is a mere function of the underlying field α at the position $\boldsymbol{r}$:

$$\rho_{\rm B} = \rho_{\rm B}\left(\alpha(\boldsymbol{r})\right). \tag{4.3.8}$$

In this case, the kernels [equation (4.3.3)] have the forms,

$$K^{(m)}(\boldsymbol{r}-\boldsymbol{x}^{(1)},\ldots,\boldsymbol{r}-\boldsymbol{x}^{(m)}) = \delta^3(\boldsymbol{r}-\boldsymbol{x}^{(1)})\cdots\delta^3(\boldsymbol{r}-\boldsymbol{x}^{(m)})R_m, \tag{4.3.9}$$

where

$$R_m = \left\langle \frac{\partial^m \rho_{\rm B}}{\partial \alpha^m} \right\rangle. \tag{4.3.10}$$

If the field α is normalized so that $\langle\alpha^2\rangle = 1$, R_m's are coefficients of the Hermite expansion of the local biasing function:

$$\rho_{\rm B}(\alpha) = \sum_{m=0}^{\infty} \frac{R_m}{m!} H_m(\alpha); \tag{4.3.11}$$

$$R_m = \frac{1}{\sqrt{2\pi}} \int_{-\infty}^{\infty} d\alpha e^{-\alpha^2/2} \rho_{\rm B}(\alpha) H_m(\alpha). \tag{4.3.12}$$

The definition of Hermite polynomials and its orthogonality relations are,

$$H_m(\alpha) = e^{\alpha^2/2}\left(-\frac{d}{d\alpha}\right)^m e^{-\alpha^2/2}, \tag{4.3.13}$$

and

$$\frac{1}{\sqrt{2\pi}} \int_{-\infty}^{\infty} dx e^{-x^2/2} H_m(x) H_n(x) = m!\,\delta_{mn}, \tag{4.3.14}$$

respectively. If the field α is not normalized and $\langle\alpha^2\rangle = \sigma^2 \neq 1$, the corresponding expansion is

$$\rho_{\rm B}(\alpha) = \sum_{m=0}^{\infty} \frac{R_m}{m!} \sigma^m H_m(\alpha/\sigma); \tag{4.3.15}$$

$$R_m = \frac{1}{\sqrt{2\pi}\sigma^{m+1}} \int_{-\infty}^{\infty} d\alpha e^{-\alpha^2/(2\sigma^2)} \rho_{\rm B}(\alpha) H_m(\alpha/\sigma). \tag{4.3.16}$$

The special form of equation (4.3.9) reduce the diagrammatic rules A-i) $\sim$ A-vi) above to the following ones:

B-i) Same as A-i)

B-ii) Same as A-ii)

B-iii) Apply the correspondence of Figure 4.2 and make the product of these factors of the graph.

B-iv) Multiply the statistical factor (4.3.6).

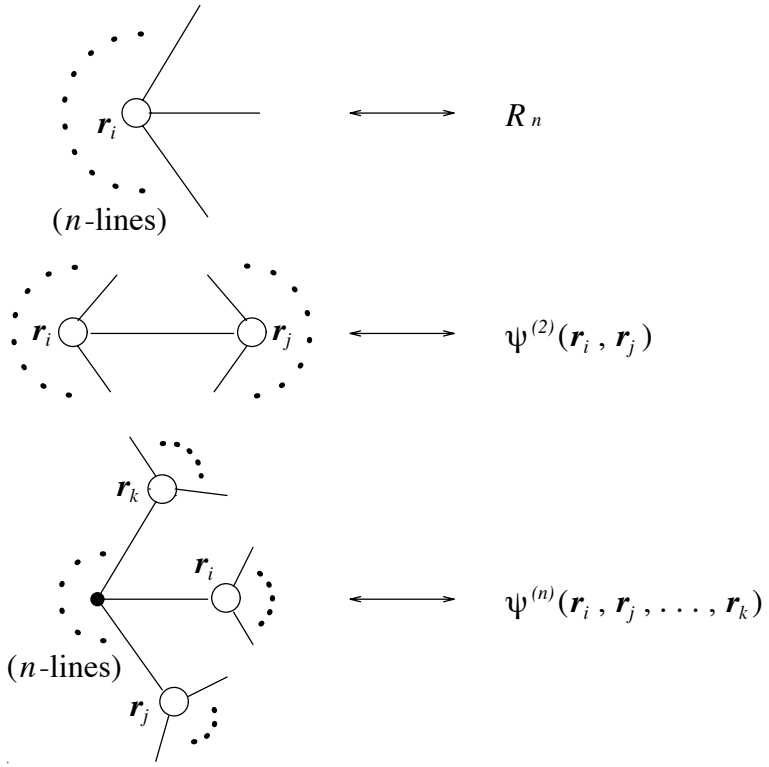

Figure 4.2: Diagrammatic rules for the local bias.

B-v) For P_N, sum up values obtained from all the possible graphs. For reduced N-point correlation function, sum up values obtained from all the connected graphs and multiply $(P_1)^{-N}$.

The above rules for P_N could be expressed by the following equation:

$$P_N(\boldsymbol{r}_1,\ldots,\boldsymbol{r}_N) = \sum_{m=0}^{\infty}\sum_{n_{11}=0}^{\infty}\cdots\sum_{n_{1N}=0}^{\infty}\cdots\sum_{n_{m1}=0}^{\infty}\cdots\sum_{n_{mN}=0}^{\infty}\frac{R_{\Sigma_j n_{j1}}\cdots R_{\Sigma_j n_{jN}}}{m!\prod_{j=1}^{m}\prod_{k=1}^{N} n_{jk}!}$$
$$\times w^{(\Sigma_k n_{1k})}(\underbrace{1,\ldots,1}_{n_{11}},\ldots,\underbrace{N,\ldots,N}_{n_{1N}})\cdots w^{(\Sigma_k n_{mk})}(\underbrace{1,\ldots,1}_{n_{m1}},\ldots,\underbrace{N,\ldots,N}_{n_{mN}}). \tag{4.3.17}$$

where

$$\begin{aligned} &w^{(0)} = 0, \\ &w^{(1)}(i) = 0, \\ &w^{(2)}(i,j) = (1-\delta_{ij})\psi^{(2)}(\boldsymbol{r}_i,\boldsymbol{r}_j) \\ &w^{(n)}(i_1,\ldots,i_n) = \psi^{(n)}(\boldsymbol{r}_{i_1}\ldots,\boldsymbol{r}_{i_n}) \qquad (n\geq 3). \end{aligned} \tag{4.3.18}$$

Identifying the underlying field α with normalized density fluctuation $\delta_R(\boldsymbol{x})/\langle\delta_R^2\rangle^{1/2}$, this formula is an alternative expression to one obtained by Borgani & Bonometto (1989, 1990) who adopted the different approach to treat the local biasing function $\rho_{\rm B}$ in evaluating the same quantity of equation (4.3.17). Our expression seems to be simpler than theirs.

When the statistics of an underlying field is random Gaussian, equation (4.3.17) reduces to

$$P_N(\boldsymbol{r}_1,\ldots,\boldsymbol{r}_N) = \sum_{m=0}^{\infty}\sum_{\{m_{kl}|m\}}\prod_{k<l}\frac{[\psi(\boldsymbol{r}_k,\boldsymbol{r}_l)]^{m_{kl}}}{m_{kl}!}\cdot\prod_{r=1}^{N}R_{m_r}, \tag{4.3.19}$$

In the above equation, $1\leq k,l\leq N$,

$$m_r = \sum_{k=1}^{r-1} m_{kr} + \sum_{k=r+1}^{N} m_{rk} \tag{4.3.20}$$

and $\sum_{\{m_{kl}|m\}}$ means the sum over m_{kl}'s $(k<l)$ which are non-negative integers with a constraint, $\sum_{k<l} m_{kl} = m$. We can see, using multinomial expansion theorem, that the equation (4.3.19) is equivalent to the formula obtained by Szalay (1988).

When the local biasing function $\rho_{\rm B}$ is given by sharp clipping:

$$\rho_{\rm B}(\alpha) = C\theta(\alpha - \nu), \tag{4.3.21}$$

then the coefficients R_m are given by

$$R_m^{(\rm sc)} = \begin{cases} \dfrac{C}{2}\mathrm{erfc}\left(\dfrac{\nu}{\sqrt{2}}\right) & (m=0) \\ \dfrac{C}{\sqrt{2\pi}} H_{m-1}(\nu) e^{-\nu^2/2} & (m \geq 1) \end{cases}, \tag{4.3.22}$$

where

$$\mathrm{erfc}(x) = 1 - \mathrm{erf}(x) = \frac{2}{\sqrt{\pi}} \int_x^\infty e^{-x^2} dt \tag{4.3.23}$$

is a complementary error function. In this case, equation (4.3.17) reduces to the formula obtained by Matarrese et al. (1986). If we, furthermore, constrain the statistics of underlying field to be Gaussian, and local biasing function to be the sharp clipping, we can find equation (4.3.19) reduces to the the formula obtained by Jensen and Szalay (1986).

High-ν limit of equation (4.3.17) for sharp-clipping biasing function (4.3.21) enables us to sum up infinite series of graphs and results in

$$P_N = \left(\frac{C}{\sqrt{2\pi}\nu e^{\nu^2/2}}\right)^N \times \exp\left[\sum_{m=2}^{\infty} \nu^m \sum_{\substack{n_1,\ldots,n_N \geq 0 \\ n_1+\cdots+n_N=m}} \frac{1}{n_1!\cdots n_N!} w^{(m)}(\underbrace{1,\ldots,1}_{n_1},\ldots,\underbrace{N,\ldots,N}_{n_N})\right] \tag{4.3.24}$$

$$= \left(\frac{C}{\sqrt{2\pi}\nu e^{\nu^2}}\right)^N Z_N\left(J_i = \nu\right), \tag{4.3.25}$$

where

$$Z_N\left(J_i = \nu\right) = \left\langle \exp\left(\nu \sum_{i=1}^N \alpha(\boldsymbol{r}_i)\right)\right\rangle, \tag{4.3.26}$$

is a N-point moment generating function $Z_N(J_i)$ in which ν is substituted for all J_i. This formula is equivalent to the one obtained by Matarrese et al. (1986). The $N = 2$ case of equation (4.3.24) has the same form obtained by Grinstein & Wise (1986).

The local bias is not relevant to the biasing through density peaks (Davis et al. 1985; Bardeen et al. 1986; Coles 1989; Lumsden et al. 1989) because density

peaks are described by not only the mere value of the underlying field but also spatial derivatives of it (see section 4.4 for details). Thus, we next consider the case that the biasing functional $\rho_{\rm B}(\boldsymbol{r},[\alpha])$ depends on $\alpha(\boldsymbol{r})$ and finite-order derivatives of it at $\boldsymbol{r}$, generally. We denote the spatial derivatives of a underlying field α as α_μ:

$$(\alpha_\mu(\boldsymbol{x})) = \left(\underbrace{\alpha(\boldsymbol{x})}_{1}, \underbrace{\frac{\partial\alpha}{\partial x^i}}_{3}, \underbrace{\frac{\partial^2\alpha}{\partial x^i \partial x^j}(i \leq j)}_{6}, \ldots \right), \tag{4.3.27}$$

where $\mu = 0, 1, 2, \ldots$. This notation enable us to write the semi-nonlocal biasing functional as

$$\rho_{\rm B}(\boldsymbol{r},[\alpha]) = \rho_{\rm B}\left(\alpha_\mu(\boldsymbol{r})\right). \tag{4.3.28}$$

In this case, kernels (4.3.3) have the forms,

$$K^{(m)}(\boldsymbol{r}-\boldsymbol{x}^{(1)},\ldots,\boldsymbol{r}-\boldsymbol{x}^{(m)}) = \sum_{\mu_1}\cdots\sum_{\mu_m}\delta_{\mu_1}(\boldsymbol{r}-\boldsymbol{x}^{(1)})\cdots\delta_{\mu_m}(\boldsymbol{r}-\boldsymbol{x}^{(m)})R_{\mu_1\cdots\mu_m}, \tag{4.3.29}$$

where δ_μ denotes the derivatives of Dirac's delta-function in the notation of equation (4.3.27), and

$$R_{\mu_1\cdots\mu_m} \equiv \left\langle \frac{\partial}{\partial\alpha_{\mu_1}}\cdots\frac{\partial}{\partial\alpha_{\mu_m}}\rho_{\rm B}(\alpha_\mu) \right\rangle_{\rm G}. \tag{4.3.30}$$

The special form of equation (4.3.29) reduce the diagrammatic rules A-i) $\sim$ A-vi) above to the following:

C-i) Same as A-i)

C-ii) Same as A-ii)

C-iii) Associate labels like μ, ν, etc. with ends of lines placed at external points.

C-iv) Apply the correspondence of Figure 4.3 and make the product of these factors of the graph.

C-v) Perform sums with respect to all the labels and multiply the statistical factor (4.3.6).

C-vi) For P_N, sum up values obtained from all the possible graphs. For reduced N-point correlation function, sum up values obtained from all the connected graphs and multiply $(P_1)^{-N}$.

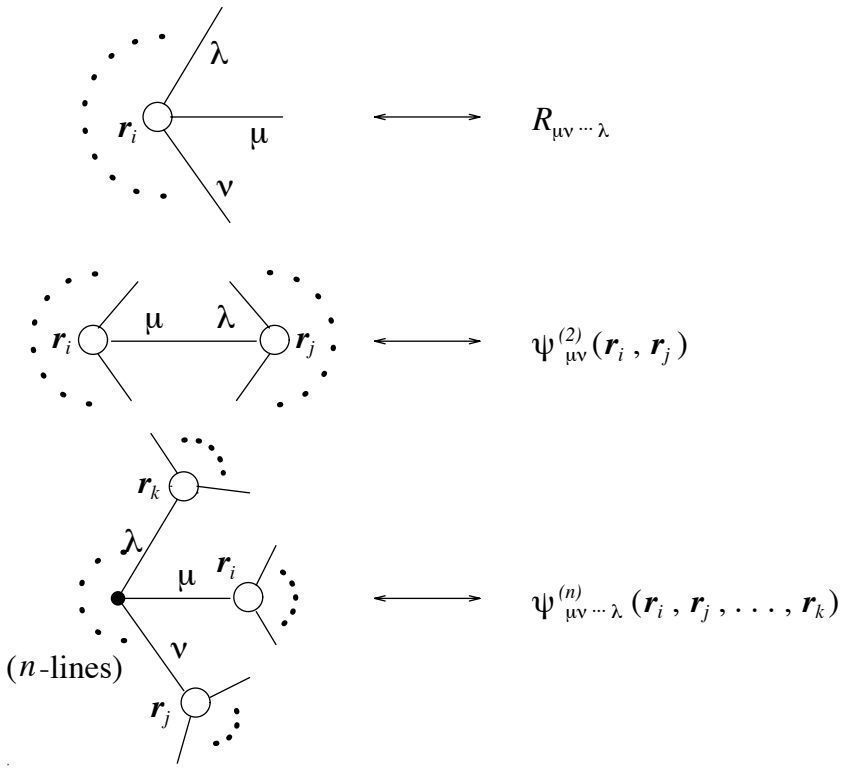

Figure 4.3: Diagrammatic rules for the semi-local bias.

In Figure 4.3, $\psi^{(2)}_{\mu\nu}(\boldsymbol{r}_i, \boldsymbol{r}_j)$ denotes the derivatives of $\psi^{(2)}$ and μ indicates the derivatives with respect to $\boldsymbol{r}_i$ according to equation (4.3.27), ν indicates the derivatives with respect to $\boldsymbol{r}_j$. Similar definition is applied to $\psi^{(n)}_{\mu\nu\cdots\lambda}(\boldsymbol{r}_i, \ldots, \boldsymbol{r}_k)$.

4.3.3 Fourier transforms

The biasing may be expressed in Fourier space rather than in coordinate space. For example, the transfer functions $T(k)$ of various cosmological models is a kind of biasing in our context through Fourier space. It may be useful for the analyses in the future to give the diagrammatic rules in Fourier space.

The Fourier transformation is a kind of the following linear transformations of a field:

$$\alpha'(\boldsymbol{k}) = \int d^3x M(\boldsymbol{k}, \boldsymbol{x})\alpha(\boldsymbol{x}) \tag{4.3.31}$$

$$\rho'_{\mathrm{B}}(\boldsymbol{p}, [\alpha']) = \int d^3r L(\boldsymbol{v}, \boldsymbol{r})\rho_{\mathrm{B}}(\boldsymbol{r}, [\alpha]), \tag{4.3.32}$$

where M and L correspond to the coefficients of the linear transformations. Fourier transformations are achieved by setting

$$M(\boldsymbol{k}, \boldsymbol{x}) = \exp(-i\boldsymbol{k}\cdot\boldsymbol{x}),\ L(\boldsymbol{p}, \boldsymbol{r}) = \exp(-i\boldsymbol{p}\cdot\boldsymbol{r}), \tag{4.3.33}$$

but we use general notations for a while. Because of the property (4.2.20), (4.2.21) of the generalized Wiener-Hermite functionals, the form of equation (4.3.5) is unchanged under linear transformations (4.3.32), if we demand the following transformation properties:

$$\psi'^{(n)}(\boldsymbol{k}_1, \ldots, \boldsymbol{k}_n) = \int d^3x_1 \cdots d^3x_n M(\boldsymbol{k}_1, \boldsymbol{x}_1)\cdots M(\boldsymbol{k}_n, \boldsymbol{x}_n)\psi^{(n)}(\boldsymbol{x}_1, \ldots, \boldsymbol{x}_n), \tag{4.3.34}$$

$$K'^{(m)}(\boldsymbol{p}; \boldsymbol{k}^{(1)}, \ldots, \boldsymbol{k}^{(m)}) = \int d^3r \int d^3x^{(1)} \cdots d^3x^{(m)} L(\boldsymbol{p}, \boldsymbol{r}) \times M^{-1}(\boldsymbol{x}^{(1)}, \boldsymbol{k}^{(1)})\cdots M^{-1}(\boldsymbol{x}^{(m)}, \boldsymbol{k}^{(m)})K^{(m)}(\boldsymbol{r} - \boldsymbol{x}^{(1)}, \ldots, \boldsymbol{r} - \boldsymbol{x}^{(m)}). \tag{4.3.35}$$

The equation (4.3.35) has the another expression,

$$K'^{(m)}(\boldsymbol{p}; \boldsymbol{k}^{(1)}, \boldsymbol{k}^{(m)}) = \left\langle \frac{\delta^m \rho'_{\mathrm{B}}(\boldsymbol{p}, [\alpha'])}{\delta\alpha'(\boldsymbol{k}^{(1)})\cdots\delta\alpha'(\boldsymbol{k}^{(m)})} \right\rangle_{\mathrm{G}}, \tag{4.3.36}$$

because of equation (4.3.3). These transformed quantities ψ' and $K'^{(m)}$ are equally applied to the diagrammatic rules i) $\sim$ vi) instead of the original quantities. This

gives a way to calculate the correlations of a biased field expressed by linearly transformed quantities (4.3.32).

Now we restrict the argument to the Fourier transformations (4.3.33). In this case, from the inverse Fourier transformation, $M^{-1}(\boldsymbol{x},\boldsymbol{k}) = \exp(i\boldsymbol{k}\cdot\boldsymbol{x})/(2\pi)^3$. Then transformed quantities are given by

$$\psi'^{(n)}(\boldsymbol{k}_1,\ldots,\boldsymbol{k}_n) = \tilde{\psi}^{(n)}(\boldsymbol{k}_1,\ldots,\boldsymbol{k}_n) = (2\pi)^3\delta^3(\boldsymbol{k}_1+\cdots+\boldsymbol{k}_n)p^{(n)}(\boldsymbol{k}_1,\ldots,\boldsymbol{k}_{n-1}), \tag{4.3.37}$$

and

$$K'^{(m)}(\boldsymbol{p};\boldsymbol{k}^{(1)},\ldots,\boldsymbol{k}^{(m)}) = (2\pi)^3\delta^3(\boldsymbol{k}^{(1)}+\cdots+\boldsymbol{k}^{(m)}-\boldsymbol{p})\frac{1}{(2\pi)^{3m}}\widetilde{K}^{(m)}(\boldsymbol{k}^{(1)},\ldots,\boldsymbol{k}^{(m)}), \tag{4.3.38}$$

where $\tilde{\psi}^{(n)}$ and $\widetilde{K}^{(m)}$ are the Fourier transformations of $\psi^{(n)}$ and $K^{(m)}$, respectively. Because of the homogeneity of a field α, the last expression of equation (4.3.37) is possible and gives a definition of the multi-spectrum $p^{(n)}$ of a field α. In the case $n=2$, $p^{(2)}$ is called power-spectrum of the field. The Fourier transform of $K^{(m)}$ is given by

$$\widetilde{K}^{(m)}(\boldsymbol{k}^{(1)},\ldots,\boldsymbol{k}^{(m)}) = (2\pi)^{3m}\left\langle\frac{\delta^m}{\delta\tilde{\alpha}(\boldsymbol{k}^{(1)})\cdots\delta\tilde{\alpha}(\boldsymbol{k}^{(m)})}\int\frac{d^3p}{(2\pi)^3}\tilde{\rho}_{\rm B}(\boldsymbol{p},[\tilde{\alpha}]\right\rangle_{\rm G}, \tag{4.3.39}$$

from the equations (4.3.36) and (4.3.38). This form is convenient if the biasing functional is expressed in Fourier space, noting that the Gaussian averaging in equation (4.3.39) is given by

$$\langle\cdots\rangle_{\rm G} = \int\cdots\prod_{\boldsymbol{k}\in{\rm uhs}}\left[\exp\left(-\frac{|\tilde{\alpha}(\boldsymbol{k})|^2}{Vp(k)}\right)\frac{2|\tilde{\alpha}(\boldsymbol{k})|d|\tilde{\alpha}(\boldsymbol{k})|}{Vp(k)}\frac{d\theta_{\boldsymbol{k}}}{2\pi}\right], \tag{4.3.40}$$

in Fourier space, where uhs means a upper half $\boldsymbol{k}$-space, $\theta_{\boldsymbol{k}}$ is a phase of $\tilde{\alpha}(\boldsymbol{k})$ so that $\tilde{\alpha}(\boldsymbol{k}) = |\tilde{\alpha}(\boldsymbol{k})|\exp(i\theta_{\boldsymbol{k}})$. The power spectrum $p(k)$ is defined by $V^{-1}\langle|\tilde{\alpha}(\boldsymbol{k})|^2\rangle$, where V is the total volume of the space. Substituting equations (4.3.37) and (4.3.38) to our rules, moments $\tilde{P}_N$ or correlations $\tilde{\xi}^{(N)}_{\rm B}$ in Fourier space are obtained. The multi-spectrum $p^{(N)}_{\rm B}(\boldsymbol{p}_1,\ldots,\boldsymbol{p}_{N-1})$ which is defined by

$$\tilde{\xi}^{(N)}_{\rm B}(\boldsymbol{p}_1,\ldots,\boldsymbol{p}_N) = (2\pi)^3\delta^3(\boldsymbol{p}_1+\cdots+\boldsymbol{p}_N)p^{(N)}_{\rm B}(\boldsymbol{p}_1,\ldots,\boldsymbol{p}_{N-1}), \tag{4.3.41}$$

is more popular than $\tilde{\xi}^{(N)}_{\rm B}$.

The procedures to obtain $\tilde{P}_N$ are summarized as the following rules:

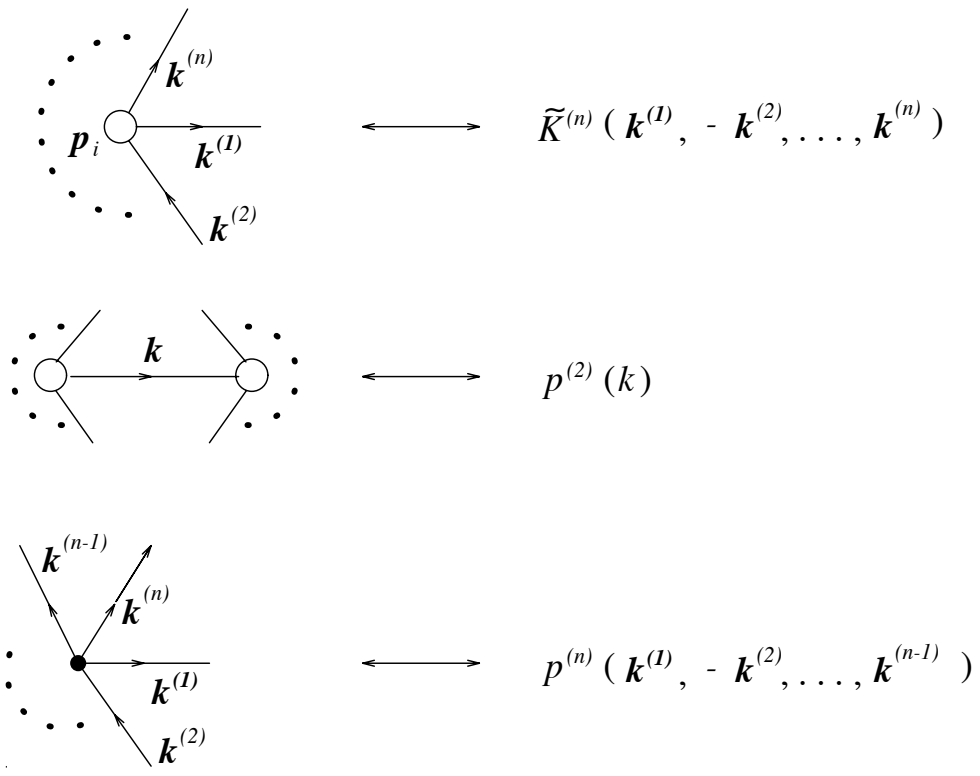

Figure 4.4: Diagrammatic rules in Fourier space.

D-i) Draw N open circles corresponding to $\boldsymbol{p}_1, \ldots, \boldsymbol{p}_N$ which we call external points.

D-ii) Same as ii)

D-iii) Define orientations to all lines and associate labels like $\boldsymbol{k}, \boldsymbol{l}$, etc. to all lines. The orientations of a line $\boldsymbol{k}$ is regarded as a direction of a current $\boldsymbol{k}$. The sum of currents flowing into a vertex should vanish and the sum of currents flowing from a external point i should be $\boldsymbol{p}_i$ (these rules are due to the δ-function in equations (4.3.37) and (4.3.38)).

D-iv) Apply the correspondence of Figure 4.4 for the external points, lines between external points and vertices. Make the product of these factors of the graph.

D-v) Perform integration $\int d^3k/(2\pi)^3$ for each label $\boldsymbol{k}$ and multiply the statistical factor (4.3.6).

D-vi) Sum up values obtained from all the possible graphs and multiply $(2\pi)^3\delta^3(\boldsymbol{p}_1 + \cdots + \boldsymbol{p}_N)$.

From the value of $\widetilde{P}_1$ which can be evaluated by the above rules, the mean density of biased field $P_1 = \bar{\rho}_{\rm B}$ is given by

$$\widetilde{P}_1(\boldsymbol{p}) = (2\pi)^3\delta^3(\boldsymbol{p})\bar{\rho}_{\rm B}. \tag{4.3.42}$$

Using $\bar{\rho}_{\rm B}$, the rules for obtaining the multi-spectrum $p_{\rm B}^{(N)}$ of biased fields are as follows:

E-i) Draw N open circles corresponding to $\boldsymbol{p}_1, \ldots, \boldsymbol{p}_{N-1}$ and $\boldsymbol{p}_N = -(\boldsymbol{p}_1 + \cdots + \boldsymbol{p}_{N-1})$ which we call external points.

E-ii) Same as ii)

E-iii) Define orientations to all lines and associate labels like $\boldsymbol{k}, \boldsymbol{l}$, etc. to all lines. The sum of currents flowing into a vertex should vanish and the sum of currents flowing from a external point i should be $\boldsymbol{p}_i$.

E-iv) Apply the correspondence of Figure 4.4 for the external points, lines between external points and vertices. Make the product of these factors of the graph.

E-v) Same as D-v)

E-vi) Sum up values obtained from all the connected graphs and multiply $(\bar{\rho}_{\rm B})^{-N}$.

4.4 THEORETICAL APPLICATIONS

4.4.1 The Edgeworth expansion of density probability distribution function

Recently, the Edgeworth expansion of probability distribution function $P(\delta)$ of cosmological density contrast δ is suggested to be useful in cosmology (Scherrer & Bertschinger 1991; Juszkiewicz et al. 1994; Bernardeau & Kofman 1994). This expansion is suitable to obtain approximately density probability distribution function when restricted number of cumulants are known. The expansion is (Bernardeau & Kofman 1994)

$$P(\delta) = \frac{1}{\sqrt{2\pi\sigma^2}} e^{-\nu^2/2}\left[1 + \sigma\frac{S_3}{6}H_3(\nu) + \sigma^2\left(\frac{S_4}{24}H_4(\nu) + \frac{S_3^2}{72}H_6(\nu)\right)\right.$$
$$\left. + \sigma^3\left(\frac{S_5}{120}H_5(\nu) + \frac{S_3S_4}{144}H_7(\nu) + \frac{S_3^3}{1296}H_9(\nu)\right) + \cdots\right], \tag{4.4.1}$$

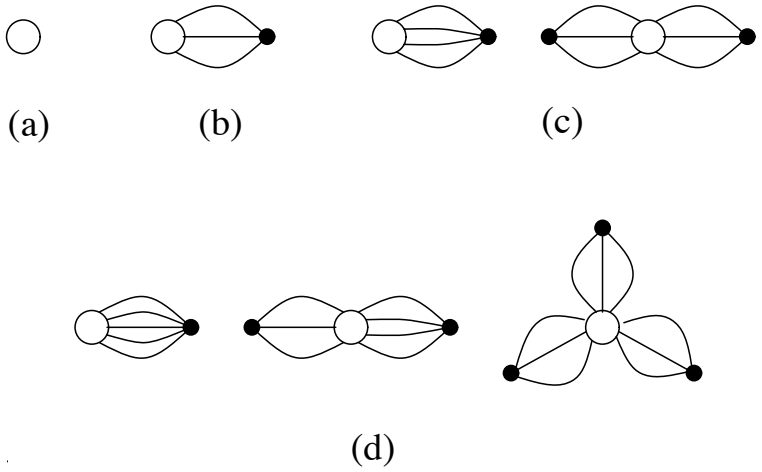

Figure 4.5: Diagrams for the Edgeworth expansion.

where $\sigma = \sqrt{\langle \delta^2 \rangle}$ is *rms* of density contrast, $\nu = \delta/\sigma$ is a normalized density contrast, and $S_n = \langle \delta^n \rangle_c / \langle \delta^2 \rangle^{n-1}$ are normalized cumulants. We can see the coefficients of Edgeworth expansion at arbitrary order are very easily calculated in our diagrammatic methods as follows.

Density probability distribution function expressed as

$$P(\delta) = \langle \delta_D(\delta - \nu\sigma) \rangle \tag{4.4.2}$$

is appropriate to our purpose. Setting $\rho_B = \delta_D(\alpha\sigma - \nu\sigma)$, Eq. (4.3.12) reduces to

$$R_m = \frac{1}{\sqrt{2\pi\sigma^2}} e^{-\nu^2/2} H_m(\nu). \tag{4.4.3}$$

Because $\psi^{(n)}(\boldsymbol{r}, \ldots, \boldsymbol{r}) = S_n \sigma^{n-2}$, a vertex with n-lines corresponds to order σ^{n-2}. Thus, diagrams of Figure 4.5 (a), (b), (c), (d), ... give all the coefficients of order σ^0, σ^1, σ^2, σ^3, ..., respectively. Applying rules B-i) $\sim$ B-iv), the expansion (4.4.1) is easily obtained. This example shows that our diagrammatic method can save the labor of calculation.

4.4.2 Density peaks of Gaussian random fields

We focus on the statistics of density peaks in this section. Bardeen et al. (1986) investigated the statistics of density peaks of random Gaussian fields identifying the density peaks of primordial fluctuation with the sites for galaxy or cluster formation. They gave practical approximations to the N-point correlation functions of the

density peaks. We show, in the following, that our method applied to density peaks of random Gaussian field provides the improved approximations to the correlation functions along the strategy of theirs.

In this section, the field α is identified with normalized density fluctuation $\delta_R(\boldsymbol{x})/\langle\delta_R^2\rangle^{1/2}$. The number density of peaks of the field α greater than a threshold ν is given by (Bardeen et al. 1986)

$$\rho_{\rm pk}(\boldsymbol{r}) = \theta(\alpha(\boldsymbol{r})-\nu)\delta^3\left(\partial_i\alpha(\boldsymbol{r})\right)(-1)^3\det\left(\partial_i\partial_j\alpha(\boldsymbol{r})\right)\theta\left(\lambda_1(\boldsymbol{r})\right)\theta\left(\lambda_2(\boldsymbol{r})\right)\theta\left(\lambda_3(\boldsymbol{r})\right), \tag{4.4.4}$$

which is a semi-nonlocal bias in our context. In the above, λ_1, λ_2, λ_3 are eigenvalues of a matrix $-(\partial_i\partial_j\alpha)$. The approximation, which is common to Bardeen et al. (1986), is to neglect all the derivatives of the two-point correlation $\psi^{(2)}$. Other correlations $\psi^{(N)}$ $(N \geq 3)$ do not exist because of the assumption of Gaussianity of underlying fluctuation. As an illustration, let us consider the case the power spectrum of background fluctuation has the power-law form with spectral index n. In this case, the two-point correlation $\psi^{(2)}(\boldsymbol{r})$ falls off as $|\boldsymbol{r}|^{-(n+3)}$ and the m-th derivative of the function falls off as $|\boldsymbol{r}|^{-(n+3+m)}$. When $n < -2$, all the derivatives of two-point correlation function can be neglected even if $\psi \sim 1$.

Adopting the above approximation, the rules C-i) $\sim$ C-vi) for the semi-nonlocal bias of random Gaussian underlying field are reduced to the rules A-i) $\sim$ A-vi) for the local bias of random Gaussian field with

$$R_m = \left\langle\left(\frac{\partial}{\partial\alpha_0}\right)^m\rho_{\rm B}(\alpha_\mu)\right\rangle_{\rm G}. \tag{4.4.5}$$

Note that this simplicity does not hold in non-Gaussian underlying field. Further assumptions for higher-order correlations which can hardly be justified are needed to have this simplicity for general non-Gaussian field (see the next section).

For the density peaks, equation (4.4.5) can be calculated using equation (A.18) of Bardeen et al. (1986) and results in

$$R_m^{\rm (pk)}(\nu) = \int d\alpha\mathcal{N}_{\rm pk}^{\rm (G)}(\alpha)\left(\frac{\partial}{\partial\alpha}\right)^m\theta(\alpha-\nu) = \begin{cases} {\rm n}_{\rm pk}^{\rm (G)}(\nu) & (m=0), \\ \left(-\dfrac{d}{d\nu}\right)^{m-1}\mathcal{N}_{\rm pk}^{\rm (G)}(\nu) & (m\geq 1). \end{cases} \tag{4.4.6}$$

where

$${\rm n}_{\rm pk}^{\rm (G)}(\nu) = \int_\nu^\infty d\alpha\mathcal{N}_{\rm pk}^{\rm (G)}(\alpha) \tag{4.4.7}$$

$$\mathcal{N}_{\rm pk}^{\rm (G)}(\nu) = \frac{1}{(2\pi)^2 R_*^3} e^{-\nu^2/2} G(\gamma, \gamma\nu) \tag{4.4.8}$$

$$G(\gamma, x_*) = \int_0^\infty dx f(x) \frac{\exp\left[-\dfrac{(x-x_*)^2}{2(1-\gamma^2)}\right]}{[2\pi(1-\gamma^2)]^{1/2}} \tag{4.4.9}$$

$$\begin{aligned} f(x) = {} & \frac{x^3 - 3x}{2}\left\{\mathrm{erf}\left[\left(\frac{5}{2}\right)^{1/2} x\right] + \mathrm{erf}\left[\left(\frac{5}{2}\right)^{1/2}\frac{x}{2}\right]\right\} \\ & + \left(\frac{2}{5\pi}\right)^{1/2}\left[\left(\frac{31x^2}{4} + \frac{8}{5}\right)e^{-5x^2/8} + \left(\frac{x^2}{2} - \frac{8}{5}\right)e^{-5x^2/2}\right] \end{aligned} \tag{4.4.10}$$

and $\mathrm{erf}(x)$ is an error function:

$$\mathrm{erf}(x) = \frac{2}{\sqrt{\pi}} \int_0^x e^{-x^2} dt. \tag{4.4.11}$$

Spectral parameters σ_j, γ, R_* are defined by

$$\sigma_j^2 = \int \frac{dk}{2\pi^2} k^{2j+2} P(k), \tag{4.4.12}$$

$$\gamma = \frac{\sigma_1^2}{\sigma_2\sigma_0}, \quad R_* = \frac{\sqrt{3}\sigma_1}{\sigma_2}, \tag{4.4.13}$$

where $P(k)$ is a power spectrum:

$$P(k) = \sigma^2 \int d^3x e^{-i\boldsymbol{k}\cdot\boldsymbol{x}} \psi^{(2)}(\boldsymbol{x}). \tag{4.4.14}$$

equation (4.4.6) can be represented as one-dimensional integrations as derived in Appendix D:

$$R_m^{\rm (pk)}(\nu) = \begin{cases} \dfrac{1}{8\pi^2 R_*^3} \displaystyle\int_0^\infty dx f(x) e^{-x^2/2} \mathrm{erfc}\left(\frac{\nu - \gamma x}{\sqrt{2(1-\gamma^2)}}\right) & (m = 0) \\ \dfrac{e^{-\nu^2/2}}{(2\pi)^{5/2} R_*^3 (1-\gamma^2)^{m/2}} \displaystyle\int_0^\infty dx f(x) H_{m-1}\left(\frac{\nu - \gamma x}{\sqrt{1-\gamma}}\right) \exp\left[-\frac{(x-\gamma\nu)^2}{2(1-\gamma^2)}\right] & (m \geq 1) \end{cases} \tag{4.4.15}$$

which have to be integrated numerically. In the high ν limit, these coefficients reduce to

$$R_m^{\rm (pk)}(\nu) \stackrel{\nu\to\infty}{\longrightarrow} \frac{1}{12\sqrt{3}\pi^2} \frac{\sigma_1}{\sigma_0} H_{m+2}(\nu) e^{-\nu^2/2}. \tag{4.4.16}$$

To see the behavior of two-point correlation function of density peaks on large scales which was described in Bardeen et al. (1986), we consider the case, $\psi^{(2)} \to 0$.

The two-point correlation function of peaks calculated by our method is, to lowest order in $\psi^{(2)}$,

$$\xi_{\rm pk}(\boldsymbol{r}_1,\boldsymbol{r}_2)=\left(\frac{\mathcal{N}_{\rm pk}^{(\rm G)}(\nu)}{\mathrm{n}_{\rm pk}^{(\rm G)}(\nu)}\right)^2\psi^{(2)}(\boldsymbol{r}_1,\boldsymbol{r}_2). \tag{4.4.17}$$

The corresponding expression in Bardeen et al. (1986) [equation (6.12) of their paper] is

$$\xi_{\rm pk}=\langle\widetilde{\alpha}\rangle^2\psi^{(2)}, \tag{4.4.18}$$

where

$$\langle\widetilde{\alpha}\rangle\equiv\frac{1}{(2\pi)^2R_*^3\mathrm{n}_{\rm pk}^{(\rm G)}(\nu)}\int_\nu^\infty d\alpha e^{-\alpha^2/2}\int_0^\infty dx f(x)\frac{\exp\left[-\dfrac{(x-\gamma\alpha)^2}{2(1-\gamma^2)}\right]}{[2\pi(1-\gamma^2)]^{1/2}}\frac{\alpha-\gamma x}{1-\gamma^2}. \tag{4.4.19}$$

The above two expressions are equivalent. In fact, explicit calculation (see Appendix E) shows

$$\langle\widetilde{\alpha}\rangle=\frac{\mathcal{N}_{\rm pk}^{(\rm G)}(\nu)}{\mathrm{n}_{\rm pk}^{(\rm G)}(\nu)}. \tag{4.4.20}$$

In high ν limit, $\xi_{\rm pk}=\nu^2\psi^{(2)}$ which corresponds to Kaiser's result (Kaiser 1984).

Jensen and Szalay (1986) give the expression of the autocorrelation functions of regions in which the value of a field α is higher than a threshold ν. Autocorrelation functions of the thresholded regions are regarded as approximations for correlation functions of peaks in high ν limit in the context of biased structure formation in astrophysics. Their formula can be derived by our method as shown in the previous section: equations (4.3.19) and (4.3.22) derive their formula [equation (4) of their paper],

$$\frac{P_N(\boldsymbol{r}_1,\ldots,\boldsymbol{r}_N)}{{P_1}^N}=\sum_{m=0}^\infty\sum_{\{m_{kl}|m\}}\prod_{k<l}\frac{[\psi(\boldsymbol{r}_k,\boldsymbol{r}_l)]^{m_{kl}}}{m_{kl}!}\cdot\prod_{r=1}^N A_{m_r}^{(\rm sc)}, \tag{4.4.21}$$

where

$$A_m^{(\rm sc)}=\frac{R_m^{(\rm sc)}}{R_0^{(\rm sc)}}=\begin{cases}1 & (m=0),\\ \dfrac{\sqrt{2}H_{m-1}(\nu)}{\sqrt{\pi}e^{\nu^2/2}\mathrm{erfc}(\nu/\sqrt{2})} & (m\geq 1).\end{cases} \tag{4.4.22}$$

Note that the definition of the Hermite polynomials are different from that in Jensen & Szalay (1986). In the case of density peaks, it is obvious that the above quantities $A_m^{(\rm sc)}$ should be replaced as follows:

$$A_m^{(\rm sc)}(\nu)\to A_m^{(\rm pk)}$$

$$= \begin{cases} 1 & (m=0), \\ \sqrt{\frac{2}{\pi}} \frac{e^{-\nu^2/2}}{(1-\gamma^2)^{m/2}} \frac{\int_0^\infty dx f(x) H_{m-1}\left(\frac{\nu-\gamma x}{\sqrt{1-\gamma^2}}\right) \exp\left[-\frac{(x-\gamma\nu)^2}{2(1-\gamma^2)}\right]}{\int_0^\infty dx f(x) e^{-x^2/2} \mathrm{erfc}\left(\frac{\nu-\gamma x}{\sqrt{2(1-\gamma^2)}}\right)} & (m \geq 1). \end{cases} \tag{4.4.23}$$

This quantities are easily evaluated by one-dimensional numerical integrations. This expression for N-point correlation function [equation (4.4.21) and equation (4.4.23)] of density peaks in Gaussian random fields is efficient than the methods developed in Bardeen et al. (1986), especially for higher N. In practice, the expansion is summed for arbitrary accuracy as in the Jensen and Szalay's formula. Figure 4.6 shows the various approximations for the two-point correlation function of peaks including the approximations of Jensen and Szalay [equation(6) of Jensen & Szalay (1986)], Bardeen et al. [equation (6.22) of their paper with $n = 2$], peak-background splitting method developed by Bardeen et al. [equation (6.46) of their paper], Lumsden et al. (1989)*, comparing with our method [equation (4.4.21) and equation (4.4.23)].

In the plot, the underlying fluctuation is assumed to be random Gaussian. We use the smoothed power spectrum of standard cold dark matter model given in Bardeen et al. (1986) with parameters $\Omega = 1, \Lambda = 0$, and a Hubble constant of 50 km/s/Mpc. The smoothing length R is $0.2h^{-1}$Mpc and the Gaussian window (4.2.2) is adopted. Figure 4.7 shows the three-point correlation functions of peaks in equilateral configuration for the approximations of Jensen and Szalay [equation (4) of their paper with $N = 3$], peak-background splitting method [equation (6.53) of Bardeen et al. (1986)], Jensen and Szalay with effective thresholds, comparing with our method for the same underlying spectrum as in Figure 4.6. In the effective threshold method, we use the same effective threshold as in the two-point correlation function. In Figure 4.8 plotted the normalized three-point correlation function

$$Q \equiv \frac{\xi^{(3)}(\boldsymbol{r}_1, \boldsymbol{r}_2, \boldsymbol{r}_3)}{\xi^{(2)}(\boldsymbol{r}_1, \boldsymbol{r}_2)\xi^{(2)}(\boldsymbol{r}_2, \boldsymbol{r}_3) + \xi^{(2)}(\boldsymbol{r}_2, \boldsymbol{r}_3)\xi^{(2)}(\boldsymbol{r}_3, \boldsymbol{r}_1) + \xi^{(2)}(\boldsymbol{r}_3, \boldsymbol{r}_1)\xi^{(2)}(\boldsymbol{r}_1, \boldsymbol{r}_2)}, \tag{4.4.24}$$

for approximations same as in Figure 4.7.

*They used Jensen and Szalay's formula with effective threshold $\nu_{\rm eff}$ which is determined by matching the two-point correlation function of Jensen and Szalay with that of peaks in large-separation limit, i.e., $\nu_{\rm eff}$ is the solution of the implicit equation, $A_1^{(\rm sc)}(\nu_{\rm eff}) = \langle\widetilde{\alpha}\rangle(\nu)$ for each true threshold ν.

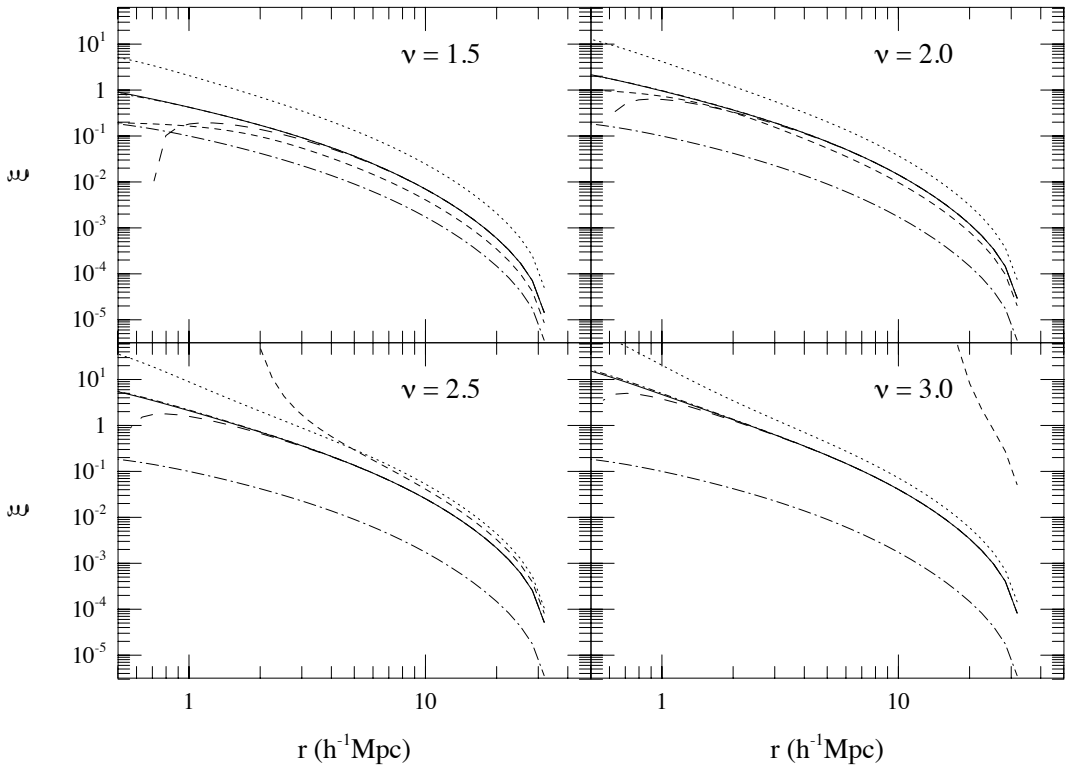

Figure 4.6: Various approximations for the two-point correlation function of peaks in CDM model ($h = 0.5$) for thresholds $\nu = 1.5$, $\nu = 2.0$, $\nu = 2.5$, and $\nu = 3.0$. The smoothing length is $0.2h^{-1}$Mpc and the Gaussian window function is adopted. *Solid lines*: our method. *Dotted lines*: Jensen and Szalay (1986). *Short Dash lines*: peak-background splitting. *Long dash lines*: Bardeen et al. (1986). *Dot-short dash lines*: Lumsden et al. (1989). *Dot-long dash lines*: original correlation function of CDM model for reference. Normalization is not relevant for our analysis.

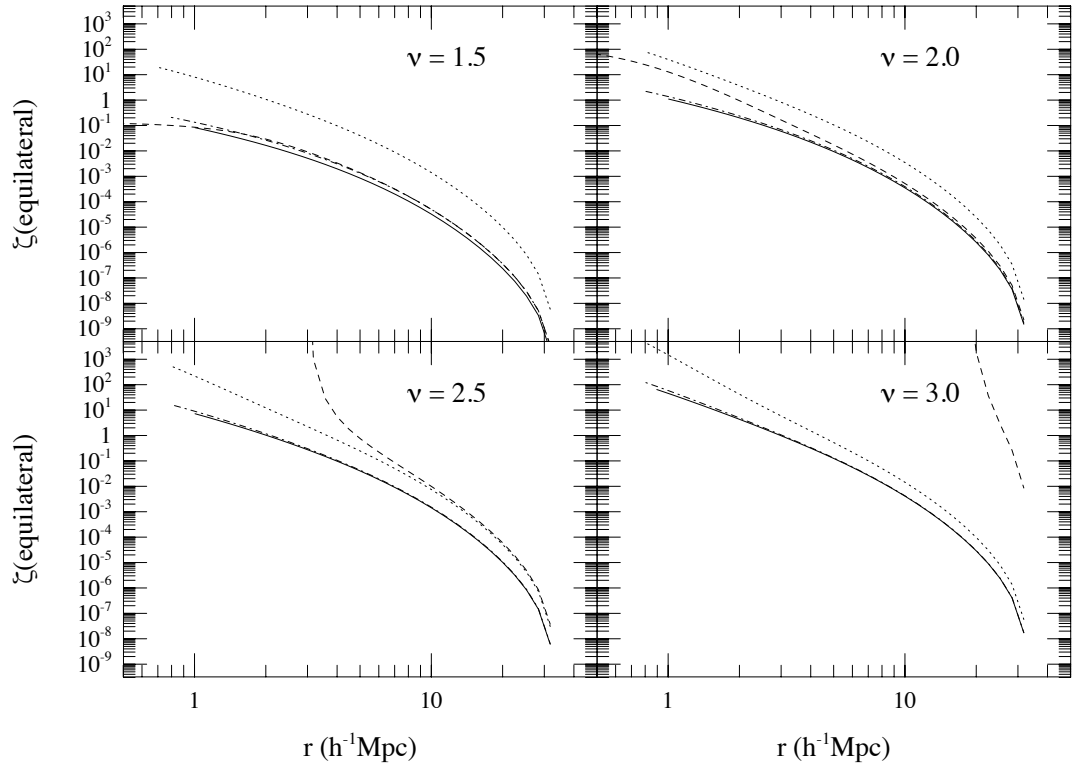

Figure 4.7: Various approximations for the three-point correlation function of peaks in CDM model. The configurations of three-points is equilateral and the length of edges of the equilateral triangle is the horizontal axis. *Solid lines*: our method. *Dotted lines*: Jensen and Szalay (1986). *Short Dash lines*: peak-background splitting. *Dot-short dash lines*: Jensen and Szalay with effective thresholds.

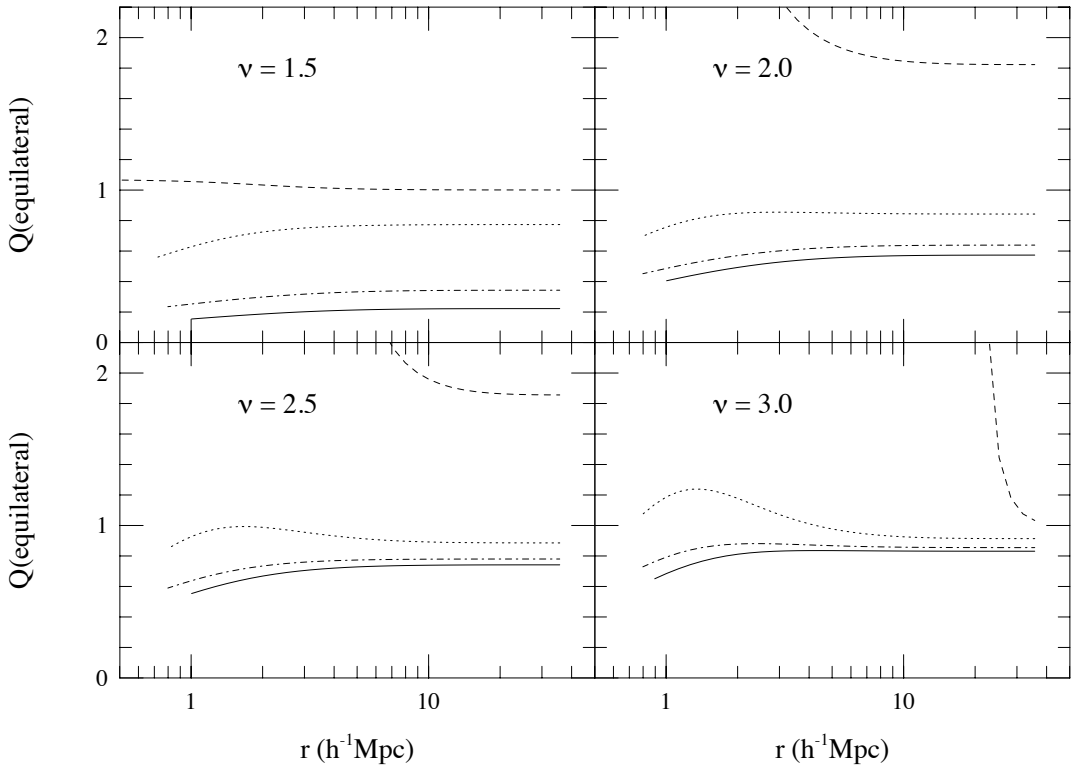

Figure 4.8: The normalized three-point correlation function of equilateral configuration for the same approximations as in Figure 4.7.

4.4.3 Weighted density extrema of non-Gaussian random field

The approximation adopted in the previous section does not work when the background fluctuation is not Gaussian random field. This is because in calculating the biasing of the non-Gaussian random field, the higher order correlations at the same point including derivatives such as $\langle\alpha^2(\boldsymbol{x})\triangle\alpha(\boldsymbol{x})\rangle$ can not reasonably neglected. In this section, we consider the density extrema with weighted factor according to the second derivatives of the field (see below) above some threshold ν, which can serve as an approximation of the density peaks for high threshold. The method to evaluate the density extrema of non-Gaussian random field to arbitrary accuracy is given in the following.

The number density of weighted density extrema above threshold ν we consider in this section is

$$\rho_{\rm ext}(\boldsymbol{r}) = \theta(\alpha(\boldsymbol{r})-\nu)\delta^3\left(\partial_i\alpha(\boldsymbol{r})\right)(-1)^3\det\left(\partial_i\partial_j\alpha(\boldsymbol{r})\right), \tag{4.4.25}$$

[*cf.* equation (4.4.4)]. This number density field is for density extrema with weight factor $-$sign[det $(\partial_i\partial_j\alpha(\boldsymbol{r}))$]. For large threshold ν, the number of maxima dominates the number of minima and saddle points, and equation (4.4.25) is a reasonable approximation for density peaks because the weight factor for density maxima is $+1$. Otto et al. (1986) and Cline et al. (1987) investigated the average number density and the correlation functions of this type of weighted extrema for Gaussian random fields approximately. We are in the place to generalize these analyses for non-Gaussian random fields.

The coefficients for the semi-nonlocal bias (4.4.25) is

$$\begin{aligned} R_{\mu_1\cdots\mu_m} &= R(k;l_1,l_2,l_3;p_{11},p_{22},p_{33},p_{23},p_{13},p_{12}) \\ &\equiv \frac{1}{(2\pi)^2}\left(\frac{\sigma_1}{\sqrt{3}\sigma_0}\right)^{3-\sum_i l_i-2\sum_{i\le j}p_{ij}} H_{l_1}(0)H_{l_2}(0)H_{l_3}(0) \\ &\quad\times e^{-\nu^2/2}\left[H_{k+2}(\nu)J_0(\{p_{ij}\}) - H_{k+1}(\nu)J_1(\{p_{ij}\})\right. \\ &\quad\left. +H_k(\nu)J_2(\{p_{ij}\}) - H_{k-1}(\nu)J_3(\{p_{ij}\})\right]. \end{aligned} \tag{4.4.26}$$

The derivation of this result is given in Appendix F. In the above notation, the number of indices corresponding to α, $\partial\alpha/\partial x^i$, $\partial^2\alpha/\partial x^i\partial x^j$ $(i\le j)$ among $\mu_1,\ldots,\mu_m$ are k, l_i, p_{ij}, respectively. For $k=0$, we use the notation,

$$H_{-1}(\nu) \equiv \sqrt{\frac{\pi}{2}}e^{\nu^2/2}{\rm erfc}\left(\frac{\nu}{\sqrt{2}}\right). \tag{4.4.27}$$

(a) (b)

Figure 4.9: Diagrams for $n_{\rm ex.}$ and $\xi_{{\rm ex},\nu}$.

Table 5.1 gives the definition of J_0, J_1, J_2 and J_3 as functions of $\{p_{ij}\}$. For cases not listed in Table 5.1, J_i's are all vanish. We can calculate the number density and the correlation functions of weighted density extrema of non-Gaussian field to arbitrary accuracy in principle by using the coefficients (4.4.26) and rules C-i) $\sim$ C-iv) provided that the diagrammatic expansion converges. As primary examples, the number density of weighted extrema $n_{\rm ex}(\nu)$ and the two-point correlation function $\xi_{{\rm ex},\nu}(r)$ of Gaussian random fields to leading order in ψ are, from diagrams in Figure 4.9,

$$n_{\rm ex}(\nu) = \frac{1}{(2\pi)^2}\left(\frac{\sigma_1}{\sqrt{3}\sigma_0}\right)^3 e^{-\nu^2/2}H_2(\nu), \tag{4.4.28}$$

$$\xi_{{\rm ex},\nu}(r) = \nu^2\left(\frac{\nu^2-3}{\nu^2-1}\right)^2\frac{\xi(r)}{\sigma_0^2} - \frac{6\nu^2(\nu^2-3)}{(\nu^2-1)^2}\frac{\triangle\xi(r)}{\sigma_1^2} + \frac{9\nu^2}{(\nu^2-1)^2}\frac{\sigma_0^2\triangle^2\xi(r)}{\sigma_1^4}, \tag{4.4.29}$$

where $\xi(r) = \sigma_0^2\psi(r)$. Otto et al. (1986) and Catelan et al. (1988) derived the leading and sub-leading contribution of ν to $\xi_{{\rm ex},\nu}$. Our method provides a way to calculate the same quantity not relying on the expansion in ν.

In the high ν limit, the leading contribution of ν in each diagram is come from the term which maximize k for each external point as seen from the expression (4.4.26). Thus, considering the leading contribution of ν is equivalent to considering the local bias with coefficients

$$R_k = \frac{1}{(2\pi)^2}\left(\frac{\sigma_1}{\sqrt{3}\sigma_0}\right)^3 \nu^{k+2}e^{-\nu^2/2}. \tag{4.4.30}$$

Substituting these coefficients to equation (4.3.17), we obtain

$$P_N = \left[\frac{1}{(2\pi)^2}\left(\frac{\sigma_1}{\sqrt{3}\sigma_0}\right)^3 \nu^2 e^{-\nu^2}\right]^N Z_N(J_i=\nu). \tag{4.4.31}$$

The number density is

$$P_1 = \frac{1}{(2\pi)^2}\left(\frac{\sigma_1}{\sqrt{3}\sigma_0}\right)^3 \nu^2 e^{-\nu^2} Z_1(\nu), \tag{4.4.32}$$

which was previously derived by Catelan et al. (1988) by using a different method. The correlation function is calculated by taking the connected part of the following quantity,

$$\frac{P_N}{P_1^N} = \frac{Z_N(J_i = \nu)}{[Z_1(\nu)]^N}, \tag{4.4.33}$$

which is the same as in the biasing with sharp clipping in high ν limit [equation (4.3.25)].

4.4.4 Biasing and hierarchical underlying fluctuations

In this section, we consider the case that the underlying fluctuation satisfy the hierarchical model of correlation functions (White 1979; Fry 1984);

$$\xi^{(N)}(\boldsymbol{x}_1, \ldots, \boldsymbol{x}_N) = \sum_{\text{trees}\,(a)} Q_a^{(N)} \sum_{\text{labelings}} \prod_{\text{edges}\,(AB)}^{N-1} \xi^{(2)}(\boldsymbol{x}_A, \boldsymbol{x}_B). \tag{4.4.34}$$

In the above symbolic notation, the edge (AB) is one of the edges in a tree graph (a) which is a set of connected $N-1$ edges linking N points, $\boldsymbol{x}_1, \ldots, \boldsymbol{x}_N$ without making any loop. All the distinct tree graphs are labeled by (a) and "labelings" indicate the symmetric sum with respect to the N-points (Fry 1984). $Q_a^{(N)}$ are constants for each tree topology (a). If $Q_a^{(N)} = 0$ for all $N \geq 3$, the hierarchical model reduces to random Gaussian fluctuation. Fry & Gaztañaga (1993) showed that the local bias which can be expanded as Taylor series by density contrast δ of background field,

$$\rho_{\rm B}(\delta) = \sum_{k=0}^{\infty} \frac{a'_k}{k!} \delta^k, \tag{4.4.35}$$

leads the hierarchical form (4.4.34) of biased field in the leading order of $\xi^{(2)}$. In this argument, the coefficients a'_k are assumed to be the zero-th order of $\xi^{(2)}$. This argument can not be applied to biasing by sharp clipping (4.3.21) because sharp clipping can not be expanded as Taylor series. Moreover, even if we approximate the sharp clipping by some smooth function, it is a function of δ/σ and the coefficients a'_k are no longer the zero-th order of $\xi^{(2)} \sim \mathcal{O}(\sigma^2)$. We complement, in the following, Fry and Gaztañaga's argument by investigate the case biasing is a local function of normalized density contrast δ/σ which has not to be expanded as a Taylor series as in the sharp clipping bias or in density peaks in the approximation of the preceding section.

In the following, the background field α is identified with the normalized density contrast δ/σ. The field δ is also assumed to satisfy the hierarchical model (4.4.34).

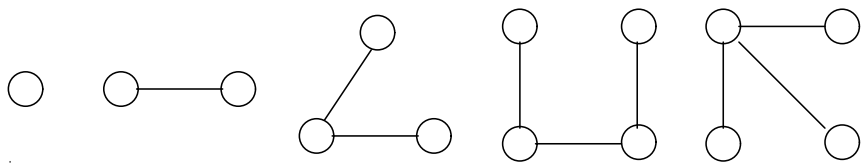

Figure 4.10: Diagrams for hierarchical underlying fluctuation.

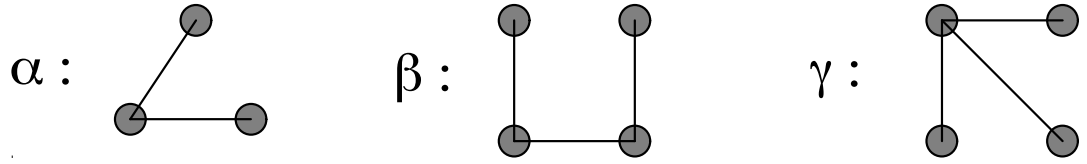

Figure 4.11: Definitions for tree graphs α, β, γ.

The j-vertex, in this case, contributes the order σ^{j-1} and we need not to consider any vertex if we only consider the leading order in σ. Evaluating diagrams in Figure 4.10, the following results are obtained to the leading order both in σ and $\psi^{(2)}$:

$$P_1 = R_0, \tag{4.4.36}$$

$$\xi^{(2)}_{\mathrm{B},12} = \left(\frac{R_1}{R_0}\right)^2 \psi_{12}, \tag{4.4.37}$$

$$\xi^{(3)}_{\mathrm{B},123} = \frac{R_1^2 R_2}{R_0^3}(\psi_{12}\psi_{23} + \text{cyc.}), \tag{4.4.38}$$

$$\xi^{(4)}_{\mathrm{B},1234} = \frac{R_1^2 R_2^2}{R_0^4}(\psi_{12}\psi_{23}\psi_{34} + \text{sim.}(12)) + \frac{R_1^3 R_3}{R_0^4}(\psi_{12}\psi_{13}\psi_{14} + \text{sim.}(4)). \tag{4.4.39}$$

The higher orders of $\psi^{(2)}$ is omitted for we are interested in large-separation limit. Thus, the parameters $Q^{(B)}_{N,a}$ of hierarchical model of a biased field are

$$Q^{(\mathrm{B})}_{3,\alpha} = \frac{R_0 R_2}{R_1^2}, \tag{4.4.40}$$

$$Q^{(\mathrm{B})}_{4,\beta} = \frac{R_0^2 R_2^2}{R_1^4}, \qquad Q^{(\mathrm{B})}_{4,\gamma} = \frac{R_0^2 R_3}{R_1^3}, \tag{4.4.41}$$

to leading order. The indices of tree graphs α, β, γ are defined in Figure 4.11. For arbitrary N, it is obvious from above calculation that $\xi^{(N)}_{\mathrm{B}}$ satisfy the hierarchical model to leading order in $\xi^{(2)}_{\mathrm{B}} \sim \mathcal{O}(\sigma^2)$ and, moreover, the parameters $Q^{(\mathrm{B})}_{N,a}$ can be

directly obtained from the topology (a) by simple rules as follows: let m_j be the number of external points which is attached by j lines in a connected tree graph (a) $(\sum_j m_j = N, \sum_j j m_j = 2(N-1))$, then

$$Q^{(\mathrm{B})}_{N,a} = \left(\frac{R_1}{R_0}\right)^{-2(N-1)} \frac{\prod_j R_j^{m_j}}{R_0^N} = A_1^{-2(N-1)} \prod_j A_j^{m_j}, \tag{4.4.42}$$

where $A_j = R_j/R_0$. In the biasing by sharp clipping, equation (4.4.22) is applied. In the biasing by density peaks, equation (4.4.23) is applied in the approximation of the preceding section. In high ν limit, both biasing via sharp clipping and via density peaks have the same behavior, $A_m(\nu) \stackrel{\nu\to\infty}{\longrightarrow} \nu^m$, and always $Q^{(\mathrm{B})}_{N,a} = 1$.

4.4.5 Gravitational evolution as nonlocal biasing

In our formalism, the gravitational nonlinear evolution of the density field can be seen as a kind of nonlocal biasing from the initial fluctuation field. In this section, we give explicit relation between our formalism and the perturbation theory of gravitational instability and apply our formalism to the calculation of correlation functions of density field. We consider the non-relativistic collisionless self-gravitating system in the fluid limit for Einstein-de Sitter universe $(\Omega = 1, \Lambda = 0, p = 0)$ as an example. The mass density contrast $\delta(\boldsymbol{x}, t)$ and the peculiar velocity field $\boldsymbol{v}(\boldsymbol{x}, t)$ are governed by the equations (Peebles 1980):

$$\frac{\partial \delta}{\partial t} + \frac{1}{a}\nabla \cdot [(1+\delta)\boldsymbol{v}] = 0, \tag{4.4.43}$$

$$\frac{\partial \boldsymbol{v}}{\partial t} + \frac{\dot{a}}{a}\boldsymbol{v} + \frac{1}{a}(\boldsymbol{v}\cdot\nabla)\boldsymbol{v} + \frac{1}{a}\nabla\phi = 0, \tag{4.4.44}$$

$$\triangle\phi = 4\pi G\bar{\rho}a^2\delta, \tag{4.4.45}$$

where ∇ denotes the derivative by means of comoving coordinate $\boldsymbol{x}$, $\bar{\rho}$ and $a(t)$ are the average density and expansion factor, respectively, and are given by $\bar{\rho} = (6\pi G t^2)^{-1}$, $a \propto t^{2/3}$ in the Einstein-de Sitter universe. The linear solution is derived by linearizing equations (4.4.43)-(4.4.45). The growing mode of the linear solution has the form,

$$\delta^{(1)}(\boldsymbol{x}, t) = \left(\frac{t}{t_{\mathrm{r}}}\right)^{2/3} \epsilon(\boldsymbol{x}), \tag{4.4.46}$$

where t_{r} is initial time or recombination time, $\epsilon(\boldsymbol{x})$ is interpreted as the primordial fluctuation. The second order perturbative solution for growing mode (Peebles 1980)

is given by

$$\delta^{(2)}(\boldsymbol{x},t)=\left(\frac{t}{t_{\rm r}}\right)^{4/3}\left\{\frac{5}{7}\epsilon^2(\boldsymbol{x})+\nabla\epsilon(\boldsymbol{x})\cdot\nabla U(\boldsymbol{x})+\frac{2}{7}\left[\partial_i\partial_j U(\boldsymbol{x})\right]\left[\partial_i\partial_j U(\boldsymbol{x})\right]\right\}, \tag{4.4.47}$$

where

$$U(\boldsymbol{x})=-\frac{1}{4\pi}\int d^3x'\frac{\epsilon(\boldsymbol{x}')}{|\boldsymbol{x}-\boldsymbol{x}'|}. \tag{4.4.48}$$

The mass density,

$$\rho_{\rm pt}(\boldsymbol{x},t)=\bar{\rho}(t)[1+\delta^{(1)}(\boldsymbol{x},t)+\delta^{(2)}(\boldsymbol{x},t)+\mathcal{O}(\epsilon^3)], \tag{4.4.49}$$

is regarded as nonlocal biasing where the background field α is identified with normalized primordial fluctuation ϵ/σ, where $\sigma^2=\langle\epsilon^2\rangle$. The kernels are derived to be

$$K^{(0)}=\bar{\rho}(t), \tag{4.4.50}$$

$$K^{(1)}(\boldsymbol{x})=\sigma\left(\frac{t}{t_{\rm r}}\right)^{2/3}\bar{\rho}(t)\delta^3(\boldsymbol{x})+\mathcal{O}(\sigma^3), \tag{4.4.51}$$

$$\begin{aligned}K^{(2)}(\boldsymbol{x},\boldsymbol{y})=\sigma^2\left(\frac{t}{t_{\rm r}}\right)^{4/3}\bar{\rho}(t)\Bigg[&\frac{10}{7}\delta^3(\boldsymbol{x})\delta^3(\boldsymbol{y})-\frac{1}{4\pi}\frac{\partial\delta^3(\boldsymbol{x})}{\partial x_i}\frac{\partial|\boldsymbol{y}|^{-1}}{\partial y_i}\\&-\frac{1}{4\pi}\frac{\partial\delta^3(\boldsymbol{y})}{\partial y_i}\frac{\partial|\boldsymbol{x}|^{-1}}{\partial x_i}+\frac{1}{28\pi^2}\frac{\partial^2|\boldsymbol{x}|^{-1}}{\partial x_i\partial x_j}\frac{\partial^2|\boldsymbol{y}|^{-1}}{\partial y_i\partial y_j}\Bigg]+\mathcal{O}(\sigma^4),\end{aligned} \tag{4.4.52}$$

$$K^{(n)}=\mathcal{O}(\sigma^n)\qquad(n\geq 3), \tag{4.4.53}$$

which are nonlocal. Using these kernels, and assuming that the primordial fluctuation ϵ is Gaussian, our rules A-i) $\sim$ A-vi) for two- and three-point correlation function give the following results after lengthy algebra:

$$\xi_{\rm pt}(\boldsymbol{r}_1,\boldsymbol{r}_2;t)=\left(\frac{t}{t_{\rm r}}\right)^{4/3}\xi_{\rm in}(r_{12})+\mathcal{O}(\sigma^4), \tag{4.4.54}$$

$$\begin{aligned}\zeta_{\rm pt}(\boldsymbol{r}_1,\boldsymbol{r}_2,\boldsymbol{r}_3;t)=\left(\frac{t}{t_{\rm r}}\right)^{8/3}\Bigg[\Bigg[&\frac{2}{7}(5+2\cos^2\theta_2)\xi_{\rm in}(r_{12})\xi_{\rm in}(r_{23})\\&+\cos\theta_2\left[\frac{\xi'_{\rm in}(r_{12})J_3^{\rm in}(r_{23})}{r_{23}^2}+\frac{\xi'_{\rm in}(r_{23})J_3^{\rm in}(r_{12})}{r_{12}^2}\right]\\&+\frac{4}{7}\Bigg\{3(3\cos^2\theta_2-1)\frac{J_3^{\rm in}(r_{12})J_3^{\rm in}(r_{23})}{r_{12}^3r_{23}^3}\\&+(1-3\cos^2\theta_2)\left[\frac{\xi_{\rm in}(r_{12})J_3^{\rm in}(r_{23})}{r_{23}^3}+\frac{\xi_{\rm in}(r_{23})J_3^{\rm in}(r_{12})}{r_{12}^3}\right]\Bigg\}\Bigg]\\&+\text{cyc.(3 terms)}+\mathcal{O}(\sigma^6).\end{aligned} \tag{4.4.55}$$

In the above, the two-point correlation function of the primordial field is

$$\xi_{\rm in}(r_{12}) = \langle \epsilon(\boldsymbol{r}_1)\epsilon(\boldsymbol{r}_2)\rangle \tag{4.4.56}$$

where $r_{12} = |\boldsymbol{r}_1 - \boldsymbol{r}_2|$; θ_2 is an angle between two vectors, $\boldsymbol{r}_1 - \boldsymbol{r}_2$ and $\boldsymbol{r}_3 - \boldsymbol{r}_2$; and $J_3^{\rm in}(r) = \int_0^r dr'^2 \xi_{\rm in}(r')$. Recently, Bharadwaj (1994) independently obtained the same result for three-point correlation function (4.4.55). Putting $\xi_{\rm in} \propto r^{\gamma_{\rm in}}$ in equation (4.4.55), we rederive Fry's result (Fry 1984). For equilateral configuration, $r_{12} = r_{23} = r_{31}$, the hierarchical amplitude, $Q_{pt} = \zeta_{\rm pt}/(3\xi_{\rm pt}^2)$ is

$$Q_{\rm pt}({\rm equilateral}) = \frac{18\gamma_{\rm in}^2 - 89\gamma_{\rm in} + 102}{7(3-\gamma_{\rm in})^2}. \tag{4.4.57}$$

5

Summary

In this *Thesis*, we deal with several topics from author's recent work mainly on the relation between mechanisms of structure formation and statistics. The pattern of large-scale structure of the Universe provides invaluable clues to both the nature of the primordial density fluctuations and their evolutionary processes. Therefore quantifying the large-scale structure of the universe rigorously is of fundamental importance in understanding the physics in the universe. We consider observable measures of galaxy distribution in the universe and study how these measures depend on initial fluctuation and how they evolve under gravitational instability. We employ some strategies to this subject, i.e., numerical method (section 3.2), semi-analytic method (section 3.4), analytic method (section 3.3, 3.6) and calculating formulation (chapter 4). In the below, the summary of what we found in previous chapters and further discussion is presented.

In chapter 2, the some basic concepts and methods to investigate the evolution of our universe are presented. Perturbation theories are only methods that enable us to investigate the nonlinear evolution analytically in general situation. As the survey volume of distribution of galaxies will be enlarged, the weakly nonlinear effect which is tractable by perturbative method will becomes one of the main subjects of investigation. As is shown, the weakly nonlinear effect is not sensitive to the cosmological parameters, Ω and Λ, in intersted ranges. Thus, comparison of data and perturbation theories in a weakly nonlinear regime provides the test of gravitational instability almost independently of the poorly determined Ω and λ. Skewness, probability distribution function and topology in a weakly nonlinear regime are among such directly observable quantities.

In chapter 3, the dynamical evolution of correlation functions and statistics of isodensity contours are explored together with the important effect, redshift contamination, to these measures.

In section 3.2, we compute two-, three- and four-point correlation functions in several cosmological models, and explicitly examine their departure from the hierarchical clustering ansatz (3.1.9) by treating separately the different triplet and quartet configurations. We find that the ansatz holds in almost all scales in these models approximately, but that there exists a weak but clear departure from it in a strict sense. The degree of this departure sensitively depends on the shape of underlying fluctuation spectrum, and also on the specific triplet and quartet configurations.

We also look for a possible effect of the peculiar velocity field which should persist for all catalogues from existing and future redshift surveys. In the case of an LCDM model, we find that the ansatz (3.1.2) for three-point correlation function holds remarkably in redshift space even though it is clearly broken in real space. The ansatz (3.1.4) for four-point correlation function holds better in redshift space. Therefore the results from the observations should be interpreted with caution. Alimi et al. (1990) and Maurogordato et al. (1992), for example, analyzed the CfA redshift survey or the SSRS (Southern Sky Red Shift Survey) data and found the evidence that the scaling law (3.1.6) holds by the method of count-in-cells. Nevertheless our results indicate that their conclusion should not be directly extended to the real space distribution. It is quite possible that the scaling law holds very well simply due to the redshift space contamination.

It is interesting and important to stress here that all the present findings are in complete agreement with the previous count-in-cells analysis by Lahav et al. (1993). In fact, they found the similar dependence of skewness and kurtosis on the degree of the density inhomogeneity. Since their analysis mostly used the cubic sampling volume, it would mix up several triplet configurations considered above, but would mostly correspond to our [1,1,1] shape. Then in the case of LCDM in particular, the tendency that Q increases as the fluctuations become more inhomogeneous is at least qualitatively consistent with their finding on the behavior of skewness. Also they found that skewness tend to behave like a constant in redshift space as we find for Q_s. Let us emphasize that this behavior would not be detected when averaging out over the triplet configurations; the probability that all the three separations of a triplet fall in small separation bins where the deviation from the scaling is most remarkable, is very small, and thus it is not easy to detect the scale-dependence properly.

Although we have shown that the hierarchical clustering ansatz (3.1.9) is weakly broken in a systematic manner, it is of great value to examine the extent to which the

ansatz extends to the higher-order correlation functions even if in an averaged sense as argued here. Also of interest is the three-point correlation analysis of clusters of galaxies (Tóth et al. 1989; Gott et al. 1991) and its comparison with theoretical predictions. The latter issue was explored by Watanabe et al. (1994).

In section 3.3, several statistics of isodensity contours are considered including genus statistics, 2D genus statistics, area statistics, length statistics and level crossing statistics. The dynamical evolution of these statistics is analytically evaluated by second order perturbation theory of gravitational instability.

As seen by equations (3.3.17)–(3.3.19), the nonlinear correction of first order in σ generates asymmetry between high-density region and low-density region in the symmetric or anti-symmetric curve of the statistics as functions of the threshold. The pattern of the asymmetry in the curve of smoothed density field depends on initial power spectra. Thus, in principle, observations of the curve can restrict the properties of initial fluctuation, such as Gaussianity, the shape of the spectrum, by the amplitude and the pattern of asymmetry of the curve. The presently available redshift data of galaxies are not enough to have the statistically sufficient accuracy on isodensity-contour statistics of the large-scale structure. The projects as Sloan Digital Sky Survey (SDSS), however, will enable us to have a large amount of redshift data in near future and the analysis indicated in this section will be important one.

The effect of biasing between the galaxy distribution and the matter distribution on the genus curve is an important issue. Quite generally, the correlation functions arose from local bias approach to the hierarchical model in the large-scale limit (Szalay 1988; Fry & Gaztañaga 1993; Matsubara 1994d; section 4.4). The parameter Q in hierarchical model is determined by individual biasing mechanisms. The effect of biasing on the genus curve is approximately expressed by equations (3.3.17)–(3.3.19).

In section 3.4, we derive a formula (3.4.9) connecting N-point correlation functions in real space and in redshift space on small scales, first neglecting velocity correlations. Then we propose a modified model (3.4.27) which partially takes into account the effect of velocity correlations. Using the above model (3.4.9) or (3.4.27) and the models for correlation functions in real space and for velocity distribution, we give analytic expression for direction-averaged two- and three-point correlation functions in redshift space. We find that the correlation functions are systematically lower in redshift space: when the power-law indices for two- and three-point correlations in real space are $-\gamma$ and -2γ respectively, the redshift space counterparts

are $1-\gamma$ and $2-2\gamma$ respectively on very small scales (equations (3.4.37), (3.4.44) and Figure 3.14. The hierarchical structure (3.1.2) is roughly preserved on all scales. We conjecture that when the power-law indices for N-point correlation function in real space is $-(N-1)\gamma$, the redshift-space counterpart is $N-1-(N-1)\gamma$ on very small scales and hierarchical structure (3.1.9) is roughly preserved on all scales.

These analyses are compared with N-body simulation data, SCDM and LCDM models, which proved good agreement between directly calculated correlation functions in redshift space in simulations and the above velocity-correlation-modified model. Although there are many approximations for velocity correlation adopted in the present model, our model turn out to successfully explain the redshift space distortions in correlation functions. The best fitted values σ_2 and σ_3 are obtained in each model and the property $\sigma_3/\sigma_2 \sim 1.7$ is found independently of cosmological models and velocity-distribution models $f_\sigma(v)$. As noted in section 3.4.3 (just below the equation [3.4.23]), the difference between the values σ_2 and σ_3 is interpreted to be the difference of expected potentials so it would be interesting if the ratio σ_3/σ_2 is fairly independent of cosmological models or detailed forms of velocity distribution functions.

In section 3.6, the redshift distortion of statistics of isodensity contours are examined using linear perturbation theory. We show directly that the redshift distortion affects only on amplitude of the statistics as functions of density threshold. the redshift distortion is fairly weak for genus and area statistics for interested values of $\Omega b^{-5/3}$. One can, therefore, use redshift data for Gaussianity test of primordial fluctuation as if the redshift data represent the real space distribution.

Quite interestingly, the direction dependent statistics, i.e., 2D genus, length statistics, level crossing statistics are fairly dependent on $\Omega b^{-5/3}$ and the direction to defining the statistics. These dependences provide ways to determine the density parameter of our Universe from redshift data.

In chapter 4, we develope a formalism to explore the statistics of biased field in large-scale structure of the universe. In particular, the general nonlocal biasing can be treated in this formalism. The underlying field is not necessarily assumed to be a random Gaussian field. The formalism is based on diagrammatic series expansion of the correlation functions of a biased field. As for local biasing, the form of series expansion of a biased field is known by previous works, but it is very complicated expression (Borgani & Bonometto 1989, 1990). Our formalism, when applied to local biasing problem, simplify this complexity.

In quantum field theory and statistical physics, the Feynman diagrams play roles more than mere simplification of calculations. It would be interesting if our formalism could play similar roles. In fact, our diagrammatic expansion can be conceived to be the generalization of the Edgeworth expansion which is useful in connecting dynamics and statistics in large-scale structure by the argument in section 4.4.

We apply our formalism to the problems which have been studied previously to show the effectiveness of our method. Application to peak statistics improves the technique developed by Bardeen et al. (1986). In particular, we can evaluate the higher order correlations of peaks successfully for which technique of Bardeen et al. had difficulty. For statistics of weighted extrema, which could be an approximation to peak statistics, we show the general way of calculation not depending on the high-threshold expansion. Weighted extrema *is* observable in surveys of large-scale structure and our result can be directly compared with observations. The similar technique is applied to the isodensity statistics of weakly non-Gaussian field in section 3.3. The conservation of hierarchical model of correlation functions subjected to local biasing, which is studied by Fry and Gaztañaga (1993), is revisited using our formalism. We complement their results by investigating a local biasing through normalized density contrast which may not be represented by Taylor series, as in sharp-clipping biasing. The gravitational evolution of primordial fluctuation also falls under the category of nonlocal biasing.

Those problems have been studied individually so far. Our formalism enables more detailed examination of those problems. Those examples show that our formalism is not only a general method but also a practically powerful way to investigate various problems. The formalism developed in chapter 4 may be an influential method for future investigations of large-scale structure of the universe.

As a concluding remark, it is important to stress that which statistic is the most suitable for quantifying the pattern of large-scale structure of the universe can not be determined. The answer of this question depends on the initial fluctuation and the mechanism of structure formation which are indeed what we want to investigate through the pattern of large-scale structure. Although the hierarchy of correlation functions provides the complete description of the statistical properties of large-scale structure, it is practically difficult to determine accurately higher order correlation functions from observations. So we need alternative statistical measures to further discriminate various cosmological models. Count-in-cells statistics, void probability functions, probability distribution functions, fractal analysis, cluster correlation

functions and isodensity-contour statistics are fairly popular measures. In the comparison between theory and observation, these statistical measures are inevitable tools. The correct theory of structure formation in the universe must passes statistical tests using these measures. The redshift data of galaxies are extending rapidly so there is no doubt that the confrontation between theories and observations in the near future will bring us a new exciting stage of investigations of our Universe.

Acknowledgements

It is my great pleasure to thank my supervisor, Prof. Yoshio Sumi and Prof. Haruo Ui at Hiroshima University for their continuous advice, encouragement and support during the preparation of the present thesis. Thanks are also due to Prof. Yasushi Suto, who is my adviser at Yukawa Institute for Theoretical Physics and at The University of Tokyo and is a collaborator of parts of the present work, for stimulating discussions and continuous encouragement. I would like to thank Dr. Takuya Watanabe for useful discussions and kind help in plotting Figures 4.6, 4.7 and 4.8. The genus curve from numerical simulations is computed using the code kindly provided by Prof. David. H. Weinberg. I appreciate Prof. Hideo Kodama, Dr. Nobuyoshi Makino, Prof. Katsuhiko Sato, Prof. Jiro Soda, Dr. Tatsushi Suginohara, Prof. Kenji Tomita, Dr. Toshio Tsuchiya, Dr. Haruhiko Ueda, Dr. Kazuhiro Yamamoto, Prof. Jun'ichi Yokoyama for discussions. I am grateful to my parents for their continuous support.

This research was supported in part by the Grants-in-Aid for Scientific research from Ministry of Education, Science and Culture of Japan (No. 0042). I acknowledge the support by the Fellowships of the Japan Society for the Promotion of Science for Japanese Junior Scientists.

Numerical calculations were carried out on Hitac S-820/80 at KEK (National Laboratory of High Energy Physics in Japan), on CRAY Y-MP2E at Supercomputer Laboratory, Institute for Chemical Research, Kyoto University, on SUN SPARC stations at Uji Research Center, Yukawa Institute for Theoretical Physics, Kyoto University.

Appendices

A THE PROOF OF THE CUMULANT EXPANSION THEOREM

In this appendix, the proof of the cumulant expansion theorem is shown. We consider the general random variable, $\phi_1, \phi_2, \ldots$, which is not restricted to have the zero-mean. These variables are not necessarily all different, but can be overlapped. Especially in the case of a single variable, $\phi_1, \phi_2, \ldots$ represent the same variable. The cumulants $\langle \phi_1 \phi_2 \cdots \phi_N \rangle_{\rm c}$ are defined from the moments $\langle \phi_1 \phi_2 \cdots \phi_N \rangle$ iteratively from the following equations:

$$\langle \phi_1 \rangle = \langle \phi_1 \rangle_{\rm c} , \tag{A.1}$$

$$\langle \phi_1 \phi_2 \rangle = \langle \phi_1 \rangle_{\rm c} \langle \phi_2 \rangle_{\rm c} + \langle \phi_1 \phi_2 \rangle_{\rm c} , \tag{A.2}$$

$$\begin{aligned} \langle \phi_1 \phi_2 \phi_3 \rangle = & \langle \phi_1 \rangle_{\rm c} \langle \phi_2 \rangle_{\rm c} \langle \phi_3 \rangle_{\rm c} + \langle \phi_1 \rangle_{\rm c} \langle \phi_2 \phi_3 \rangle_{\rm c} + \langle \phi_2 \rangle_{\rm c} \langle \phi_3 \phi_1 \rangle_{\rm c} + \langle \phi_3 \rangle_{\rm c} \langle \phi_1 \phi_2 \rangle_{\rm c} \\ & + \langle \phi_1 \phi_2 \phi_3 \rangle_{\rm c} , \end{aligned} \tag{A.3}$$

$$\begin{aligned} \langle \phi_1 \phi_2 \phi_3 \phi_4 \rangle = & \langle \phi_1 \rangle_{\rm c} \langle \phi_2 \rangle_{\rm c} \langle \phi_3 \rangle_{\rm c} \langle \phi_4 \rangle_{\rm c} + \langle \phi_1 \phi_2 \rangle_{\rm c} \langle \phi_3 \rangle_{\rm c} \langle \phi_4 \rangle_{\rm c} + \text{sym.}(6) \\ & + \langle \phi_1 \phi_2 \rangle_{\rm c} \langle \phi_3 \phi_4 \rangle_{\rm c} + \text{sym.}(3) + \langle \phi_1 \rangle_{\rm c} \langle \phi_2 \phi_3 \phi_4 \rangle_{\rm c} + \text{sym.}(4) \\ & + \langle \phi_1 \phi_2 \phi_3 \phi_4 \rangle_{\rm c} , \end{aligned} \tag{A.4}$$

$$\vdots \qquad\qquad \vdots$$

where sym.(n) means the addition of terms to symmetrizing the previous term resulting in n terms in total. As is obvious from above equations, the cumulants are interpreted as true contribution to correlations. The contribution from the lower order moments are eliminated in cumulants. The general expression of above equations is

$$\langle \phi_1 \phi_2 \cdots \phi_N \rangle = \sum_{\text{grouping}} \prod_{\text{groups}\,(a)} \left\langle \prod_{i \in I_\alpha} \phi_i \right\rangle_{\rm c} , \tag{A.5}$$

where $\sum_{\text{grouping}}$ means the summation for all the possible ways of grouping variables, $\phi_1, \phi_2, \ldots$, α is an index of groups for a fixed grouping, and I_α is the set of indices of the variables in a group α. Since ϕ_j appears once in the left hand side of equation

(A.5), the cumulant $\langle\phi_1\cdots\phi_N\rangle_{\rm c}$ is linear for each variable ϕ_j:

$$\left\langle\phi_1\cdots(\phi_j+\phi_j')\cdots\phi_N\right\rangle_{\rm c}=\langle\phi_1\cdots\phi_j\cdots\phi_N\rangle_{\rm c}+\left\langle\phi_1\cdots\phi_j'\cdots\phi_N\right\rangle_{\rm c}, \tag{A.6}$$

as easily seen from induction.

The N-moment for a random variable Φ is, from equation (A.5),

$$\left\langle\Phi^N\right\rangle=\sum_{\rm grouping}\prod_{\alpha}\langle\Phi^{n_\alpha}\rangle_{\rm c}, \tag{A.7}$$

where n_α is the number of elements in a group α. Let m_j be the number of groups which has $n_\alpha=j$ elements for a fixed grouping. Note the condition $\sum_j jm_j=N$. Some different grouping give the same set of numbers, $(m_1,m_2,\ldots)$. Using the number of redundancy $n(m_1,m_2,\ldots;N)$ of this correspondence, equation (A.7) reduces to

$$\left\langle\Phi^N\right\rangle=\sum_{m_1=0}^{\infty}\sum_{m_2=0}^{\infty}\cdots\delta\left(N-\sum_j jm_j\right)n(m_1,m_2,\ldots;N)\,\langle\Phi\rangle_{\rm c}^{m_1}\left\langle\Phi^2\right\rangle_{\rm c}^{m_2}\left\langle\Phi^3\right\rangle_{\rm c}^{m_3}\cdots, \tag{A.8}$$

where $\delta(m)$ is either 1 if $m=0$ or 0 if $m\neq 0$. The number of redundancy n is the product of the number of ways to divide N objects to groups of $m_1,2m_2,3m_3,\ldots$ elements and the number of ways to divide jm_j elements in each group to subgroups of j elements:

$$n(m_1,m_2,\ldots;N)=\frac{N!}{m_1!(2m_2)!(3m_3)!\cdots}\times\prod_j\frac{(jm_j)!}{m_j!(j!)^{m_j}}=N!\prod_j\frac{1}{m_j!(j!)^{m_j}}. \tag{A.9}$$

The following equation is derived from equations (A.8), (A.9):

$$\left\langle e^{\Phi}\right\rangle=\sum_{N=0}^{\infty}\frac{\left\langle\Phi^N\right\rangle}{N!}=\exp\left(\sum_{N=1}^{\infty}\frac{\left\langle\Phi^N\right\rangle_{\rm c}}{N!}\right). \tag{A.10}$$

Setting $\Phi=-iJ\phi$ in equation (A.10), the cumulant expansion theorem for a single variable is obtained:

$$\ln\langle\exp(-iJ\phi)\rangle=\sum_{N=1}^{\infty}\frac{(-i)^N}{N!}J^N\left\langle\phi^N\right\rangle_{\rm c}. \tag{A.11}$$

Setting $\Phi=-i\sum_j J_j\phi_j$ in equation (A.10), the cumulant expansion theorem for multiple variables is obtained:

$$\ln\left\langle\exp\left(-i\sum_j J_j\phi_j\right)\right\rangle=\sum_{N=1}^{\infty}\frac{(-i)^N}{N!}\sum_{j_1}\cdots\sum_{j_N}J_{j_1}\cdots J_{j_N}\langle\phi_{j_1}\cdots\phi_{j_N}\rangle_{\rm c}. \tag{A.12}$$

Setting $\Phi = -i \int dx J(x)\phi(x)$ in equation (A.10), the cumulant expansion theorem for a continuum variable is obtained:

$$\ln \left\langle \exp\left(-i \int dx J(x)\phi(x)\right)\right\rangle = \sum_{N=1}^{\infty} \frac{(-i)^N}{N!} \int dx_1 \cdots \int dx_N J(x_1)\cdots J(x_N) \left\langle \phi(x_1)\cdots\phi(x_N)\right\rangle_{\mathrm{c}}. \quad \text{(A.13)}$$

The cumulant expansion theorem is extremely important because the cumulants which are defined order by order are simply related by a single equation through generating functions.

As an illustrative application of the cumulant expansion theorem, let us calculate the cumulants c_N for a single variable of zero mean in terms of moments μ_N. From equation (A.11),

$$c_N = \frac{\partial^N}{\partial t^N} \ln \left\langle e^{t\phi}\right\rangle \Big|_{t=0}. \quad \text{(A.14)}$$

Evaluation of this equation provided $\mu_1 = 0$ is straightforward. We list below the first ten cumulants for use:

$$c_1 = 0, \quad \text{(A.15)}$$

$$c_2 = \mu_2, \quad \text{(A.16)}$$

$$c_3 = \mu_3, \quad \text{(A.17)}$$

$$c_4 = \mu_4 - 3\mu_2^2, \quad \text{(A.18)}$$

$$c_5 = \mu_5 - 10\mu_2\mu_3, \quad \text{(A.19)}$$

$$c_6 = \mu_6 - 15\mu 2\mu 4 - 10\mu_3^2 + 30\mu_2^3, \quad \text{(A.20)}$$

$$c_7 = \mu_7 - 21\mu_2\mu_5 - 35\mu_3\mu_4 + 210\mu_2^2\mu_3, \quad \text{(A.21)}$$

$$c_8 = \mu_8 - 28\mu_2\mu_6 - 56\mu_3\mu 5 - 35\mu_4^2 + 420\mu_2^2\mu_4 + 560\mu_2\mu_3^2 - 630\mu_2^4, \quad \text{(A.22)}$$

$$c_9 = \mu_9 - 36\mu_2\mu_7 - 84\mu_3\mu_6 - 126\mu_4\mu_5 + 756\mu_2^2\mu_5 + 2520\mu_2\mu_3\mu_4 + 560\mu_3^3 - 7560\mu_2^3\mu_3, \quad \text{(A.23)}$$

$$c_{10} = \mu_{10} - 45\mu_2\mu_8 - 120\mu_3\mu 7 - 210\mu_4\mu_6 + 1260\mu_2^2\mu_6 - 126\mu_5^2 + 5040\mu_2\mu_3\mu_5 + 3150\mu_2\mu_4^2 + 4200\mu_3^2\mu_4 - 18900\mu_2^3\mu_4 - 37800\mu_2^2\mu_3^2 + 22680\mu_2^5. \quad \text{(A.24)}$$

In astrophysical applications, the density contrast $\rho/\bar{\rho} - 1$ (ρ is the density at some point and $\bar{\rho}$ is the average density) is taken as a random variable with zero mean. The parameter $S_N = c_N/c_2^{N-1}$ is often used in analyzing astrophysical density fields. S_3 is called skewness and S_4 is called kurtosis.

B EXPECTATION VALUES OF PRODUCTS OF GENERALIZED WIENER-HERMITE FUNCTIONALS

Imamura, Meecham & Siegel (1965) gives the method to calculate symbolically the expectation values of products of Wiener-Hermite functionals. In this Appendix, we generalize their method to the case of generalized Wiener-Hermite functionals. The quantity we need to calculate is

$$\left\langle \prod_{i=1}^{s} \mathcal{H}_{(m_i)}\left(\boldsymbol{x}_i^{(1)}, \ldots, \boldsymbol{x}_i^{(m_i)}\right) \right\rangle_{\mathrm{G}} . \tag{B.1}$$

To derive the method to calculate this quantity, there are at least two ways, i.e., using operators and using generating functionals. We present both ways here although either is sufficient to our purpose.

B.1 The method using operators

The method using operators is to use the operator representation of generalized Wiener-Hermite functionals. This method is similar to the derivation of Feynman rules in operator formalism in quantum field theory.

We define the annihilation operator $a(\boldsymbol{x})$ and creation operator $a^\dagger(\boldsymbol{x})$ as

$$a(\boldsymbol{x}) = \frac{1}{2}\int d^3y \psi^{-1}(\boldsymbol{x},\boldsymbol{y})\alpha(\boldsymbol{y}) + \frac{\delta}{\delta\alpha(\boldsymbol{x})}, \tag{B.2}$$

$$a^\dagger(\boldsymbol{x}) = \frac{1}{2}\alpha(\boldsymbol{x}) - \int d^3y \psi(\boldsymbol{x},\boldsymbol{y})\frac{\delta}{\delta\alpha(\boldsymbol{y})}. \tag{B.3}$$

Annihilation and creation operators transform as covariant and contravariant vectors, respectively under the linear transformation (4.2.19). These operators indeed satisfy the following commutation relations as annihilation and creation operators:

$$\left[a(\boldsymbol{x}), a^\dagger(\boldsymbol{y})\right] = \delta^3(\boldsymbol{x}-\boldsymbol{y}), \tag{B.4}$$

$$[a(\boldsymbol{x}), a(\boldsymbol{y})] = \left[a^\dagger(\boldsymbol{x}), a^\dagger(\boldsymbol{y})\right] = 0. \tag{B.5}$$

In terms of annihilation and creation operators, the generalized Wiener-Hermite functionals are represented by

$$\mathcal{H}_{(m)}(\boldsymbol{x}_1, \ldots, \boldsymbol{x}_m) = :\prod_{i=1}^{m}\left[\tilde{a}(\boldsymbol{x}_i) + a^\dagger(\boldsymbol{x}_i)\right]:, \tag{B.6}$$

where

$$\tilde{a}(\boldsymbol{x}) \equiv \int d^3y \psi(\boldsymbol{x},\boldsymbol{y})a(\boldsymbol{y}), \tag{B.7}$$

is a contravariant vector. The notation $:\cdots:$ means the Wick product (Wick 1950): place all the annihilation operators to the left of all the creation operators in the Wick product. For example,

$$:\left[\tilde{a}(\boldsymbol{x})+a^{\dagger}(\boldsymbol{x})\right]\left[\tilde{a}(\boldsymbol{y})+a^{\dagger}(\boldsymbol{y})\right]:=\tilde{a}(\boldsymbol{x})\tilde{a}(\boldsymbol{y})+\tilde{a}(\boldsymbol{x})a^{\dagger}(\boldsymbol{y})+\tilde{a}(\boldsymbol{y})a^{\dagger}(\boldsymbol{x})+a^{\dagger}(\boldsymbol{x})a^{\dagger}(\boldsymbol{y}), \tag{B.8}$$

and so on. The representation (B.6) is proved by induction using the recursion relation (4.2.23).

We then define the "vacuum state" $|0\rangle$ as

$$|0\rangle \equiv \{P_{\mathrm{G}}[\alpha]\}^{1/2}, \tag{B.9}$$

where $P_{\mathrm{G}}[\alpha]$ is an infinite dimensional Gaussian distribution functional given by equation (4.2.24). The "n particle states" ($n \geq 0$) are defined using vacuum state as

$$|\boldsymbol{x}_1,\ldots,\boldsymbol{x}_n\rangle = a^{\dagger}(\boldsymbol{x}_1)\cdots a^{\dagger}(\boldsymbol{x}_n)|0\rangle, \tag{B.10}$$

which are the bases of the Fock space $\mathcal{F}$. The following properties hold for n particle state:

$$a^{\dagger}(\boldsymbol{y})|\boldsymbol{x}_1,\ldots,\boldsymbol{x}_n\rangle = |\boldsymbol{y},\boldsymbol{x}_1,\ldots,\boldsymbol{x}_n\rangle, \tag{B.11}$$

$$a(\boldsymbol{y})|0\rangle = 0, \tag{B.12}$$

$$a(\boldsymbol{y})|\boldsymbol{x}_1,\ldots,\boldsymbol{x}_n\rangle = \sum_{i=1}^{n}\delta^3(\boldsymbol{y}-\boldsymbol{x}_i)|\boldsymbol{x}_1,\ldots,\boldsymbol{x}_{i-1},\boldsymbol{x}_{i+1},\ldots,\boldsymbol{x}_n\rangle. \tag{B.13}$$

We define the inner product of n particle state $|\boldsymbol{x}_1,\ldots,\boldsymbol{x}_n\rangle$ and m particle state $|\boldsymbol{y}_1,\ldots,\boldsymbol{y}_m\rangle$ in the Fock space $\mathcal{F}$ by

$$\begin{aligned}\langle\boldsymbol{x}_1,\ldots,\boldsymbol{x}_n|\boldsymbol{y}_1,\ldots,\boldsymbol{y}_m\rangle \equiv \delta_{nm}\int d^3z_1\cdots d^3z_n\psi^{-1}(\boldsymbol{x}_1,\boldsymbol{z}_1)\cdots\psi^{-1}(\boldsymbol{x}_n,\boldsymbol{z}_n)\\ \times\int[d\alpha]|\boldsymbol{z}_1,\ldots,\boldsymbol{z}_n\rangle|\boldsymbol{y}_1,\ldots,\boldsymbol{y}_n\rangle,\end{aligned} \tag{B.14}$$

where we employ Dirac's notation for the inner product. The annihilation operator and the creation operator are Hermite conjugate to each other under this definition of the inner product in the Fock space. The inner product (B.14) can be calculated explicitly by commutation relations (B.4), (B.5) and the properties (B.13) resulting in

$$\begin{aligned}\langle\boldsymbol{x}_1,\ldots,\boldsymbol{x}_n|\boldsymbol{y}_1,\ldots,\boldsymbol{y}_m\rangle &= \left\langle 0\left|a(\boldsymbol{x}_1)\cdots a(\boldsymbol{x}_n)a^{\dagger}(\boldsymbol{y}_1)\cdots a^{\dagger}(\boldsymbol{y}_m)\right|0\right\rangle\\ &= \delta_{mn}\left[\delta^3(\boldsymbol{x}_1-\boldsymbol{y}_1)\cdots\delta^3(\boldsymbol{x}_n-\boldsymbol{y}_n)+\mathrm{sym.}(\boldsymbol{y}_1,\ldots,\boldsymbol{y}_n)\right],\end{aligned} \tag{B.15}$$

where sym.$(\boldsymbol{y}_1,\ldots,\boldsymbol{y}_n)$ represents the symmetric summation of the previous term with respect to $\boldsymbol{y}_1,\ldots,\boldsymbol{y}_n$. If $F[a,a^\dagger]$ is a c-number, i.e., the operator which simply multiplies the real number to the operand, then

$$\left\langle F\left[a,a^\dagger\right]\right\rangle_{\mathrm{G}} = \left\langle 0\middle|F\left[a,a^\dagger\right]\middle|0\right\rangle. \tag{B.16}$$

The quantity (4.4.53) is, after all, represented as

$$\begin{aligned}&\left\langle\prod_{j=1}^{s}\mathcal{H}_{(m_j)}\left(\boldsymbol{x}_j^{(1)},\ldots,\boldsymbol{x}_j^{(m_j)}\right)\right\rangle_{\mathrm{G}}\\ &\quad=\left\langle 0\middle|:\prod_{i=1}^{m_1}\left[\tilde{a}\left(\boldsymbol{x}_1^{(i)}\right)+a^\dagger\left(\boldsymbol{x}_1^{(i)}\right)\right]:\cdots:\prod_{i=1}^{m_s}\left[\tilde{a}\left(\boldsymbol{x}_s^{(i)}\right)+a^\dagger\left(\boldsymbol{x}_s^{(i)}\right)\right]:\middle|0\right\rangle.\end{aligned} \tag{B.17}$$

Expanding the products in *r.h.s*, and using the commutation relations (B.4), (B.5) and the properties (B.11)-(B.13), this quantity is calculated algebraically. But more convenient diagrammatic calculation can be introduced. The "particle" created by a creation operator should be annihilated by an annihilation operator placed left of that creation operator. In a single $\mathcal{H}_{(m_i)}$ represented by Wick product, the creation operators are already placed to the left of annihilation operators, and the "particles" created in some $\mathcal{H}_{(m_i)}$ can not annihilated by the annihilation operator in the same $\mathcal{H}_{(m_i)}$. These observations show the following diagrammatic rules for calculating equation (B.17):

i) Corresponding each $\mathcal{H}_{(m_j)}$, draw m_j points labelled by $\boldsymbol{x}_j^{(1)},\ldots,\boldsymbol{x}_j^{(m_j)}$.

ii) Make $\sum_j m_j/2$ pairs out of those points such that the two points in the same $\mathcal{H}_{(m_j)}$ are not paired. If $\sum_j m_j/2$ is an odd number, the equation (B.17) vanishes.

iii) Associate factor $\psi(\boldsymbol{x}_a^{(p)},\boldsymbol{x}_b^{(q)})$ for each pair, $\boldsymbol{x}_a^{(p)}$ and $\boldsymbol{x}_b^{(q)}$ and make products of these factors.

iv) Sum up those products obtained from all the possible pairings.

For example, the quantities,

$$\left\langle\mathcal{H}_{(1)}(\boldsymbol{x})\mathcal{H}_{(1)}(\boldsymbol{y})\mathcal{H}_{(2)}(\boldsymbol{z},\boldsymbol{w})\right\rangle_{\mathrm{G}}, \tag{B.18}$$

are evaluated by the diagrams in Figure 5.1. Applying the above rules we obtain

Figure 5.1: An example of diagrams for expectation values of products of generalized Wiener-Hermite functionals.

$$\psi(\boldsymbol{x},\boldsymbol{z})\psi(\boldsymbol{y},\boldsymbol{w})+\psi(\boldsymbol{x},\boldsymbol{w})\psi(\boldsymbol{y},\boldsymbol{z}). \tag{B.19}$$

When the generalized Wiener-Hermite functionals of type $\mathcal{H}^{(m)}$ are contained in the *l.h.s.* of equation (B.17), the factor $\psi(\boldsymbol{x}_a^{(p)},\boldsymbol{x}_b^{(q)})$ or $\delta^3(\boldsymbol{x}_a^{(p)}-\boldsymbol{x}_b^{(q)})$ or $\psi^{-1}(\boldsymbol{x}_a^{(p)},\boldsymbol{x}_b^{(q)})$ are associated for each pairs and which factor should be associated can be determined by the fact that the result should be transformed correctly under linear transformation (4.2.19).

The following orthogonality relation can be derived by the above rules:

$$\begin{aligned}&\left\langle\mathcal{H}_{(n)}(\boldsymbol{x}_1,\ldots,\boldsymbol{x}_n)\mathcal{H}^{(m)}(\boldsymbol{y}_1,\ldots,\boldsymbol{y}_m)\right\rangle_{\mathrm{G}}\\&\quad=\delta_{mn}\left[\delta^3(\boldsymbol{x}_1-\boldsymbol{y}_1)\cdots\delta^3(\boldsymbol{x}_m-\boldsymbol{y}_m)+\mathrm{sym.}(\boldsymbol{y}_1,\ldots,\boldsymbol{y}_m)\right].\end{aligned} \tag{B.20}$$

B.2 The method using generating functional

The second method using generating functionals is to derive rules i) $\sim$ iv) using generating functional of generalized Wiener-Hermite functionals. This method is similar to the derivation of Feynman rules in path integral formalism in quantum field theory.

The generating functional of generalized Wiener-Hermite functionals is defined by

$$\mathcal{G}[\alpha,J]=\sum_{m=0}^{\infty}\frac{1}{m!}\int d^3x_1\cdots d^3x_m J(\boldsymbol{x}_1)\cdots J(\boldsymbol{x}_m)\mathcal{H}^{(m)}(\boldsymbol{x}_1,\ldots,\boldsymbol{x}_m), \tag{B.21}$$

so that

$$\mathcal{H}^{(m)}(\boldsymbol{x}_1,\ldots,\boldsymbol{x}_m)=\left.\frac{\delta^m\mathcal{G}[\alpha,J]}{\delta J(\boldsymbol{x}_1)\cdots\delta J(\boldsymbol{x}_m)}\right|_{J=0}. \tag{B.22}$$

We consider the following functional:

$$F[J-\alpha]=\exp\left\{-\frac{1}{2}\int d^3xd^3y[J(\boldsymbol{x})-\alpha(\boldsymbol{x})]\psi^{-1}(\boldsymbol{x},\boldsymbol{y})[J(\boldsymbol{y})-\alpha(\boldsymbol{y})]\right\}, \tag{B.23}$$

and expand this functional with respect to J:

$$F[J-\alpha]=\sum_{m=0}^{\infty}\frac{1}{m!}\int d^3x_1\cdots d^3x_m J(\boldsymbol{x}_1)\cdots J(\boldsymbol{x}_m)\left.\frac{\delta^m F[J-\alpha]}{\delta J(\boldsymbol{x}_1)\cdots\delta J(\boldsymbol{x}_m)}\right|_{J=0}. \quad \text{(B.24)}$$

Because

$$\begin{aligned}\left.\frac{\delta^m F[J-\alpha]}{\delta J(\boldsymbol{x}_1)\cdots\delta J(\boldsymbol{x}_m)}\right|_{J=0}&=(-1)^m\left.\frac{\delta^m F[J-\alpha]}{\delta\alpha(\boldsymbol{x}_1)\cdots\delta\alpha(\boldsymbol{x}_m)}\right|_{J=0}\\&=(-1)^m\left.\frac{\delta^m F[\alpha]}{\delta\alpha(\boldsymbol{x}_1)\cdots\delta\alpha(\boldsymbol{x}_m)}\right|_{J=0}=F[\alpha]\mathcal{H}^{(m)}(\boldsymbol{x}_1,\ldots,\boldsymbol{x}_m), \quad \text{(B.25)}\end{aligned}$$

we see

$$\begin{aligned}\mathcal{G}[\alpha,J]&=\frac{F[J-\alpha]}{F[\alpha]}\\&=\exp\left\{-\frac{1}{2}\int d^3xd^3y J(\boldsymbol{x})\psi^{-1}(\boldsymbol{x},\boldsymbol{y})J(\boldsymbol{y})+\int d^3xd^3y\alpha(\boldsymbol{x})\psi^{-1}(\boldsymbol{x},\boldsymbol{y})J(\boldsymbol{y})\right\}. \quad \text{(B.26)}\end{aligned}$$

Using this representation of generating functional, we can derive the following equation:

$$\langle\mathcal{G}[\alpha,J_1]\cdots\mathcal{G}[\alpha,J_s]\rangle_{\mathrm{G}}=\exp\left[\sum_{i<j}^{s}\int d^3xd^3y J_i(\boldsymbol{x})\psi^{-1}(\boldsymbol{x},\boldsymbol{y})J_j(\boldsymbol{y})\right]. \quad \text{(B.27)}$$

The rules i) $\sim$ iv) are derived by operating

$$\frac{\delta^{m_1}}{\delta J_1\left(\boldsymbol{x}_1^{(1)}\right)\cdots\delta J_1\left(\boldsymbol{x}_1^{(m_1)}\right)}\cdots\frac{\delta^{m_s}}{\delta J_s\left(\boldsymbol{x}_s^{(1)}\right)\cdots\delta J_s\left(\boldsymbol{x}_s^{(m_s)}\right)}, \quad \text{(B.28)}$$

to the both side of equation (B.27), and putting $J_1=J_2=\cdots=J_s=0$.

C THE CALCULATION OF THE STATISTICAL FACTOR

In the expression (4.3.5) the points associated with $\mathcal{H}^{(n_1+\cdots+n_m)},\mathcal{H}_{(m_i)}$ are classified into $m+N$ groups with $n_1,\ldots,n_m;m_1,\ldots,m_N$ members respectively. These points in each group are symmetric about permutations. We distinguish these $m+N$ groups by labels like α,β, and so on. In evaluating the Gaussian average of the product of generalized Wiener-Hermite functionals using diagrammatic method described in Appendix A, we denote the number of lines connecting the members of two groups α and β as a symmetric matrix $M_{\alpha\beta}$ with vanishing diagonal elements. Obviously, graphs which have the same value of the matrix $M_{\alpha\beta}$ give the same contribution to P_N. Thus we need to calculate the degree of multiplicity of the graphs which have the same value of $M_{\alpha\beta}$.

We designate the number of points in a group α as M_α. The number of ways to divide the M_α points into $M_{\alpha,1},\ldots,M_{\alpha,m+N}$ parts for all groups α's is

$$\prod_\alpha \left(\frac{M_\alpha!}{M_{\alpha,1}!\cdots M_{\alpha,m+N}!} \right) = \frac{\prod_\alpha M_\alpha!}{\left(\prod_{\alpha<\beta} M_{\alpha\beta}! \right)^2}. \tag{C.1}$$

The number of ways to connect these points is given by $\prod_{\alpha<\beta} M_{\alpha\beta}!$ and thus the multiplicity of the graphs is

$$\frac{n_1!\cdots n_m! m_1!\cdots m_N!}{\prod_{\text{ends}} a_{\text{ends}}}. \tag{C.2}$$

The numerator cancels out in equation (4.3.5) and the statistical factor

$$\frac{1}{m! \prod_{\substack{\text{identical}\\ \text{lines}}} n_{\mathrm{L}}!}. \tag{C.3}$$

follows. It is obvious that the m vertices are distinguished in the above evaluation. We can further take the indistinguishability of the same kind of vertices into account. This corresponds to multiplying

$$\frac{m!}{\prod_{\substack{\text{identical}\\ \text{vertices}}} n_{\mathrm{V}}!}, \tag{C.4}$$

and the statistical factor

$$\frac{1}{\prod_{\substack{\text{identical}\\ \text{lines}}} n_{\mathrm{L}}! \prod_{\substack{\text{identical}\\ \text{vertices}}} n_{\mathrm{V}}!}, \tag{C.5}$$

follows.

D EVALUATION OF $R_m^{(\mathrm{pk})}(\nu)$

This Appendix is devoted to the derivation of equation (4.4.15). The following identity is convenient for our purpose:

$$\frac{x^2}{2} + \frac{(y-\gamma x)^2}{2(1-\gamma^2)} = \frac{y^2}{2} + \frac{(x-\gamma y)^2}{2(1-\gamma^2)}. \tag{D.1}$$

From this identity, equation (4.4.8) reduces to

$$\mathcal{N}_{\rm pk}^{\rm (G)}(\nu)=\frac{1}{(2\pi)^2R_*^3}\int_0^\infty dxf(x)e^{-x^2/2}\frac{\exp\left[-\dfrac{(\nu-\gamma x)^2}{2(1-\gamma^2)}\right]}{[2\pi(1-\gamma^2)]^{1/2}}, \tag{D.2}$$

and the integral in equation (4.4.7) can easily be calculated:

$$\mathrm{n}_{\rm pk}^{\rm (G)}(\nu)=\frac{1}{8\pi^2R_*^3}\int_0^\infty dxf(x)e^{-x^2/2}\mathrm{erfc}\left(\frac{\nu-\gamma x}{\sqrt{2(1-\gamma^2)}}\right). \tag{D.3}$$

The latter expression (D.3) was previously derived by Mann, Heavens & Peacock (1993). Differentiating equation (D.2) and using the identity (D.1) again, we obtain

$$\left(-\frac{d}{d\nu}\right)^{m-1}\mathcal{N}_{\rm pk}^{\rm (G)}(\nu)= \frac{e^{-\nu^2/2}}{(2\pi)^{5/2}R_*^3(1-\gamma^2)^{m/2}}\int_0^\infty dxf(x)H_{m-1}\left(\frac{\nu-\gamma x}{\sqrt{1-\gamma^2}}\right)\exp\left[-\frac{(x-\gamma\nu)^2}{2(1-\gamma^2)}\right], \tag{D.4}$$

for $m\geq 1$. Thus,

$$R_m^{\rm (pk)}(\nu)= \begin{cases} \dfrac{1}{8\pi^2R_*^3}\displaystyle\int_0^\infty dxf(x)e^{-x^2/2}\mathrm{erfc}\left(\frac{\nu-\gamma x}{\sqrt{2(1-\gamma^2)}}\right) & (m=0) \\ \dfrac{e^{-\nu^2/2}}{(2\pi)^{5/2}R_*^3(1-\gamma^2)^{m/2}}\displaystyle\int_0^\infty dxf(x)H_{m-1}\left(\frac{\nu-\gamma x}{\sqrt{1-\gamma}}\right)\exp\left[-\frac{(x-\gamma\nu)^2}{2(1-\gamma^2)}\right] & (m\geq 1) \end{cases} \tag{D.5}$$

is proved.

E PROOF OF $\langle\tilde{\alpha}\rangle=\mathcal{N}_{\rm pk}^{\rm (G)}(\nu)/\mathrm{n}_{\rm pk}^{\rm (G)}(\nu)$

In this Appendix, we calculate $\langle\tilde{\alpha}\rangle$ defined by equation (4.4.19). Using the identity (D.1), the equation (4.4.19) reduces to

$$\langle\tilde{\alpha}\rangle=\frac{1}{(2\pi)^2R_*^3\mathrm{n}_{\rm pk}^{\rm (G)}(\nu)}\int_0^\infty dxf(x)e^{-x^2/2}\int_\nu^\infty d\alpha\frac{\exp\left[-\dfrac{(\alpha-\gamma x)^2}{2(1-\gamma^2)}\right]}{[2\pi(1-\gamma^2)]^{1/2}}\frac{\alpha-\gamma x}{1-\gamma^2}. \tag{E.1}$$

The integration with respect to α is straightforward by a transformation $\beta=\alpha-\gamma x$. Comparing the result with equation (D.2), this quantity has the simple form,

$$\langle\tilde{\alpha}\rangle=\frac{\mathcal{N}_{\rm pk}^{\rm (G)}(\nu)}{\mathrm{n}_{\rm pk}^{\rm (G)}(\nu)}. \tag{E.2}$$

F DERIVATION OF COEFFICIENTS FOR DENSITY EXTREMA

In this Appendix, we derive the coefficients (4.4.26). The quantity we should calculate is

$$R(k,\{l_i\},\{p_{ij}\}) = \left\langle \left(\frac{\partial}{\partial\alpha}\right)^k \prod_{i=1}^{3}\left(\frac{\partial}{\partial\beta_i}\right)^{l_i} \prod_{i\le j}^{3}\left(\frac{\partial}{\partial\omega_{ij}}\right)^{p_{ij}} \theta(\alpha-\nu)\delta^3(\beta_i)(-1)^3\det(\omega_{ij})\right\rangle_{\rm G} \tag{F.1}$$

$$= -\frac{1}{(2\pi)^5\sqrt{\det M}}\int_{-\infty}^{\infty} d\alpha \prod_{i=1}^{3} d\beta_i \prod_{i\le j}^{3} d\omega_{ij} \exp\left[-\frac{1}{2}\sum_{\mu,\nu} A_\mu (M^{-1})_{\mu\nu} A_\nu\right] \times \frac{\partial^k\theta(\alpha-\nu)}{\partial\alpha^k}\prod_{i=1}^{3}\frac{\partial^{l_i}\delta(\beta_i)}{\partial\beta_i^{l_i}}\prod_{i\le j}^{3}\left(\frac{\partial}{\partial\omega_{ij}}\right)^{p_{ij}}\det\omega, \tag{F.2}$$

where ten dimensional vector A_μ is

$$(A_\mu) = (\alpha,\beta_1,\beta_2,\beta_3,\omega_{11},\omega_{22},\omega_{33},\omega_{23},\omega_{13},\omega_{12}). \tag{F.3}$$

The correlation matrix $M_{\mu\nu} = \langle A_\mu A_\nu\rangle$ is explicitly

$$M = \left[\begin{array}{c|c|c|c} 1 & \boldsymbol{O}_V^T & -\frac{\sigma_1^2}{3\sigma_0^2}\boldsymbol{I}_V^T & \boldsymbol{O}_V^T \\ \hline \boldsymbol{O}_V & \frac{\sigma_1^2}{3\sigma_0^2}\boldsymbol{I} & \boldsymbol{O} & \boldsymbol{O} \\ \hline -\frac{\sigma_1^2}{3\sigma_0^2}\boldsymbol{I}_V^T & \boldsymbol{O} & \frac{\sigma_2^2}{15\sigma_0^2}\boldsymbol{B} & \boldsymbol{O} \\ \hline \boldsymbol{O}_V & \boldsymbol{O} & \boldsymbol{O} & \frac{\sigma_2^2}{15\sigma_0^2}\boldsymbol{I} \end{array}\right], \tag{F.4}$$

where

$$\boldsymbol{O}_V = \begin{bmatrix}0\\0\\0\end{bmatrix}, \boldsymbol{I}_V = \begin{bmatrix}1\\1\\1\end{bmatrix}, \boldsymbol{O} = \begin{bmatrix}0&0&0\\0&0&0\\0&0&0\end{bmatrix}, \boldsymbol{I} = \begin{bmatrix}1&0&0\\0&1&0\\0&0&1\end{bmatrix}, \boldsymbol{B} = \begin{bmatrix}3&1&1\\1&3&1\\1&1&3\end{bmatrix}. \tag{F.5}$$

This is the consequence of spatial homogeneity and isotropy (see Bardeen et al. 1986). We introduce new variables $\tilde{\omega}_{ij}$ as

$$\tilde{\omega}_{ij} = \omega_{ij} + \delta_{ij}\frac{\sigma_1^2}{3\sigma_0^2}\alpha, \tag{F.6}$$

then the non-vanishing correlations among variables α, β_i, $\tilde{\omega}_{ij}$ are

$$\langle\alpha^2\rangle = 1, \langle\beta_1^2\rangle = \langle\beta_2^2\rangle = \langle\beta_3^2\rangle = \frac{\sigma_1^2}{3\sigma_0^2},$$
$$\langle\tilde{\omega}_{11}^2\rangle = \langle\tilde{\omega}_{22}^2\rangle = \langle\tilde{\omega}_{33}^2\rangle = \frac{\sigma_2^2}{5\sigma_0^2}\left(1-\frac{5}{9}\gamma^2\right),$$

p_{11}	p_{22}	p_{33}	p_{23}	p_{13}	p_{12}	J_0	J_1	J_2	J_3
0	0	0	0	0	0	1	0	0	0
1	0	0	0	0	0	0	1	0	0
0	1	0	0	0	0	0	1	0	0
0	0	1	0	0	0	0	1	0	0
1	1	0	0	0	0	0	0	1	0
1	0	1	0	0	0	0	0	1	0
0	1	1	0	0	0	0	0	1	0
0	0	0	2	0	0	0	0	−2	0
0	0	0	0	2	0	0	0	−2	0
0	0	0	0	0	2	0	0	−2	0
1	1	1	0	0	0	0	0	0	1
1	0	0	2	0	0	0	0	0	−2
0	1	0	0	2	0	0	0	0	−2
0	0	1	0	0	2	0	0	0	−2
0	0	0	1	1	1	0	0	0	2

Table 5.1: The definition of J_i. For other values of p_{ij} not listed in this table, $J_i = 0$.

$$\langle\tilde{\omega}_{11}\tilde{\omega}_{22}\rangle = \langle\tilde{\omega}_{22}\tilde{\omega}_{33}\rangle = \langle\tilde{\omega}_{11}\tilde{\omega}_{33}\rangle = \frac{\sigma_2^2}{15\sigma_0^2}\left(1 - \frac{5}{3}\gamma^2\right),$$
$$\langle\tilde{\omega}_{12}^2\rangle = \langle\tilde{\omega}_{23}^2\rangle = \langle\tilde{\omega}_{13}^2\rangle = \frac{\sigma_2^2}{15\sigma_0^2}, \tag{F.7}$$

and all other correlations vanish. The coefficients (F.1) is represented by new variables, α, β_i, ω_{ij} as

$$R(k,\{l_i\},\{p_{ij}\}) = -\left\langle \prod_{i=1}^{3} \frac{\partial^{l_i}\delta(\beta_i)}{\partial\beta_i^{l_i}} \right\rangle_{\mathrm{G}} \left\langle \frac{\partial^k\theta(\alpha-\nu)}{\partial\alpha^k} \prod_{i\le j}^{3} \left(\frac{\partial}{\partial\tilde{\omega}_{ij}}\right)^{p_{ij}} W(\alpha,\tilde{\omega}) \right\rangle_{\mathrm{G}}, \tag{F.8}$$

where

$$\begin{aligned} W(\alpha,\tilde{\omega}) = &-\left(\frac{\sigma_1^2}{3\sigma_0^2}\right)^3\alpha^3 + \left(\frac{\sigma_1^2}{3\sigma_0^2}\right)^2(\tilde{\omega}_{11}+\tilde{\omega}_{22}+\tilde{\omega}_{33})\,\alpha^2 \\ &+\frac{\sigma_1^2}{3\sigma_0^2}\left(\tilde{\omega}_{23}^2+\tilde{\omega}_{13}^2+\tilde{\omega}_{12}^2-\tilde{\omega}_{22}\tilde{\omega}_{33}-\tilde{\omega}_{11}\tilde{\omega}_{33}-\tilde{\omega}_{11}\tilde{\omega}_{22}\right)\alpha \\ &+\tilde{\omega}_{11}\tilde{\omega}_{22}\tilde{\omega}_{33}+2\tilde{\omega}_{23}\tilde{\omega}_{13}\tilde{\omega}_{12}-\tilde{\omega}_{11}\tilde{\omega}_{23}^2-\tilde{\omega}_{22}\tilde{\omega}_{13}^2-\tilde{\omega}_{33}\tilde{\omega}_{12}^2. \end{aligned} \tag{F.9}$$

We see, from equation (F.9), that the equation (F.8) survives only when integers p_{ij} take the values listed in Table 5.1. Using $J_i(\{p_{ij}\})$ defined by Table 5.1, the multivariate Gaussian integral by $\tilde{\omega}$ of the second factor of the equation (F.8) reduces

to

$$-\left(\frac{\sigma_1^2}{3\sigma_0^2}\right)^{3-\sum_{i\le j}p_{ij}}\left\langle\frac{\partial^k\theta(\alpha-\nu)}{\partial\alpha^k}\left[H_3(\alpha)J_0(\{p_{ij}\})-H_2(\alpha)J_1(\{p_{ij}\})+\right.\right.$$
$$\left.\left.+H_1(\alpha)J_2(\{p_{ij}\})-J_3(\{p_{ij}\})\right]\right\rangle_{\rm G}. \qquad \text{(F.10)}$$

Defining

$$H_{-1}(\nu)=\sqrt{\frac{\pi}{2}}e^{\nu^2/2}\mathrm{erfc}\left(\frac{\nu}{\sqrt{2}}\right), \qquad \text{(F.11)}$$

we find

$$\left\langle\frac{\partial^k\theta(\alpha-\nu)}{\partial\alpha^k}H_n(\alpha)\right\rangle_{\rm G}=\frac{1}{\sqrt{2\pi}}H_{k+n-1}(\nu)e^{-\nu^2/2}, \qquad \text{(F.12)}$$

for $n=0,1,2,\ldots$. The first factor of equation (F.8) is

$$\frac{1}{(2\pi)^{3/2}}\left(\frac{\sigma_1}{\sqrt{3}\sigma_0}\right)^{-\sum_i l_i-3}H_{l_1}(0)H_{l_2}(0)H_{l_3}(0), \qquad \text{(F.13)}$$

where

$$H_l(0)=\begin{cases}0 & (l\text{: odd}),\\ (-1)^{l/2}(l-1)!! & (l\text{: even}).\end{cases} \qquad \text{(F.14)}$$

Therefore, we finally get the explicit form of the kernels:

$$R(k,\{l_i\},\{p_{ij}\})=\frac{1}{(2\pi)^2}\left(\frac{\sigma_1}{\sqrt{3}\sigma_0}\right)^{3-\sum_i l_i-2\sum_{i\le j}p_{ij}}H_{l_1}(0)H_{l_2}(0)H_{l_3}(0)$$
$$\times e^{-\nu^2/2}\left[H_{k+2}(\nu)J_0(\{p_{ij}\})-H_{k+1}(\nu)J_1(\{p_{ij}\})\right.$$
$$\left.+H_k(\nu)J_2(\{p_{ij}\})-H_{k-1}(\nu)J_3(\{p_{ij}\})\right]. \qquad \text{(F.15)}$$

References

Adler R. J. 1981, *The Geometry of Random Fields* (Wiley: Chichester)

Alimi J.-M., Blanchard, A. & Schaeffer, R. 1990, *Astrophys. J.*, **349**, L5

Allen T. J., Grinstein B. & Wise M. B. 1987, *Phys. Lett.*, **B197**, 66

Appel P. & de Fériet J. K. 1926, *Fonctions Hypergéométriques et Hypersphériques, Polynômes d'Hermite* (Ganthier-Villars: Paris)

Babul A. & White S. D. M. 1991, *Monthly Notices Roy. Astron. Soc.*, **253**, 31P

Bahcall N. A. & Soneira R. M. 1983, *Astrophys. J.*, **270**, 20

Balian R. & Schaeffer R. 1989a, *Astron. Astrophys.*, **220**, 1

Balian R. & Schaeffer R. 1989b, *Astron. Astrophys.*, **226**, 373

Bardeen J. M., Bond J. R., Kaiser N. & Szalay A. S. 1986, *Astrophys. J.*, **304**, 15

Bardeen J. M., Steinhardt P. J. & Turner M. S. 1983, *Phys. Rev.*, D**28**, 679

Bernardeau F. 1992, *Astrophys. J.*, **392**, 1

Bernardeau F. 1994, *Astrophys. J.*, **433**, 1

Bernardeau F. & Kofman L. 1994, preprint IFA-94-19 (astro-ph/9403028).

Bernardeau F., Juszkiewicz R., Dekel A. & Bouchet F. R. 1994, preprint CITA 94-15 (astro-ph/9404052).

Bertschinger E. 1993, in *New Insights into the Universe* eds. Martínez, V. J., Portilla, M. & Sáez, D., (Springer-Verlag: Berlin-Heidelberg)

Bharadwaj S. 1994, *Astrophys. J.*, **428**, 419

Bond J. R. & Szalay A. S. 1983, *Astrophys. J.*, **274**, 443

Bond J. R. & Efstathiou G. 1987, *Monthly Notices Roy. Astron. Soc.*, **226**, 655

Borgani S. & Bonometto S. A. 1989, *Astron. Astrophys.*, **215**, 17

Borgani S. & Bonometto S. A. 1990, *Astrophys. J.*, **348**, 398

Bouchet F. R., Juszkiewicz R., Colombi S. & Pellat R. 1992, *Astrophys. J. Letters*, **394**, L5

Bouchet F. R., Colombi S., Hivon E. & Juszkiewicz R. 1995, Astron. Astrophys, *296*, **575**,

Bower R. G., Coles P., Frenk C. S. & White S. D. M. 1993, *Astrophys. J.*, **405**, 403

Buchert T. 1992, *Monthly Notices Roy. Astron. Soc.*, **254**, 729

Buchert T. 1994, *Monthly Notices Roy. Astron. Soc.*, **267**, 811

Buchert T. & Ehlers J. 1993, *Monthly Notices Roy. Astron. Soc.*, **264**, 375

Catelan P., Lucchin F. & Matarrese S. 1988, *Phys. Rev. Lett.*, **61**, 267

Cen R. & Ostriker J. P. 1992, *Astrophys. J. Letters*, **399**, L113

Cen R. & Ostriker J. P. 1993, *Astrophys. J.*, **417**, 415

Cline J. M., Politzer H. D., Rey S.-J. & Wise M. B. 1987, *Commun. Math. Phys.*, **112**, 217

Cole S., Fisher K. B. & Weinberg D. H. 1994, *Monthly Notices Roy. Astron. Soc.*, **267**, 785

Coles P. 1988, *Monthly Notices Roy. Astron. Soc.*, **234**, 509

Coles P. 1989, *Monthly Notices Roy. Astron. Soc.*, **238**, 319

Coles P. & Frenk C. S. 1991, *Monthly Notices Roy. Astron. Soc.*, **253**, 727

Colombi S., Bouchet F. R. & Schaeffer R. 1994Astron. Astrophys., *281*, **301**,

Croft R. A. & Efstathiou G. 1994, *Monthly Notices Roy. Astron. Soc.*, **267**, 390

Davis M., Efstathiou G., Frenk C. S. & White S. D. M. 1985, *Astrophys. J.*, **292**, 371

Davis M. & Peebles P. J. E. 1977, *Astrophys. J. Suppl.*, **34**, 425

Davis M. & Peebles P. J. E. 1983, *Astrophys. J.*, **267**, 465

de Lapparent V., Geller M. J. & Huchra J. P. 1988, *Astrophys. J.*, **332**, 44

Doroshkevich A. G. 1970, *Astrophysics*, **6**, 320 (transl. from *Astrofizika*, 6, 581 [1970])

Efstathiou G., Frenk C. S., White S. D. M. & Davis M. 1988, *Monthly Notices Roy. Astron. Soc.*, **235**, 715

Efstathiou G., Kaiser N., Saunders W., Lawrence A., Rowan-Robinson M., Ellis R. S. & Frenk C. S. 1990, *Monthly Notices Roy. Astron. Soc.*, **247**, 10P

Efstathiou G., Sutherland W. J. & Maddox S. J. 1990, *Nature*, **348**, 705

Freedman W. L., Madore B. F., Mould J. R., Hill R., Ferrarese L., Kennicutt Jr. R. C., Saha A., Stetson P. B., Graham J. A., Ford H., Hoessel J. G., Huchra J., Hughes S. M. & Illingworth G. D. 1994, *Nature*, **371**, 757

Friedberg R. & Lee T. D. 1984, *Nucl.Phys.*, **B242**, 145

Fry J. N. 1984a, *Astrophys. J. Letters*, **277**, L5

Fry J. N. 1984b, *Astrophys. J.*, **279**, 499

Fry J. N. 1986, *Astrophys. J. Letters*, **308**, L71

Fry J. N. & Gaztañaga E. 1993, *Astrophys. J.*, **413**, 447

Fry J. N. & Gaztañaga E. 1994, *Astrophys. J.*, **425**, 1

Fry J. N., Melott A. L. & Shandarin S. F. 1992, *Astrophys. J.*, **393**, 431

Fry J. N. & Peebles P. J. E. 1978, *Astrophys. J.*, **221**, 19

Gaztañaga E. 1992, *Astrophys. J. Letters*, **398**, L17

Goroff M. H., Grinstein B., Rey S.-J. & Wise M. B. 1986, *Astrophys. J.*, **311**, 6

Gott J. R., Park C., Juszkiewicz R., Bies W. E., Bennett D. P., Bouchet F. R. & Stebbins A. 1990, *Astrophys. J.*, **352**, 1

Gott J. R., Gao B. & Park C. 1991, *Astrophys. J.*, **383**, 90

Gott J. R., Mao S., Park C. & Lahav O. 1992, *Astrophys. J.*, **385**, 26

Gott J. R., Melott A. L. & Dickinson M. 1986, *Astrophys. J.*, **306**, 341

Gott J. R., Miller J., Thuan T. X., Schneider S. E., Weinberg D. H., Gammie C., Polk K., Vogeley M., Jeffrey S., Bhavsar S. P., Melott A. L., Giovanelli R., Haynes M. P., Tully R. B. & Hamilton A. J. S. 1989, *Astrophys. J.*, **340**, 625

Gott J. R., Weinberg D. H. & Melott A. L. 1987, *Astrophys. J.*, **319**, 1

Gramann M., Cen R. & Gott J. R. 1994, *Astrophys. J.*, **425**, 382

Grinstein B. & Wise M. B. 1986, *Astrophys. J.*, **310**, 19

Groth E. J,. & Peebles P. J. E. 1977, *Astrophys. J.*, **217**, 385

Guth A. & Pi S.-Y. 1982, *Phys. Rev. Lett.*, **49**, 1110

Hamilton A. J. S. 1988, *Astrophys. J.*, **332**, 67

Hamilton A. J. S. 1988, *Publ. Astron. Soc. Pacific*, **100**, 1343

Hamilton A. J. S. 1992, *Astrophys. J. Letters*, **385**, L5

Hamilton A. J. S. 1993, *Astrophys. J. Letters*, **406**, L47

Hamilton A. J. S., Gott J. R. & Weinberg D. H. 1986, *Astrophys. J.*, **309**, 1

Harrison E. R. 1970, *Phys. Rev.*, D**1**, 2726

Hauser M. G. & Peebles P. J. E. 1973, *Astrophys. J.*, **185**, 757

Hawking S. 1982, *Phys. Lett.*, **115B**, 295

Hivon E., Bouchet F. R., Colombi S. & Juszkiewicz R. 1994preprint (astro-ph/9407049),

Hodges H. M., Blumenthal G. R., Kofman L. A. & Primack J. R. 1990, *Nucl. Phys.*, **B335**, 197.

Ikeuchi S. 1981, *Publ. Astron. Soc. Japan*, **33**, 211

Imamura T. & Meecham W. C., Siegel A. 1965, *J. Math. Phys.*, **6**, 695

Itoh M, Suginohara T. & Suto Y. 1992, *Publ. Astron. Soc. Japan*, **44**, 481

Jensen L. G. & Szalay A. S. 1986, *Astrophys. J. Letters*, **305**, L5

Juszkiewicz R., Bouchet F. R. & Colombi S. 1993, *Astrophys. J. Letters*, **412**, L9

Juszkiewicz R., Weinberg D. H., Amsterdamski P., Chodorowski M. & Bouchet F. R. 1994, preprint (astro-ph/9308012) *Astrophys. J.* in press

Kaiser N. 1984, *Astrophys. J. Letters*, **284**, L9.

Kaiser N. 1987, *Monthly Notices Roy. Astron. Soc.*, **227**, 1

Kauffmann G. & White S. D. M. 1992, *Monthly Notices Roy. Astron. Soc.*, **258**, 511

Klypin A. A. & Kopylov A. I. 1983, *Sov. Astron. Lett.*, **9**, 41

Kofman L. A. & Linde A. D. 1985, *Nucl. Phys.*, **B282**, 555

Kolb E. M. & Turner M. S. 1990, *The Early Universe* (Addison-Wesley: New York

Lahav O., Lilje P. B., Primack J. R. & Rees M. J. 1991, *Monthly Notices Roy. Astron. Soc.*, **251**, 128)

Lahav O., Itoh M., Inagaki S. & Suto Y. 1993, *Astrophys. J.*, **402**, 387

Lilje P. B. & Efstathiou G. 1989, *Monthly Notices Roy. Astron. Soc.*, **236**, 851

Łokas E. L., Juszkiewicz R., Weinberg D. H. & Bouchet F. R. 1995, *Monthly Notices Roy. Astron. Soc.*, **274**, 730

Lumsden S. L., Heavens A. F. & Peacock J. A. 1989, *Monthly Notices Roy. Astron. Soc.*, **238**, 293

Ma S.-K. 1985, *Statistical Mechanics* (World Scientific: Philadelphia

Maddox S. J., Efstathiou G., Sutherland W. J. & Loveday J. 1990, *Monthly Notices Roy. Astron. Soc.*, **242**, 43P)

Mann R. G., Heavens A. F. & Peacock J. A. 1993, *Monthly Notices Roy. Astron. Soc.*, **263**, 798

Martel H. 1991, *Astrophys. J.*, **377**, 7

Matarrese S., Lucchin F. & Bonometto S. A. 1986, *Astrophys. J. Letters*, **310**, L21

Matsubara T. 1994a, *Astrophys. J.*, **424**, 30

Matsubara T. 1994b, *Astrophys. J. Letters*, **434**, L43

Matsubara T. 1994c, *Astrophys. J.*, in press

Matsubara T. 1994d, *Astrophys. J. Suppl.*, **101**, in press.

Matsubara T. 1995a, in *Proceedings of the 11th Potsdam Cosmology Workshop* in press

Matsubara T. 1995b, in preparation.

Matsubara T. & Suto Y. 1994, *Astrophys. J.*, **420**, 497.

Matsubara T. & Suto Y. 1995, in preparation

Maurogordato S., Schaeffer R. & da Costa L. N. 1992, *Astrophys. J.*, **390**, 17.

McGill C. 1990, *Monthly Notices Roy. Astron. Soc.*, **242**, 428

Meiksin A., Szapudi I. & Szalay A. S. 1992, *Astrophys. J.*, **394**, 87

Melott A. L., Weinberg D. H. & Gott J. R. 1988, *Astrophys. J.*, **328**, 50

Melott A. L., Cohen A. P., Hamilton A. J. S., Gott J. R. & Weinberg D. H. 1989, *Astrophys. J.*, **345**, 618

Moore B., Frenk C. S., Weinberg D. H., Saunders W., Lawrence A., Ellis R. S., Kaiser N., Efstathiou G. & Rowan-Robinson M. 1992, *Monthly Notices Roy. Astron. Soc.*, **256**, 477

Okun B. L. 1990, *J. Stat. Phys.*, **59**, 523

Olive K. A., Schramm D. N., Steigman G. & Walker T. P. 1990Phys. Lett., *B236*, **454**,

Ortolan A., Lucchin F. & Matarrese S. 1989, *Phys. Rev.*, D**40**, 290

Ostriker J. P. & Cowie L. L. 1981, *Astrophys. J. Letters*, **284**, L9

Otto S., Politzer H. D. & Wise M. B. 1986, *Phys. Rev. Lett.*, **56**, 1878

Park C. 1991, *Astrophys. J. Letters*, **382**, L59

Park C. & Gott J. R. 1991, *Astrophys. J.*, **378**, 457

Park C., Gott J. R. & da Costa L. N. 1992, *Astrophys. J. Letters*, **392**, L51

Park, C., Gott. J. R., Melott, A. L. & Karachentsev, I. D. 1992, *Astrophys. J.*, **387**, 1

Peacock J. A. 1993, *New Insights into the Universeeds. Martínez, V. J., Portilla, M. & Sáez, D.* (Springer-Verlag: Berlin-Heidelberg)

Peebles P. J. E. 1980, *The Large-Scale Structure of the Universe* (Princeton University Press: Princeton)

Peebles P. J. E. & Groth E. J. 1975, *Astrophys. J.*, **196**, 1

Pierce M. J., Welch D. L., McClure R. D., Bergh S., Racine R. & Stetson P. B. 1994, *Nature*, **371**, 385

Politzer H. D. & Wise M. B. 1984, *Astrophys. J. Letters*, **285**, L1

Postman M., Huchra J. P. & Geller M. J. 1992, *Astrophys. J.*, **384**, 404

Readhead A. C. S., Lawrence C. R., Myers S. T., Sargent W. L. W., Hardebeck H. E. & Moffet A. T. 1989, *Astrophys. J.*, **346**, 566

Rhoads J. E., Gott J. R. & Postman M. 1994, *Astrophys. J.*, **421**, 1

Ryden B. S. 1988, *Astrophys. J. Letters*, **333**, L41

Ryden B. S., Melott A. L., Craig D. A., Gott J. R., Weinberg D. H., Scherrer R. J., Bhavsar S. P., & Miller J. M. 1989, *Astrophys. J.*, **340**, 647

Salopek D. S. 1992, *Phys. Rev.*, D**45**, 1139

Salopek D. S. & Bond J. R. 1990, *Phys. Rev.*, D**42**, 3936

Salopek D. S., Bond J. R. & Efstathiou G. 1989, *Phys. Rev.*, D**40**, 1753

Sargent W. L. W. & Turner E. L. 1977, *Astrophys. J. Letters*, **212**, L3

Saunders W., Rowan-Robinson M. & Lawrence A. 1992, *Monthly Notices Roy. Astron. Soc.*, **258**, 134

Scherrer R. J. & Bertschinger E. 1991, *Astrophys. J.*, **381**, 349

Sharp N. A. 1981, *Monthly Notices Roy. Astron. Soc.*, **195**, 857

Sharp N. A., Bonometto S. A. & Lucchin F. 1984, *Astron. Astrophys.*, **130**, 79

Smith M. S., Kawano L. H. & Malaney R. A. 1993, *Astrophys. J. Suppl.*, **85**, 219

Smoot G. F., Bennett C. L., Kogut A., Wright E. L., Aymon J., Boggess N. W., Cheng E. S., DeAmici G., Gulkis S., Hauser M. G., Hinshaw G., Lineweaver C., Loewenstein K., Jackson P. D., Janssen M., Kaita E., Kelsall T., Keegstra P., Lubin P., Mather J. C., Meyer S. S., Moseley S. H., Murdock T. L., Rokke L., Silverberg R. F., TenorioL., Weiss R. & Wilkinson D. T. 1992, *Astrophys. J. Letters*, **396**, L1

Starobinskii A. A. 1982, *Phys. Lett.*, **117B**, 175

Suginohara T., Suto Y., Bouchet F. R. & Hernquist L. 1991, *Astrophys. J. Suppl.*, **75**, 631

Suginohara T. & Suto Y. 1991, *Publ. Astron. Soc. Japan*, **43**, L17

Suto Y. 1993, *Astrophys. J. Letters*, **404**, L1

Suto Y. & Matsubara T. 1994, *Astrophys. J.*, **420**, 504

Suto Y. & Suginohara T. 1991, *Astrophys. J. Letters*, **370**, L15

Szalay A. S. 1988, *Astrophys. J.*, **333**, 21

Szapudi I., Szalay A. S. & Boschán P. 1992, *Astrophys. J.*, **390**, 350

Tóth G., Hollósi J. & Szalay A. S. 1989, *Astrophys. J.*, **344**, 75

Totsuji H. & Kihara T. 1969, *Publ. Astron. Soc. Japan*, **21**, 221

Ueda H., Itoh M., & Suto Y. 1993, *Astrophys. J.*, **408**, 3

Uson J. M. & Wilkinson D. T. 1984, *Nature*, **312**, 427

Vilenkin A. 1985, *Phys. Rep.*, **121**, 263

Vogeley M. S., Geller M. J. & Huchra J. P. 1991, *Astrophys. J.*, **382**, 44

Vogeley M. S., Park C., Geller M. J., Huchra J. P. & Gott J. R. 1994, *Astrophys. J.*, **420**, 525

Walker T. P., Steigman G., Schramm D. N., Olive K. A. & Kang H.-S. 1991, *Astrophys. J.*, **376**, 51

Watanabe T., Matsubara T. & Suto Y. 1994, *Astrophys. J.*, **432**, 17

Weinberg D. H. & Cole S. 1992, *Monthly Notices Roy. Astron. Soc.*, **259**, 652

Weinberg D. H., Gott J. R. & Melott A. L. 1987, *Astrophys. J.*, **321**, 2

Weinberg S. 1972, *Gravitation and Cosmology* (Wiley: New York)

White S. D. M. 1979, *Monthly Notices Roy. Astron. Soc.*, **186**, 145

Wick G. C. 1950, *Phys. Rev.*, **80**, 268

Zel'dovich Ya. B. 1970, *Astron. Astrophys.*, **5**, 84

Zel'dovich Ya. B. 1973, *Astrophysics*, **6**, 164

Zel'dovich Ya. B. 1972, *Monthly Notices Roy. Astron. Soc.*, **160**, 1P